The meteorological and chemical processes influencing UK air quality investigated using satellite observations and modelling

Richard James Pope

University of Leeds

School of Earth and Environment

Submitted in accordance with the requirements for a degree of

Doctor of Philosophy

December 2014

Declaration of Authorship

The candidate confirms that the work submitted is his/her own, except where work which has formed part of jointly authored publications has been included. The contribution of the candidate and the other authors to this work has been explicitly indicated below. The candidate confirms that appropriate credit has been given within the thesis where reference has been made to the work of others.

Chapter 4 includes model evaluation using satellite data which has been published, with co-authors, in Atmospheric Chemistry and Physics Discussions. The reference is **Pope, R.J., M.P. Chipperfield, N.H. Savage, C. Ordóñez, L.S. Neal, L.A. Lee, S.S. Dhomse, and N.A.D. Richards, Evaluation of a regional air quality model using satellite column NO$_2$: treatment of observational errors and model boundary conditions and emissions,** $ACPD$**, 14, 21749-217484, doi:10.5194/acpd-14-21749-2014, 2014**. MP Chipperfield and NH Savage supervised the student. C Ordóñez wrote AQUM's aerosol surface area code for the heterogeneous chemistry. LS Neal provided code/advise on model emissions files. LA Lee provided knowledge on statistical methods. SS Dhomse and NAD Richards gave advice on satellite observations.

In Chapter 5, the work comparing OMI column NO$_2$ with the LWTs has been published in Atmospheric Science Letters. The reference is **Pope, R.J., N.H. Savage, M.P. Chipperfield, S.R. Arnold and T.J. Osborn, The influence of synoptic weather regimes on UK air quality: Analysis of satellite column NO$_2$,** $Atmos.Sci.Letts$**., doi:10.1002/asl2.492, 2014**. MP Chipperfield and NH Savage supervised the student. SR Arnold provided insight into tropospheric chemistry and TJ Osborn advised the student on the LWTs.

This copy has been supplied on the understanding that it is copyright material and that no quotation from the thesis may be published without proper acknowledgement.

The right of Richard James Pope to be identified as Author of this work has been asserted by him in accordance with the Copyright, Designs and Patents Act 1988.

©2014 The University of Leeds and Richard James Pope

Acknowledgements

I firstly would like to express my thanks to my academic supervisors Martyn Chipperfield and Nick Savage. Their advice, patience and help have been invaluable in my completion of this PhD thesis. Martyn has always been there to discuss results, ideas and give advice guiding me through the thesis. Nick has provided great input teaching me how to run the model and helping debug any issues in the model code and setup. I would also like to thank Lucy Neal, Carlos Ordóñez and Paul Agnew in the Air Quality Group at the Met Office. They have provided useful code, advice and model data throughout my PhD. Special thanks to Carlos for writing the aerosol surface area code, which I know was a big job with lots of coding issues involved.

I would like to thank NERC's National Centre for Earth Observation (NCEO) who provided the funding for this PhD and the Met Office who provided the CASE Award.

Several members of the School of Earth and Environment have been a massive help as well throughout the PhD. Sandip Dhomse and Nigel Richards have provided helpful advice on satellite observations of atmospheric trace gases. Richard Rigby, in IT support, and Cara Healy, Reception, have been a great help as well with computing and administrative issues. A big thanks to all the people in the Office who have put up with me for 3 years including, Tamsin Farmer, Miroslav Provod, Sarah Dennis, Becky Jansen, Nsikanabasi Umo and Lindsay Lee.

My friends also deserve a mention: Bev O'kane, Abi Marshall, Adam Davison, Adam Burwell, Maria Perez, Chris Webb and many more. My parents, Nigel and Ruth Pope, and sister, Lucy Pope, have been vital to me, not only in this PhD, but throughout my life with unconditional support of every form. Thank you!! A massive acknowledgement goes to my parents' daft cocker spaniel dog Weasley!! She is always excited to see me and up for a play fight with the stuffed teddy. Best dog ever!!!! Finally, a special thanks goes to my awesome girlfriend Laura Tymon who has been there for me throughout my PhD.

Abstract

Poor UK air quality has important social and economic impacts with $\sim$29,000 premature deaths and costs to society of $\sim$£20 billion, annually. It is important to understand the controlling factors and be able to forecast it. Therefore, the operational UK Met Office Air Quality in the Unified Model (AQUM), a short-range forecast model of atmospheric chemistry and aerosols, has been designed to predict hazardous air quality events. This study presents the first evaluation of AQUM using satellite observations of trace gases. These satellite observations, in comparison with AQUM, have also been used to investigate the influence of synoptic weather on UK air quality.

Satellite data are prone to large random, systematic and smoothing errors. An algorithm has been developed to calculate and reduce the random error component of time-averaged Differential Optical Absorption Spectroscopy (DOAS) NO_2 retrievals. It reduces the time-averaged tropospheric NO_2 errors by 30-70% through the cancellation of random errors, which allows for a more critical evaluation of regional models.

Comparisons with the processed observations of tropospheric column NO_2 for 2006 show that AQUM overestimates column NO_2 over northern England and Scotland in summer and across the domain in winter. Sensitivity experiments suggest that the model's treatment of NO_x point source (power station) emissions and missing N_2O_5 heterogeneous chemistry are the cause of these column NO_2 overestimations.

Satellite column NO_2 composited under daily classifications of UK synoptic weather indicate that unstable (stable) cyclonic (anticyclonic) conditions lead to column NO_2 transport (accumulation) away from (over) UK source regions. Wind direction influences column NO_2 as source region leeward transport can be detected from space. AQUM, composited using the same methodology, successfully captures these air quality - synoptic weather relationships, giving confidence in its ability to forecast air pollution under different synoptic conditions.

Contents

List of Figures

List of Tables

Abbreviations

AK	**A**veraging **K**ernel
AMF	**A**ir **M**ass **F**actor
AOD	**A**erosol **O**ptical **D**epth
AQ	**A**ir **Q**uality
AQUM	**A**ir **Q**uality in the **U**nified **M**odel
AURN	**A**utomated **U**rban and **R**ural **N**etwork
DAQI	**D**aily **A**ir **Q**uality **I**ndex
DEFRA	**D**epartment for **E**nvironment, **F**ood and **R**ural **A**ffairs
DOAS	**D**ifferential **O**ptical **A**bsorption **S**pectroscopy
ECMWF	**E**uropean **C**entre for **M**edium **R**ange **W**eather **F**orecasts
EMEP	**E**uropean **M**onitoring and **E**valuation **P**rogramme
FGE	**F**ractional **G**ross **E**rror
GEMS	**G**lobal and regional **E**arth-system **M**onitoring using **S**atellite and in-situ data
GOME	**G**lobal **O**zone **M**onitoring **E**xperiment
LWT	**L**amb **W**eather **T**ype
MACC	**M**onitoring **A**tmospheric **C**omposition and **C**limate
MB	**M**ean **B**ias
MLS	**M**icrowave **L**imb **S**ounder
MNMB	**M**odified **N**ormalised **M**ean **B**ias
MODIS	**M**oderate **R**esolution **I**maging **S**pectroradiometer
NAEI	**N**ational **A**tmospheric **E**missions **I**nventory
NWP	**N**umerical **W**eather **P**rediction
OMI	**O**zone **M** onitoring **I**nstrument
PM	**P**articulate **M**atter
PWC	**P**ast **W**eather **C**ode
RMSE	**R**oot **M**ean **S**quare **E**rror
SCIAMACHY	**SC**anning **I**maging **A**bsorption **S**pectro**M**eter for **A**tmospheric **CH**artograph**Y**
TES	**T**ropospheric **E**mission **S**pectrometer
VOC	**V**olitile **O**rganic **C**ompound
WHO	**W**orld **H**ealth **O**rganisation
WMO	**W**orld **M**eteorological **O**rganisation
WRT	**W**ilcoxon **R**ank **T**est

Chapter 1

Introduction

1.1 Motivation

The World Health Organisation (WHO) states that the major air pollutants are O_3, Particulate Matter ($PM_{2.5\&10}$), NO_2 and SO_2. They impose safe health concentration limits of 100 $\mu g/m^3$ 8-hour mean, 25 and 50 $\mu g/m^3$ daily mean, 200 $\mu g/m^3$ hourly mean and 20 $\mu g/m^3$ daily mean, respectively (WHO, 2014). These pollutants can trigger health effects such as lung disease and cancer, cardiovascular problems and asthma.

In the UK, air pollution has a major impact socially and economically. The Committee on Medical Effects of Air Pollution (CMEAP, 1998) stated that poor air quality conservatively results in approximately 12,000-14,000 premature deaths in the UK per year. The House of Commons Environmental Audit Report (HCEA): Air Quality: Vol 1 (2009-2010) suggests that the number of premature deaths due to poor air quality is approximately 50,000 per year (HoC, 2010). More recently though, Public Health England (PHE, 2014) suggests it is closer to approximately 29,000 premature deaths per year. Poor air quality also results in an average decrease of 7-8 months in life expectancy (HoC, 2010) (also quoted by DEFRA (2011a)). The HoC (2010) highlights the effect of extreme events such as the heatwave in 2003 where high concentrations of ozone and particulate matter, in August, resulted in an extra 207 and 225-593 premature deaths, respectively.

In 2005, UK air pollution cost the UK economy approximately £8.5-20.2 billion, whereas The Air Quality Resource Centre (DEFRA, 2011a) advises that it is approximately £10.7 billion per annum. Between 2007-2008, asthma related hospital admissions (74,000) cost society £2.3 billion (HoC, 2010). The economic cost of air pollution also extends to crops where urban air pollution is transported to rural regions. For example, Hollaway et al. (2012) shows that ozone concentrations of over 20-40 ppbv can result in significant yield losses.

UK air quality issues are also influenced by European Union legislation. In 2008, the EU, in an attempt to improve European air quality, introduced the Ambient Air Quality Directive (DEFRA, 2011b), which sets legally binding limits on concentrations
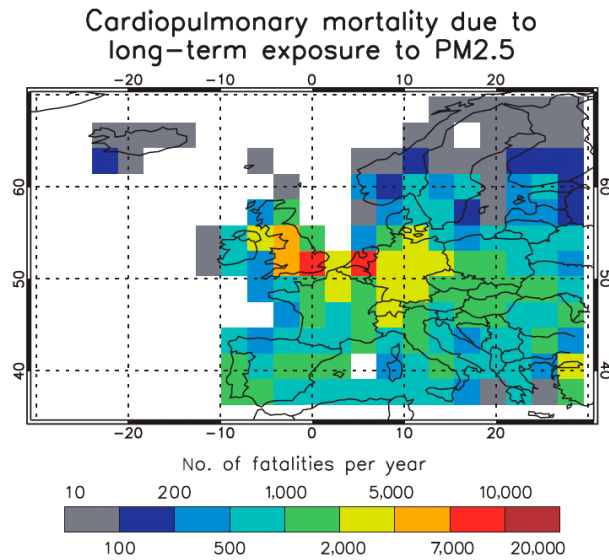
Figure 1.1: Number of excess cardiopulmonary fatalities in the year following the onset of a Laki-style eruption due to long-term exposure to $PM_{2.5}$ (shown as a mean of the 2003 and 2005 simulations (Schmidt et al., 2011)).

in outdoor air for major air pollutants. This legislation was introduced to the UK in 2010 as the Air Quality Standards Regulations. For the emission of air pollutants (from e.g. power stations), legislation set by the UNECE Gothenburg Protocol determined the national emission limits on species like SO_2, NO_x and nitric acid. Similar limits have been set in the past in EU law such as the 2001 National Emission Ceilings Directive, which was introduced into the UK in 2002 under the National Emissions Ceilings Regulations (DEFRA, 2011b). The UK is divided into 43 zones for assessing the compliance with EU air quality limits. So far the UK meets most of these limits for air pollution, but in London urban centres these limits are exceeded. Therefore, the UK has to submit a report to the EU commission explaining why these targets were not met and what the plans are to address the issues. As of 2014, the EU has started legal proceedings against the UK for not meeting NO_2 pollution targets with annual fines of £300 millions (BBC, 2014)(Guardian, 2014). Therefore, fully understanding the processes controlling air pollution and its impact on the UK are vitally important.

In the UK, the Department of Environment, Food and Rural Affairs (DEFRA) uses the Daily Air Quality index (DAQI) to categorise air pollution levels using a scale of 1-10 (DEFRA, 2013) with additional descriptors of low, moderate, high and very high. The Automated Urban and Rural Network (AURN), funded by DEFRA (DEFRA, 2012), provides real time measurements of UK air pollution at multiple urban and rural sites. These two combined give the general public warning of dangerous air pollution episodes.

An example of using models to investigate the risks of air quality is provided by Schmidt
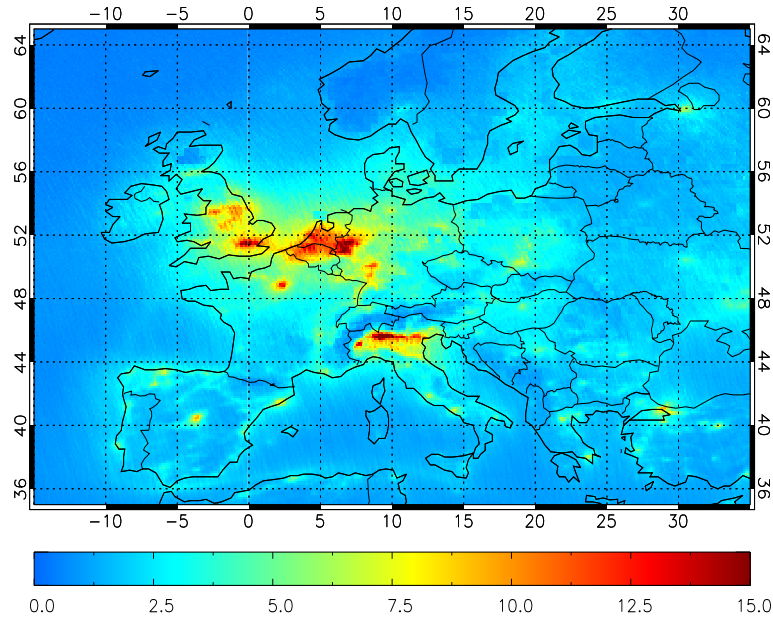
Figure 1.2: European tropospheric column NO_2 measured from space ($\times 10^{15}$ molecules/cm^2, 2005-2013 average).

et al. (2011). They used GLOMAP (Global Model of Aerosol Processes) to look at the potential scenario of a future Laki-style Icelandic eruption. The Laki Icelandic eruption occurred in 1783-84, and records at the time suggest it had a significant impart on human health. Therefore, the eruption was simulated using the meteorology in 2003 and 2005 (years of predominantly northwesterlies so pollution from the eruption transported into Europe) to investigate the effect of a low probability event of this nature on air quality. They suggest that the poor air quality would result in approximately 142,000 deaths across Europe. Figure 1.1 highlights the potential impacts of such an eruption.

Satellites over the past few decades have provided us with space-borne observations of air pollutants (e.g. NO_2, O_3 and aerosol optical depth). Figure 1.2 shows the 9-year (2005-2013) tropospheric column NO_2 average from the Ozone Monitoring Instrument (OMI) aboard the NASA AURA satellite, illustrating how air pollution can now be observed from space. The air pollution hot spots are over the UK, Benelux region and the Po Valley. The peak concentrations are over 15×10^{15} molecules/cm^2 and are a good proxy for elevated air pollution.

1.2   Aim of Thesis

The Met Office operational Air Quality in the Unified Model (AQUM) is a short-term forecast model of atmospheric chemistry and aerosols up to 5 days. The forecasts from AQUM are binned into air quality warnings, such as Low, Medium, High and Very High, for the general public and are based on the UK Daily Air Quality Index (DAQI). The

AQUM has only been validated against surface observations, i.e. point measurements, of air quality from the UK AURN, maintained by DERFA, which is sparse spatially. Therefore, this project uses satellite observations of air pollutants (e.g. NO_2, O_3) to evaluate the performance of AQUM and better understand regional air quality as satellite observations have better spatial coverage. The pixel size (km^2) of satellite instruments also gives a fairer comparison with the AQUM grid box area (km^2).

The project also investigates the influence of synoptic weather on air quality by using circulation indices to composite observations of atmospheric chemistry, both satellite and surface, into different weather regimes. AQUM is then used to reproduce the relationships found in the observations and investigates how important atmospheric chemistry, meteorology and emissions are in governing them.

This thesis has three results chapters with the following scientific questions and objectives:

- Can satellite observations of atmospheric trace gases (e.g. O_3, NO_2) be used for evaluating limited area air quality models? How does the AQUM perform against satellite observations of tropospheric NO_2?

- Are there statistically significant relationships between synoptic weather and observations of atmospheric chemistry (air quality)?

- In the evolution of UK air quality events, does synoptic weather, atmospheric chemistry or emissions have a more significant controlling influence?

1.3 Thesis Layout

This thesis consists of 6 further chapters. Chapter 2 discusses the background of tropospheric chemistry, methods of quantifying UK air quality and previous literature on global/regional air quality model - satellite comparisons. Chapter 3 describes the model configuration and a short case study of initial comparisons between AQUM and satellite observations for multiple chemical species. Chapter 4 presents the evaluation of AQUM against satellite measurements of column NO_2. This covers the assessment of retrieval error budgets, sensitivity of the model to perturbed boundary conditions and emissions and introduction of N_2O_5 heterogeneous chemistry. Chapter 5 shows the relationships between synoptic weather and precipitation types on UK air quality. Chapter 6 uses the model to reproduce the synoptic weather - satellite column NO_2 results and uses passive tracer experiments to assess the atmospheric dynamic and chemical control on such relationships. Chapter 7 presents our conclusions.

Chapter 2

Background

2.1 Introduction

This chapter provides a background to atmospheric chemistry, discusses literature on model-satellite comparisons of air quality pollutants and summarises measures to quantify levels of pollution. Section 2.2 introduces the Earth's atmosphere and standard tropospheric chemistry. Section 2.3 presents previous studies using satellite observations to evaluate atmospheric chemistry models. A description of the previous AQUM validation study is in Section 2.4. Section 2.5 describes the DAQI, which is a measure to quantify poor air quality.

2.2 Earth's Atmosphere

2.2.1 The Structure and Dynamics of Earth's Atmosphere

The Earth's atmosphere is a mixture of different gases, which surrounds the planet. The majority of the atmosphere is made up of nitrogen (78%), oxygen (21%), argon and water vapour (<1% each). All other gases exist in trace amounts in the atmosphere. In total, the Earth's atmosphere weights about 5×10^{18} kg (Wayne, 2000). The atmosphere is divided into four layers (approximately 100km from the surface to the edge of space); the troposphere, stratosphere, mesosphere and thermosphere. The atmospheric pressure and temperature profiles are shown in Figure 2.1. Pressure decreases exponentially with height from approximately 10^5 Pa at the surface and is heavily dependent on gravity and temperature. The Earth's temperature varies across the atmospheric layers. In the troposphere, between 0-18 km, temperature is approximately 288 K at the surface reducing to approximately 225 K at the tropopause. In the stratosphere, which is highly stratified, temperature increases again to about 270 K at 50 km (Wayne, 2000). Ozone in the stratosphere also absorbs incoming UV radiation, which warms that part of the atmosphere, creating the temperature inversion. This temperature inversion starts at the tropopause where the stratosphere is dynamically stable (dry air) with negligible convection.
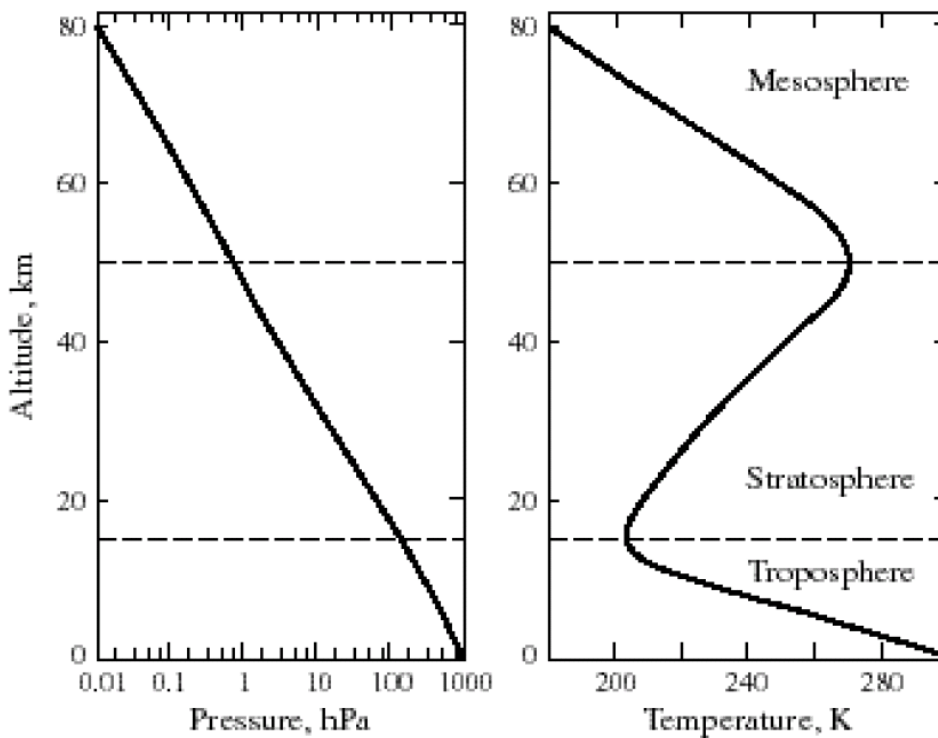
Figure 2.1: Typical pressure (left panel) and temperature (right panel) vertical profiles in the atmosphere at 30° N for March. From from Jacob (1999).

The UK meteorology is very variable because of its geographical location in North-West Europe (i.e. located between the Atlantic and continental Europe) and the different air mass types (e.g. Tropical Maritime, Polar Maritime, Tropical Continental and Polar Continental) it is exposed too. The mixing of different air masses over/around the UK can lead to atmospheric instabilities. Following the Norwegian model (Figure 2.2), the barrier between the tropical maritime/continental and polar air masses (polar front) produces frequent atmospheric depressions. As a result, these frontal systems or mid-latitude depressions subject the UK to advecting warm and cold air masses and along the fronts (barrier between cold and warm air) precipitation often occurs. In periods of intense surface heating, convective systems will occur where moist air masses can ascend, cool and precipitate out in the form of short showers or intensive downpours from cumulus type clouds. Stratus clouds are normally associated with more stable frontal systems (e.g. a warm front catching a cold front and producing drizzle).

As well as mid-latitude depressions, the UK can experience high pressure systems known as "blocking". This results in prolonged periods of stable weather with reduced cloud cover and weaker winds. Strong blocking events in summer can result in significantly increased temperatures and cause mild/extreme drought conditions. In winter, blocking events have the opposite effects. The stable weather can result in below freezing tempera-

tures (often clear skies and the escape of long wave radiation) leading to frosty, foggy and sometimes snowy conditions.
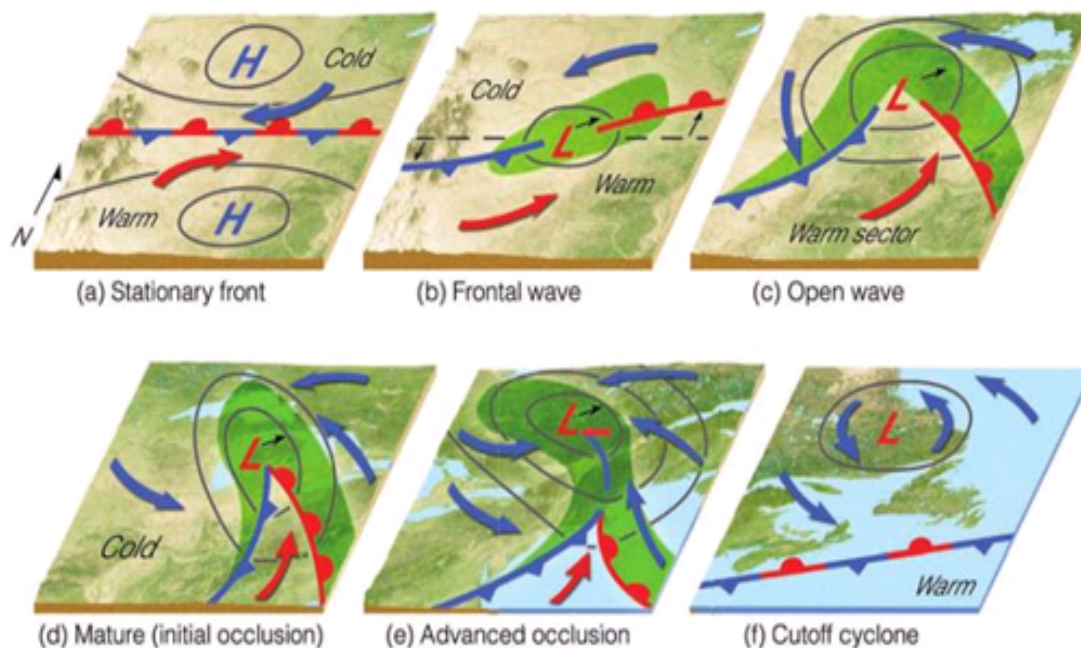
Figure 2.2: Development of mid-latitude depressions. Taken from Ahrens (2009).

These meteorological processes are important in governing the spatial distribution of air pollution from both anthropogenic and natural sources. Under unstable weather, increased advection can transport pollution away from source regions. Stable weather, e.g. summer anticyclonic conditions, can trap air pollutants over populated areas which also react to form secondary pollutants, e.g. NO_x and volatile organic compounds (VOCs) leading to ozone formation. Transport from polluted regions like continental Europe can influence UK air quality as pollution is advected to the UK from easterly winds.

2.2.2 Tropospheric Chemistry and Aerosols

This section discusses the important atmospheric chemistry related to air quality and is based on Wayne (2000), Wallace and Hobbs (2006) and Seinfeld and Pandis (2006). For more information the reader is referred to these publications.

2.2.2.1 Emission, Transport and Loss Processes

Atmospheric pollutants have sources and sinks and a range of lifetimes. Pollutants can be described as either primary or secondary. Primary pollutants are produced directly from sources (e.g. combustion), whereas secondary pollutants are formed after chemical reactions of the primary pollutants. For example SO_2, a primary pollutant, is oxidised by

Table 2.1: Volume mixing ratios and tropospheric lifetimes of key trace species. Volume mixing ratios are reported for clean and polluted tropospheric regions. Taken from the thesis of Hollaway (2012).

Species	Volume Mixing Ratio (ppbv)		Life Time
	Clean Troposphere	Polluted Troposphere	
Ozone (O_3)	10-100	10-350	≈ 22 days[a]
Nitric Oxide (NO)	0.005-0.1	0.05-300	≈ 1 days[b]
Nitrogen Dioxide (NO_2)	0.01-0.3	0.2-200	≈ 1 days[b]
Carbon Monoxide (CO)	40-200	2000-10,000	≈ 2 months[c]
Methane (CH_4)	1800	1800-2500	7.3-10.3 years[d]
PAN ($CH_3.O_2NO_2$)	0.002-0.1	10-35	1 hour - 5 months[e]

[a] Mean lifetime from 25 model simulations (Stevenson et al., 2006) [b] Mean lifetime of NO_x (Jacob, 1999)

[c] Mean lifetime for oxidation by OH (Jacob, 1999) [d] Mean lifetime oxidation by OH (Lawrence et al., 2001)

[e] Mean lifetime varies with temperature between 1h at 298 K and $\approx$ 5m at 250 K (Singh, 1967)

OH to form sulphuric acid, a secondary pollutant (Wayne, 2000). Sources and emissions of pollutants are defined as the processes that led to their formation, typically though chemical reactions, or emission into the atmospheric system (e.g. CO_2 from the biosphere), respectively. Sinks are defined as the loss of a species from the atmospheric system, such as dry/wet deposition, photolysis or chemical reactions (e.g. with the hydroxyl radical OH). The life/residence time of any species is defined by the mean concentration in the system divided by the loss rate (i.e. flow time through the system (Wayne, 2000)). As the system tends to steady state conditions, i.e. production = loss, the residency time becomes constant. For example, CH_4 has a residence time of approximately 9 years. As stated in Chapter 1, key air pollutants include O_3, NO_2, NO and CO. Table 2.1 from the thesis of Hollaway (2012) shows the quantity and lifetime of these species.

2.2.2.2 Tropospheric and Stratospheric Ozone (O_3)

Ozone in the stratosphere absorbs incoming short-wave solar radiation, which can be harmful to the biosphere. However, in the troposphere, ozone is an air pollutant and can have adverse effects on human health and vegetation. Production of ozone in the stratosphere is a significant source of troposphere ozone, through dynamical stratospheric-tropospheric exchanges. However, this source of ozone cannot alone account for elevated ozone levels seen in polluted regions. Stratospheric ozone is produced by photolysis of oxygen, where higher energy photons ($\lambda < 242$ nm) are able to break the O_2 bond:

$$O_2 + h\nu \ (\lambda < 242nm) \rightarrow 2O \qquad [R1]$$

The molecular oxygen then reacts with O_2 to form ozone.

$$O + O_2 + M \rightarrow O_3 + M \qquad [R2]$$
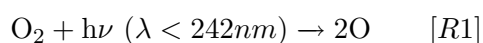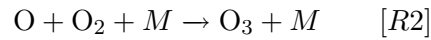
$R2$ can also be a source of ozone in the troposphere where O_2 reacts with O to form O_3. The molecular oxygen can come from several pathways, but the destruction of ozone through photolysis at wavelengths greater than 320 nm is one example ($R3$).

$$O_3 + h\nu \ (\lambda > 320nm) \rightarrow O_2 + O \qquad [R3]$$
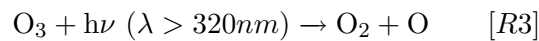
The production and loss of O_3 from $R2$ and $R3$ represent a null cycle (i.e. no net production or loss) on their own. Therefore, the reaction of the O_3 cycle with with NO_x ($NO + NO_2$) and VOCs will lead to the net production or loss of O_3.

2.2.2.3 Nitric Oxide and Nitrogen Dioxide (NO_x)

Anthropogenic processes are a strong source of NO_x, e.g. combustion and power generation, and are a cause of poor air quality. Natural sources of NO_x include soil emissions and lightning. Sinks of NO_x include oxidation, photolysis and dry and wet deposition.

In a set of cyclical reactions, NO_x can lead to the production and loss of O_3. From $R4$, nitric oxide reacts with ozone (sink) to produce nitrogen dioxide and oxygen. The nitrogen dioxide is then photolysed at wave lengths greater than 424 nm to form NO and molecular oxygen. This molecular oxygen then reacts with O_2 to form ozone again (source).

$$NO + O_3 \rightarrow NO_2 + O_2 \qquad [R4]$$

$$NO_2 + h\nu \ (\lambda < 424nm) \rightarrow NO + O \qquad [R5]$$

$$O_2 + O + M \rightarrow O_3 + M \qquad [R6]$$
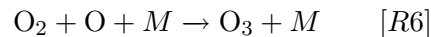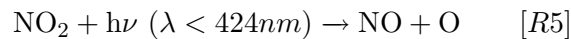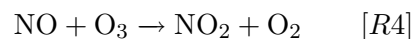
$R4$-$R6$ on their own represent a null cycle where there is no net production or loss of ozone or NO_x; $d[NO_x]/dt=d[O_3]/dt=0$. The photochemical steady state between NO_x and O_3 can be expressed by the Leighton Relationship. From $R4$ the loss of NO can be expressed as $d[NO]/dt=-k_4[NO][O_3]$ and the production can be expressed as $d[NO]/dt = j_5[NO_2]$. This gives the overall NO reaction rate of $d[NO]/dt=j_5[NO_2]-k_4[NO][O_3]$. Now if the system is in steady state then $d[NO]/dt=d[O_3]/dt=0$ and the Leighton Relationship is $j_5[NO_2]=k_4[O_3][NO]$ and can be rearranged to get $[O_3]=(j_5/k_4)[NO_2]/[NO]$. j_5 and k_4 are the photolysis rate and rate coefficient of $R5$ and $R4$, respectively. The reaction of NO with OH ($R9$) or VOCs increases the concentration of O_3 as more NO_2 is produced to be photolysed and form O_3 ($R5$ and $R6$).

2.2.2.4 Hydroxyl Radical (OH)

The hydroxyl radical, OH, is extremely reactive with an atmospheric lifetime of less than a second. The dominant sink of the OH radical is its oxidation of other tropospheric trace gases. For this reason, the OH radical has been named the cleansing agent of the troposphere. However, multiple reactions result in the production of OH. For instance, the reaction of an excited oxygen atom $O(^1D)$ with either water or methane. When radiation is less than 320 nm ozone can be photolysed to form the exited oxygen atom.

$$O_3 + h\nu \ (\lambda < 320nm) \rightarrow O(^1D) + O_2 \qquad [R7]$$

$$O(^1D) + H_2O \rightarrow +2OH \qquad [R8]$$
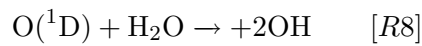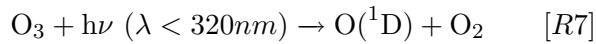
The photodissociation of O_3 results in the production of molecular oxygen and an excited oxygen atom. This atom then reacts with water to form the OH radical. The reaction between NO and the hydroperoxyl radical (HO_2) also results in OH production. Here, NO can also be oxidised by HO_2 to form NO_2 and OH:

$$NO + HO_2 \rightarrow NO_2 + OH \qquad [R9]$$

This production of NO_2 will lead to a net production of O_3.

2.2.2.5 NO_x Sinks

An example of NO_2 loss is through reaction with OH to form nitric acid:

$$NO_2 + OH + M \rightarrow HNO_3 + M \qquad [R10]$$

OH is the dominant cleansing agent during the day, but at night, when photolytic processes cease, the nitrate radical (NO_3) becomes the dominant oxidant. Even though NO_3 is much less reactive than OH, the night time concentrations are sufficient to be a significant oxidant. The nitrate radical is produced through the reaction of NO_2 with O_3:

$$NO_2 + O_3 \rightarrow NO_3 + O_2 \qquad [R11]$$
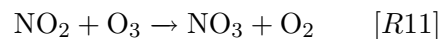
However, during the day it is rapidly destroyed by photolysis:

$$NO_3 + h\nu \rightarrow NO + O_2 \qquad [R12]$$

$$NO_3 + h\nu \rightarrow NO_2 + O \qquad [R13]$$
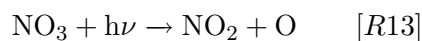
NO_3 can react with NO_2 to form N_2O_5, another NO_y product (all oxides of nitrogen), which is reversible (in thermal equilibrium).

$$NO_3 + NO_2 \rightleftharpoons N_2O_5 \qquad [R14]$$
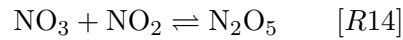
N_2O_5 is then lost on aerosol through the heterogeneous reaction:

$$N_2O_5 + H_2O_l \xrightarrow{aerosol} 2HNO_{3(aq)} \qquad [R15]$$
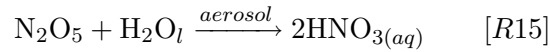
This is therefore a sink of NO_x.

2.2.2.6   Carbon Monoxide (CO)

Carbon monoxide is emitted from both natural and anthropogenic (e.g. incomplete combustion) sources. The oxidation and loss of CO is also part of a cyclic system which produces ozone, through the production of HO_2. Firstly, CO is oxidised by OH resulting in CO_2 and H, where H reacts with O_2 to form HO_2:

$$CO + OH \rightarrow CO_2 + H \qquad [R16]$$

$$H + O_2 + M \rightarrow HO_2 + M \qquad [R17]$$
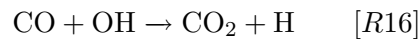
CO, however, can be produced by the oxidation of methane as seen below.

2.2.2.7   Methane (CH_4)

The loss and oxidation (OH) of methane can result in the production of formaldehyde (HCHO), CO and re-balance the loss of the OH radical:

$$CH_4 + OH \rightarrow CH_3 + H_2O \qquad [R18]$$

The CH_3 molecule then reacts with $2O_2$ and NO to form HCHO and HO_2:

$$CH_3 + O_2 + M \rightarrow CH_3O_2 + M \qquad [R19]$$

$$CH_3O_2 + NO \rightarrow CH_3O + NO_2 \qquad [R20]$$

$$CH_3O + O_2 \rightarrow HCHO + HO_2 \qquad [R21]$$

The CH_3O_2 molecule can also react with the HO_2 (not shown). $R20$ is important as the reaction of CH_3O_2 with NO produces NO_2, which can also lead to the net production of O_3.

2.2.2.8 Formaldehyde (HCHO)

For the HCHO molecule, both photolysis and oxidation result in CO production:

$$HCHO + h\nu \rightarrow HO_2 + CO \qquad [R22]$$

$$HCHO + OH \rightarrow HCO + H_2O \qquad [R23]$$

$$HCO + O_2 \rightarrow HO_2 + CO \qquad [R24]$$
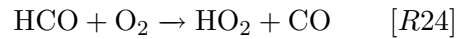
Both anthropogenic and natural (e.g. C_5H_8) VOCs can form HCHO, which when oxidised or photolysed can produce HO_2. This can then go on to react with NO to form O_3.

2.2.2.9 Tropospheric Ozone Production
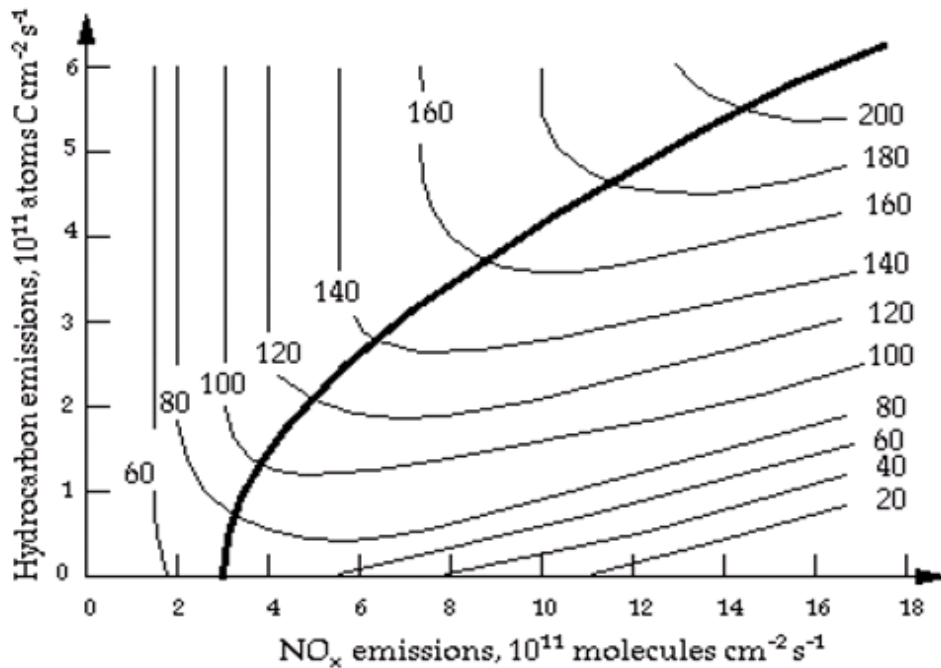
Figure 2.3: Ozone concentrations (ppbv) as a function of NO_x and hydrocarbon emissions. Taken from Jacob (1999).

As stated above, ozone can be produced and lost through the NO_x cycle. However, when NO_x is present in the troposphere, the presence of CO, CH_4 and VOCs when oxidised by OH can result in net ozone production. VOCs have similar oxidation pathways as CH_4, but with higher order hydrocarbons. A hydrocarbon (RH) is oxidised by OH to form the alkyl (R) radical and H_2O. This R radical can then react with oxygen to form RO_2, which in turn reacts with NO to from NO_2 (similar to $R9$, where $RO_2=HO_2$). In Figure 2.3, the production of O_3 from NO_x and VOCs are not linearly related. The black line represents

the separation between NO_x and VOC limited regions. On the left hand side of this line is the NO_x limited region where NO_x increases result in O_3 increases, independent of VOC emissions. On the right hand side is the VOC limited region where O_3 concentrations are sensitive to changes in both NO_x and VOCs. If both NO_x and VOCs increase then O_3 also increases. If NO_x increases and VOCs stay constant then O_3 will decrease. If VOCs increase and NO_x stay constant, then O_3 increases.

2.2.2.10 Aerosols

Aerosols are solid or liquid particles, made up of two or more molecules, which are suspended in a gas and range in scales of nm to μm in diameter. Aerosols are typically classified by mass or number, where large aerosols have greater mass than smaller aerosols but are much lower in concentration. In the mass classification there are two modes: Accumulation (0.1-2.5 μm in diameter) and Coarse (2.5-50μm in diameter). Within the Accumulation mode there are submodes; Condensation and Droplet modes. Accumulation mode is mainly aerosols from primary emissions; condensation of secondary sulphates, nitrates and organics from the gas-phase. The two overlapping submodes, Condensation and Droplet, represent the growth of the smaller aerosols via coagulation or vapour condensation and the cloud processing of Accumulation-mode particles, respectively. The Coarse mode is produced by mechanical processes like wind or erosion (dust, seasalts, pollen, etc). Classifying aerosols by the number of particles has the two modes; Nucleation (under 10 nm) and Aitken (10-100 nm). The Nucleation mode particles are usually fresh aerosols created in-situ from gas-phase nucleation. Aitken mode particles are primary particles onto which secondary material condenses as they are transported through the atmosphere.

From an air quality perspective, aerosol concentrations can be quantified in two ways; mass concentration (an in situ measurement, usually made at the surface) and Aerosol Optical Depth (AOD) (column). $PM_{2.5}$ and PM_{10} are measurements of the mass concentration of particles with aerodynamic diameters less than 2.5 and 10 μm, respectively. AOD is a measure of atmospheric opaqueness and can represent where there are higher loadings of atmospheric aerosol. Therefore, from satellites, the AOD is an indicator of potentially hazardous air quality events. At the surface, observation sites record concentrations of $PM_{2.5}$ and PM_{10} (μg/m^3) to detect poor air quality.

There are different sources of aerosol from primary and secondary natural and anthropogenic sources. Examples of primary natural aerosols include sea salt and volcanic ash and while secondary sources include biogenic emissions (e.g. the condensation of isoprene from a gas to a liquid). Anthropogenic primary sources typically come from internal combustion engines and fossil fuel burning (e.g. soot (black carbon)). Secondary anthropogenic aerosols include ammonium nitrate and ammonium sulphate.

2.3 Atmospheric Chemistry Models and Satellite Observations

Atmospheric chemistry models have been developed to investigate and predict many important processes and interactions. This includes atmospheric composition, influences on dynamical processes and radiation, interaction between biosphere & health, climate change and changes in natural and anthropogenic emissions.

Typically there are regional and global models, which are classed as either Chemistry-Transport Models (CTM) or Chemistry Climate Models (CCM). Regional models focus on sub-global regions such as Europe or the UK and have much higher resolution temporally and spatially. The chemistry schemes used by the regional models also tend to be more complex than global models. However, regional models require lateral boundary conditions throughout the simulation, whereas global models, once started with the initial conditions, essentially generate their own boundary conditions (i.e. a set grid box can always get information from its neighbour). CCMs, such as AQUM, are known as "on-line" models and simulate both interactive chemistry and weather at each time step. CTMs, like TOMCAT (Monks et al., 2012), are purely chemistry-aerosol models and read in meteorology from external sources (e.g. ECMWF winds for TOMCAT) for transport processes. However, the changes in chemistry do not feed back onto the meteorology through changes in aerosol radiative forcings.

Before satellite data was readily available, validation of tropospheric chemistry models or data assimilation was limited to observations from surface stations, weather balloons, ozonesondes and aircraft campaigns. One of the first satellite instruments, BUV (Backscatter Ultra-Violet Spectrometer), measured ozone data back in the 1970s (Gottwald and Bovernsmann, 2006). Since then, many more missions have resulted in both a good temporal and spatial range of observations from space for multiple species at different altitudes.

Below is a selected collection of relevant case studies comparing atmospheric chemistry models and satellite data. They provide background into the different satellite instruments used and how the data can improve models. They also show how models can be used in tandem with satellite observations for research and not just validation.

Savage et al. (2004) looked at comparisons of tropospheric NO_2 columns between TOMCAT (using POET (Precursors of Ozone and their Effects in the Troposphere) emissions) and the Global Ozone Monitoring Experiment (GOME) on the global scale. Overall, TOMCAT overestimated NO_2 columns from GOME in the polluted regions. To evaluate the data more quantitatively, regional sections were devised and correlation and ordinary least squares regression were used. Looking at the seasonal cycles, TOMCAT and GOME were highly correlated in polluted regions, but the model concentrations were too high

in the summer. Savage et al. (2004) suggested that the emissions datasets do not play a significant role in the TOMCAT-GOME differences and that meteorology is the dominant factor.

Savage et al. (2008) investigated European tropospheric column NO_2 interannual variability (IAV), 1996-2000, by comparing GOME with the TOMCAT. The best comparisons were found in the JFM and AMJ seasons, especially over western Europe. They also found that synoptic meteorology had more influence on NO_2 IAV than NO_x emissions did.

Huijnen et al. (2010) compared OMI tropospheric column NO_2 against a European global-regional air quality model ensemble median for 2008-2009. The ensemble compared better with the OMI data than any one model, with good agreement over the urban hotspots. Overall, the spread in the models was greatest in the summer (with deviations from the mean OMI tropospheric column in the range of 40-62%), due to the more active NO_x chemistry in this season and the differences in chemistry schemes among the contributing models, when compared to winter (20-34%). Several of the regional models successfully detected the shipping lane seen by OMI.

Han et al. (2011) investigated tropospheric column NO_2 over the Korean Peninsula through comparisons between OMI data and the Community Multi-scale Air Quality Model (CMAQ) (Foley et al., 2010). In summer, both observed and simulated, that North and South Korea have similar column NO_2. However, in winter South Korea, a more developed nation with greater infrastructure, had significantly greater NO_2 concentrations than North Korea. Overall, CMAQ overestimated OMI NO_2 concentrations by factors of 1.38-1.87 and 1.55-7.46 over South and North Korea, respectively.

Peters et al. (2002) describe several model-satellite comparison methods and used a Monte-Carlo approach to simulate model natural variability. They used the CTM, TM3, to compare with the NIMBUS-7 tropospheric ozone column satellite record (1979-1992). The model-satellite differences were represented by the correlation, η_1, and absolute deviation (normalised by the standard deviation), η_2, between the two datasets. Then to better understand the errors between TM3 and NIMBUS-7, the model data was perturbed by +/- 10% (Monte-Carlo approach with an ensemble sample size of 100) to represent anomalous winds, convective venting or unexpected emissions of ozone, which could disturb the ozone concentration in a non-systematic way resulting in a spread of η_1 and η_2 values. Overall, they found that the North Atlantic had the greatest absolute deviation (5σ) and that η_1 is higher with a correlation of 0.84 when using real/perturbed annual meteorological conditions than a 14 year climatology in TM3 to simulate column O_3 with a correlation of 0.7.

Peters et al. (2002) also use labelled traces to show that the main sources of the modelled ozone columns are photochemical ozone production from lightning NO_x emissions,

biomass burning, soil NO_2 emissions and the stratospheric flux of ozone. Sensitivity experiments of these model processes, based on η_1 and η_2, showed that biomass burning and lightning emissions of NO_x had a significant impact on column O_3. Therefore, the representation of biomass burning in the model and the parameterisation of lightning needed to be improved.

Paton-Walsh et al. (2010) investigated the estimation of CO emissions from forest fires in Canberra wildfires, 2003, using MODIS (Moderate-Resolution Imaging Spectroradiometer) AOD measurements at 0.55 microns and combined with the Model for Ozone And Related chemical Tracers (MOZART) CTM. MODIS retrievals were interpolated onto a $1° x 1°$ grid in the region of Canberra. To remove background aerosol (e.g. dust, sea spray/salt and old smoke from other fires) the average AOD measured at 0.11 before the fires (8-26th January 2003) was used.

Paton-Walsh et al. (2010) outlined the potential uncertainties in the MODIS retrievals of AOD caused by forest fires. These included smoke plumes mistaken as clouds, clouds misinterpreted as smoke, smoke transported out of the region before the satellite can sample it and smoke double counting. So Paton-Walsh et al. (2010) used MOZART to predict the transport/dispersion of smoke plumes to help avoid the issues above. To calculate the CO concentration, the half-life of CO/aerosols was applied to the CO burden within the model and was corrected for the double counting of smoke from other days. The emission of CO compared well with the GFED2 inventory of the emissions for this period. The greatest uncertainty in the Paton-Walsh et al. (2010) method is the conversion of AOD into trace gas concentrations. However, it has advantages over direct satellite measurements of CO because AOD has better sensitivity in the boundary layer, where the fires/smoke plumes occur.

2.4 AQUM Validation

Savage et al. (2013) performed the first evaluation of AQUM operational forecast for the period May 2010-April 2011 by using surface O_3, NO_2 and particulate matter (PM) observations from AURN. Among other model-observation metrics they used the mean bias (MB), root mean square error (RMSE), modified normalised mean bias (MNMB) and the Fractional Gross Error (FGE) (Seigneur et al., 2000). Savage et al. (2013) found that AQUM overestimated O_3 by 8.38 μg/m^3 (MNMB=0.12), with a positive bias at urban sites but no systematic bias at rural sites. The model-observation correlation was reasonably high at 0.68. For NO_2, there was a bias of -6.10 μg/m^3, correlation of 0.57 and MNMB of -0.26. At urban sites there was a large negative bias while rural sites had marginal positive biases. They argued that the coarse resolution of AQUM (12 km) led to an underestimation at urban sites because the NO_x emissions are instantaneously spread

over the entire grid box. The particulate matter (PM_{10}) prediction skill was lower with a correlation and bias of 0.52 and -9.17 $\mu g/m^3$, respectively.

2.5 Air Quality Index

Figure 2.4: Example Daily Air Quality Index tables for O_3, NO_2 and SO_2. The ten index levels represent four classifications; low, moderate, high and very high forecast warnings (DEFRA, 2013).

Because of the health issues and costs discussed in Chapter 1, the Committee On Medical Effects of Air Pollutants (COMEAP) recommended the adoption of the DAQI to communicate current and predicted pollution levels. This index is based on the concentration of the pollutants O_3, NO_2, SO_2 and $PM_{2.5\&10}$ (DEFRA, 2013). The overall DAQI is formed from the highest index of the different pollutants. Figure 2.4 shows DAQI for O_3, NO_2 and SO_2. There are ten indices for each pollutant representing different ranges of potentially hazardous concentrations. These ten indices are then separated into four warning levels; low, moderate, high and very high. Therefore, as the index increases, the concentrations become more hazardous to human health. The index ranges are set to account for the safe/unsafe concentrations of air pollutants set by the WHO. The index also comes with health advice for both the general public and vulnerable groups. In AQUM forecasts, taking O_3 as an example, the AQUM calculates 8 hour running means and takes the peak surface 8 hour mean value per day. This peak O_3 value is then binned into the DAQI and presented to the general public through the Met Office, DEFRA and BBC websites.

Chapter 3

AQUM configuration, model-satellite comparison methodology and initial results

3.1 Introduction

One aim of the PhD is to investigate whether satellite observations of atmospheric trace gases can be used to monitor UK air quality and to evaluate AQUM. The surface observations currently used to evaluate AQUM, while having good temporal resolution, have limited horizontal coverage and no vertical information. Therefore, evaluating a 3D model using only sparse surface information limits the assessment of its forecasting skill. Satellite observations give good spatial coverage over the model domain and contain vertical information of the species in the atmosphere. However, using these observations poses a challenge as they come with large uncertainties and errors. Therefore, to get good representation over the UK and to reduce the errors, multiple observations need to be averaged together over a certain period. In air quality, monthly averages of atmospheric species are often used. Hence, in this chapter, I use a range of satellite products to evaluate AQUM for a short case study of July 2006 (an extreme heat wave leading to hazardous air quality events) to see to what extent products are suitable for monitoring UK air quality and can be used to evaluate the model.

In July 2006, northern Europe experienced an intense heatwave which Rebetez et al. (2009) associated with persistent anticyclonic conditions favouring the advection of dry air masses. This high pressure system extended from Spain to Denmark during most of the month resulting in an enhanced surface sensible heat flux and a significant reduction in the latent heat flux. In comparison to August 2003 (another significant continental heatwave), Rebetez et al. (2009) found that UK July 2006 temperatures were significantly higher by 6.0-7.0 K (Figure 3.1). Tropospheric ozone has a strong seasonal cycle (Huijnen et al., 2010) which is greater in the summer when photochemistry is more active. As a result,

this has knock-on effects for other atmospheric chemical species such as formaldehyde
(HCHO) and NO_x. Therefore, this period is of interest because of the extreme air quality
event. Therefore, AQUM has been run for July 2006 outputting multiple species.
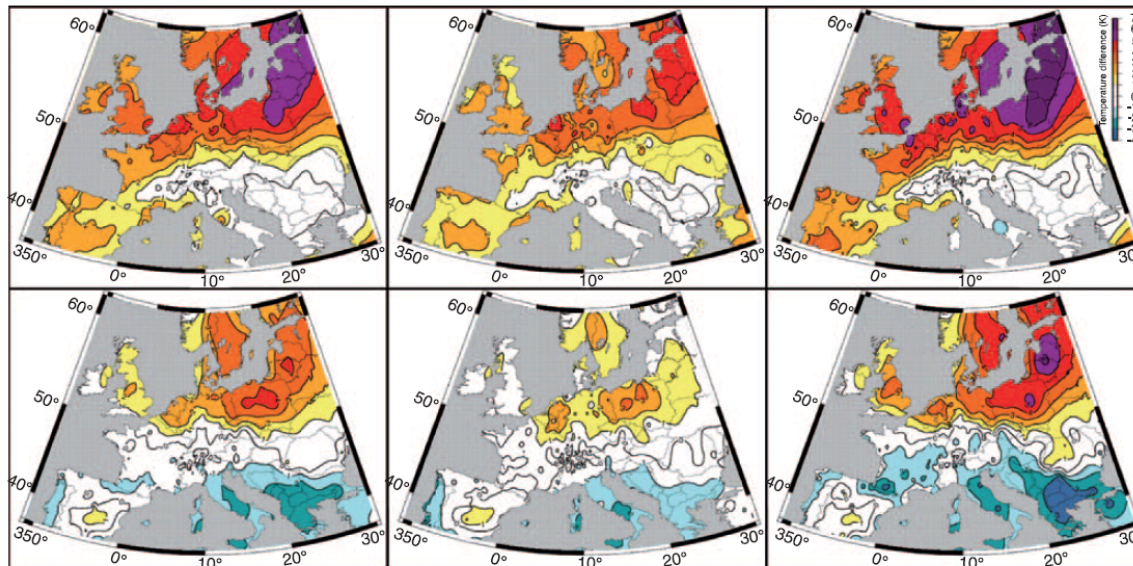
Figure 3.1: Differences between July 2006 and June 2003 (top)/August 2003 (bottom)
average (left), minimum (middle) and maximum (right) surface air temperature (K) (Re-
betez et al., 2009).

Section 3.2 describes AQUM's configuration. Section 3.3 introduces the satellite prod-
ucts used and model-satellite comparison methodologies. The initial comparisons for se-
lected species (NO_2, HCHO and AOD) are presented in Section 3.4. Section 3.5 focuses
on the use of space-borne ozone measurements for validating AQUM. Ozone is considered
in more detail than the other species as it is an important air pollutant, but out of the
many tropospheric ozone products available, few are suitable for AQUM evaluation. As
the majority of atmospheric ozone is in the stratosphere, the sensitivity of satellite instru-
ments to observing tropospheric ozone is reduced. To get accurate spatial composites of
tropospheric ozone, longer periods were needed for averaging. Therefore, we focused on
June-July-August (JJA) for 2006 and 2008. Section 3.6 summarises my results from this
chapter.

3.2   AQUM Configuration

AQUM is a regional model of chemistry and aerosols used for forecasts up to 5 days. It is
the Met Office's operational model for providing public air quality forecasts to both the
BBC and DEFRA. AQUM's domain covers the UK and part of continental Europe on a
rotated-pole co-ordinate system with the North Pole at latitude 37.5° and longitude 177.5°.

The domain ranges between approximately 45°-60° N and 12°W-12°E. It is centred near the equator meaning that the grid spacing is similar in the zonal and meridional directions. Figure 3.2 shows the model domain and an example of a daily maximum surface ozone field on the 27th June 2010. The model configuration used in this study has a horizontal resolution of 0.11° x 0.11° (approximately 12 km x 12 km) with 38 vertical levels and a top boundary at 39 km. Offline air quality models do not require such a high top boundary, but it is necessary for online air quality models in order to accurately represent weather systems (Savage et al., 2013).
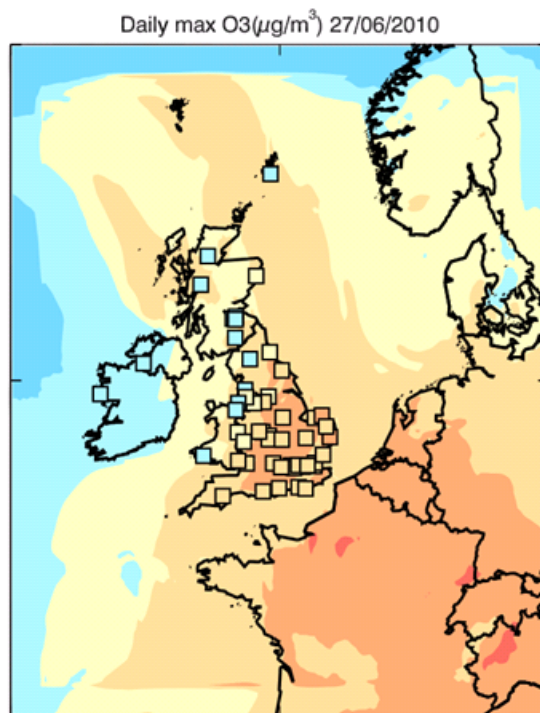
Figure 3.2: AQUM domain showing maximum modelled hourly ozone concentrations (μg/m^3) for 27th June 2010, with observed concentrations over-plotted within squares (taken from Savage et al. (2013)).

3.2.1   Model Dynamics and Physics

AQUM's physics configuration is based on the Met Office's North Atlantic and European Model (NAE) (Bush et al., 2006). The MetUM dynamical core is non-hydrostatic and fully compressible, using semi-implicit and semi-Lagrangian time integration methods. For the advection of aerosol and gases, a positive definite semi-Lagrangian tracer advection scheme is used (Davies et al., 2005). Boundary-layer mixing (including aerosols and gases) is parameterised (Lock et al., 2000). Convection is represented with a mass flux scheme with downdraughts, momentum transport and convective available potential energy closure (Gregory and Rowntree, 1990). The land surface scheme (MOSES II) is based on a nine tile

(including urban tile) flux-blended surface exchange approach (Essery et al., 2003). The model uses the Edwards-Slingo code for long-wave and short-wave radiation (Edwards and Slingo, 1996). The microphysics scheme comes from Wilson and Ballard (1999) with the addition of prognostic ice and snow, rain and graupel. AQUM's cloud scheme (diagnostic) is described by Smith (1990).

3.2.2   Gas Phase Chemistry Scheme

AQUM has a coupled, online tropospheric chemistry scheme using the United Kingdom Chemistry and Aerosols (UKCA) subroutines. The chemistry scheme (Regional Air Quality, RAQ) includes 40 tracers, 23 photolysis reactions and 116 gas-phase reactions (Savage et al., 2013) including the reaction of the nitrate radical with formaldehyde, ethene, ethane, propane, n-butane, acetaldehyde and isoprene. The standard model setup does not include any heterogeneous chemistry. Removal of gas-phase species by wet and dry deposition is considered for 19 and 16 species, respectively. The chemistry is integrated using a backward Euler solver. A complete chemical mechanism is presented in the online supplement to Savage et al. (2013) and included in the Appendix of this thesis.

3.2.3   Aerosol Scheme

To simulate aerosols, AQUM uses the Coupled Large-scale Aerosol Simulator for Studies In Climate (CLASSIC) scheme. This is a bulk scheme with the aerosols treated as an external mixture. It contains six prognostic tropospheric aerosol types: ammonium sulphate, mineral dust, fossil fuel black carbon (FFBC), fossil fuel organic carbon (FFOC), biomass burning aerosols and ammonium nitrate. In addition, there is a diagnostic aerosol scheme for sea salt and a fixed climatology of biogenic secondary organic aerosols (BSOA). For more details of the aerosol scheme see Bellouin et al. (2011). The direct radiative effects of all aerosols are included in the model feeding back onto meteorology. These effects are included using wavelength dependent scattering and absorption coefficients calculated offline according to Mie theory. This includes the effects such as the hygroscopic growth of sulphate, sea salt, nitrate, biomass burning, FFOC and biogenic aerosols. All aerosol species except mineral dust and FFBC are considered to act as cloud condensation nuclei. In common with most regional AQ forecast models in Europe, AQUM shows a small negative bias for $PM_{2.5}$ and a larger negative bias for PM_{10} (Savage et al., 2013).

3.2.4   Initial and Lateral Boundary Conditions

Meteorological initial conditions and lateral boundary conditions (LBCs) come from the Met Office's MetUM operational global model (25 km $\times$ 25 km) data. Initial chemical conditions come from the previous day's AQUM forecast and aerosol and chemistry LBCs come from the ECMWF GEMS (Global and regional Earth-system Monitoring using

Satellite and in-situ data) reanalyses (Hollingsworth et al., 2008). The GEMS fields, available at http://www.gmes-atmosphere.eu/, provide boundary concentrations for regional air quality models such as AQUM.

3.2.5 Emissions

Anthropogenic emissions used in this configuration of AQUM are from three sources. The National Atmospheric Emissions Inventory (NAEI, MacCarthy et al. (2011)) (1 km $\times$ 1 km) are used for the UK, shipping lanes come from ENTEC (Whall et al., 2010) (5 km $\times$ 5 km) and the European Monitoring and Evaluation Programme (EMEP, http://www.ceip.at /webdab-emission-database/emissions-as-used-in-emep-models/) (50 km $\times$ 50 km) are used for the rest of the model domain. The ENTEC shipping emissions are produced by ENTEC Ltd on behalf of DEFRA and represent emissions for waters around the UK (Savage et al., 2013). All of these datasets are then interpolated onto the AQUM grid of 12 km. The key anthropogenic emissions include carbon monoxide, sulphur oxide gases, volatile organic compounds, nitrogen oxides and particulate matter. These emissions are entered into the model at the 4 levels; 20m, 80m, 180m and 320m. The emissions are annual totals; however, monthly, weekly and diurnal cycles are forced onto them for the model runs. The input (ancillary) emissions files already include monthly cycles on the emissions and the weekly (i.e. week vs. weekend) and diurnal (e.g. traffic) cycles are applied in the model itself. These emissions cycles come from TNO (Visschedijk et al., 2007).

Over the UK, the NAEI emissions datasets are made up of two source types: area and point. Area sources include traffic, light industry and urban emissions, while point sources are power stations, landfill, incinerators and refineries. Typically for NO_x emissions, individual point sources are approximately 100 g/s in magnitude, while the area NO_x emissions tend to be 10 g/s. For the sensitivity experiments discussed in Chapter 4, the 2007 NO_x emissions were used instead of 2006 because the ENTEC shipping emissions (5 km $\times$ 5 km resolution) are available for this year, while only the coarse EMEP shipping emissions are available for the earlier years (Savage et al., 2013). I found the difference between the 2006 and 2007 NO_x emissions to be negligible. Therefore, 2007 emissions datasets were used. Lightning emissions of NO_x are based on a parameterisation linked to the model's convection scheme; for details see O'Connor et al. (2014). The model does not have a separate parameterisation for soil NO_x emissions but given the large emissions from transport and industry, the soil NO_x emissions are unlikely to be important in this region.

3.3   AQUM-Satellite Comparison Methodology

Earth observation of atmospheric trace gases for the July 2006 case study came from OMI and Tropospheric Emissions Spectrometer (TES), aboard the NASA EOS-AURA satellite, and MODIS, aboard NASA EOS-AQUA satellite. Both of these satellites are part of the NASA A-Train (Figure 3.3) where AQUA is approximately 10 minutes ahead of AURA. OMI solar radiation backscatter is observed in the ultra-violet (UV-VIS) range from 270-500 nm. It was launched into a sun-synchronous orbit in 2004, crossing the equator at 13:00 local time. OMI observes in the nadir and has a mean footprint resolution of 312 km^2 (Han et al., 2011). TES is an infra-red Fourier transform spectrometer that measures thermal emissions over the spectral range 650-2250 cm^{-1}. It has a nadir-viewing footprint of 45 km^2 (Richards et al., 2008). MODIS provides high radiometric sensitivity in 36 spectral bands ranging from 0.4 μm to 1.4 μm. It is nadir-viewing with a footprint of 23,300 km^2 (Paton-Walsh et al., 2010).
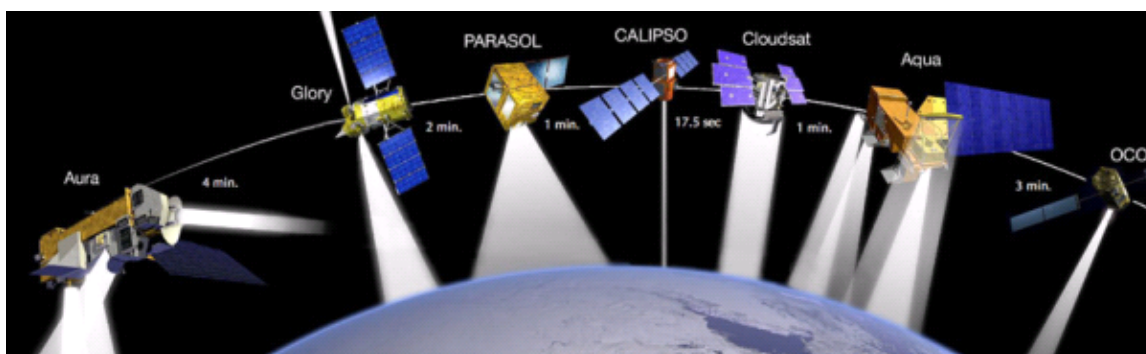
Figure 3.3: The NASA A-Train consists of satellites with various scientific missions. In the figure, AURA is on the left in the train, while AQUA is approximately 10 minutes ahead (NASA, 2012).

The chemical species investigated and their respective instruments include:

- Tropospheric column NO_2 - OMI

- Total column HCHO - OMI

- Total column AOD - OMI and MODIS

- O_3 vertical profiles - TES (discussed in Section 3.5 with other O_3 comparisons)

AQUM data needed to be converted to the quantities in the satellite products. NO_2 data is in the form of tropospheric column swath data (10^{15} molecules/cm^2). HCHO (10^{15} molecules/cm^2), and AOD (dimensionless) were total column gridded data (0.25° x 0.25°). TES O_3 data was vertical profiles in volume mixing ratio (ppbv). Satellite observations have different levels of sensitivity to the measured chemical species throughout

the atmosphere. For instance, the majority of the atmospheric O_3 is in the stratosphere. Hence, satellites tend to have greater sensitivity in this region. Therefore, model profiles and satellite retrieval are not directly comparable. In this case, where possible, to reduce comparison error, the satellite averaging kernels (AK or weighting function in the more simple case) need to be applied to the model data so satellite sensitivity is accounted for in the comparisons (i.e. the model field now looks like what the satellite sees).

Eskes and Boersma (2003) defines the AK to be a relationship between the retrieved quantities and the true distribution of the tracer. In other words, the satellite instrument's capability to retrieve a quantity is a function of altitude. The AK comes in different forms for different retrieval methods. For the Differential Optical Absorption Spectroscopy (DOAS) method, the AK is in the form of a column vector, while in Optimal Estimation, the AK is a matrix, whose dimensions are dependent on the number of pressure levels in the retrieval process. The HCHO and AOD products did not include AKs, while the OMI NO_2 AKs are discussed in Chapter 4. The AKs from TES O_3 are applied to the AQUM and discussed in Section 3.5.

Even though both the HCHO and AOD products were total column data, they are primarily tropospheric atmospheric chemical/aerosol species. Since the vertical extent of the model is limited in the stratosphere, it was reasonable to treat the products as tropospheric column data. As some of the data was in swath form, these datasets had to be interpolated onto a regular grid. HCHO was the first species to be investigated on a $0.25° \times 0.25°$ lat-lon grid, between 20°W-20° E and 43-63° N. Therefore, the model data ($0.1° \times 0.1°$ grid) was interpolated onto the same resolution as the satellite. This resolution has since been the template for further comparisons, excluding the TES data. To that end, the swath datasets (e.g. NO_2) were interpolated onto this resolution.

For the July 2006 TES data, which has a sparse sampling resolution, the closest model vertical profile to each retrieval location was converted into volume mixing ratio and then interpolated onto the satellite pressure grid (67 vertical levels). However, since the model profile had a smaller vertical range, the interpolated data above the top model pressure level was replaced by the satellite apriori. This meant that averaging kernels (AK) were applied to realistic profiles.

To compare to the OMI datasets, the model mass mixing ratios were interpolated onto the satellite pressure grid. Model species subcolumn thickness was then calculated using hydrostatic approximation between the subcolumn barrier pressure levels. These were multiplied by the interpolated mass mixing ratios and converted into molecules/cm^2. The tropospheric column was obtained by totalling all subcolumns up to the satellite tropopause level/information. However, if no such information existed then the model

chemical tropopause (where the O_3 vertical profile reached 100 ppbv) was used.

$$\text{Layer Thickness}: \quad \rho dz = -\frac{dp}{g} = \frac{p_{lower} - p_{upper}}{g} \tag{3.1}$$

where dp = the change in pressure, dz = the change in height, g = gravitational constant and ρ is the density of the air.

$$\text{Species Sub Column} \quad = \quad \text{Mass Mixing Ratio} \quad \times \quad \text{Layer Thickness} \quad (\frac{kg}{m^2}) \tag{3.2}$$

$$\text{Species Sub Column} \quad (\frac{molecules}{cm^2}) = \quad \text{Species Sub Column} \\ \times \frac{10^7 \quad \times \quad \text{Avagadro Constant}}{\text{Species Molecular Mass}} \tag{3.3}$$

For the model-observation comparisons, I used the mean bias, root mean square error, normalised mean bias, normalised root mean square error, modified normalised mean bias and the fractional gross error statistical metrics. For the HCHO, AOD and NO_2 comparisons, since the satellite daytime overpasses is 13:00 LT each day, the timeseries for each grid box contain 0-31 observations for the monthly period, where the model is sampled at the location of good satellite retrievals. Any grid boxes with no satellite data were classed as missing data, where the model is not sampled. These statistical methods were obtained from Han et al. (2011) and Savage et al. (2013). In the model validation statistical metrics, f is the model output, o is the satellite measurements, N is the total number of elements and i is the index.

- Mean Bias (MB):

$$MB = \frac{1}{N} \sum_i (f_i - o_i) \tag{3.4}$$

- Root Mean Square Error (RMSE):

$$RMSE = \sqrt{\frac{1}{N} \sum_i (f_i - o_i)^2} \tag{3.5}$$

- Normalised Mean Bias (NMB):

$$NMB = \frac{1}{N} \sum \frac{(f_i - o_i)}{o_i} \tag{3.6}$$

- Normalised Root Mean Square Error (NRMSE):

$$NRMSE = \sqrt{\frac{1}{N} \sum_i \left(\frac{f_i - o_i}{o_i}\right)^2} \tag{3.7}$$

- Modified Normalised Mean Bias (MMB):

$$MMB = \frac{2}{N} \sum_i \left(\frac{f_i - o_i}{f_i + o_i} \right) \tag{3.8}$$

- Fractional Gross Error (FGE):

$$FGE = \frac{2}{N} \sum_i \left| \frac{f_i - o_i}{f_i + o_i} \right| \tag{3.9}$$

The MB and RMSE can be non-dimensionalised to form the NMB and NRMSE using the observations (i.e. the satellite data), where the magnitude/units of different quantities (e.g. O_3 biases in ppbv or NO_2 biases in $\mu g/m^3$) are removed. The problem with this is that negative biases/errors then become limited between -1 and 0 or 0 and 1, respectively, and positive biases/errors, where the model value is much greater than the observation, can become very large. Therefore, the MNMB and FGE are used because the MB and RMSE are non-dimensionalised by the average of the model and observation values. This limits the biases to values between -2 and 2 and the errors to between 0 and 2, respectively.

The satellite retrievals used here have been filtered by time, cloud fraction and quality assurance flags. Initially, the satellite data were projected onto a spatial map for retrievals around 13:00 LT. However, this led to poor spatial coverage, so multiple time windows were tested to find the balance between spatial coverage and temporal accuracy. These were 12:30-13:30, 12:00-13:00 and 11:00-15:00 LT, where multiple observations in a grid box were averaged together over the time window. In the end, the 11:00-15:00 LT window offered the most appropriate spatial-temporal balance. Retrieved pixels with large cloud coverage result in biased retrievals because the instrument can only partially sample the vertical extent of the species in the atmosphere. Therefore, any retrievals which had geometric cloud fractions over 0.5 were rejected (this was revised to 0.2 for Chapters 4-6). Most of the satellite products also contained quality assurance flags, which indicated if there was a problem with the retrieval (e.g. instrument error, retrieval error, OMI row anomalies). Retrievals were filtered out in such cases. In the case of TES O_3 data, instead of cloud fraction data, the products included cloud optical depth. Richards et al. (2008) investigated the TES-aircraft O_3 biases, in their validation study of TES, as a function of cloud optical depth and found that they had limited dependence on them. Therefore, the TES retrievals are used without filtering for cloudcover.

3.4 AQUM - Satellite Comparisons

3.4.1 Nitrogen Dioxide

The tropospheric column data come from the TEMIS (Tropospheric Emissions Monitoring Internet Service) website, http://www.temis.nl/airpollution/no2.html (Boersma et al.,

2011b), called DOMINO version 2.0. After initial comparisons, the OMI column NO_2 dataset gave the best comparisons with AQUM and representation of air quality from space over the UK. Therefore, analysis of AQUM using OMI column NO_2 is analysed in more detail in Chapter 4 and only the initial comparisons are presented here. In Chapter 4, the errors in the product are discussed, the averaging kernels are applied to AQUM (including methodology) and longer period (i.e. summer and winter of 2006) comparisons are done. In Figure 3.4a, the maximum monthly mean AQUM NO_2 columns (around 12 $\times 10^{15}$ molecules/cm^2) are found over urban areas. Over the rural areas columns range from around 0 to 5 $\times 10^{15}$ molecules/cm^2. For urban areas, AQUM column NO_2 was expected to be highest over London, as seen by OMI at 25 $\times 10^{15}$ molecules/cm^2 (Figure 3.4b). However, the model maximum NO_2 columns occur over north east England peaking at 20-25 $\times 10^{15}$ molecules/cm^2 and are only 12-15 $\times 10^{15}$ molecules/cm^2 over London. OMI column NO_2 over north east England reaches similar values to London, but in less dense clusters. Looking at the peak NO_2 hot spots over Europe, the model underestimates places such as Paris and the Benelux region by 5-10 $\times 10^{15}$ molecules/cm^2 when compared with OMI. Figure 3.4c highlights these differences where there are negative biases over London, Paris and the Benelux region, between -10 to -5 $\times 10^{15}$ molecules/cm^2, and positive biases
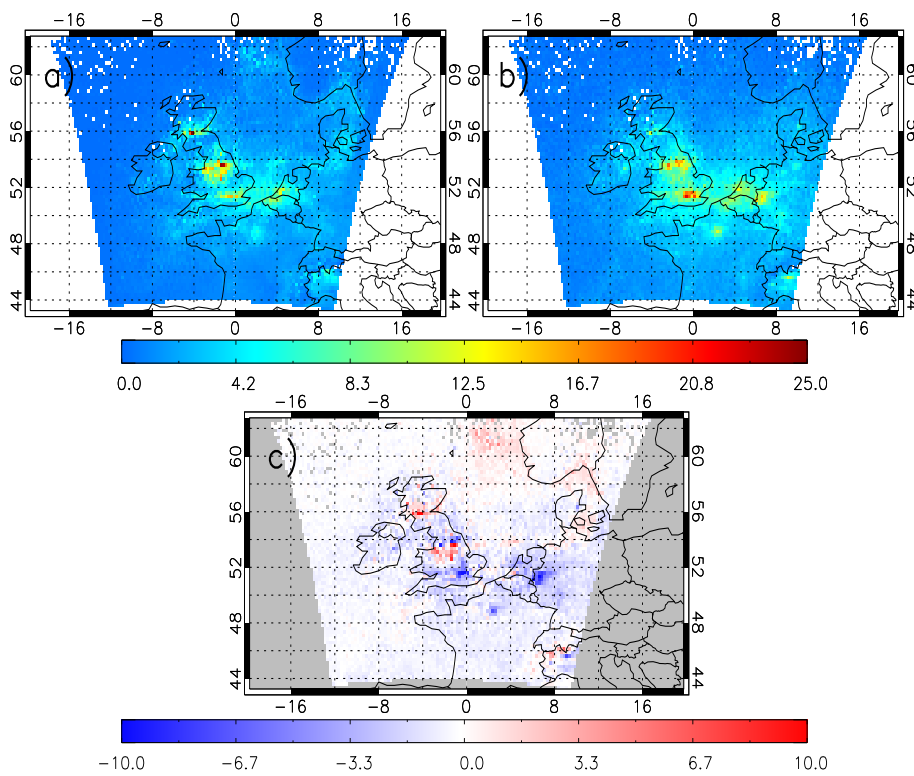
Figure 3.4: July 2006 tropospheric column NO_2 (10^{15} molecules/cm^2): a) AQUM, b) OMI and c) mean bias. White pixels in a) and b) and grey pixels in c) indicate no satellite data.

over north east England and Edinburgh, between 5-10 $\times 10^{15}$ molecules/cm^2.

3.4.2   Formaldehyde
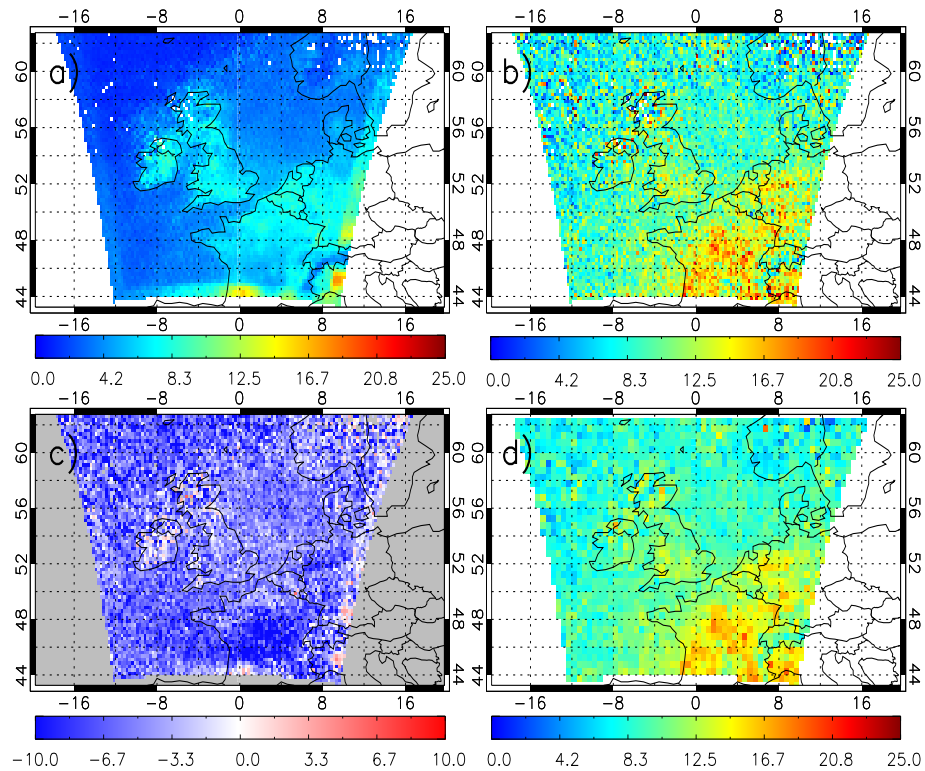
Figure 3.5: July 2006 tropospheric column HCHO (10^{15} molecules/cm^2): a) AQUM, b) OMI and c) mean bias. d) OMI column HCHO on a coarser 0.5° × 0.5° grid.

For simplicity, the total column product is treated as tropospheric as the majority of the atmospheric HCHO column resides there. Cloud filters and quality flags have been applied to the satellite data, but it is still a very noisy product. Overall, both AQUM and OMI show that the maximum/minimum HCHO columns are over the land and sea, respectively. The model generally underestimates OMI (Figure 3.5a and 3.5b) - the model and satellite land maxima reach approximately 18 and 25 $\times 10^{15}$ molecules/cm^2, respectively. Over the ocean the model predicts HCHO concentrations between 0-5 $\times 10^{15}$ molecules/cm^2, while the satellite sees 6-10 $\times 10^{15}$ molecules/cm^2. The AQUM - OMI MB (Figure 3.5c) highlights these differences with the strongest negative biases of under -10 $\times 10^{15}$ molecules/cm^2 over continental Europe. Possible reasons for these strong negative biases are that AQUM underestimates the emission of isoprene (C_5H_8) from biogenic sources (which is a precursor to HCHO over continental Europe), AQUM is missing VOCs in the chemical mechanism, there is excessive loss of HCHO in AQUM or errors in the chemistry scheme. Over the sea AQUM underestimates OMI HCHO columns by between -10 to -5 $\times 10^{15}$ molecules/cm^2.
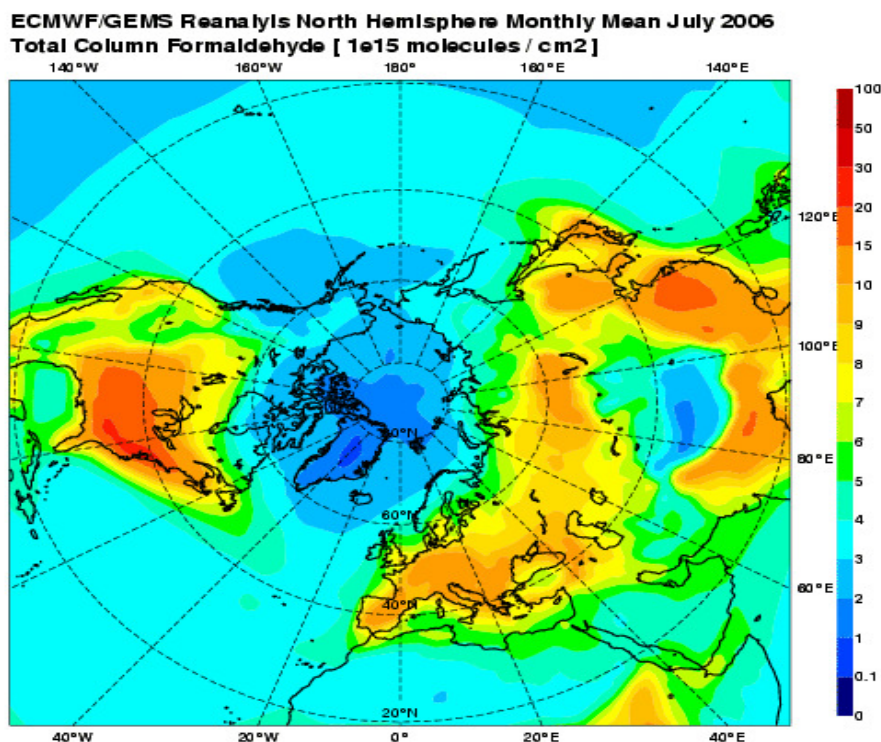
Figure 3.6:   GEMS July 2006 northern hemispheric total column HCHO (10^{15} molecules/cm^2).

The peak positive biases are over the south east boundary, where they reach 5×10^{15} molecules/cm^2. Along the eastern boundary, positive biases of approximately $0\text{-}2 \times 10^{15}$ molecules/cm^2 suggest that the GEMS boundary conditions for HCHO may be too high. Figure 3.6 represents the July 2006 mean total column HCHO GEMS reanalyses (MACC, 2014). However, the uneven AQUM boundary HCHO peaks are not seen here, where the GEMS data is lower, between $10\text{-}15 \times 10^{15}$ molecules/cm^2, than AQUM at $16\text{-}17$ $\times 10^{15}$ molecules/cm^2. The GEMS column HCHO over the UK, $5\text{-}9 \times 10^{15}$ molecules/cm^2, is closer to AQUM than OMI, $10\text{-}13 \times 10^{15}$ molecules/cm^2. Over continental Europe, GEMS/AQUM/OMI columns are $10\text{-}15/8\text{-}9/15\text{-}20 \times 10^{15}$ molecules/cm^2, respectively. Therefore, in the case of Europe, all three sources are showing different column values. However, over the UK, GEMS and AQUM HCHO columns are in agreement. In the AQUM-OMI comparisons, the positive biases of $0\text{-}2 \times 10^{15}$ molecules/cm^2 over Ireland, Scotland and the UK west coast suggest the model overestimates OMI there.

These comparisons with OMI column HCHO are noisy and show that this is not the best product to validate the AQUM. When OMI HCHO data are averaged onto a coarser gird, e.g. $0.5°$ x $0.5°$, the noise is partially averaged out spatially. In Figure 3.5d, there is a stronger sea-land contrast with column HCHO ranging between $10\text{-}15/\text{over } 30$ $\times 10^{15}$ molecules/cm^2, respectively. For better AQUM comparisons, using OMI data on

an even coarser grid and over a longer time period would give a clearer column HCHO signal. Comparisons with surface and aircraft observations of HCHO would also aid better understanding of any problems with the AQUM HCHO chemistry.

3.4.3   Aerosol Optical Depth

Both OMI and MODIS AOD products were compared with AQUM at 0.38/0.44 and 0.55 μm, respectively. The cloud filters (< 0.5) were applied to both the OMI and MODIS data. However, the quality assurance flags in the MODIS product were not consistent with the product documentation. Therefore, they were not applied in the analysis, unlike the OMI quality assurance flags. However, in comparison between the two data products, MODIS AOD has better spatial signal-to-noise ratio.
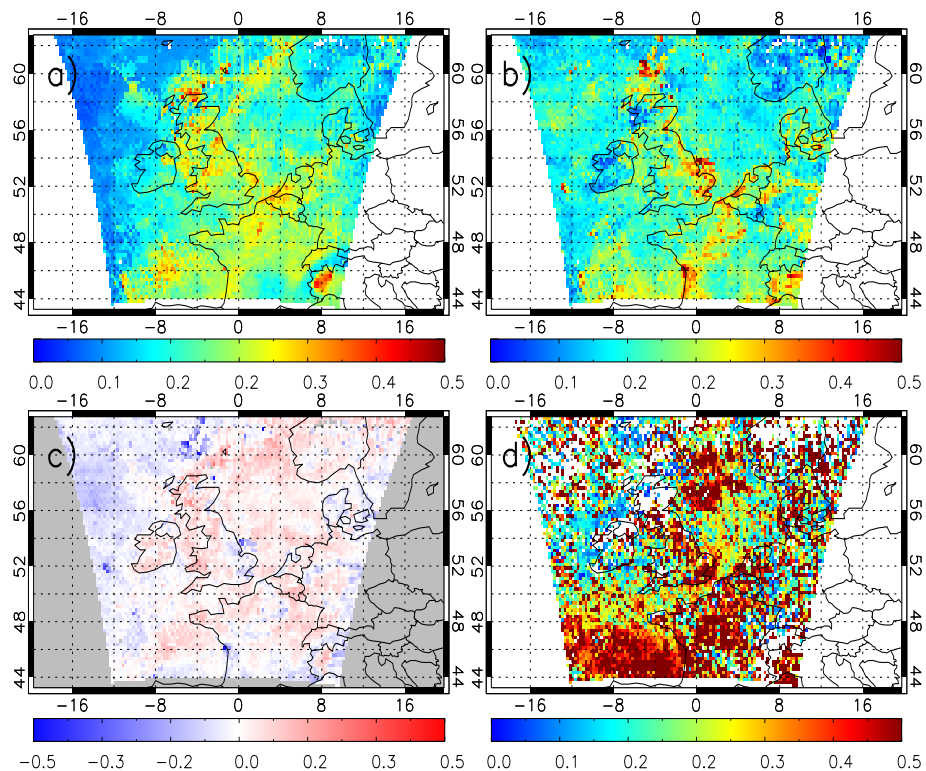
Figure 3.7: July 2006 column aerosol optical depth (AOD): a) AQUM (0.55 μm), b) MODIS (0.55 μm), c) AQUM - MODIS mean bias and d) OMI (0.44 μm).

In Figures 3.7b and 3.7d, AOD column means from MODIS (0.55 μm) and OMI (0.44 μm) show that MODIS is more coherent than OMI spatially. This AOD spatial noise is independent of AOD wavelength as OMI AOD at 0.38 μm is also extremely noisy (not shown here). Generally MODIS recorded more retrievals over the month, so potentially the retrieval noise is averaged out more in this product, compared with OMI. Therefore, only the MODIS data is used in the AQUM-satellite AOD comparisons. The MODIS data is still noisy, but AOD peaks at 0.4-0.5 over the Bay of Biscay, East Anglia, the Humber

Estuary, Scotland, Benelux region and the Po Valley. AQUM (Figure 3.7a) has peak AOD in similar locations but with lower values at generally 0.2-0.4. AQUM calculates the optical depth for several different types of aerosols (ammonium sulphate, mineral dust, sea salt, soot, biomass burning, biogenic, fossil fuel and ammonium nitrate) and the optical depths for these aerosols were totalled together to give the model AOD. However, since sea salt aerosol is a diagnostic variable and not transported, it was not included in the total model AOD.
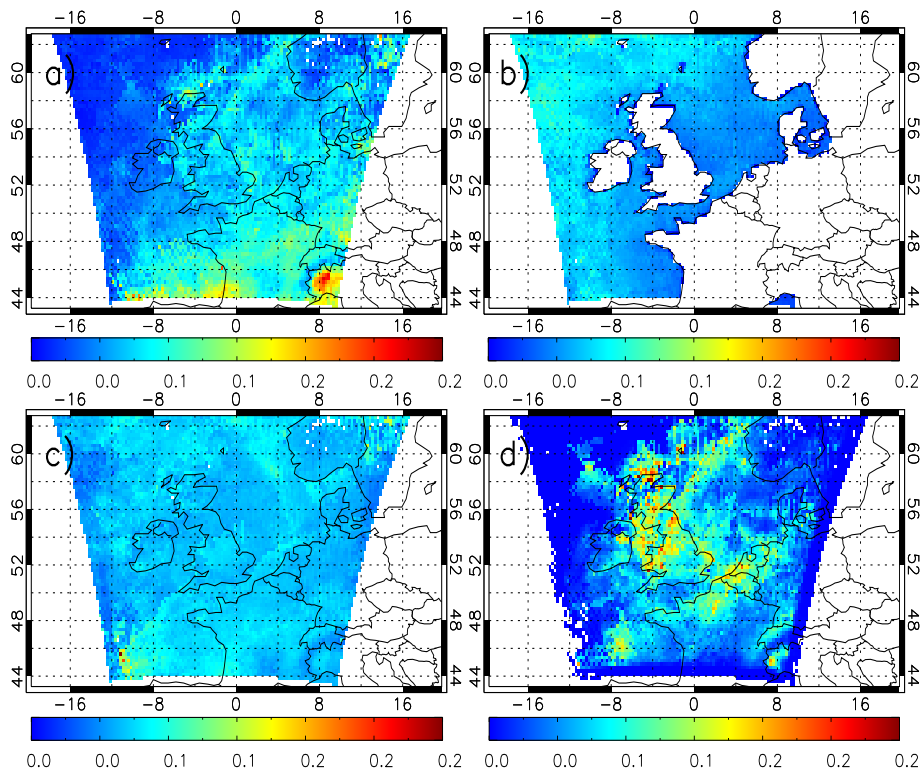
Figure 3.8: AQUM July 2006 column OD (0.55 μm): a) ammonium sulphate b) Sea Salt, c) fossil fuel burning and d) ammonium nitrate.

The AQUM - MODIS mean bias (Figure 3.7c) highlights where MODIS is greater than AQUM with values between -0.4 to -0.3 over the Bay of Biscay, north of Scotland and East Anlia/Humber Estuary. Overall, despite the noise in the MODIS product, the comparisons are reasonable with biases between -0.1 to 0.1 over most of the domain. Over the Atlantic and eastern boundary, there are some negative biases between -0.2 to 0. To further investigate the AQUM-MODIS AOD biases, the AQUM AOD was decomposed into its constituents. Figure 3.8 shows AQUM mean optical depth of ammonium sulphate, sea salt, fossil fuel and ammonium nitrate. These aerosol types have the largest OD values in the total AOD, but the other aerosol types were negligible. In Figure 3.8a and 3.8d, the ammonium sulphate and nitrate aerosols look spatially similar to the mean bias in places. The fossil fuel aerosols are more or less constant over the domain at 0.1-0.2. The

ammonium sulphate AOD peaks at 0.2-0.3 in the Po Valley and the AOD MB has a positive bias of 0.2 there. Therefore, this suggests that ammonium sulphate, with the largest optical depth in the region, might be the cause of this regional AQUM-satellite bias. Ammonium nitrate appears to correlate highly with many of the MB spatial features. This is best seen over Cape Wrath, west of the Bay of Biscay, southern Wales, the Scottish Borders and locations over the North Sea where the MBs of 0.2-0.3 match the peak ammonium nitrate AOD of 0.2-0.3. Therefore, suggesting that the majority of the AOD MBs are due to AQUM's representation of ammonium nitrate OD.

To test this more quantitatively, each AQUM type optical depth field was correlated against the AQUM - MODIS MB field. This resulted in correlations of 0.51 (ammonium sulphate), 0.26 (mineral dust), 0.6 (soot), 0.5 (biomass burning), 0.0 (biogenic), 0.22 (fossil fuel) and 0.73 (ammonium nitrate). Therefore, this confirms that the ammonium nitrate aerosol in the model has the biggest influence on the MBs.

3.5   Tropospheric Ozone

OMI column NO_2 is a reliable product with which to monitor air quality over the UK. However, other important air quality species are not so well observed from space. Ozone is also an important air quality species, but since the majority of it is in the stratosphere, satellite instruments have limited sensitivity in retrieving tropospheric ozone. Therefore, evaluation of regional air quality model O_3 can be problematic. This section explores a range of different datasets to try and find a suitable product with which to evaluate AQUM. Such products would include good signal-to-noise ratios, high resolution (e.g. $0.25°$ x $0.25°$), high tropospheric sensitivity and daily UK coverage (e.g. swath data). Unfortunately, it was difficult to find such a product for the summer of 2006; data from satellite instruments launched in 2007 have also been investigated for summer 2008.

3.5.1   TES Ozone

TES O_3 product contains vertical volume mixing ratio (vmr) profiles on 67 pressure levels ranging from the surface to 0.1 hPa. AQUM data were interpolated onto the satellite pressure profile. Compared to other instruments TES has a lower temporal sampling frequency, making it difficult to look at the spatial pattern of O_3. In July 2006, TES only observed approximately 200 retrievals over the AQUM domain. Therefore, AQUM and TES comparisons were split into four domains; UK (50-58° N, 8° W-2° E), Continental Europe (44-52° N, 0°-12° E), Western domain (44-63° N, 20-4° W) and North Sea domain (54-63° N, 1° W-12° E). All the retrievals in each domain were averaged together to give a single vertical profile.

The TES AKs, based on Optimal Estimation, were in the form of a 67×67 matrix and were applied to the AQUM O_3 as:

$$X_{final} = x_a + A(x_{model} - x_a) \tag{3.10}$$

where A is the averaging kernel, x_a is the apriori used in the retrieval, x_{model} is the comparison profile and X_{final} is the modified model retrieval (Richards et al., 2008). In Equation 3.10, low instrument sensitivity results in small averaging kernels and the profile becomes heavily weighted to the a-priori with little model information remaining.
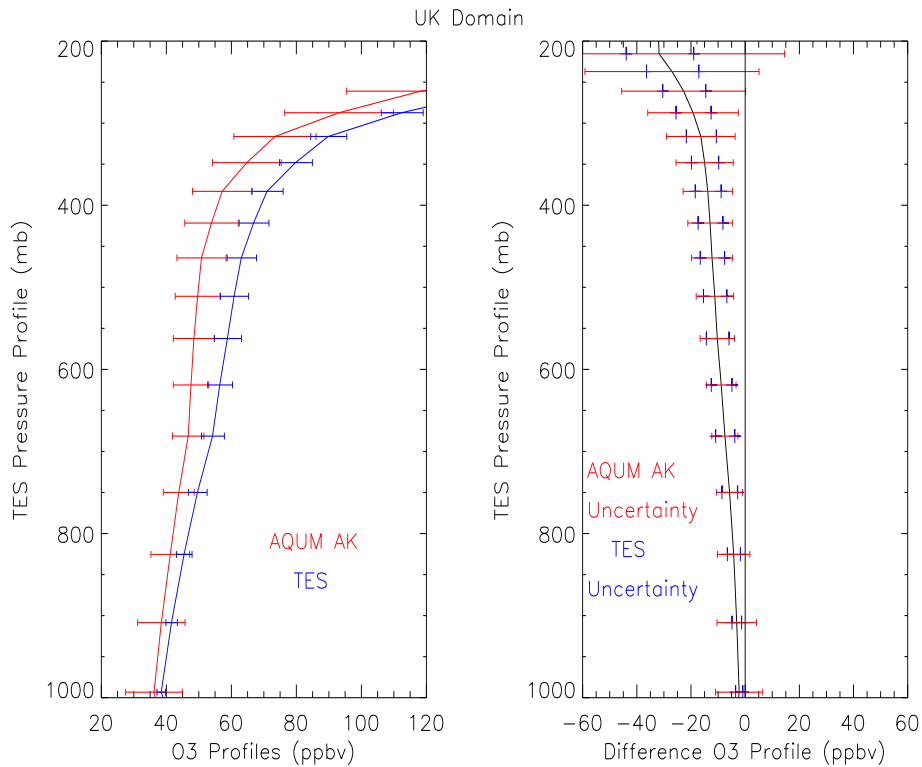
Figure 3.9: UK domain July 2006 averaged vertical profiles (ppbv) of AQUM (red), TES (blue) O_3 and the difference.

Figures 3.9 and 3.10 show the UK and Continental European domain O_3 profiles. In the UK, AQUM AK (red) and TES (blue) profiles range from 40-50 ppbv at the surface (1000 hPa) and increase near linearly to 50-70 ppbv at 400 hPa. The profiles then increase more exponentially to over 120 ppbv at approximately 300 hPa. This represents stratospheric ozone incursion in the UT (upper troposphere). In Figure 3.9 (right), there is a negative AQUM AK - TES O_3 surface bias of 0-5 ppbv, which intensifies with altitude up to 200 hPa between -35 and -30 ppbv. The continental European domain (Figure 3.10 (right)) has positive surface biases at 5 ppbv but then follows a similar pattern to the UK with biases reaching -20 ppbv between 700 to 200 hPa, suggesting that AQUM underestimates the TES observations here. In the biases plots of Figures 3.9 and 3.10, up to about 750

and 600 hPa, respectively, the differences are non-significant because the size of the bias is less than the satellite errors. However, above this up to approximately 300 hPa, AQUM significantly underestimates the observations. Therefore, AQUM upper tropospheric O_3 is too low by approximately 10 to 20 ppbv over the UK and continental European domains.
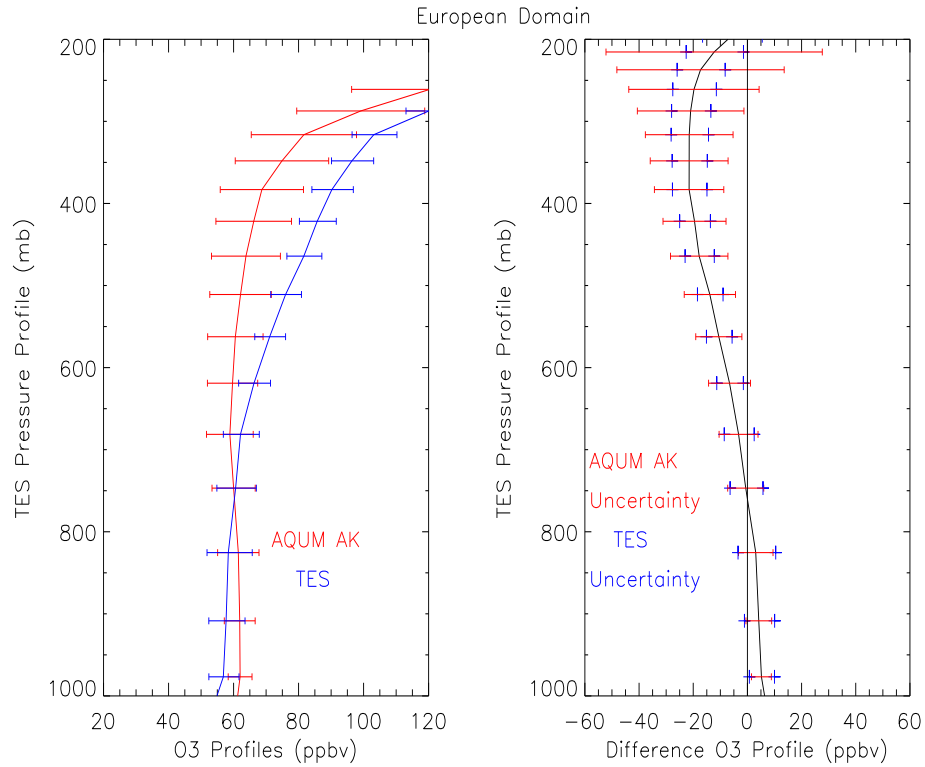
Figure 3.10: European domain July 2006 averaged vertical profiles (ppbv) of AQUM (red), TES (blue) O_3 and the difference.

Several TES validation papers suggest that its retrievals overestimate O_3, when compared with other observations at lower levels. Nassar et al. (2008) compared TES to ozonesondes over the northern latitudes in the summer and they found that TES, on average, overestimated them by 10-15 ppbv between 900-800 hPa. Richards et al. (2008), while comparing TES retrievals with the Intercontinental Chemical Transport Experiment-B (INTEX-B) aircraft campaign for March 2006, found that over the Pacific and USA TES overestimated by up to 10 ppbv near the surface. However, both Nassar et al. (2008) and Richards et al. (2008) show that the TES overestimation of O_3 steadily reduces with altitude. Osterman et al. (2008) also found total column positive biases when comparing TES with OMI and MLS (Microwave Limb Sounder) at all latitudes. Therefore, TES overestimates ozone profiles, which might account for some of the negative biases between AQUM and TES in the lower troposphere over the UK. However, this potential overestimation by TES appears to decrease with altitude, so does not explain the strong negative biases seen in the upper and mid vertical profiles. Therefore, further investigation is required for the

mid and upper tropospheric profile biases.

3.5.2 OMI Ozone

In the OMI subcolumn ozone product (OMO3PR), each retrieval has a vertical profile of 18 layers ranging from the surface to 0.3hPa. According to de Haan and Veefkind (2012) (disc.sci.gsfc.nasa.gov/Aura/data-holdings/OMI/documents/v003/OMO3PRO_README.html), the product has little tropospheric information, and the AKs have peak sensitivity in the stratosphere. Despite this, the spatial distribution of ozone over the UK in the bottom subcolumn (surface-500 hPa) is compared to the AQUM equivalent. The OMO3PR subcolumn O_3 is in the form of swath data, which was interpolated onto a $0.25° \times 0.25°$ grid.
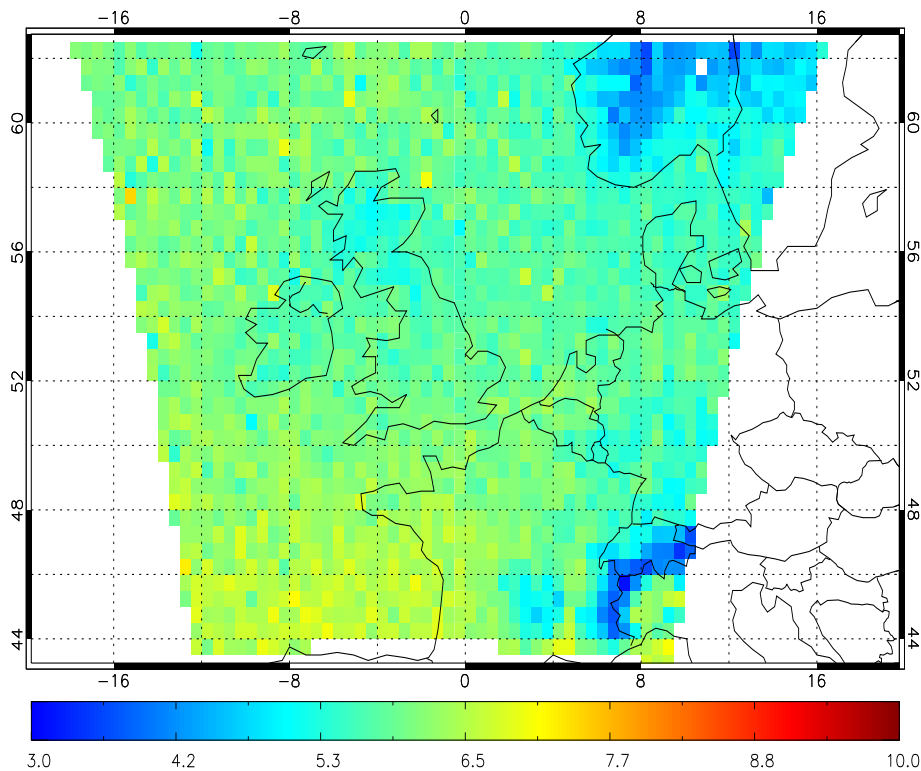
Figure 3.11: OMI subcolumn O_3 (10^{17} molecules/cm^2), surface-500 hPa, for July 2006.

Figure 3.12a shows the AQUM surface - 500 hPa subcolumn O_3, which peaks over continental Europe and the UK between approximately 6-7 $\times 10^{17}$ molecules/cm^2. The minimum subcolumn O_3 is over the Atlantic and Scandinavia between 3-4 $\times 10^{17}$ molecules/cm^2. Figure 3.11 shows that OMI O_3 is the reverse where subcolumns peak over the ocean at approximately 6-7 $\times 10^{17}$ molecules/cm^2 and only 5-6 $\times 10^{17}$ molecules/cm^2 over the UK. OMI subcolumn O_3 over the Alps and Scandinavia is consistent with AQUM as values range between 3-4 $\times 10^{17}$ molecules/cm^2. However, the spatial coherence in the OMI image is less.
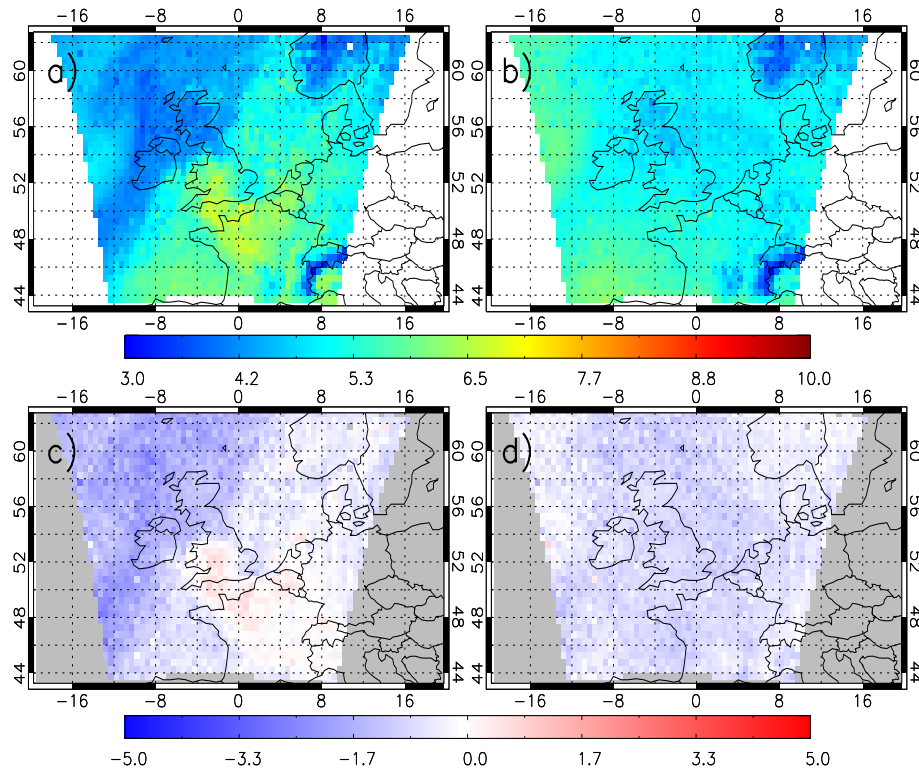
Figure 3.12: July 2006 subcolumn O_3 (10^{17} molecules/cm^2), surface-500 hPa, for a) AQUM, b) AQUM (AKs applied), c) AQUM - OMI mean bias and d) AQUM (AKs applied) - OMI mean bias.

Even though the AKs have limited tropospheric sensitivity, Figure 3.12b indicates that they have an impact on the AQUM O_3 spatial distribution (the AKs are applied using Equation 3.10). Now the peak subcolumn O_3 is over the Atlantic, approximately 6 $\times 10^{17}$ molecules/cm^2, and reduced over the UK to 4-5 $\times 10^{17}$ molecules/cm^2. The large OMI subcolumns over the Atlantic are now present in the AQUM domain because AK sensitivity is greatest here and the model O_3 is weighted accordingly. The MB (Figure 3.12c) between the normal AQUM and OMI suggests the subcolumn O_3 is similar, +/- 0.5 $\times 10^{17}$ molecules/cm^2, over the eastern half of the domain, but the AQUM underestimates O_3 over the Atlantic by -3.5 to -1.5 $\times 10^{17}$ molecules/cm^2.

In Figure 3.12d, the AQUM AK - OMI MBs are less spatially coherent where the AQUM underestimates O_3 across the domain between -2 - 0 $\times 10^{17}$ molecules/cm^2. At the East and West LBCs, O_3 subcolumn biases are near 0 and represent better agreement. However, because the AKs have less sensitivity in this subcolumn, the retrieval itself will be more dependent on the apriori information, which is based on other O_3 information such as model simulations or O_3 climatologies. Therefore, this product is not suitable for AQ model evaluation with limited sensitivity in the troposphere.

3.5.3   OMI-MLS Ozone
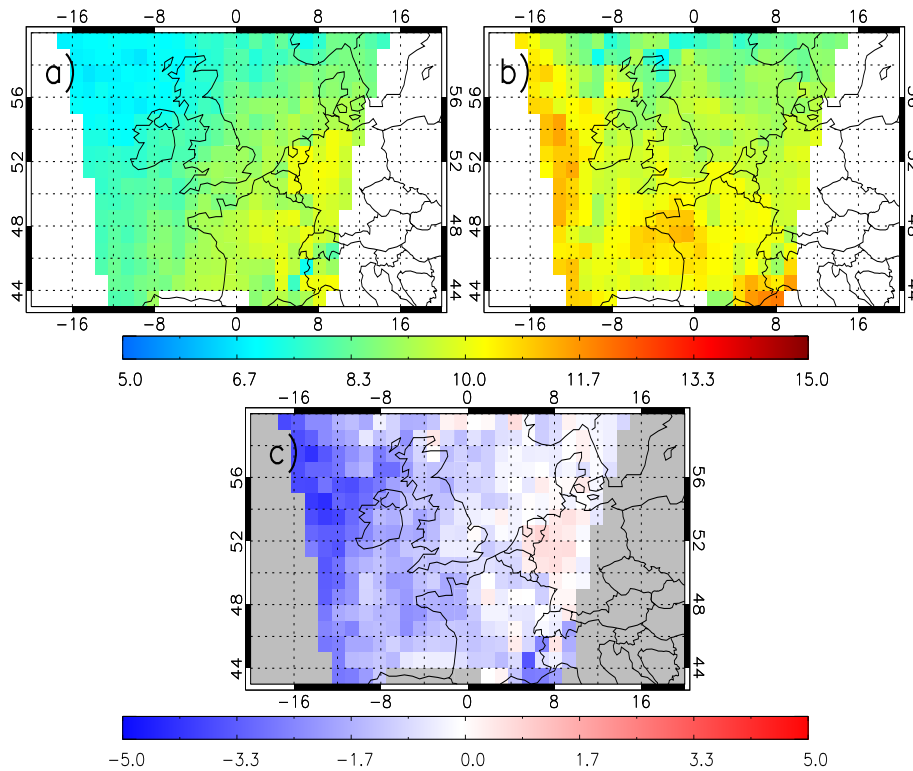
Figure 3.13: Tropospheric column O_3 (10^{17} molecules/cm^2) for a) AQUM, b) OMI/MLS
and c) AQUM - OMI/MLS biases.

The OMI/MLS (Microwave Limb Sounder) O_3 product is the derived 1° x 1° monthly
tropospheric column O_3 for July 2006. This product is found at http://acd-ext.gsfc.nasa.
gov/Data_services/cloud_slice/new_data.html (Ziemke et al., 2011) and is developed by
taking the OMI total column O_3 and subtracting the MLS stratospheric column to form
this tropospheric product. Unfortunately, as this is a gridded monthly mean product (level
3 product), it does not have information on individual retrievals such as AKs, cloud cover
and retrieval quality. Therefore, only simple grid comparisons are possible.

AQUM tropospheric column O_3 (Figure 3.13a) peaks at approximately 10×10^{17}
molecules/cm^2 over continental Europe with a strong East - West gradient, which is similar
to Figure 3.12a, to 5×10^{17} molecules/cm^2 over the Atlantic. The OMI/MLS column O_3
has a different spatial distribution, which peaks at approximately 12×10^{17} molecules/cm^2
along the western LBC and over the Po Valley. Therefore, there is some consistency
between the OMI subcolumn and OMI/MLS tropospheric column product as the spatial
differences in the model-satellite MBs are similar in places (without AKs applied). In
Figure 3.13c, the bias between AQUM and OMI/MLS is -5 $\times 10^{17}$ molecules/cm^2 over the
western LBC, but small over the eastern LBC and continental Europe.
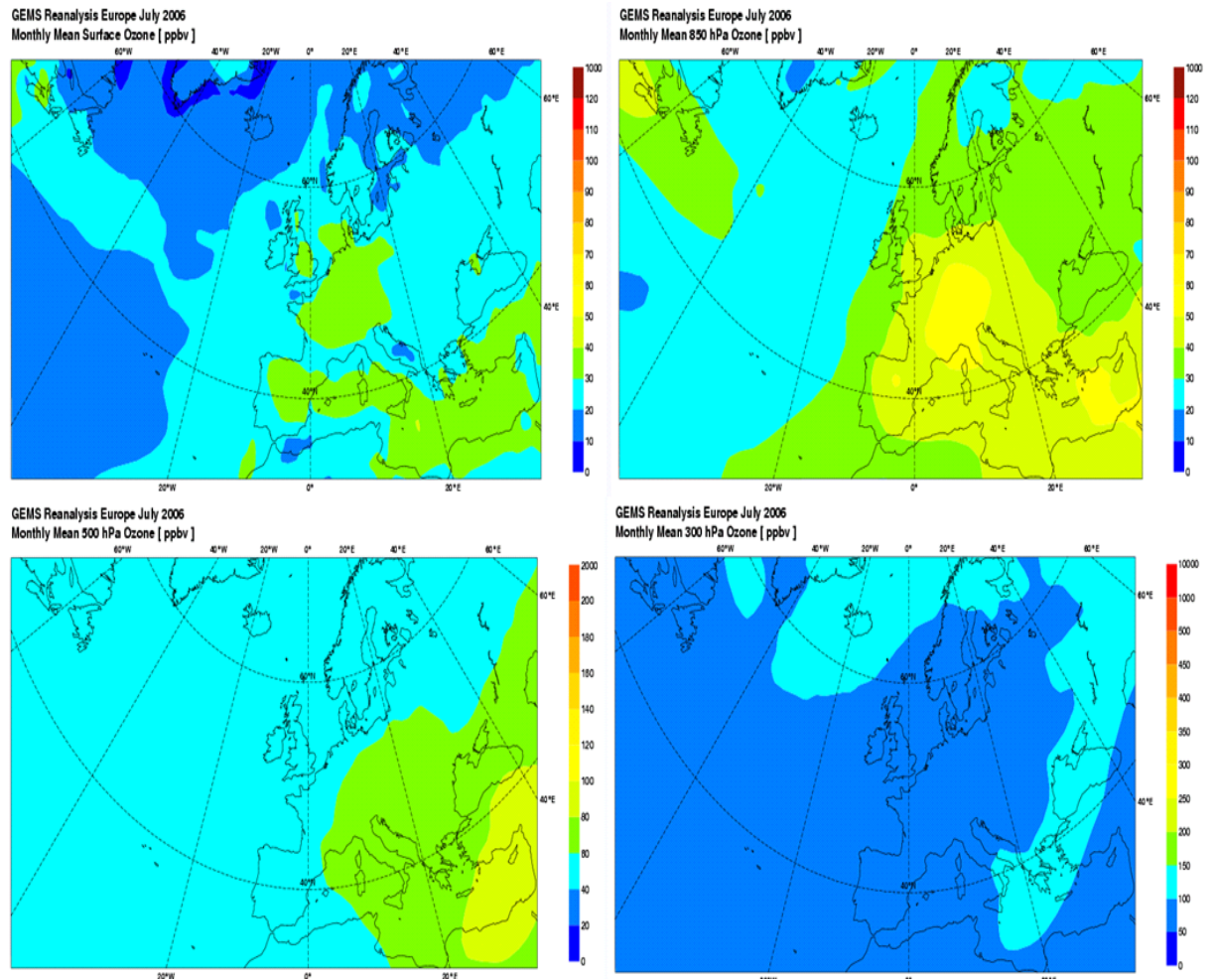
Figure 3.14: GEMS reanalysis O_3 (ppbv) for July 2006 at the surface (top left), 850 hPa (top right), 500 hPa (bottom left) and 300 hPa (bottom right).

These comparisons, although with high uncertainty, potentially suggest that AQUM underestimates tropospheric O_3 concentrations in the western section of the model domain. This could be due to the flux of O_3 through the western LBC, which is based on GEMS reanalysis data. Therefore, there seems to be some Atlantic ozone feature that the LBCs are missing, which leads to AQUM O_3 under-prediction. Figure 3.14 shows GEMS reanalysis (MACC, 2014) northern Atlantic O_3 (ppbv) at the surface, 850, 500 and 300 hPa for July 2006. At most levels there are clear East - West O_3 gradients. At the surface, O_3 concentrations over the Atlantic are 10-30 ppbv and 30-50 ppbv over continental Europe. At 850 (500) hPa, the Atlantic and continental European O_3 concentrations are 20-30 (40-60) ppbv and 40-70 (60-100) ppbv, respectively. However, the GEMS O_3 is strongly homogeneously distributed at 300 hPa, but this might be due to the colour bar used by MACC (2014). Therefore, in July 2006 for the lower-mid troposphere, the GEMs simulations used for AQUM's LBCs have an East-West O_3 gradient, which is not seen in

the satellite observations. Hence, O_3 concentrations are lower on AQUM's western LBC.

3.5.4   Atlantic Ozone
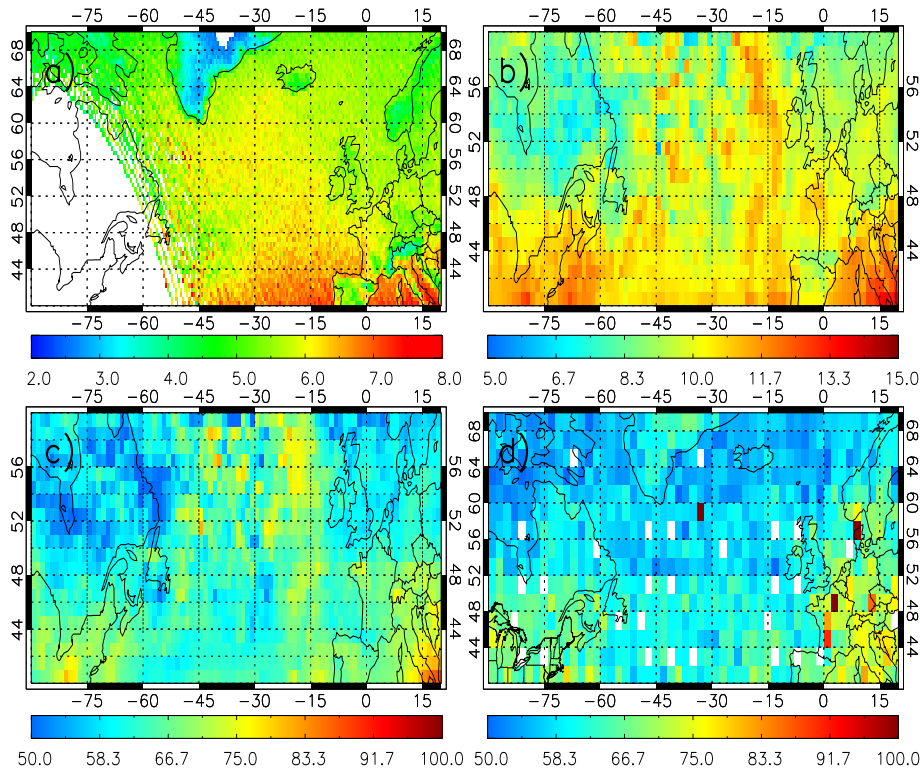
Figure 3.15: Atlantic O_3 for July 2006 for a) OMI subcolumns ($\times 10^{17}$ molecules/cm^2), surface - 500 hPa, b) OMI/MLS tropospheric columns ($\times 10^{17}$ molecules/cm^2), c) OMI/MLS tropospheric mean profiles (ppbv) and d) TES tropospheric mean profiles (ppbv) (JJA 2006).

Since the AQUM - satellite O_3 comparisons suggest that AQUM's western LBC underestimates the flux of O_3 in the domain, the satellite O_3 fields for the Atlantic have been plotted (July 2006) to see if there are enhanced O_3 concentrations over the ocean. Figures 3.15a-c show such features in the OMI subcolumn (surface - 500 hPa) and OMI/MLS (tropospheric column - $\times 10^{17}$ molecules/cm^2, ppbv) ozone fields. The OMI subcolumns over the Atlantic range around 6-7 $\times 10^{17}$ molecules/cm^2, which are higher than the UK concentrations of 3-5.5 $\times 10^{17}$ molecules/cm^2. This O_3 feature covers most of the Atlantic. The OMI/MLS column O_3 highlight more defined O_3 features with isolated O_3 concentrations just off the UK coastline ranging between 11-12 $\times 10^{17}$ molecules/cm^2 and 70-80 ppbv, while the UK and continental Europe concentrations range from 8-10 $\times 10^{17}$ molecules/cm^2 and 50-60 ppbv. I also looked at TES Jun-Jul-Aug (JJA) 2006 Atlantic O_3 concentrations. Because TES has poor spatial coverage, the slightly longer period of JJA was examined on a coarser 2.5$°$ x 2.5$°$ grid. Unfortunately, Figure 3.15d is still very

noisy and it is difficult to tell if there is an Atlantic O_3 feature or the O_3 gradient seen in the AQUM domain.

3.5.5   Ozone Comparisons JJA 2008
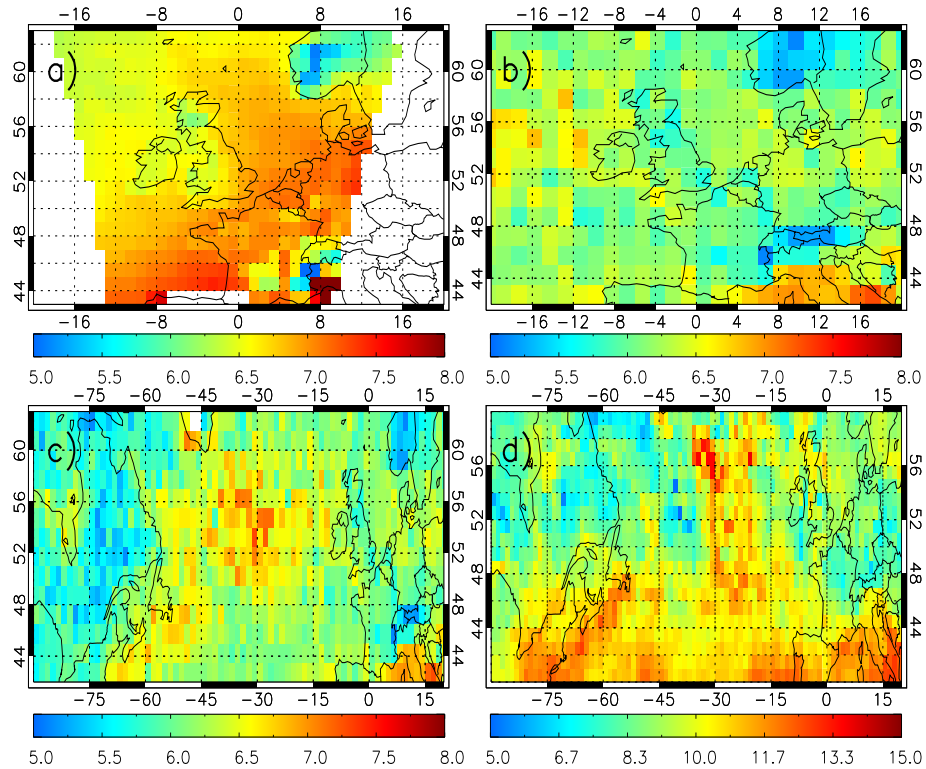
Figure 3.16: JJA 2008 subcolumn, surface - 450 hPa, O_3 (10^{17} molecules/cm^2) for a) AQUM, b) GOME-2 and c) GOME-2 Atlantic coverage. d) OML/MLS tropospheric column O_3 (10^{17} molecules/cm^2) for JJA 2008.

GOME-2 (Global Ozone Monitoring Experiment 2) subcolumn (surface-450 hPa) O_3, which is on the ESA Metop-A satellite and has a London overpass time of 9.30am LT (Richards et al., 2013), was used in this period to undertake complete full model - satellite comparisons. The product is in the form of swath data, but was interpolated onto on a 1° x 1° grid. The product includes averaging kernels, cloud filters and quality flags. Due to technical issues with the use of the averaging kernels though, the AKs were not applied to the AQUM data. Nevertheless, comparisons between AQUM and GOME-2 show similar patterns to those seen in the July 2006 case study. AQUM subcolumn O_3 peaks over continental Europe (south-western domain) at 7-8 $\times 10^{17}$ molecules/cm^2 (Figure 3.16a), with the familiar East - West O_3 gradient of smaller concentrations, 6-7 $\times 10^{17}$ molecules/cm^2, over the Atlantic. In the case of GOME-2, subcolumn O_3 is generally lower over the eastern domain of 6.0-6.5 $\times 10^{17}$ molecules/cm^2 and higher over the Atlantic between 6.5-7.0 $\times 10^{17}$ molecules/cm^2 (Figure 3.16b). The GOME-2 subcolumn
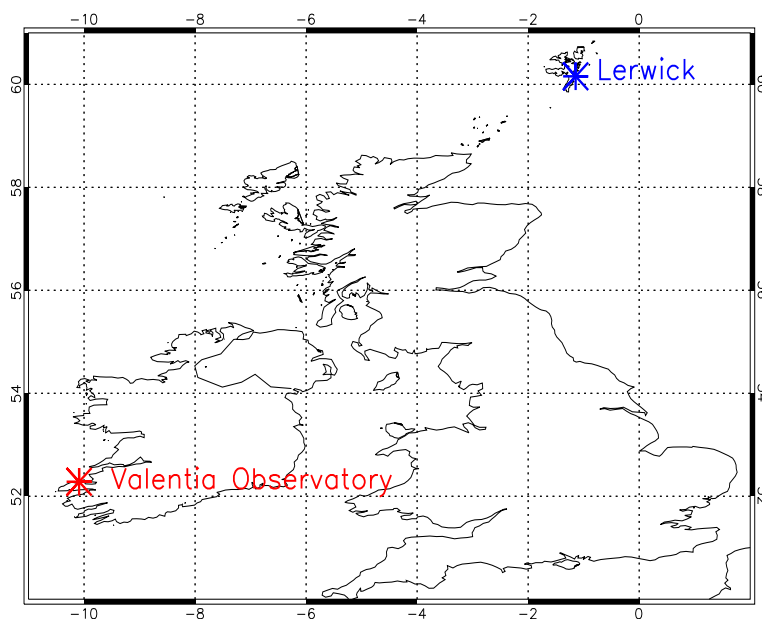
Figure 3.17: Ozonesonde release sites for 2008; Lerwick, Shetlands and the Valentia Observatory, Ireland.
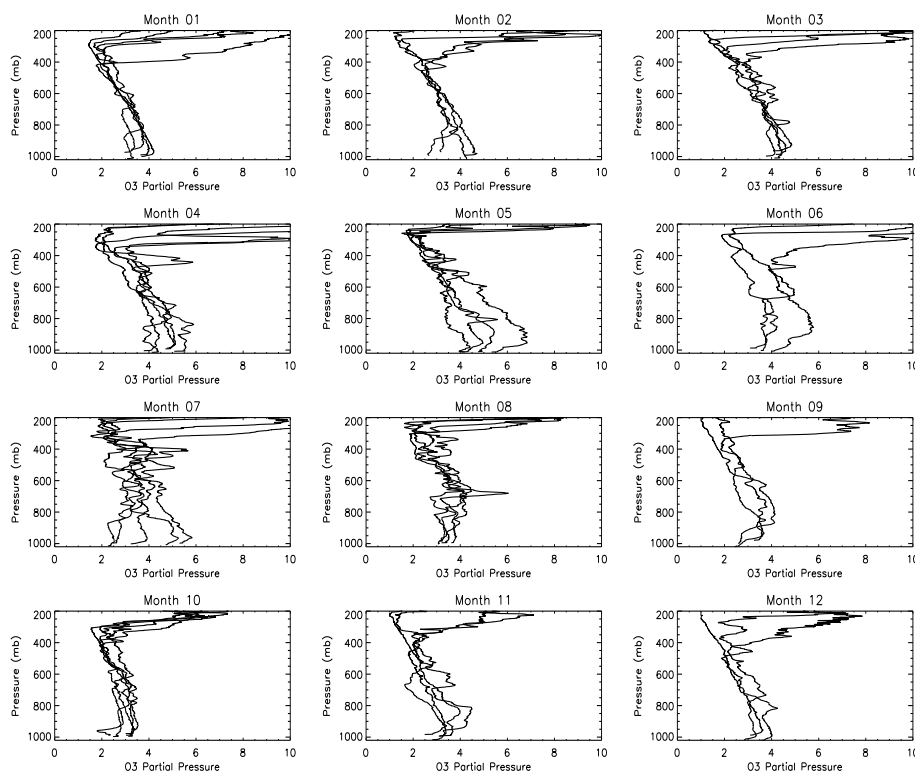
Figure 3.18: Ozonesonde profiles (partial pressure - Pa) for 2008 from Lerwick, Shetland.

O_3, although noisy, has realistic spatial patterns with peak O_3 over the Mediterranean, 7-8 $\times 10^{17}$ molecules/cm^2, and minimum subcolumn O_3 over Scandinavia and the Alps.

Overall, the AQUM overestimates GOME-2 by 1-2 $\times 10^{17}$ molecules/cm^2 across the domain (except the Atlantic).

To check if the Atlantic ozone feature, seen by multiple satellite products, did not only occur in the summer of 2006, the GOME-2 O$_3$ data for JJA 2008 was investigated. Figure 3.16c clearly highlights elevated Atlantic ozone. GOME-2 subcolumn O$_3$ over Europe and Canada range from 5-6.5 $\times 10^{17}$ molecules/cm^2, while the Atlantic peaks at 7.5 $\times 10^{17}$ molecules/cm^2. To validate the JJA GOME-2 spatial pattern, Figure 3.16d shows July 2008 OMI/MLS tropospheric column O$_3$, which will have higher values as it represents a larger vertical section of the atmosphere. It highlights similar spatial patterns with larger Atlantic O$_3$ (11-15 $\times 10^{17}$ molecules/cm^2) and lower O$_3$ over Europe/Canada (5-8 $\times 10^{17}$ molecules/cm^2).

Ozonesondes from Lerwick, Shetlands and the Valentia Observatory, Ireland (Figure 3.17), were compared (2008) to see if this Atlantic ozone feature could be seen by observations other than satellite. In Figure 3.18 and 3.19, the annual seasonal cycle of ozonesondes at Lerwick and Valentia show the vertical profile of ozone as partial pressure (Pa). A typical profile is approximately 2-4 Pa at the surface and decreases to 1-2 Pa at 250-300 hPa before increasing again to 8-10 Pa by 200 hPa because of the stratospheric O$_3$ fluxes into the upper troposphere. If the O$_3$ Atlantic feature was detected, Valentia
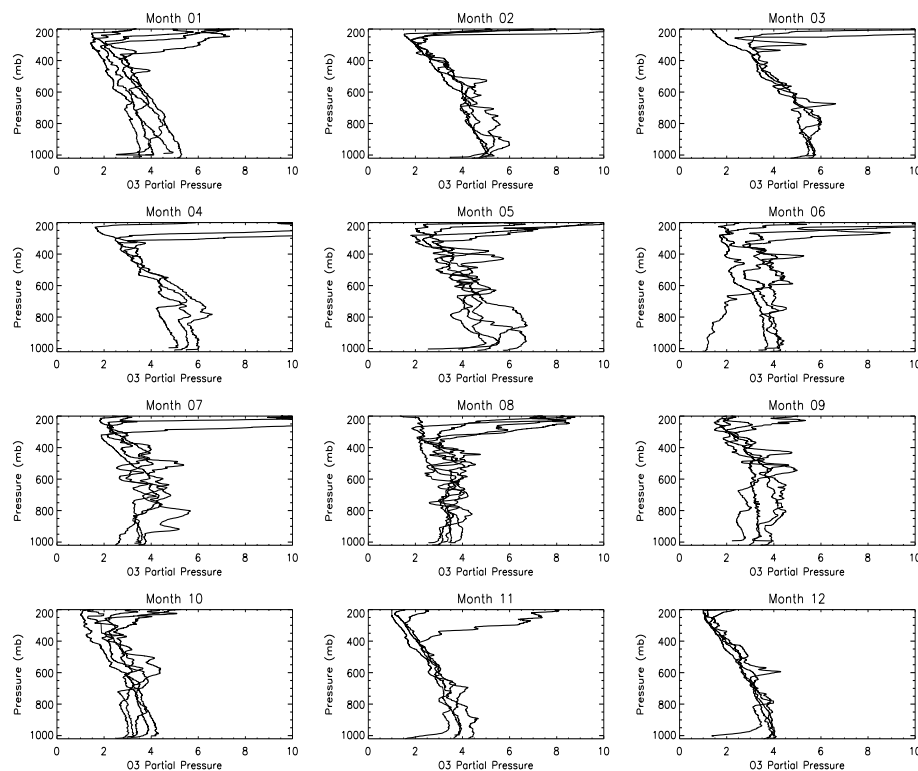
Figure 3.19: Ozonesonde profiles (partial pressure - Pa) for 2008 from the Valentia Observatory, Ireland.
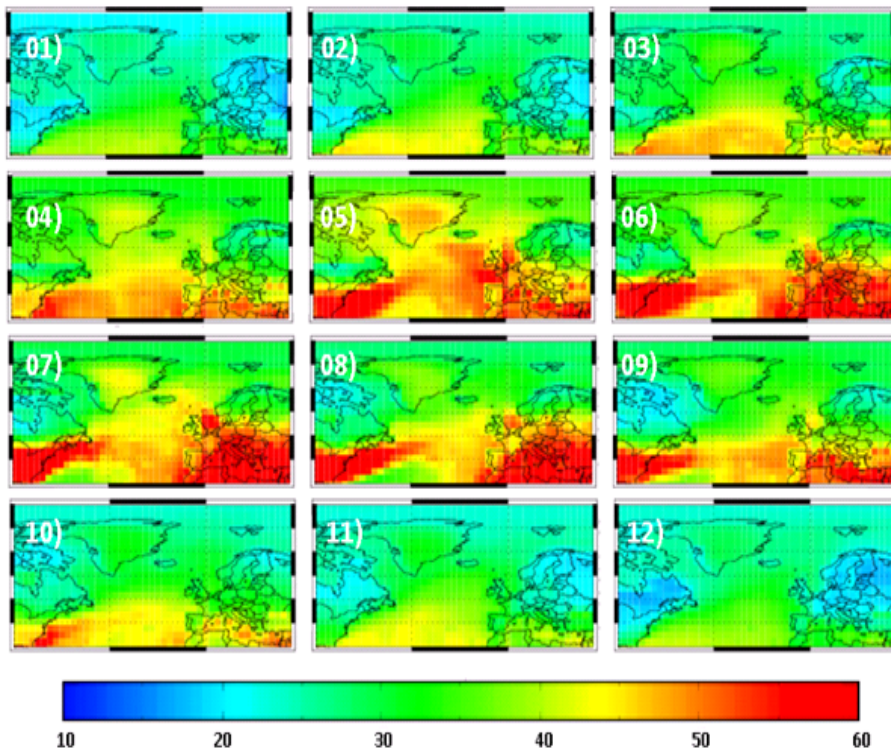
Figure 3.20: TOMCAT 2008 surface Atlantic O_3 (ppbv).

(closer to the Atlantic) would be expected to measure higher O_3 partial pressures than Lerwick in summer. However, there is no noticeable difference between the two sites. The only noticeably feature at both sites is the spring time, March-May, O_3 maximum, where the partial pressure increases to 4-6 Pa at the surface and lower troposphere from 2-4 Pa.

I looked at the skill of TOMCAT (runs performed by Nigel Richards, University of Leeds), to simulate the Atlantic ozone feature seen by the satellites. Figure 3.20 shows the annual seasonal cycle monthly means of TOMCAT surface O_3. In the winter months, there is no obvious feature as O_3 ranges between 30-40 ppbv over the Atlantic and Europe. In spring and summer however, the Atlantic O_3 increases to 40-60 ppbv, with the majority of cases showing higher O_3 over the Atlantic than the UK. Therefore, TOMCAT can represent the Atlantic O_3 feature seen by multiple satellite products, while the AQUM does not along its western LBC suggesting an insufficient O_3 flux into the domain.

3.6   Summary

This chapter has shown that the OMI column NO_2 product successfully detected coherent air quality signals over the UK for the extreme air quality month of July 2006. Peak concentrations were over the urban regions such as London and the Benelux region. The good signal-to-noise ratio and high resolution makes it a good product with which to

evaluate AQUM, which is discussed more in Chapter 4.

The HCHO and AOD data are less coherent. The OMI column HCHO data successfully detects the land-sea mask with peak concentrations over land. As the product is noisy, comparisons with AQUM were not as good as for NO_2. Ultimately, comparisons between AQUM, OMI and GEMS Western Europe column HCHO were inconclusive. The OMI AOD was also noisy over the UK, but comparisons with AQUM suggest that biases could potentially be accounted for by AQUM's representation of ammonium nitrate OD. However, it has been recently (Summer 2014) discovered by Nick Savage at the Met Office that AQUM overestimates ammonium nitrate because the nitrogen atom in the molecule was being double counted in the chemistry scheme.

It was not possible to find suitable satellite O_3 products to compare with AQUM. The OMO3PR had limited sensitivity in the troposphere, while the OMI/MLS product monthly mean gridded data had no AKs. The TES data, while providing vertical O_3 profiles, had limited sampling. By grouping the July 2006 TES retrievals together in a UK and continental Europe domain, I was able to investigate the skill of the AQUM in the vertical. In the lower-mid tropospheric, where the differences were most significant, the AQUM underestimated TES by 5-20 ppbv.

From simple AQUM - satellite comparisons (i.e. without AKs) for July 2006, the AQUM appears to underestimate O_3 along its western boundary. Investigation of GEMS O_3, used for the AQUM LBCs, showed it had a West (low) - East (high) O_3 gradient in the lower and middle troposphere. Satellite data of O_3 concentrations over the Atlantic for July 2006 showed a strong Atlantic O_3 feature with higher values than Europe. This is something GEMS and thus the AQUM are missing. To confirm this, GOME-2 data for JJA 2008 were investigated and it shows similar spatial patterns with higher O_3 over the Atlantic than Europe. Some ozonesonde sites were also investigated to see if other observation types could detect this O_3 Atlantic feature, although unsuccessfully. The TOMCAT global CTM simulates significant Atlantic O_3 features in summer 2008, where there is a West (high) - East (low) O_3 gradient at the surface between the Atlantic and UK. Therefore, in conclusion AQUM, based on the GEMS LBCs, appears to be underestimating O_3 fluxes through the western LBC of the domain.

The next chapter evaluates the AQUM against satellite and surface observations of NO_2. It discusses a range of selected sensitivity experiments on NO_x emissions, LBCs and heterogeneous chemistry to improve AQUM's skill and improve the general understanding on such topics.

Chapter 4

Evaluation of a regional air quality model against satellite and surface observed NO$_2$ concentrations

4.1 Introduction

This chapter presents the first evaluation of AQUM simulated NO$_2$ and O$_3$ concentrations against both satellite and surface observations. Multiple sensitivity experiments on the lateral boundary conditions, NO$_x$ emissions and heterogeneous chemistry have been explored to better understand model biases. This work has been submitted to ACPD, using only OMI observations to evaluate AQUM (see Declaration of Authorship). Section 4.2 discusses the tropospheric column NO$_2$ observations, averaging kernels and treatment of retrieval errors. The surface observations are discussed in Section 4.3. Section 4.4 covers the model sensitivity experiments. The results are presented in Section 4.5.

4.2 Satellite Data

To evaluate AQUM, this study uses column NO$_2$ data from OMI and the SCanning Imaging Absorption SpectroMeter for Atmospheric CHartographY (SCIAMACHY). Several studies have validated OMI column NO$_2$ against surface and aircraft measurements of tropospheric column NO$_2$. Irie et al. (2008) compared OMI and with ground based MAX-DOAS retrievals in the Mount Tai Experiment (2006). They found the standard OMI product (version 3) overestimated the MAX-DOAS measurements by approximately 1.6 $\times 10^{15}$ molecules/cm^2, but within the OMI uncertainty limits. Boersma et al. (2008a) compared the near real time (NRT) OMI product (version 0.8) with aircraft measurements in the INTEX-B campaign. Overall, they found a good correlation (0.69) between OMI and the aircraft column NO$_2$, with no significant biases. Blond et al. (2007) used the CHIMERE CTM and model transfer functions to correlate SCIAMACHY column NO$_2$

with in-situ measurements. They state good agreement between CHIMERE and both observational datasets claiming SCIAMACHY as a good daily tool for continental AQ monitoring. Therefore, the literature has confidence in the OMI and SCIAMACHY column NO$_2$ and I use them for evaluation of AQUM. However, OMI data is used as the primary satellite validation dataset.

OMI is a nadir-viewing instrument with a footprint of 312 km^2 aboard NASA's EOS-Aura satellite. It has an approximate London overpass time of 13:00 local time (LT) (Boersma et al., 2008a). SCIAMACHY is also a nadir-viewing instrument with a footprint of 1800 km^2 aboard ESA's ENVISAT satellite. It has an approximate London overpass time of 10:30 LT (Boersma et al., 2008b). In this chapter, I use the DOMINO tropospheric column NO$_2$ products from OMI version 2.0 and SCIAMACHY version 2.3, from the TEMIS (Tropospheric Emissions Monitoring Internet Service) website, http://www.temis.nl/airpollution/no2.html (Boersma et al., 2011a) (Boersma et al., 2011b). The NO$_2$ swath data from 1st January to 31st December 2006 have been binned onto a daily 13:00 LT 0.25° × 0.25° grid (OMI) and 10.30 LT 0.5° × 0.5° grid (SCIAMACHY) between 43° - 63° N and 20° W - 20° E. All satellite retrievals have been quality controlled, and retrievals/pixels with geometric cloud cover greater than 20% and poor quality data flags (flag = -1) were removed. The OMI product uses the algorithm of Braak (2010) to identify OMI pixels affected by row anomalies and sets the data flags to -1. These affected pixels are also filtered out in this study. Even though OMI and SCIAMACHY have approximate 13:00 and 10.30 LT London overpasses, all retrievals across the domain within a two hour window (1 hour either side of the overpass time) in the respective instruments are used to achieve more extensive spatial coverage.

4.2.1 Averaging Kernels

Eskes and Boersma (2003) define the averaging kernel (AK) to be a relationship between the retrieved quantities and the true distribution of the tracer. In other words, the satellite instrument's capability to retrieve a quantity is a function of altitude. For instance, the instrument may be more or less sensitive retrieving a chemical species near the boundary layer than in the stratosphere. Therefore, since satellite retrievals and model vertical profiles are not directly comparable, the AK (or weighting function) is applied to the model data, so the sensitivity of the satellite is accounted for in the comparisons. The AK comes in different forms for different retrieval methods. For the DOAS method, the AK is in the form of a column vector, while in Optimal Estimation, the AK is a matrix, whose dimensions are dependent on the number of pressure levels in the retrieval process. The OMI and SCIAMACHY retrievals use the DOAS technique and hence the

AK is a column vector. Following Huijnen et al. (2010) and the OMI/SCIAMACHY documentation (Boersma et al., 2011b), the AKs are applied to the model as:

$$y = \boldsymbol{A}.\boldsymbol{x} \tag{4.1}$$

where y is the total column, $\boldsymbol{A}$ is the AK and $\boldsymbol{x}$ is the vertical model profile. However, here the tropospheric column is needed:

$$y_{trop} = \boldsymbol{A}_{trop}.\boldsymbol{x}_{trop} \tag{4.2}$$

where $\boldsymbol{A}_{trop}$ is:

$$\boldsymbol{A}_{trop} = \boldsymbol{A}.\frac{AMF}{AMF_{trop}} \tag{4.3}$$
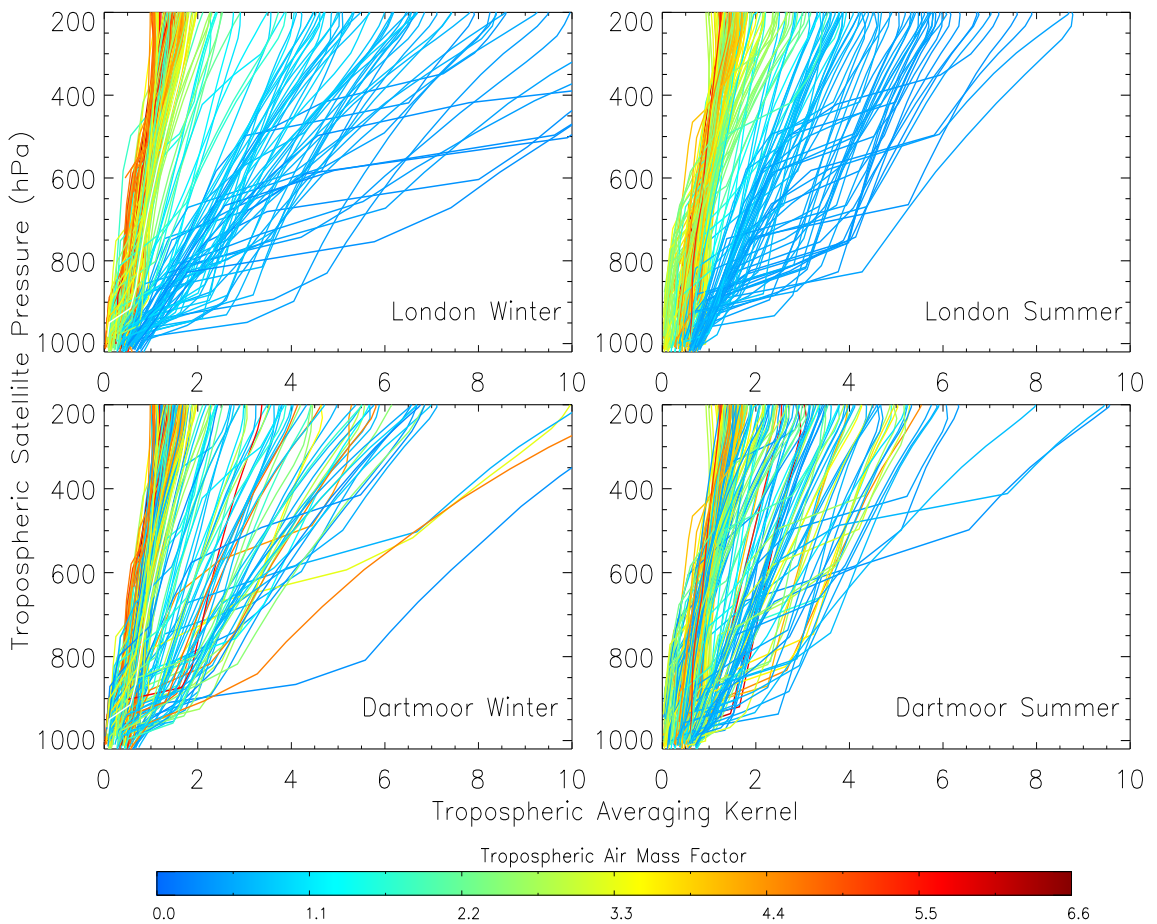
Figure 4.1: Example OMI averaging kernels for London (top) and Dartmoor (bottom) for summer (right) and winter (left) 2006. Averaging kernels have been coloured according to their respective tropospheric air mass factor values.

AMF is the atmospheric air mass factor and AMF_{trop} is the tropospheric air mass factor. For the OMI product, Huijnen et al. (2010) state that the AK tends to be lower than 1 in the lower troposphere (e.g. 0.2-0.7 up to 800 hPa) and greater than 1 in the

mid-upper troposphere. Therefore, the OMI AKs reduce model NO$_2$ subcolumns in the lower troposphere and increase them in the mid-upper troposphere (Huijnen et al., 2010). Figure 4.1 shows example tropospheric AKs for summer and winter profiles over London (urban - higher column NO$_2$) and Dartmoor (rural area in southwest England - lower column NO$_2$), which have been coloured by their respective tropospheric AMF. In the lower troposphere for both seasons and locations the tropospheric AKs range around 0-1. However, in the mid-upper troposphere, the London tropospheric AKs tend to be greater than Dartmoor in both seasons. London tropospheric AKs are most pronounced in winter, with many tropospheric AKs over 8, while in the summer they range around 1-8. In both seasons, the largest tropospheric AMFs between 5-6 are in the lower range tropospheric AKs of 0-1, and the smaller AMFs of 0-1.5 range in the larger tropospheric AKs over 2. If the tropospheric AMFs are small (i.e. near 0 inferring peak NO$_2$ concentrations in the lower London boundary layer) they will return large tropospheric AKs from Equation 4.3, which increase with height. Also, in winter over London, the shallower boundary layer will trap larger winter emissions of NO$_2$ closer to the surface. Therefore, the tropospheric AMF will be smaller and the winter mid-upper tropospheric AKs will be larger as seen in Figure 4.1. Over Dartmoor, the AKs show less seasonal variation and the majority range around 1-6 for both summer and winter. This is also seen in the tropospheric AMF, which ranges between approximately 0-6, but has no clear pattern in the Dartmoor tropospheric AKs in either season.

4.2.2   Satellite Errors

The DOAS retrievals are subject to random, systematic and smoothing errors in the retrieval process. Random (quasi-systematic) errors include fitting errors, cloud errors, instrument noise and signal corruption. Systematic errors include absorption cross-sections, surface albedo and stratospheric correction uncertainties. Finally, smoothing errors include biases in the a priori profiles and sensitivity of the satellite when recording the slant column through the atmosphere. If multiple retrievals are averaged together, as in this study, the random errors will partially cancel leading to the random error being reduced by a factor of $\frac{1}{\sqrt{N}}$ (where N is the number of retrievals). In contrast, systematic errors are unaffected by cancelling through averaging. This section investigates the different error components of the satellite retrievals and derives an expression for the error in the averaged retrievals. This methodology should give smaller errors which are more representative of the time-averaged retrieval error and so allow a stricter test of the model.

Boersma et al. (2004) describe the error in the DOAS NO$_2$ retrievals as:

$$\sigma_{trop}^2 = \left(\frac{\sigma_{total}}{AMF_{trop}} \right)^2 + \left(\frac{\sigma_{strat}}{AMF_{trop}} \right)^2 + \left(\frac{(X_{total} - X_{strat})\, \sigma_{AMF_{trop}}}{AMF_{trop}^2} \right)^2 \qquad (4.4)$$

where σ_{trop}, σ_{strat} and σ_{total} are the uncertainties in the tropospheric, stratospheric and total slant columns, respectively. AMF_{trop} is the tropospheric air mass factor, $\sigma_{AMF_{trop}}$ is the error in the tropospheric air mass factor, X_{total} is the total slant column and X_{strat} is the stratospheric slant column. σ_{total} is made up of both random and systematic error, where the random error component can be reduced by $\frac{1}{\sqrt{N}}$. We assume that the systematic and random errors can be combined in quadrature. In Equation 4.6 there are two terms for σ_{total}; $\sigma_{total_{ran}}$ and $\sigma_{total_{sys}}$, which are the random and systematic error components of the total slant column, respectively. Boersma et al. (2004) state that $\sigma_{total_{sys}}$ can be expressed as $\sigma_{total_{sys}} = 0.03X_{total}$. This study treats σ_{strat} here as systematic as both the OMI standard and DOMINO products estimate the stratospheric slant column using TM4 chemistry transport model simulations and data assimilation (Dirksen et al., 2011). According to the DOMINO OMI product documentation (which references Boersma et al. (2004), Boersma et al. (2007) and Dirksen et al. (2011)), the error in the stratospheric slant column is estimated to be 0.25×10^{15} molecules/cm^2 in all cases. Boersma et al. (2004) state that the tropospheric column is calculated as:

$$N_{trop} = \frac{X_{total} - X_{strat}}{AMF_{trop}} \tag{4.5}$$

where N_{trop} is the vertical tropospheric column and can be substituted, including the σ_{total} and σ_{strat} approximations, into Equation 4.4. This leads to:

$$\sigma_{trop}^2 = \left(\frac{\sigma_{total_{ran}}}{AMF_{trop}}\right)^2 + \left(\frac{0.03X_{total}}{AMF_{trop}}\right)^2 + \left(\frac{0.25 \times 10^{15}}{AMF_{trop}}\right)^2 + \left(\frac{N_{trop}\,\sigma_{AMF_{trop}}}{AMF_{trop}}\right)^2 \tag{4.6}$$

σ_{trop} is reduced in the model-satellite comparisons when the AK is applied to the model data. Therefore, the error product, $\sigma_{trop_{ak}}$, from the OMI retrieval files with the smoothing error removed is used instead of σ_{trop} in Equation 4.4 and Equation 4.6.

Boersma et al. (2007) suggest that the uncertainty in the tropospheric AMF is between 10-40%. Therefore, a conservative estimate of $\sigma_{AMF_{trop}} = 0.4 \times AMF_{trop}$ is taken. This leads to the new retrieval error approximation of:

$$\sigma_{trop_{ak}}^2 = \left(\frac{\sigma_{total_{ran}}}{AMF_{trop}}\right)^2 + \left(\frac{0.03X_{total}}{AMF_{trop}}\right)^2 + \left(\frac{0.25 \times 10^{15}}{AMF_{trop}}\right)^2 + (0.4N_{trop})^2 \tag{4.7}$$

All of these terms are known apart from $\sigma_{total_{ran}}$. This can then be rearranged to calculate $\sigma_{total_{ran}}$ based on other variables provided in the OMI product files. This leads to:

$$\left(\frac{\sigma_{total_{ran}}}{AMF_{trop}}\right)^2 = \sigma_{trop_{ak}}^2 - (0.4N_{trop})^2 - \left(\frac{0.03X_{total}}{AMF_{trop}}\right)^2 - \left(\frac{0.25 \times 10^{15}}{AMF_{trop}}\right)^2 \tag{4.8}$$

In the rare case that the left hand side is negative, the random error component cannot be found as it would be complex, so the random error component is then set to 50% (personal communication with Eskes (2012)). Now, rearranging for $\sigma_{total_{ran}}$, and assuming the left hand side is positive, Equation 4.8 becomes:

$$\sigma_{total_{ran}} = AMF_{trop}\sqrt{\left(\sigma_{trop_{ak}}^2\right) - (0.4N_{trop})^2 - \left(\frac{0.03X_{total}}{AMF_{trop}}\right)^2 - \left(\frac{0.25 \times 10^{15}}{AMF_{trop}}\right)^2} \quad (4.9)$$

This quantity was calculated for each retrieval in each grid square and then the new seasonal retrieval error was calculated taking the reduced random component into account:

$$\overline{\sigma_{trop_{ak}}} = \sqrt{\left(\frac{\overline{\sigma_{total_{ran}}}}{\sqrt{N}AMF_{trop}}\right)^2 + \left(\frac{0.03\overline{X_{total}}}{AMF_{trop}}\right)^2 + \left(\frac{0.25 \times 10^{15}}{AMF_{trop}}\right)^2 + \left(0.4\overline{N_{trop}}\right)^2} \quad (4.10)$$

where a bar superscript represents the seasonal time average.

The same methodology is used for assessing the SCIAMACHY random error component. The uncertainty stated by Boersma et al. (2007) is the same for both OMI and SCIAMACHY ranging between 10-40%. Boersma et al. (2007) also quote the same error in the SCIAMACHY stratospheric slant column as the DOMINO product documentation for OMI column NO$_2$ does of 0.25×10^{15} molecules/cm^2. The systematic error in the total slant column of 3% stated by Boersma et al. (2004) for GOME DOAS retrievals is used here for both OMI and SCIAMACHY.
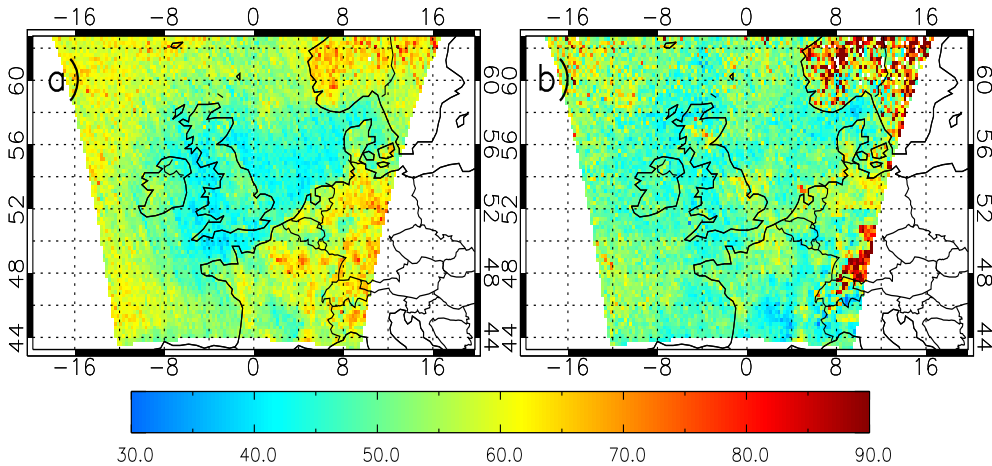
Figure 4.2: New seasonal satellite mean error, obtained by reduction of random error using the methodology described in Section 4.2.2, as a percentage of the simple seasonal mean of satellite total error for 2006. Smoothing errors have been removed. (a) Summer and (b) winter.

Figure 4.2 shows how averaging, by decreasing the random error component, reduces the seasonal satellite tropospheric column error as calculated by the DOAS random error

reduction algorithm. The figure compares the simple mean of the total satellite column NO_2 error (calculated for each pixel) with our new method which reduces the estimated random error component by one over the square root of the number of observations. The reduction in the satellite column error is then presented as a percentage of the original satellite column seasonal mean error. In both summer and winter, the seasonal mean column error is reduced to 30-70% across the domain, therefore making the OMI data a much more rigorous test of model skill. Only for a few retrievals over Scandinavia, does this methodology of reducing the random error component increase the overall column error (not shown here).

4.3   Surface Data

As well as satellite observations, surface observations of NO_2 and O_3 from the Automatic Urban Rural Network (AURN) have been used to validate AQUM. AURN is a network of 175 (106 operational - 127 operational in 2006) surface sites, which has monitored air pollution (O_3, NO_2, $PM_{2.5\&10}$) from 1973-present day (DEFRA, 2012). However, this study uses approximately 70 rural, remote, urban background and suburban sites, although not all species are measured at every site. Kerbside and roadside sites are not used as they are only representative of local conditions and not the background state. The coarse resolution of AQUM will also struggle to reproduce such fine scale measurements. More information about AURN, maintained by DEFRA, including the location of all sites, is available at http://uk-air.defra.gov.uk/networks/network-info?view=aurn.

4.4   Model

4.4.1   Sensitivity Experiments

This study performed one control and seven sensitivity experiments to investigate the AQUM's skill of simulating column NO_2. Two experiments used different LBCs, four experiments used modified point source emissions and two included heterogeneous chemistry. These are summarised in Table 4.1. Run MACC investigates the sensitivity of AQUM column NO_2 to different chemical LBCs from the global Monitoring Atmospheric Composition and Climate (MACC) reanalyses, which is the follow-on project of GEMS (Inness et al., 2012). Savage et al. (2013) have undertaken a similar analysis of the MACC LBCs in AQUM. They showed that when compared with the AURN observations of O_3, AQUM-MACC performs well during the first quarter of 2006 and overestimates observations afterwards, while AQUM-GEMS has a negative bias during the first quarter of the year but compares well with observations afterwards.

Table 4.1: List of AQUM runs and experiments.

Run ID	Run Description
C	Control run (GEMS LBCs)
MACC	MACC LBCs
E1	No point sources emissions
E2	Idealised point source tracer
E3	Split point and area sources
E4	Altered seasonal cycle
N$_2$O$_5$Low	N$_2$O$_5$ heterogeneous chemistry with γ=0.001
N$_2$O$_5$High	N$_2$O$_5$ heterogeneous chemistry with γ=0.02

Additional runs were performed to examine the impact of the point source emissions over the UK on column NO$_2$. Each of these runs are done independently of each other. The motivation behind Run E1 was to determine the impact of the NO$_x$ point sources on the simulated column NO$_2$ budget, as it was hypothesised that AQUM's representation of them was the cause of the AQUM - OMI column NO$_2$ positive biases. Run E2 uses an idealised passive tracer from the point sources with a lifetime of one day to examine if the tracer columns correlated with summer AQUM-OMI positive biases. Run E3 split the area and point source NO$_x$ emissions, where the point source emissions were entered at 1 km vertically. This was to better represent the stack height of power stations and the plume buoyancy. With emissions injected higher in the lower troposphere, I hypothesised that enhanced lateral transport would reduce AQUM - OMI positive biases. Run E4 introduced an artificial seasonal cycle, essentially reducing the JJA 2006 NO$_x$ emissions by 50% (artificial emissions seasonal cycle (SC) = 1-0.5sin(π(m$_0$....m$_{11}$)/(n-1)), where n = number of months = 12, m=0,1...n-1 and was forced onto the emissions but only JJA were used for Run E4), to determine the emissions reduction factor needed for better AQUM - OMI summer comparisons. See section 4.5.3 for more results.

Runs N$_2$O$_5$High and N$_2$O$_5$Low investigate the impact of heterogeneous chemistry on NO$_2$ columns. Tropospheric NO$_x$ (NO + NO$_2$) sources are dominated by anthropogenic emissions and the loss of NO$_2$ to HNO$_3$ is through two pathways:

$$NO_2 + OH + M \rightarrow HNO_3 + M \qquad\qquad [R1]$$

$$NO_2 + O_3 \rightarrow NO_3 + O_2 \qquad\qquad [R2]$$

$$NO_3 + NO_2 + M \rightleftharpoons N_2O_5 + M \qquad\qquad [R3]$$

$$N_2O_5 + H_2O \xrightarrow{aerosol} 2HNO_{3(aq)} \qquad\qquad [R4]$$
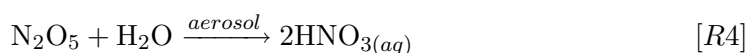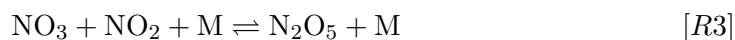
The standard configuration of AQUM does not include any heterogeneous reactions such as the hydrolysis of N_2O_5 on aerosol surfaces (see details of the chemistry scheme in the Appendix).

Previous global modelling studies have shown that this process can be a significant NO_x sink at mid-latitudes in winter (e.g. Tie et al. (2003), Macintyre and Evans (2010)). Following those analyses, we have implemented this reaction, with rate k (s^{-1}) calculated as:

$$k = \frac{A\gamma\omega}{4} \tag{4.11}$$

where A is the aerosol surface area (cm^2/cm^3), γ is the uptake coefficient of N_2O_5 on aerosols (non-dimensional) and $\omega = 100[8RT/(M)]$ (cm/s) is the root-mean square molecular speed of N_2O_5 at temperature T (K), M is the molecular mass of N_2O_5 (kg/mol) and R = 8.3145 J/mol K. Here, γ is assumed to be representative of the uptake of N_2O_5 on all aerosols.

Other studies have introduced this chemistry into AQ models:

- Foley et al. (2010) discuss the use of N_2O_5 heterogeneous chemistry in the Community Multiscale Air Quality (CMAQ) model over the eastern US. They base their updated γ parameter on work done by Davis et al. (2008). This was developed using comprehensive laboratory data and is based on temperature, RH and inorganic particle composition in the model. The CMAQ γ varies between 0-0.06.

- In the French CTM CHIMERE (Menut et al., 2013), N_2O_5 is converted to HNO_3 via heterogeneous pathways by oxidation on aqueous aerosols. The uptake coefficient for N_2O_5 is assumed to be temperature-dependent in the range between 0.01-1. CHIMERE also includes the reaction of N_2O_5 with gaseous water.

- Zhang et al. (2013) compared WRF-Chem with two different aerosol modules called MADRID and Polyphemus. WRF/Chem-MADRID does not treat heterogeneous chemistry, but Polyphemus includes heterogeneous reactions of HO_2, NO_3 and N_2O_5 on the surface of aqueous particles and cloud droplets.

- Sarwar et al. (2013) compares results of the Carbon Bond mechanism with updated toluene chemistry and Regional Atmospheric Chemistry Mechanism Version 2.0 (RACM2) in CMAQ. Both chemical mechanisms in the model include homogeneous and heterogeneous hydrolisis of N_2O_5.

- Macintyre and Evans (2010) investigated the sensitivity of N_2O_5 loss on aerosol by using a range of uptake values (0.0, 10^{-6}, 10^{-4}, 10^{-3}, 5×10^{-3}, 10^{-2}, 2×10^{-2}, 0.1, 0.2, 0.5 and 1.0). They found that limited sensitivity occurs at low and high values of gamma. At low values, the uptake pathway is an insignificant route for NO_x loss.

At high values, the loss of NO_x through heterogeneous removal of N_2O_5 is limited
by the rate of production of NO_3, rather than the rate of heterogeneous uptake.
However, in the northern extra-tropics (including the AQUM domain), intermediate
values of (0.001-0.02) show a significant loss of NO_x.

Therefore, we experimented with $\gamma=$ 0.001 and 0.02 to investigate the sensitivity of
AQUM column NO_2 to heterogeneous chemistry. The aerosol surface area, A, includes
the contribution of seven aerosol types present in CLASSIC: sea salt aerosol, ammonium
nitrate, ammonium sulphate, biomass burning aerosol, fossil fuel black carbon, fossil fuel
organic carbon (FFOC) and biogenic secondary organic aerosol (BSOA). To account for
hydroscopic growth of the aerosols, the formulation of Fitzgerald (1975) is used for growth
above the deliquescence point for ammonium sulphate (RH = 81%), sea salt (RH = 75%)
and ammonium nitrate (RH = 61%) up to 99.5% RH. A linear fit between the efflorescence
(RH = 30% for sulphate, 42% for sea-salt and 30% for nitrate) and deliquescence points
was applied. There is no hydroscopic growth below the efflorescence point. Look-up tables
are used for the other aerosol types. Biomass burning and FFOC aerosol growth rates are
taken from Magi and Hobbs (2003), BSOA growth rates come from Varutbangkul et al.
(2006) and black carbon is hydrophobic (no growth). By including this reaction in the
AQUM, there is an extra sink for N_2O_5 and NO_x on aerosol, but also acts as another
production source for HNO_3.

The initial run of AQUM with heterogeneous chemistry implemented was JFM 2006
to investigate the realism of the model aerosol surface density and fields of NO_x, NO_y
and NO_z. Comparisons of column NO_2 using the implemented chemistry were also done
with OMI. This process is predominately active at night time and in winter with longer
days. Therefore, I looked at winter months JFM, which gave sufficient OMI data to get
a good satellite composite average. The MACC LBCs were used as the standard for the
heterogeneous chemistry initial runs because we intended to do a 5 year simulation to
compare to the results discussed in Chapter 6, where the GEMS LBCs only exist up until
the end of 2008. It should be noted that the ammonium nitrate bug of double counting
the nitrogen atoms, discussed in Chapter 3, has been corrected here.

In Figure 4.3, 13.00 LT (to match the OMI overpass) JFM 2006 total aerosol, sea
salt, ammonium nitrate and ammonium sulphate surface area have been plotted ($\times 10^{-7}$
cm^2/cm^3). The total aerosol surface area is greatest over continental Europe between
40-50 $\times 10^{-7}$ cm^2/cm^3, but also high over the ocean, 25-40 $\times 10^{-7}$ cm^2/cm^3. However,
there is a strong land - sea mask in the surface area in the vicinity of the UK and Norway,
where the aerosol surface area is much lower than over continental Europe (0-25 $\times 10^{-7}$
cm^2/cm^3).

This mask is a result of AQUM's representation of sea salt, which is a diagnostic
scheme based on the wind speed over sea points and not a transported tracer. Sea salt
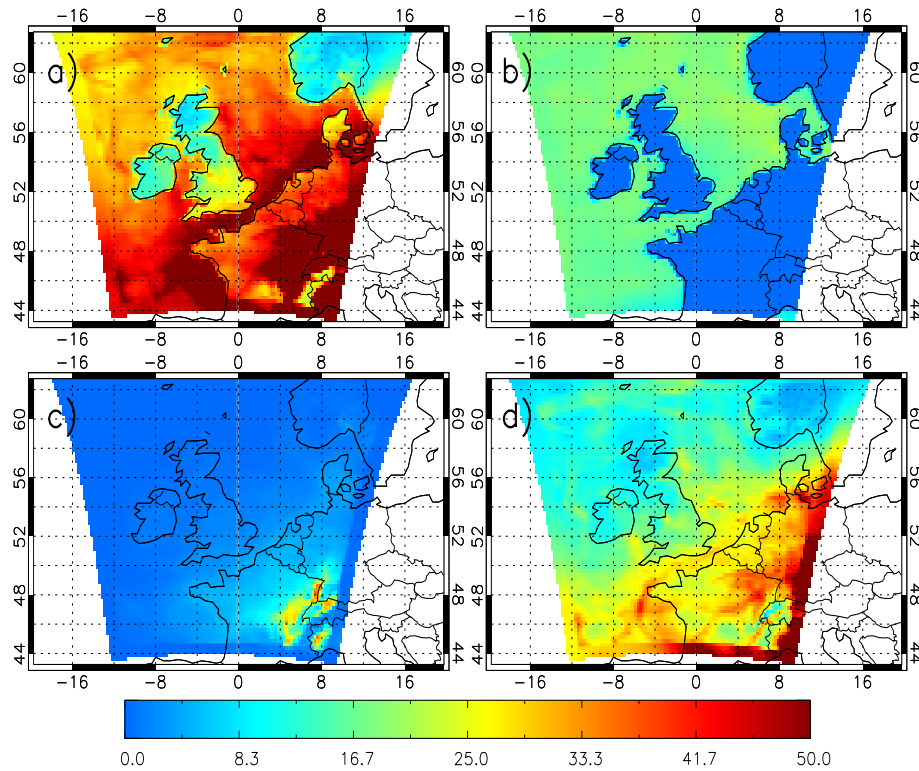
Figure 4.3: AQUM aerosol surface area ($\times 10^{-7}$ cm^2/cm^3) for JFM 2006 of a) total aerosol, b) sea salt, c) ammonium nitrate and d) ammonium sulphate.

aerosol is often not used in the AQUM operational forecasts as it results in overestimation of PM$_{10}$. Therefore, there is a strong land-sea mask in this aerosol type resulting in lower aerosol surface area over the UK. When looking at the ammonium nitrate, the aerosol surface area is low compared with other types except for either side of the Alps, 25×10^{-7} cm^2/cm^3. The ammonium sulphate surface area is the largest component of the total aerosol surface area, but restrained to continental Europe, 30-50 $\times 10^{-7}$ cm^2/cm^3. We suspect that lower UK emissions of ammonium sulphate precursor gases, compared with the rest of Europe, mean the total aerosol surface area is lower here. Also, ammonium nitrate and ammonium sulphate have similar continental emissions, but since ammonium sulphate is much more hydroscopic, the surface area is larger. Barnaba and Gobbi (2001) used lidar measurements to look at marine and dust aerosol properties. They present the aerosol surface area between 10^{-9} and 10^{-4} cm^2/cm^3. Even though this is a different region to Europe, the magnitude of the aerosol surface area gives me confidence that the AQUM diagnostic is reasonable. Therefore, from Figure 4.3 and Barnaba and Gobbi (2001), the total aerosol surface area looks reasonable and we use these fields to calculate the loss of N$_2$O$_5$ on aerosol.

Table 4.2 summarises the effects of heterogeneous chemistry on NO$_x$, NO$_y$ and NO$_z$ at the surface, 180 and 1000 metres. AQUM NO$_y$ includes NO, NO$_2$, NO$_3$, N$_2$O$_5$, HNO$_3$,

HO$_2$NO$_2$, PAN, ISON, ORGNIT, RNC$_2$H$_4$ and RNC$_3$H$_6$. The control (γ=0.0) and exper-
iment (γ=0.001 & 0.02) runs had no aerosol radiative feedbacks so any changes in AQUM
aerosols due to the heterogeneous processes will not alter the meteorology. Therefore,
comparisons between the control and the experiments will only be looking at the influence
of the heterogeneous losses and not indirect feedbacks on meteorology. AQUM column
NO$_2$ was also compared with OMI using the standard model and including heterogeneous
chemistry with γ= 0.001 and γ=0.02, thus providing a test with aerosol radiative feed-
backs switched on. This study found that over a longer time period average (more than a
few days), the aerosol radiative feedback has little feedback on the chemistry (not shown
here). The effect of the heterogeneous chemistry on AQUM column NO$_2$ improves the
JFM comparisons with OMI, again not shown here for JMF 2006, as is discussed later
using the GEMS LBCs in winter 2006 (Section 4.5.4).

4.5 Results

4.5.1 Control

Figures 4.4 and 4.6 show seasonal composites of OMI and SCIAMACHY column NO$_2$ and
the AQUM equivalent. In summer, Figure 4.4c, OMI column NO$_2$ ranges between 16-20
$\times10^{15}$ molecules/cm^2 over London and 10-15 $\times10^{15}$ molecules/cm^2 over northern England
and the Benelux region. The background state ranges between 4-8 $\times10^{15}$ molecules/cm^2
over the UK and 0-3 over the sea. In winter (Figure 4.4d) the background state has a
larger spatial extent ranging between 6-11 $\times10^{15}$ molecules/cm^2. UK source region column
NO$_2$ is reduced to 9-14 $\times10^{15}$ molecules/cm^2 due to winter time dynamics (see Chapter 6
and Pope et al. (2014a)), while Benelux column NO$_2$ rises to 12-20 $\times10^{15}$ molecules/cm^2
from higher emissions. SCIAMACHY column NO$_2$ in both seasons, Figure 4.6c & 4.6d,
has similar spatial patterns to OMI, however, the concentrations are higher. In summer,
source region column NO$_2$ ranges between 16-20 $\times10^{15}$ molecules/cm^2 across the UK
and Benelux region; not just London. In winter, UK source region column NO$_2$ ranges
between 16-20 $\times10^{15}$ molecules/cm^2 with a larger spatial extent. Over the Benelux region
and western Germany column NO$_2$ is larger, again due to increased emissions, between
15-25 $\times10^{15}$ molecules/cm^2.

The SCIAMACHY overpass time coincides with high NO$_x$ emissions from morning
rush hour traffic. Boersma et al. (2008b) compared global OMI and SCIAMACHY ob-
servations for August 2006 and found that over the source regions that SCIAMACHY
observed 40% more column NO$_2$. This implies that SCIAMACHY retrievals are higher in
regions of morning rush hour traffic as more NO$_2$ and NO are emitted. The higher levels
of NO can react with O$_3$ to form more NO$_2$ indirectly. At the OMI midday overpass time,
photochemical loss of NO$_2$ is faster and loss through reaction with OH will increase as OH
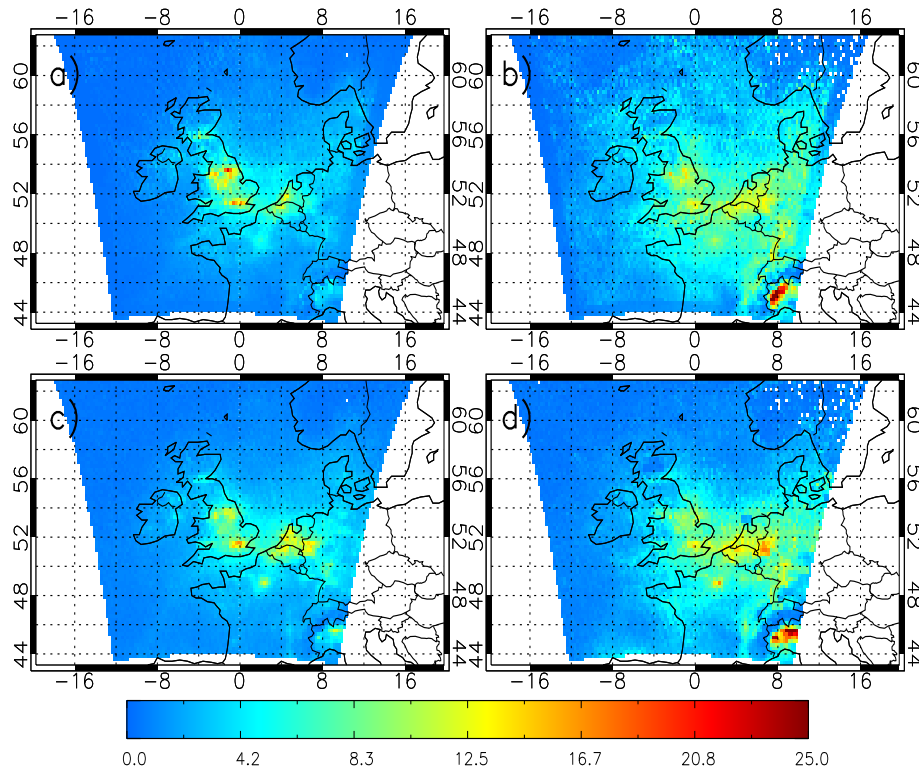
Figure 4.4: Tropospheric NO_2 column ($\times 10^{15}$ molecules/cm^2) for 2006 of (a) AQUM Run C (with averaging kernels (AK) applied) summer, (b) AQUM Run C (with AKs applied) winter, (c) OMI summer and (d) OMI winter.

concentrations peak around midday. The transport of NO_x away from source regions by midday will also have an impact on the levels of NO_2 observed. Boersma et al. (2008b) investigated if retrieval differences could account for the observed column variations by investigating the retrieved slant columns and AMFs. However, they found that the retrieval differences were not a retrieval artefact as the differences in the slant columns were down to spectral fitting and the AMF differences were small.

Figure 4.4 also compares observed column NO_2 with the AQUM control Run C (with AKs applied). The AQUM and OMI averages have similar spatial patterns, with maximum and minimum column NO_2 over the urban and rural/ocean regions, respectively. In summer, AQUM and OMI background concentrations are around 0-3 $\times 10^{15}$ molecules/cm^2. While OMI sees peak column NO_2 of 16-20 $\times 10^{15}$ molecules/cm^2 over London, AQUM simulates peak concentrations are over northern England at over 20 $\times 10^{15}$ molecules/cm^2. However, AQUM London column NO_2 is similar to that of OMI. In winter, the background column NO_2 has larger spatial coverage and concentrations in AQUM, as well as OMI, ranging between 0-6 $\times 10^{15}$ molecules/cm^2. However, the spatial extent of AQUM background column NO_2 is larger than that of OMI. Over London, AQUM and OMI column NO_2 ranges between 12-13 $\times 10^{15}$ molecules/cm^2. However, AQUM peak column NO_2 is
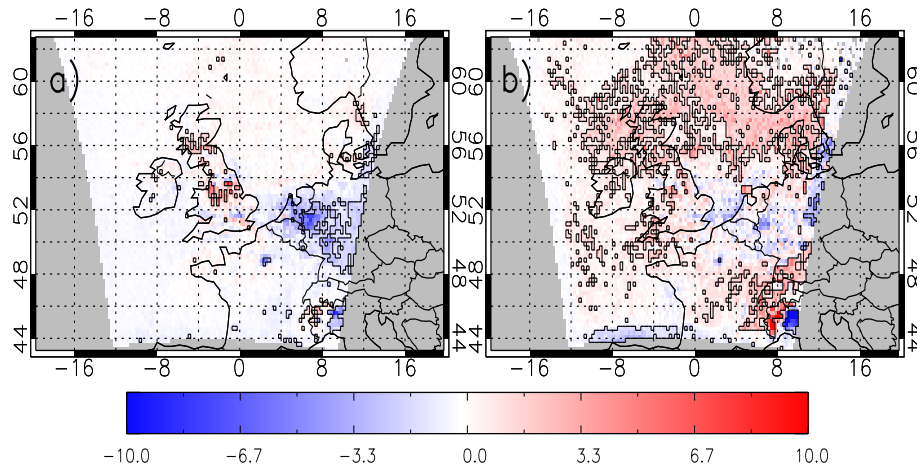
Figure 4.5: Mean bias in tropospheric NO$_2$ column ($\times 10^{15}$ molecules/cm^2) for 2006 between AQUM Run C (with AKs applied) and OMI for (a) summer (RMSE=3.68$\times 10^{15}$ molecules/cm^2 and FGE=0.65) and (b) winter (5.12$\times 10^{15}$ molecules/cm^2 and FGE=0.63). The RMSE and FGE are over the UK between 8°W-2°E and 50-60°N and black polygoned regions show significant differences. Also the same for other mean bias plots below in this chapter.

over northern England at 12-16 $\times 10^{15}$ molecules/cm^2. Therefore, independent of season, AQUM overestimates northern England column NO$_2$.

Figure 4.5 shows the MB in AQUM Run C versus OMI. The black polygoned regions show significant differences, i.e. where the magnitude of the MB is greater than the satellite error. In summer, there are significant positive, 5-10 $\times 10^{15}$ molecules/cm^2, and negative, -10 to -1 $\times 10^{15}$ molecules/cm^2, biases in northern England and the Benelux region, respectively. The negative biases are potentially linked to the coarser resolution EMEP NO$_x$ emissions datasets (50 km $\times$ 50 km) which average emissions over a larger grid square causing AQUM to simulate lower column NO$_2$ than seen by OMI. I hypothesise that the northern England biases are linked to the point source (power station) NO$_x$ emissions from the NAEI. This is further discussed in Section 4.5.3. In winter, AQUM overestimates OMI by 1-3 $\times 10^{15}$ molecules/cm^2 over the North Sea and Scotland, as the modelled winter background column NO$_2$ is larger; this is further investigated in Section 4.5.4 by including an additional NO$_x$ sink in the chemistry scheme of the model. The northern England biases seen in summer also extend to winter, 3-5 $\times 10^{15}$ molecules/cm^2, suggesting the northern England biases are annual instead of seasonal. Finally, the large bias dipole in the Po Valley appears to be related to the LBCs or the winter emissions, as summer biases are small here.

AQUM column NO$_2$, sampled at the SCIAMACHY 10.30 LT overpass time and interpolated onto a 0.5° x 0.5° grid resolution, is reduced through averaging over a coarser grid. Therefore, AQUM column NO$_2$ over London and northern England in
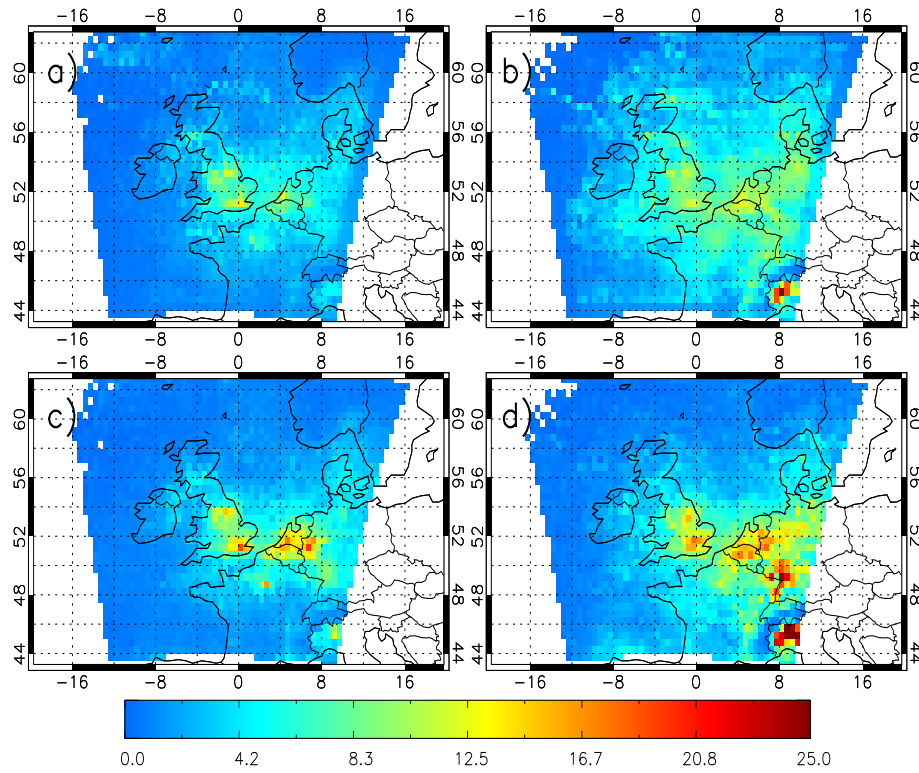
Figure 4.6: Tropospheric NO_2 column ($\times 10^{15}$ molecules/cm^2) for 2006 of (a) AQUM Run C (with AKs applied) summer, (b) AQUM Run C (with AKs applied) winter, (c) SCIAMACHY summer and (d) SCIAMACHY winter.
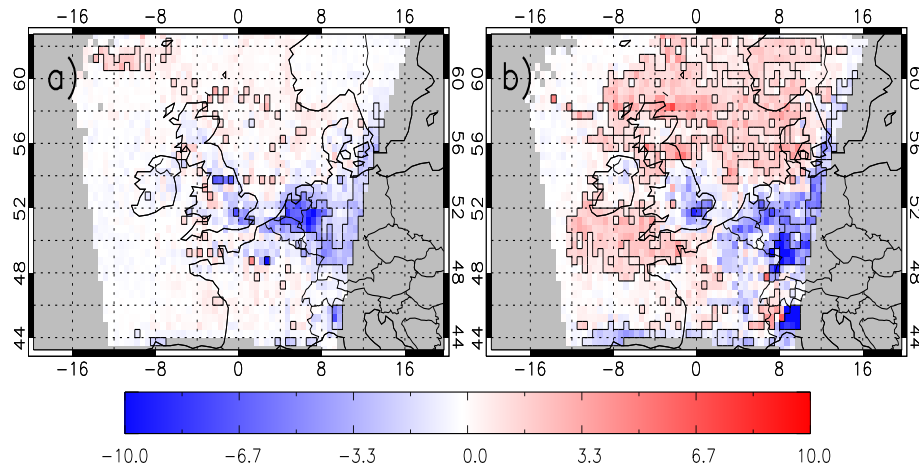
Figure 4.7: Mean bias in tropospheric NO_2 column ($\times 10^{15}$ molecules/cm^2) for 2006 between AQUM Run C (with AKs applied) and SCIAMACHY for (a) summer (RMSE=4.55$\times 10^{15}$ molecules/cm^2 and FGE=0.63) and (b) winter (6.77$\times 10^{15}$ molecules/cm^2 and FGE=0.70).

summer is 12-15 $\times 10^{15}$ molecules/cm^2 (Figure 4.6) while over 20 $\times 10^{15}$ molecules/cm^2 on the higher grid resolution. In winter, the AQUM, like in the OMI comparisons, has

larger background column NO$_2$ and spatial extent between 0-7 $\times 10^{15}$ molecules/cm^2. In
the SCIAMACHY winter average, the background column NO$_2$ range from 0-5 $\times 10^{15}$
molecules/cm^2. The peak AQUM regions, northern England and London, are approxi-
mately 12 $\times 10^{15}$ molecules/cm^2, while peak SCIAMACHY column NO$_2$ is significantly
higher at 16-20 $\times 10^{15}$ molecules/cm^2 (over 25 $\times 10^{15}$ molecules/cm^2 in the Po Valley).

In Figure 4.7, the summer AQUM - SCIAMACHY MB shows near zero background
column NO$_2$ biases, similar to the AQUM - OMI MB. The continental Europe negative
biases are consistent with OMI (4.5) ranging between -5 and 0 $\times 10^{15}$ molecules/cm^2.
Again these biases are potentially linked to the coarser EMEP emissions. However, while
AQUM overestimates OMI column NO$_2$ over London and northern England, AQUM un-
derestimates SCIAMACHY columns there by -10 to -3 $\times 10^{15}$ molecules/cm^2. This has
not been explored extensively, but this study suggests that the coarser SCIAMACHY grid,
the different instrument overpass times or the instruments biases might be the cause.

However, a closer look at the application of the SCIAMACHY AKs to the AQUM data
(not shown here) resulted in a summer decrease of 2-3 $\times 10^{15}$ molecules/cm^2 over north-
ern England. This potentially implies reduced SCIAMACHY sensitivity over the region.
Summer 2006 AQUM column NO$_2$ sampled at 10.30 and 13.00 LT on its native grid shows
that it is higher over the majority of the UK at 10.30 LT. However, over northern England,
13.00 LT column NO$_2$ is higher by 1-2 $\times 10^{15}$ molecules/cm^2. Therefore, the representation
of NO$_x$ emission in the AQUM in the region may be leading to different biases rather than
instruments biases. In the winter (Figure 4.7), the AQUM-SCIAMACHY MB domain is
dominated by positive biases, 3-5 $\times 10^{15}$ molecules/cm^2, similar to the OMI comparisons.
However, there are significant negative biases, -10 to -3 $\times 10^{15}$ molecules/cm^2, over the
continental Europe, again, possibly due to coarser European emissions.

To further evaluate AQUM, the AURN data were gridded, 0.25° x 0.25° longitudinally
and latitudinally, and sampled at 13.00 LT to determine if the model biases versus AURN
and OMI NO$_2$ were consistent spatially. The gridded AURN data attempts to provide
more representative comparisons to AQUM as point and area comparisons will introduce
systematic biases. It also attempts to increase the spatial coverage of the AURN data.
However, there are cases where there is only one AURN site in a grid cell. In summer
(Figure 4.8c), peak, approximately 40 μg/m^3, and minima, under 15 μg/m^3, AURN NO$_2$
occur over London and the rural regions (East Anglia and Wales), respectively. The
AQUM surface NO$_2$ concentrations (Figure 4.8a) are lower with peak concentrations over
London of 15-20 μg/m^3 and 0-13 μg/m^3 over the rest of the UK. In winter (Figure 4.8d),
AURN NO$_2$ peaks at over 50 μg/m^3 in London and between 40-50 μg/m^3 in parts of
northern England. Winter AQUM surface NO$_2$ concentrations increase by approximately
5 μg/m^3 over the majority of the domain.

Figure 4.8: Surface NO$_2$ (μg/m^3) for 2006 of (a) AQUM Run C summer, (b) AQUM Run C winter, (c) AURN summer and (d) AURN winter.

Figure 4.9: Surface NO$_2$ (μg/m^3) AQUM Run C - AURN mean bias for 2006 of (a) summer and (b) winter. AQUM - AURN MNMB and FGE for (c) summer and (d) winter.

AQUM underestimates surface NO$_2$ in both seasons. Significant (95% confidence level using the student t-test) negative biases under -20 μg/m^3 range across the UK (Figures 4.9a

Figure 4.10: Surface O_3 (μg/m^3) for 2006 of (a) AQUM Run C summer, (b) AQUM Run C winter, (c) AURN summer and (d) AURN winter.
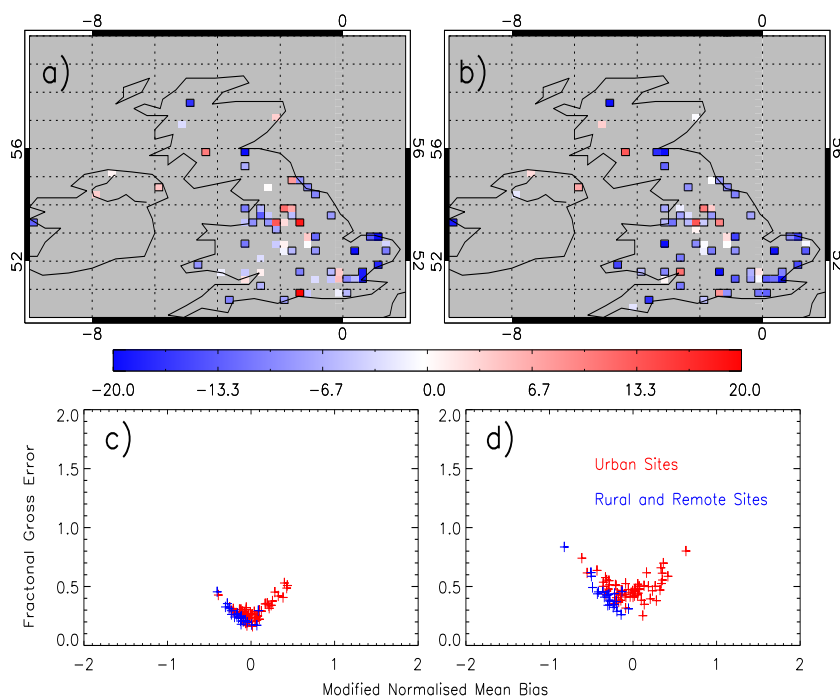
Figure 4.11: Surface O_3 (μg/m^3) AQUM Run C - AURN mean bias for 2006 of (a) summer and (b) winter. AQUM - AURN MNMB and FGE for (c) summer and (d) winter.

& 4.9b). Significant biases are highlighted by polygoned areas. This is similar to Savage et al. (2013) who state AQUM underestimates the urban AURN data due to its coarse

12 km $\times$ 12 km resolution, where NO_x emissions are averaged out over the Eulerian grid. AURN rural NO_x are prone to overestimation of NO_2 as its molybdenum converters suffer from inferences due to NO_z (Steinbacher et al., 2007), which may degrade comparisons. The MNMB vs. FGE comparisons in Figure 4.9c & 4.9d are where the AQUM is sampled to the closest AURN site. For winter and summer the MNMB plotted against FGE shows that at urban sites the AQUM underestimates AURN with negative biases between 0 to -2 and FGE between 0-2. Rural comparisons are prone to smaller magnitude positive biases, especially in winter, between 0-0.5 and 0-1 for the MNMB and FGE, similar to Savage et al. (2013).

Both AQUM and AURN summer O_3 peak over South East England at approximately 70 and 100 μg/m^3, respectively (Figure 4.10a & 4.10c). Over the rest of the UK AQUM and AURN agree. In winter (Figure 4.10d & 4.10b), the AURN and AQUM O_3 concentrations are lower ranging between 25-55 μg/m^3 across the UK. The summer MB (Figure 4.11a) shows that the AQUM significantly underestimates surface O_3 at multiple locations across the UK by 10 μg/m^3, but by 10-20 μg/m^3 over South East England. The winter MB pattern is similar but more extensive. Typically, AQUM underestimates rural sites with MNMB and FGE between -0.5 to 0 and 0-0.5 in summer. However, there are larger biases and errors in winter. At urban sites (Figure 4.11c & 4.11d), AQUM overestimates O_3 with a summer (winter) MNMB and FGE of 0-0.5 (0-0.5) and 0-1.0 (0-1.0), respectively. Therefore, not enough O_3 is lost in urban regions and could partially account for AQUM's underestimation of urban NO_2 as destroyed O_3 leads to the formation of NO_2.

4.5.2 Lateral Boundary Conditions

Figure 4.12 shows results of the sensitivity run with the MACC boundary conditions (Run MACC) versus OMI which can be compared with Figure 4.5. The MACC LBCs have a limited impact on summer column NO_2 with peak concentrations over London and northern England between 15-20 $\times 10^5$ molecules/cm^2 for both runs MACC and C. However, in winter Run MACC increases column NO_2 from approximately 12×10^{15} to 16×10^{15} molecules/cm^2 over the UK and Benelux region. When compared with OMI the limited summer impact of the MACC LBCs (Figure 4.12c) results in biases which are similar to those in Figure 4.5a from the control run, with biases over northern England, 5-10 $\times 10^5$ molecules/cm^2, and continental Europe, -5 to -3 $\times 10^5$ molecules/cm^2. In winter Run MACC has enhanced column NO_2 resulting in biases with OMI of between 2-5 $\times 10^5$ molecules/cm^2 across the whole domain, unlike Run C with GEMS LBCs in Figure 4.5b. The peak positive biases of 5 $\times 10^5$ molecules/cm^2 are again over northern England (and the Po Valley) suggesting that AQUM overestimates NO_2 in the region, at the OMI overpass time, independent of season or LBCs. Therefore, the GEMs LBCs appear to give
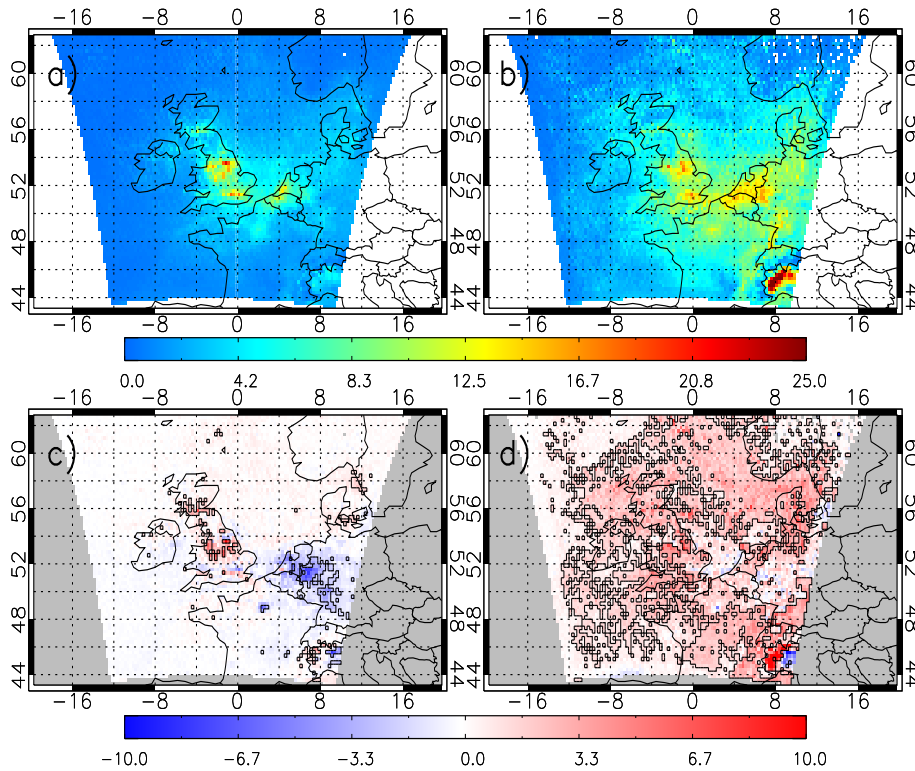
Figure 4.12: Tropospheric column NO_2 ($\times 10^{15}$ molecules/cm^2) for 2006 from AQUM Run MACC (AKs applied) for (a) summer and (b) winter. AQUM Run MACC (AKs applied) and OMI mean bias for (c) summer (RMSE=3.74×10^{15} molecules/cm^2 and FGE=0.63) and (d) winter (RMSE=6.00×10^{15} molecules/cm^2 and FGE=0.65).

better AQUM column NO_2 forecast skill than MACC does, which is consistent with the findings of Savage et al. (2013) for the comparisons with surface ozone.

Figure 4.13 shows Run MACC column NO_2 sampled at 10.30 LT versus SCIAMACHY. There are increases in both summer and winter NO_2 columns when compared with Run C. The summer field increases slightly by approximately 1-2 $\times10^5$ molecules/cm^2 over the source regions. In winter, peak column NO_2 increases occur over source regions as well, but from 10 $\times10^5$ molecules/cm^2 to 12-16 $\times10^5$ molecules/cm^2. The background concentrations increase also by 1-2 $\times10^5$ molecules/cm^2, especially over the ocean. The Run MACC - SCIAMACHY MBs, Figure 4.13c, do not significantly change in summer over the UK. However, the significant London and continental Europe negative biases seen in Run C (Figure 4.7a), under -5 $\times10^5$ molecules/cm^2 have reduced in magnitude and spatially. In winter, significant positive biases seen from Run C (Figure 4.7b), have spread across the majority of the domain ranging between 3-5 $\times10^5$ molecules/cm^2.

Run MACC shows similar impacts on the surface AQUM NO_2 to that of column NO_2. In summer (Figure 4.14a), surface NO_2 from Run C to Run MACC increases by 1-2 μg/m^3 over the source regions. However, the winter AQUM concentrations increase
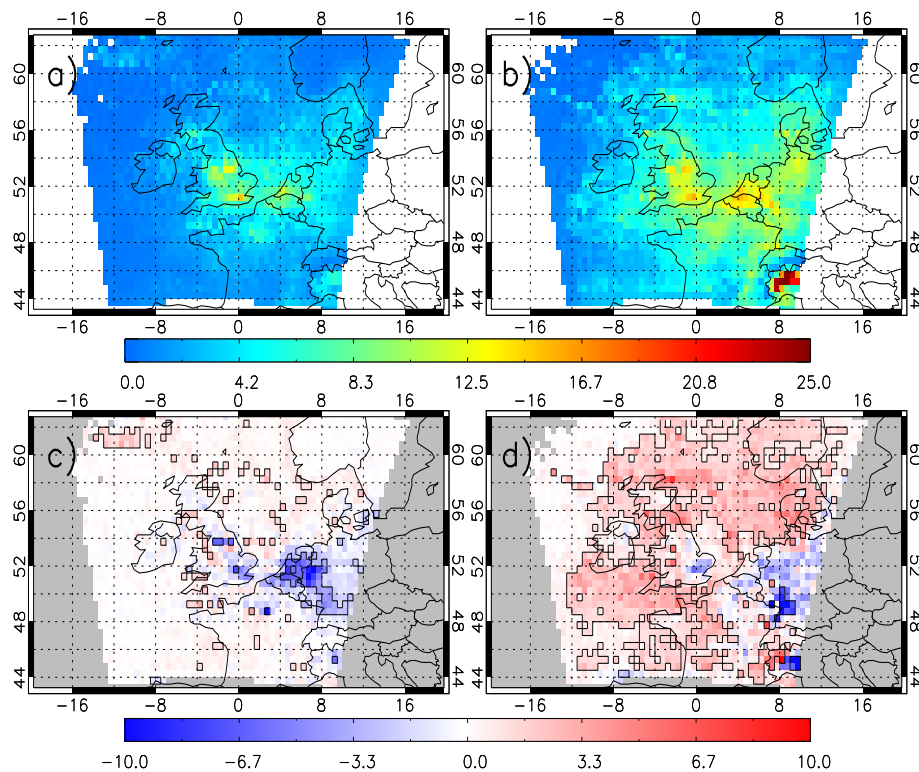
Figure 4.13: Tropospheric column NO_2 ($\times 10^{15}$ molecules/cm^2) for 2006 from AQUM Run MACC (AKs applied) for (a) summer and (b) winter. AQUM Run MACC (AKs applied) and SCIAMACHY mean bias for (c) summer (RMSE=4.51$\times 10^{15}$ molecules/cm^2 and FGE=0.60) and (d) winter (RMSE=6.83$\times 10^{15}$ molecules/cm^2 and FGE=0.70).

by approximately 5-10 μg/m^3, Figure 4.14b. Figure 4.15b highlights this as the AQUM underestimation of AURN winter NO_2 improves from -35 to -15 to -25 to -10 μg/m^3 over the urban regions. However, the surface NO_2 MNMB-FGE values do not vary significantly from Run MACC for either season.

In summer and winter, Run MACC simulates elevated surface O_3 in comparison to Run C by 20-40 μg/m^3 across the full domain (Figure 4.16a & 4.16b). Figure 4.17 highlights this as winter/summer Run MACC - AURN biases increase to over 20 μg/m^3. Savage et al. (2013) found similar results when they compared AQUM with the AURN Yarwood site for 2006. AQUM with GEMS LBCs struggled to reproduce the spring time O_3 peak seen in the observations. AQUM, using the MACC LBCs, correctly predicted the spring time maxima, but from June onwards AQUM-GEMS more accurately captures the Yarwood annual cycle. For the rest of the year AQUM-MACC is offset by approximately 20-30 μg/m^3. In Figure 4.11, for summer and winter, Run C underestimates and overestimates rural and urban O_3. However, Run MACC (Figure 4.17c & 4.17d) overestimates both rural and urban O_3 concentrations where the rural and urban MNMB (FGE) ranges from 0-0.5 (0-0.5) and 0-1 (0-1), respectively, in both seasons.
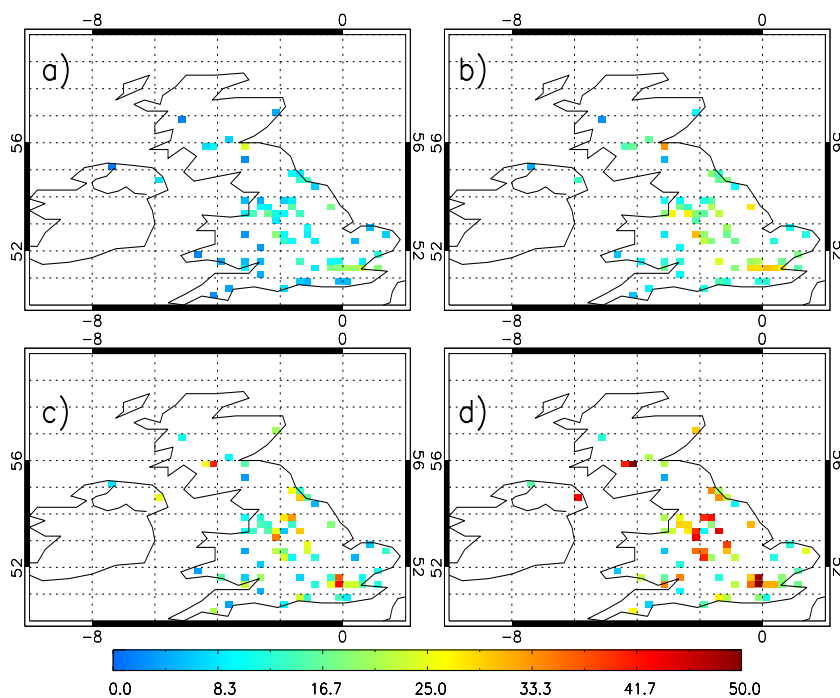
Figure 4.14: Surface NO$_2$ (μg/m^3) for 2006 of (a) AQUM Run MACC summer, (b) AQUM Run MACC winter, (c) AURN summer and (d) AURN winter.
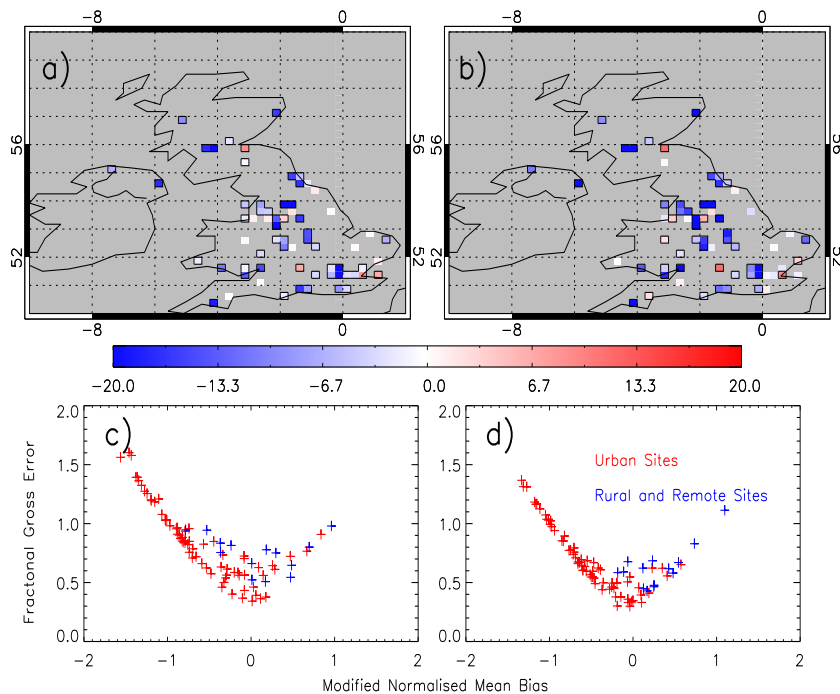
Figure 4.15: Surface NO$_2$ (μg/m^3) AQUM Run MACC - AURN mean bias for 2006 of (a) summer and (b) winter. AQUM - AURN MNMB and FGE for (c) summer and (d) winter.
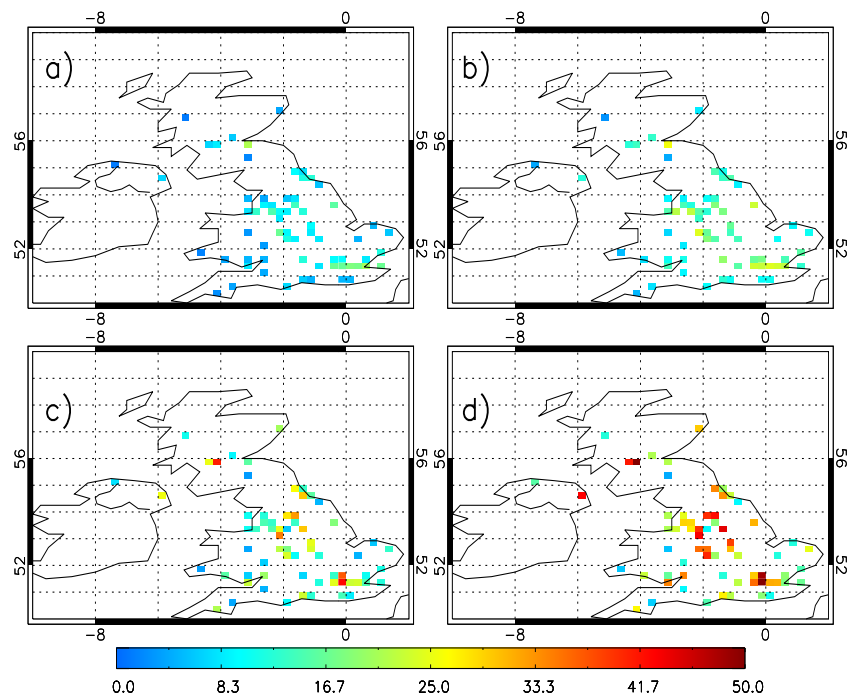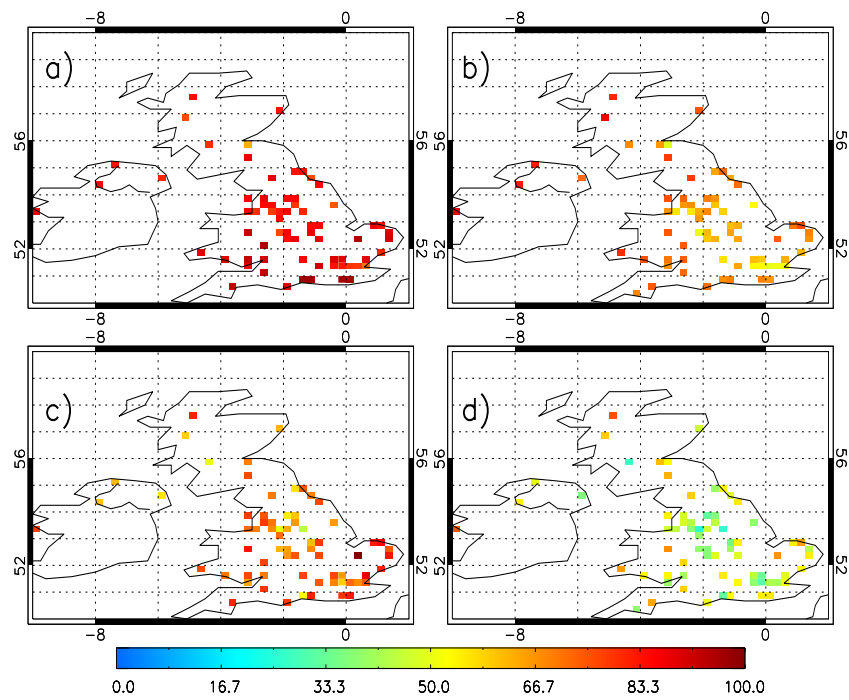
Figure 4.16: Surface O$_3$ (μg/m^3) for 2006 of (a) AQUM Run MACC summer, (b) AQUM Run MACC winter, (c) AURN summer and (d) AURN winter.
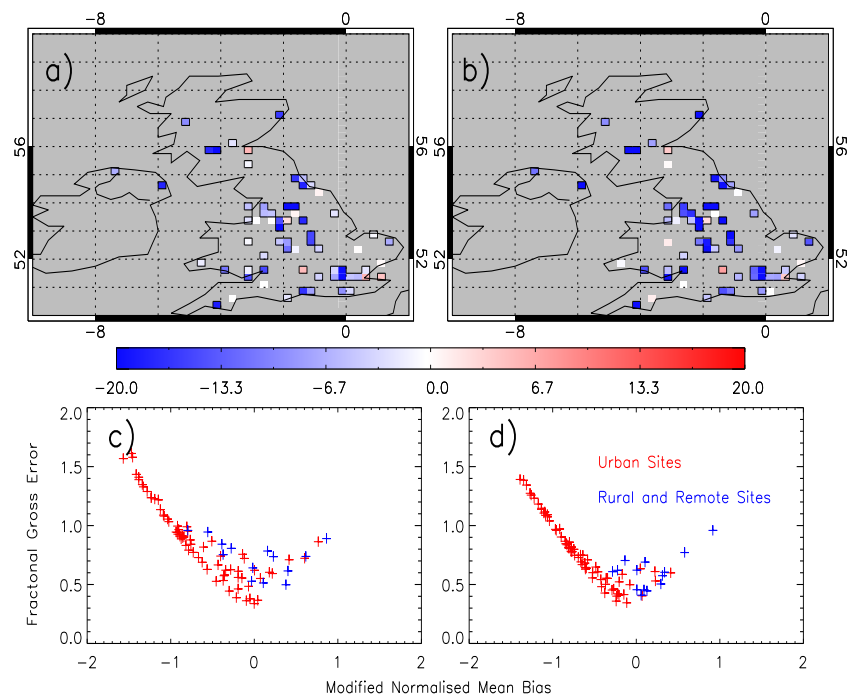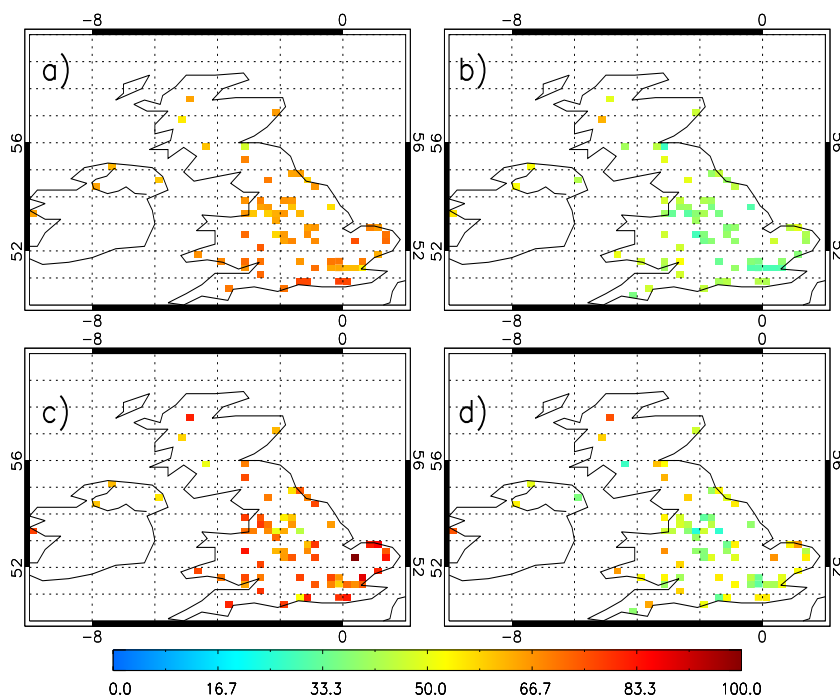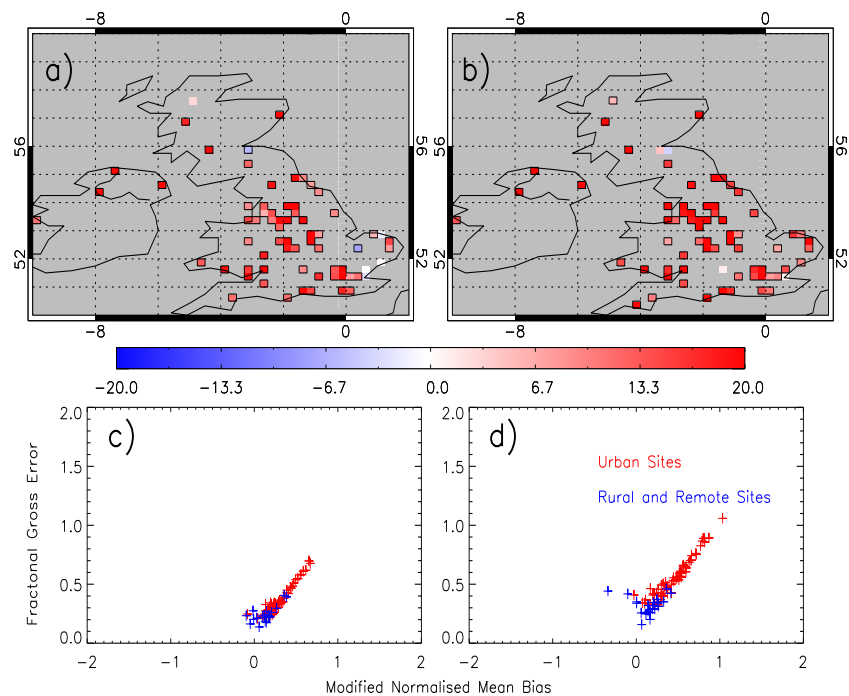

Figure 4.17: Surface O$_3$ (μg/m^3) AQUM Run MACC - AURN mean bias for 2006 of (a) summer and (b) winter. AQUM - AURN MNMB and FGE for (c) summer and (d) winter.

4.5.3   Emissions Sensitivity Experiments

The hypothesis that significant summer Run C - OMI positive biases in northern England
and Scotland (Figure 4.5a) are caused by errors in AQUM's representation of point source
(mainly power station) NO$_x$ emissions is tested in this section. To better understand these
biases, sensitivity experiments for June-July-August (JJA) on NO$_x$ emissions (Table 4.1)
2006 have been carried out. Figure 4.18a shows JJA Run C - OMI positive biases and
acts as the baseline to compare the sensitivity experiments too.
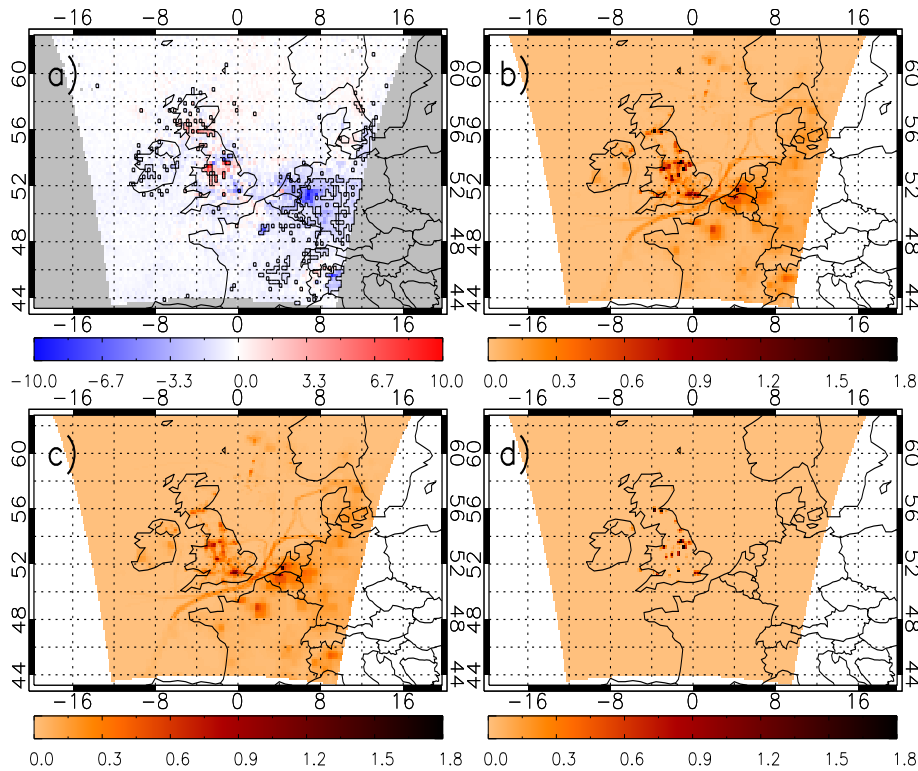
Figure 4.18: a) AQUM Run C (AKs applied) - OMI tropospheric NO$_2$ column ($\times 10^{15}$
molecules/cm^2) JJA 2006 mean bias. These are the control MBs to compare to the point
source sensitivity experiments (RMSE = 3.64 $\times 10^{15}$ molecules/cm^2 and FGE = 0.66).
NO$_x$ emissions ($\times 10^{-9}$ kg/m^2/s), JJA 2006, used in AQUM for (b) Run C and (c) Run
E1. Panel (d) shows the difference between panels (b) and (c).

Figure 4.18b, c & d shows the JJA AQUM NO$_x$ emissions for runs C and E1 (with
point sources removed) and their difference. The peak Run C NO$_x$ emissions are over 1.8
$\times 10^9$ kg/m^2/s. The peak differences between the emissions are over 1.8 $\times 10^9$ kg/m^2/s in
point source locations, showing that they make up significant part of the emissions budget
in certain areas.

Figure 4.19a & 4.19b show the impact on NO$_2$ columns of removing point sources.
Column NO$_2$ over northern England reduces from 15-25 $\times 10^5$ molecules/cm^2 to 4-5 $\times 10^5$
molecules/cm^2. The Run E1 - OMI MB now ranges between -10 to -6 $\times 10^5$ molecules/cm^2,

while the Run C - OMI MB (Figure 4.18a) is between 6-10 $\times 10^5$ molecules/cm^2. Therefore, the switch in sign of the biases, of similar magnitude, indicates that the point source emissions play a significant role in the AQUM column NO$_2$ budget.
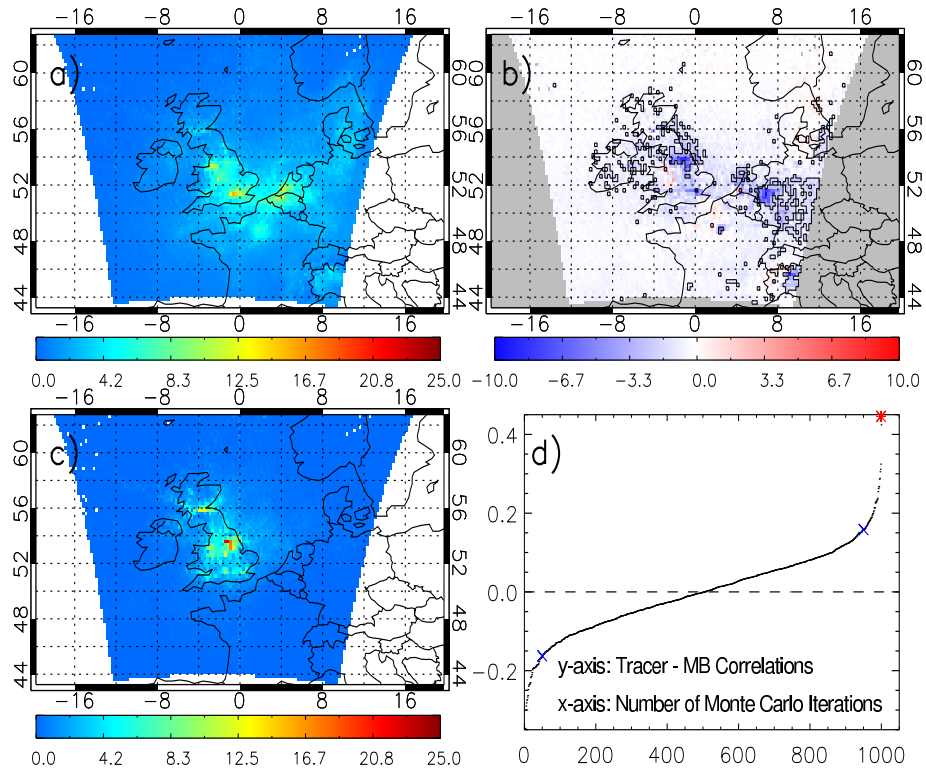
Figure 4.19: Tropospheric column ($\times 10^{15}$ molecules/cm^2) for JJA 2006 of (a) AQUM Run E1 NO$_2$ (AKs applied), (b) AQUM Run E1 NO$_2$ (AKs applied) - OMI (RMSE=3.02$\times 10^{15}$ molecules/cm^2 and FGE=0.68) and (c) AQUM Run E2 Tracer (AKs applied). (d) Peak Run E2 and co-located Run C-OMI MB correlation (red star) significance distribution. Black dots are Run E2 and random Run C-OMI MB correlations. Blue X=5th and 95th percentiles of the 1000 size sample.

Run E2 aimed to test whether the point sources were responsible for the positive biases in Figure 4.18a by using an idealised (non-reacting) tracer of the power station emissions. Here the tracer emissions are equal to that of the point source NO$_x$ emissions. Figure 4.19c shows the JJA tracer column with the OMI AKs applied, where peak columns range around 16-20 $\times 10^5$ molecules/cm^2 over northern England. Figures 4.18a and 4.19c suggest that the peak tracer columns overlap with the large Run C - OMI positive biases. The correlation between the largest 100 tracer column pixels in Figure 4.19c and the MB over the same locations in Figure 4.18a, is 0.45. To test the statistical significance of this correlation, a Monte-Carlo approach has been used. A random sample of 100 of the land-based MB pixels (land bias pixels only are used as the biases in Figure 4.18a are over land) were correlated against the largest 100 tracer sample. This was repeated 1000 times

and then sorted from lowest to highest. The 5th and 95th percentiles of the correlation distribution were calculated to be -0.162 and 0.158, respectively. If the point sources are responsible for the peak Run C - OMI biases, then the peak tracer concentrations, which represent the point source emissions, should be in the same location as the peak biases. Since 0.45 is above the 95th percentile, this shows that the tracer-MB peak correlation value is significant (it is actually the greatest correlation - see Figure 4.19d). Therefore, AQUM's representation of point source emissions can be linked to the AQUM overestimation of column NO$_2$ in northern England and Scotland.
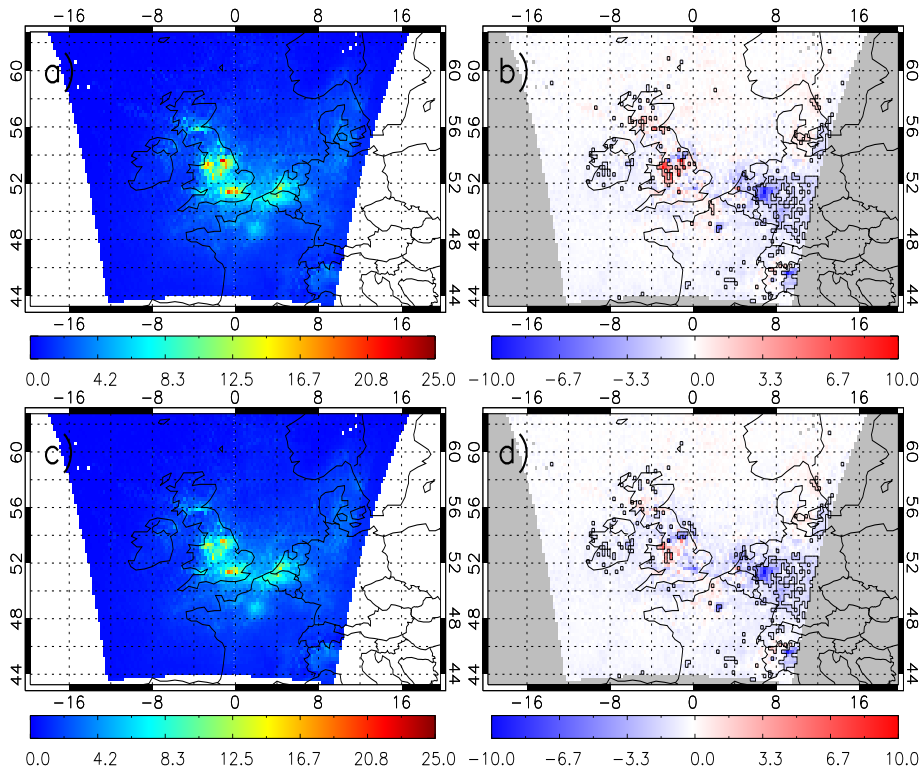
Figure 4.20: Tropospheric column NO$_2$ ($\times 10^5$ molecules/cm^2) for JJA 2006 of (a) AQUM Run E3 and (c) AQUM Run E4. AQUM - OMI MB for (b) Run E3 (RMSE=3.51$\times 10^5$ molecules/cm^2 and FGE=0.66) and (d) Run E4 (RMSE=3.15$\times 10^5$ molecules/cm^2 and FGE=0.66).

Having found a significant positive correlation, to the 95% confidence level, between the column tracer and AQUM - OMI JJA positive biases, Run E3 split the emissions into point and area sources. The point sources were emitted at 1 km to better represent power station stack height and plume buoyancy, and area sources were entered at the surface. In Figure 4.20a, the peak column NO$_2$ still resides over northern England and London, between 20-25 $\times 10^5$ molecules/cm^2; similar to Run C JJA (Figure 4.18a). However, Run E3 appears to reduce the comparison skill in places as several more pixels become significantly biased between 5-10 $\times 10^5$ molecules/cm^2 (Figure 4.20b). The comparisons in

Scotland improve though, with a reduction in the number of significantly different pixels. Overall, the change in emissions does improve the comparisons as the UK RMSE (over UK domain 8°W - 2°E and 50-60° N) drops from 3.64×10^5 molecules/cm^2 to 3.51×10^5 molecules/cm^2 and the FGE stays the same.
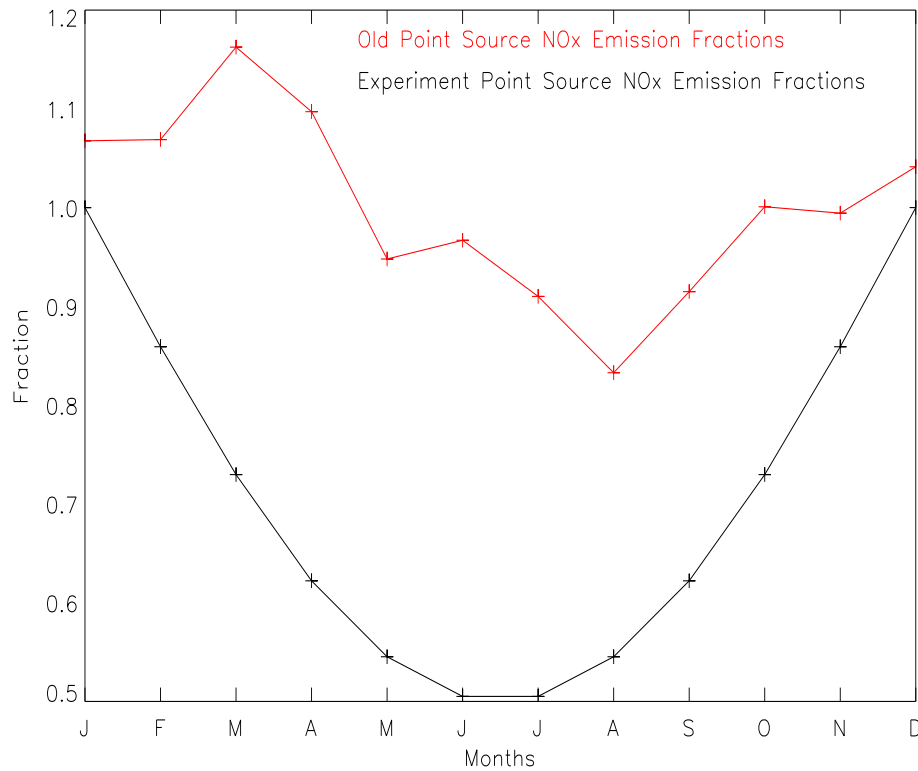
Figure 4.21: Seasonal cycles forced onto the NAEI NO$_x$ emissions; Red is the old seasonal cycle (SC) and black is the experiment based on SC = 1-0.5sin(π(m$_0$....m$_{11}$)/(n-1)), where n = number of months = 12 and m=0,1...n-1.

Run E4 introduces an idealised seasonal cycle into the point sources after removing the initial season cycle, focusing on JJA. Hence we effectively reduce the JJA point source NO$_x$ emissions by 50%. This is seen in Figure 4.21 where the seasonal cycle of the old and Run E4 emission fractions are plotted. Under the original seasonal cycle the fractions, for both area and point sources, range around 0.8-1.0 for JJA, but the Run E4 cycle reduces these fractions to 0.5-0.55 for the point sources. The result (Figure 4.20d) improves the summer comparison where the northern England biases in Figure 4.18a have reduced from 5-10 $\times 10^{15}$ and 3-6 $\times 10^5$ molecules/cm^2 in northern England and Scotland, respectively. The domain RMSE reduces from 3.64 x 10^{15} to 3.15×10^5 molecules/cm^2, while the FGE stays around 0.66. This suggests that the seasonal cycle of the power station emissions in this region is not well captured by the emissions profiles chosen for the AQUM.

Runs E1 - E4 show that the AQUM's representation of point source NO$_x$ emissions is incorrect. The implementation of heterogeneous chemistry, see next section, partially

masks this but there are still some issues. Run E4 shows that reducing the emissions can solve the problem but is unrealistic. I think that the point and area sources, though degrading the comparisons here, should be split, but using more sophisticated methods such as experimenting with the introduction of a stack plume model into the AQUM. This would give better representation of plume buoyancy and emission height. The vertical mixing rate in AQUM could potentially be too slow. This implies that too much NO$_2$ is trapped lower down in the atmosphere, below 1 km, and cannot be more efficiently transported laterally in the free troposphere where horizontal wind speeds are stronger.

4.5.4   N$_2$O$_5$ Heterogeneous Chemistry Sensitivity Experiments

Runs N$_2$O$_5$Low and N$_2$O$_5$High investigate the implementation of N$_2$O$_5$ heterogeneous chemistry with uptake values of $\gamma = 0.001$ and $\gamma = 0.02$. Since AQUM does not include this chemistry as standard, this study investigates whether it will explain either AQUM winter background or summer northern point source positive biases found in Section 4.5.1. Table 4.2 shows the impact of the N$_2$O$_5$ chemistry on the model fields for γ=0.001 and γ=0.02 at night (23.00 LT) and day (13.00 LT) at the surface, 180 and 1000m. At the surface for both times and gamma values the largest losses are in NO$_y$, which is to be expected as NO$_y$ = NO$_x$ + NO$_z$. The average losses of NO$_y$ across the domain are -0.46 (13.00 LT) and -0.50 (23.00 LT) for γ=0.001 and -0.99 (13.00 LT) and -1.32 ppbv (23.00 LT) for $\gamma = 0.02$. The loss of NO$_z$ is greater than NO$_x$ at night as NO$_3$ and N$_2$O$_5$ are taken up on aerosol, which are the loss pathway of NO$_x$. However, at 13.00 LT, when this process is less efficient, the loss of NO$_y$ is dominated by NO$_x$ loss. In all cases, the larger γ value results in more loss of NO$_x$, NO$_y$ and NO$_z$. These patterns are consistent further up in the atmosphere, where larger γ values and night time lead to the largest loss of NO$_y$. Again, during the day NO$_x$ forms the dominant component of NO$_y$ loss, but at night NO$_z$ becomes the dominant loss species. The magnitude of the loss, however, always decreases with height as the aerosol loading decreases with altitude.

Figure 4.22 shows the winter and summer MBs between AQUM (with LBCs from GEMS) and OMI when heterogeneous hydrolysis of N$_2$O$_5$ is implemented in the model with γ=0.001 (Run N$_2$O$_5$Low) and $\gamma = 0.02$ (Run N$_2$O$_5$High). In the Run C summer case (see Figure 4.5a) there are positive northern England and Scotland biases of around 5-10 $\times10^{15}$ molecules/cm^2. I have shown that these positive biases are likely to be linked to AQUM's representation of point source emissions. However, by introducing N$_2$O$_5$ heterogeneous chemistry these positive biases are significantly reduced. In Run N$_2$O$_5$Low (Figure 4.22a) there is some impact on the biases as RMSE decreases from 3.68 $\times10^{15}$ to 3.39 $\times10^{15}$ molecules/cm^2 and FGE also reduces slightly. In Run N$_2$O$_5$High (Figure 4.22c) many of the positive biases over point sources are now insignificant and the RMSE decreases to 3.08 $\times10^{15}$ molecules/cm^2. However, over parts of continental Europe the intensity and

Table 4.2: The average domain bias sensitivity of NO_x, NO_y and NO_z (ppbv) at the surface, 180 m and 1 km to $\gamma = 0.001$ and 0.02 for the reaction of $N_2O_5 + H_2O$ on aerosol. Comparisons are at 13.00 LT (OMI overpass time) and 23.00 LT for JFM 2006. Here the aerosol radiative feedbacks are switched off.

Experiment -	$\gamma = 0.001$		$\gamma = 0.02$	
Control (ppbv)	**13.00 LT**	**23.00 LT**	**13.00 LT**	**23.00 LT**
NO_x **Surface**	-0.45	-0.22	-0.96	-0.60
NO_y **Surface**	-0.46	-0.50	-0.99	-1.32
NO_z **Surface**	-0.01	-0.28	-0.02	-0.72
NO_x **180 m**	-0.42	-0.17	-0.93	-0.44
NO_y **180 m**	-0.43	-0.47	-0.94	-1.25
NO_z **180 m**	-0.00	-0.29	-0.02	-0.81
NO_x **1000 m**	-0.12	-0.05	-0.32	-0.13
NO_y **1000 m**	-0.13	-0.13	-0.35	-0.39
NO_z **1000 m**	-0.01	-0.08	-0.03	-0.27

spread of negative biases has increased, thus suggesting that $\gamma = 0.02$ might be too strong an uptake here. The FGE does go up slightly to 0.67 and it is likely that this is due to the introduction of negative biases over relatively clean or moderately polluted areas (e.g. the Irish Sea and parts of the continent).

Note that the correction of errors of large magnitude (e.g. over point sources) reduces RMSE because this metric penalises the large deviations between the model and the satellite-retrieved columns, while the introduction of errors of low magnitude over less polluted areas might increase the normalised errors given by FGE. The changes at the point source locations are most significant because of the large emissions of NO_x and aerosols suitable for this heterogeneous process to take place. Therefore, we suggest that while AQUM's representation of point sources results in the summer northern England/Scotland positive biases, including N_2O_5 heterogeneous chemistry with $\gamma = 0.02$ will partially account for this. In winter, the positive biases seen in Figure 4.5b, 2-5 $\times 10^{15}$ molecules/cm^2, decrease as γ increases, similarly as found for summer. In Run N_2O_5Low (Figure 4.22b) the spatial spread of significantly positive biases is only partially reduced, resulting in small decreases of RMSE (from 5.12 $\times 10^{15}$ to 5.05 $\times 10^{15}$ molecules/cm^2) and FGE (from 0.63 to 0.62). For Run N_2O_5High (Figure 4.22d) the cluster of significantly positive biases has decreased spatially yielding the best comparisons, with RMSE and FGE values of 4.48 $\times 10^{15}$ molecules/cm^2 and 0.60, respectively.

Overall, the implementation of N_2O_5 heterogeneous chemistry with $\gamma = 0.02$ into AQUM improves the winter and summer comparisons with OMI. Therefore, this process should be included in the operation AQUM, especially for winter. In summer and winter over continental Europe the chemistry with $\gamma = 0.02$ might be too aggressive degrading comparisons
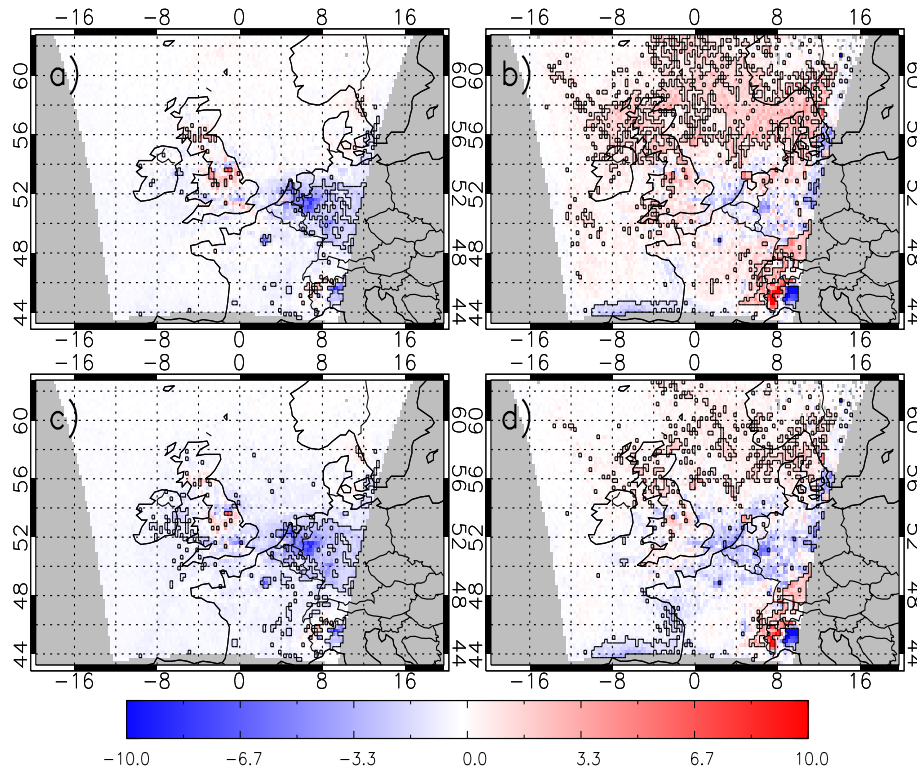
Figure 4.22: MB in tropospheric NO$_2$ column ($\times 10^{15}$ molecules/cm^2) for 2006 between AQUM (AKs applied) - OMI for (a) summer γ=0.001 (RMSE=3.39$\times 10^{15}$ molecules/cm^2 and FGE=0.65), (b) winter γ=0.001 (RMSE=5.05$\times 10^{15}$ molecules/cm^2 and FGE=0.62), (c) summer γ=0.02 (RMSE=3.08$\times 10^{15}$ molecules/cm^2 and FGE=0.67) and (d) winter γ=0.02 (RMSE=4.48$\times 10^{15}$ molecules/cm^2 and FGE=0.60).

here. However, as shown for both OMI and SCIAMACHY, especially for summer, the AQUM control run underestimates column NO$_2$ and I suspect there are significant limitations in the EMEP emission datasets here. Their coarseness will always lead to AQUM underestimation of column NO$_2$ and can be important if European pollution events extend to the UK. Therefore, a new source of emissions datasets (e.g. satellite top-down derived emissions) for continental Europe might be more appropriate in future AQUM emissions datasets.

4.6   Conclusions

This chapter describes the use of OMI satellite observations of column NO$_2$ over the UK to further explore the AQUM performance, extending the previous validation of the model which had only used surface data. In order to do this we have looked in detail at the satellite errors (random, systematic and smoothing) and derived an algorithm which reduces the retrieval random error component when averaging retrievals. This allows more critical AQUM-satellite comparisons as the time average random error component

can be reduced by 30-70% in all seasons. SCIAMACHY and AURN observations have also provided useful insights into the skill of AQUM.

Based on the summer and winter comparisons, the standard (operational) AQUM over-estimates OMI column NO_2 over northern England/Scotland by 5-10 $\times10^{15}$ molecules/cm^2 and over the northern domain by 2-5 $\times10^{15}$ molecules/cm^2, in summer and winter, respectively. Comparisons with SCIAMACHY column NO_2 also show that AQUM overestimates column NO_2 in winter. The use of a different set of lateral boundary conditions (from the MACC reanalysis), which are known to increase AQUM's surface ozone positive bias (Savage et al., 2013), further increases AQUM's overestimate of column NO_2. This increase in AQUM surface ozone is also detected in this study's comparisons using AURN O_3. AQUM column NO_2 is increased, especially in winter, by 2-5 $\times10^{15}$ molecules/cm^2, resulting in poorer comparisons with OMI. Therefore, despite the MACC being the follow-on project to GEMS, the GEMS product provides more realistic fluxes of O_3 through the AQUM boundaries and indirectly, resulting in better AQUM representation of NO_2.

From multiple sensitivity experiments on the UK NO_x point source emissions I conclude that it was AQUM's representation of these emissions which caused the northern England/Scotland summer biases. By emitting an idealised tracer in the NO_x point sources we found a significant correlation of the peak tracer columns to the AQUM - OMI MBs. Finally, introducing N_2O_5 heterogeneous chemistry into AQUM improves the AQUM - OMI comparisons in both seasons. In winter, the spatial extent of positive biases, 2-5 $\times10^{15}$ molecules/cm^2, decreases. In summer, the northern England biases decrease both spatially and in magnitude from 5-10 to 0-5 $\times10^{15}$ molecules/cm^2. Therefore, this suggests that in summer the AQUM's representation of NO_x point sources is inaccurate but can be partially masked by the introduction of N_2O_5 heterogeneous chemistry.

Overall, AQUM treatment of point source NO_x emissions, especially in summer, is inaccurate and needs modifying. Heterogeneous chemistry partially masks this but investigation of new methods to treat these point source emissions is needed. For instance, the experimentation of a stack plume model for AQUM point source emissions at known power station locations. The hydrolysis of N_2O_5 with the reaction of water on aerosol is a standard reaction and an important sink of NO_x. Therefore, this chemistry should be included in the operational AQUM, with an uptake value of 0.02. The NO_x emission over continental Europe are also a concern as comparisons with both satellite instruments showing that AQUM NO_2 here is significantly underestimated. So in the future, as new improved emission datasets become available (e.g. satellite top-down emissions), the coarse EMEP emissions should be replaced.

Chapter 5

Influence of synoptic weather regimes on observed UK air quality

5.1 Introduction

Regional weather exerts a strong influence on local air quality (AQ) through aiding both the accumulation and dispersal of emitted pollutants, and controlling their transport on a regional scale. Models have been developed to predict AQ, but need to be evaluated against observations. Satellite data provide an important source of data for such evaluation, as demonstrated by Huijnen et al. (2010), and greater knowledge of such observations allow for enhanced model development (e.g. detection of an observational seasonal cycle can then improve model representation of such features). This chapter analyses observations of tropospheric trace gases over the UK, to determine the influence of specific climatological patterns of meteorology on regional species distributions.

Multiple studies have investigated the link between atmospheric chemistry and synoptic meteorology using the Lamb Weather Types (LWT) in both an observational and modelling sense. However, most studies have used surface weather station data and the use of the LWTs to investigate synoptic patterns in the satellite atmospheric chemistry data has not been done. LWTs provide a useful tool to classify synoptic meteorology over the UK (Jones et al., 2013). They are a subjective/objective description of the daily midday atmospheric circulation over the UK based on mean sea level pressure reanalysis data. O'Hare and Wilby (1995) used the LWTs to look at synoptic patterns in surface station ozone data across the UK. They found that prevailing LWTs (A, C, W - see Table 5.1) significantly influenced surface ozone, where the A and E regimes lead to enhanced in-situ production of ozone. The N and W regimes resulted in peak ozone concentrations at Mace Head and Dursey because the turbulent mixing associated with these flows enhanced free troposphere ozone incursion at the surface and reduced loss mechanisms.

Table 5.1: The non-bold elements show the 27 basic Lamb Weather Types with their number coding. LWTs also include -1 (unclassified) and -9 (non-existent day). In this work these LWTs are grouped into 3 circulation types and 8 wind directions, indicated in the outer row and column.

This Work	Anticyclonic	Neutral Vorticity	Cyclonic
	0 A		20 C
North-easterly	1 ANE	11 NE	21 CNE
Easterly	2 AE	12 E	22 CE
South-easterly	3 ASE	13 SE	23 CSE
Southerly	4 AS	14 S	24 CS
South-westerly	5 ASW	15 SW	25 CSW
Westerly	6 AW	16 W	26 CW
North-westerly	7 ANW	17 NW	27 CNW
Northerly	8 AN	18 N	28 CN

Lesniok et al. (2010) investigated the influence of air pollution in the region of Upper Silesia in Southern Poland. The authors used a similar weather classification system to the LWTs called the Niedzweidz's Manual Classification. Using the surface station network in the region, Lesniok et al. (2010) made seasonal composites of the different surface chemical data for the different circulation types. Davies et al. (1991) used the LWTs to look at the patterns in anthropogenic ion content of precipitation. They found that the total annual deposition of ions is affected mainly by Cyclonic, Westerly and Anticyclonic LWTs.

Demuzere et al. (2009) used the LWT data and surface ozone data from several sites in the rural Netherlands to investigate the link between air pollution and meteorology on the local and synoptic scales. In JJA, they found that ozone is positively correlated with temperature, negatively correlated with temperature on cloudy days, windspeed and relative humidity. Ozone surface production is often limited in turbulent weather with high windspeed, cloudy weather (reduced photochemical activity) and relative humidity. Clear skies, high pressure and high temperatures are better for ozone production. In DJF, however, surface zone is positively correlated with wind speed and surface pressure as a result of increased tropopause folding, also discussed by O'Hare and Wilby (1995).

Tang et al. (2011) used the LWTs applied to a Synoptic-Regression Model (SRM) to investigate the influence of meteorology on NO_2 concentrations in Gothenberg. The SRM is a combination of circulation and regression based methods, where the circulation information came from the LWTs, for the SRM to predict NO_2 concentrations. The regression method, based on local meteorological variables, reflects the impact of local meteorological conditions. A Multiple Linear Regression model was also used to try and simulate the observations from surface weather stations in Gothenberg. Both models successfully captured the daily, weekly and seasonal cycles of observed surface NO_2 in

Gothenburg, but in comparison, the SRM was more accurate with greater correlation and lower RMSE. Therefore, highlighting the potential skill of the LWTs in a modelling case study.

Other studies have looked at the connection between meteorology and NO_2 tropospheric columns. Beirle et al. (2011) used OMI column NO_2 and wind forecasts (below 500m) to analyse NO_2 transport from the isolated megacity Riyadh, Saudi Arabia, detecting leeward NO_2 plume transport. Hayn et al. (2009) performed a similar analysis of wind direction and column NO_2 over Johannesburg, South Africa. Zhou et al. (2012) found significant impacts of wind speed and precipitation on OMI column NO_2 over western Europe. Savage et al. (2008) investigated the interannual variability (IAV) of satellite NO_2 columns over Europe finding that meteorology influences NO_2 IAV more than emissions.

van der A et al. (2008) used GOME and SCIAMACHY data, 1996-2006, to look at column NO_2 seasonal patterns and trends. Over Europe, the peak industrial column NO_2 occurs during winter. They inferred that reduced photolysis (increased NO_2 lifetime), not increased NO_x emissions, are the main cause. The UK is the exception as the meteorological variability and increased soil emissions of NO_x lead to peak NO_2 columns in July. However, Zhou et al. (2012) found that days with peak column NO_2 values over the UK are in winter/spring and state they cannot detect peak column NO_2 described by van der A et al. (2008).

To this study's knowledge, LWTs have not previously been used to investigate synoptic patterns in fields of satellite observations of atmospheric chemistry. The aim of this chapter is to investigate the influence of UK surface circulation patterns on atmospheric trace gas distributions by using the LWTs to classify distributions of air pollutants under different weather regimes. Section 5.2.1 discusses how the LWTs are derived and how we use them in this study. Section 5.3 presents the results of a study into the relationships between the LWTs and column NO_2, HCHO and surface O_3 and NO_2. Section 5.3.1 has been published in Pope et al. (2014a). Section 5.3 also introduces the Past Weather Code (PWC) and its relationship with OMI column NO_2. Finally, in Section 5.4, this Chapter's results are summarised.

5.2 Data

5.2.1 Lamb Weather Types

Lamb Weather Types were originally derived using a manual method of classifying the atmospheric circulation patterns (mostly using sea level pressure) according to the wind direction and circulation type over the UK (Lamb, 1972). Jenkinson and Collison (1977) created an automated classification scheme based on the mean sea level pressure at sixteen points over Western Europe (centred on UK). From the pressure field at these points the

direction, strength and vorticity of the mean flow over the UK are calculated. Each day is then assigned both a vorticity typed and a wind flow direction. Three vorticity types are used (neutral vorticity, cyclonic and anticyclonic) and eight wind flow directions (N, NE, E, SE, S, SW, W and NW) unless the flow vorticity is much stronger than the flow strength, when the day is classified solely as cyclonic or anticyclonic. There is also an unclassified LWT.
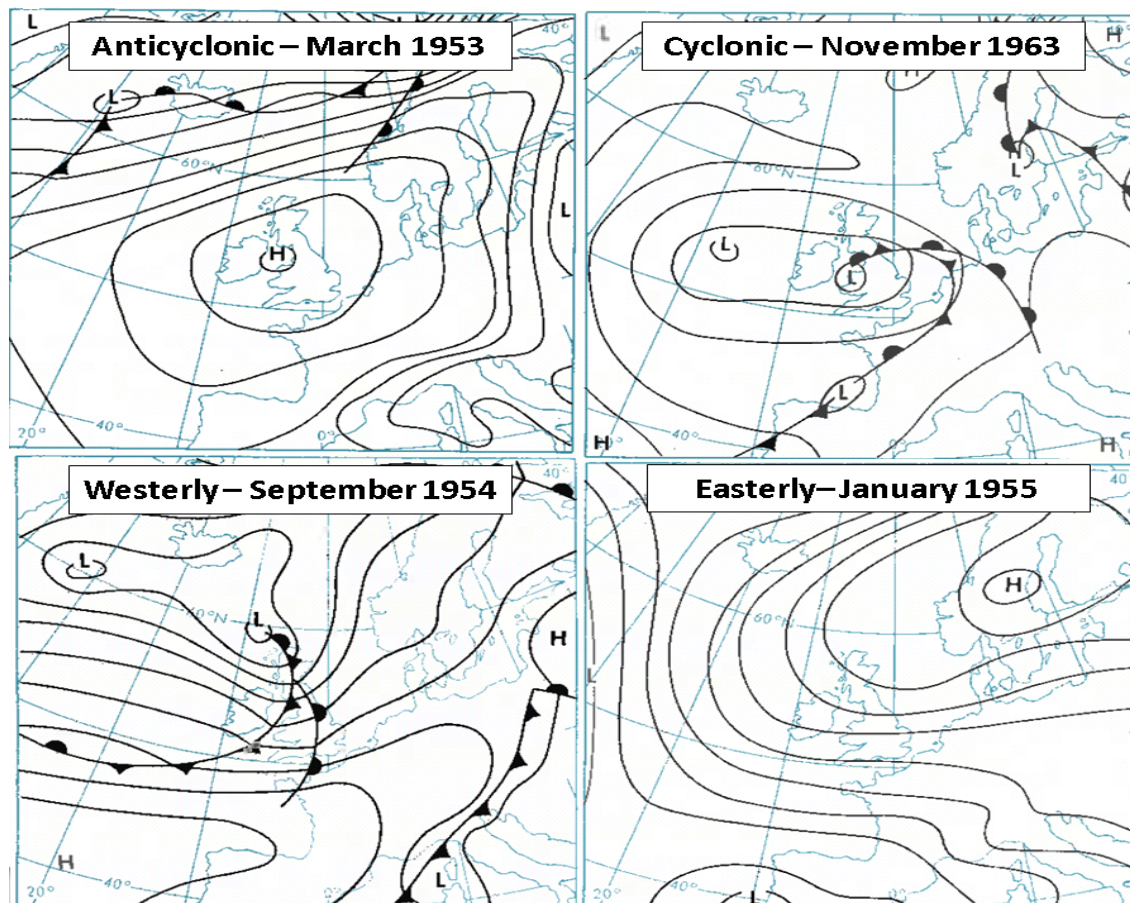
Figure 5.1: Digitised example synoptic charts of LWT classifications from Lamb (1972).

Table 5.1 summarises the LWT codes. For more details of the classification scheme see Jones et al. (2013). Examples of the original LWT classification synoptic charts are in Figure 5.1. This study uses the dataset of Jones et al. (2013) which extends the objective LWT dataset by using daily midday (12.00 UT) grid-point mean sea level pressure data from NCEP/NCAR reanalysis (Kalnay et al., 1996). This data can be obtained from the Climatic Research Unit (CRU) at the University of East Anglia (www.cru.uea.ac.uk/cru/data /lwt/).

It is likely that it would prove difficult to find statistically significant associations between the NO_2 columns and each individual LWT because their occurrence frequency is too low during the period of OMI data. Therefore, the LWTs were merged into 11 classes,

similar to O'Hare and Wilby (1995) and Tang et al. (2011), to increase the amount of data in each category (Table 5.1). There are 3 synoptic classes: neutral vorticity (LWTs 11-18); cyclonic (20-28) and anticyclonic (0-8). There are 8 flow directions: NE, E, SE, NW, W, SW, N and S (e.g. the south-westerly type is a combination of LWTs 5, 15 and 25). It should be noted that there is only one LWT definition per day, but each day is included in two of this study's weather classes (unless it is unclassified or are LWTs 0 or 20 as they have no flow direction). For example, LWT 27 is in the Cyclonic and North-westerly groups. For the 7-year (2556-day) period 2005-2011, the percentage occurrence was calculated for each of the 11 classes. The relative occurrence of the synoptic conditions was: neutral vorticity 38.9%; cyclonic 26.1% and anticyclonic 33.7%. The most frequent wind flow directions were the W and SW directions at 16.7% and 14.4%, respectively.

5.3 Atmospheric Chemistry - Weather Relationships

5.3.1 Tropospheric Column NO_2
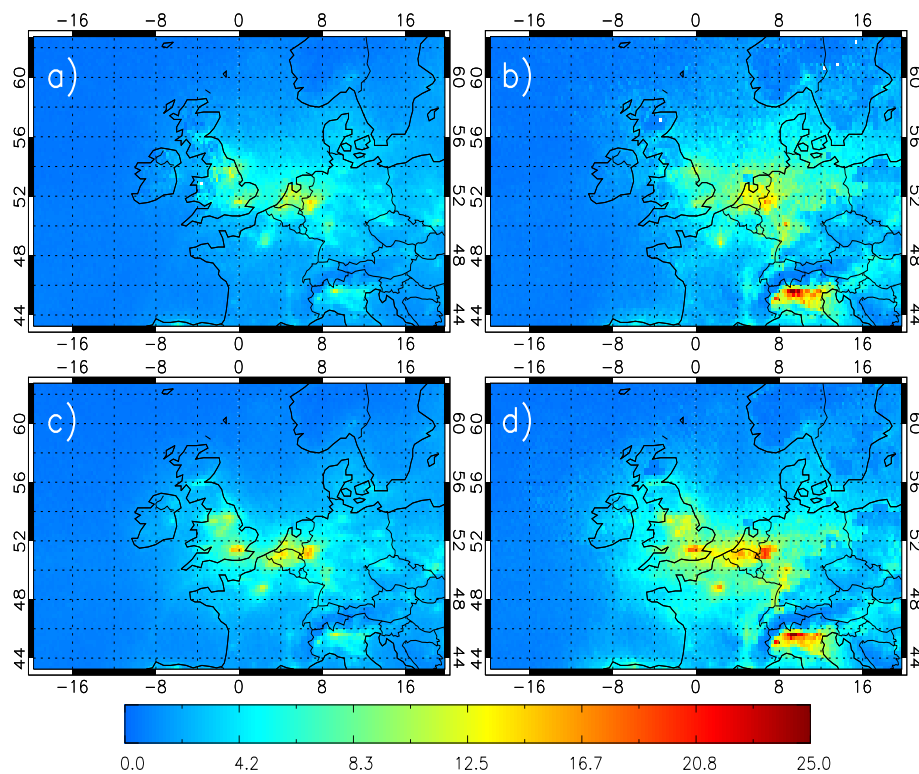
Figure 5.2: Composites of OMI column NO_2 ($\times 10^{15}$ molecules/cm^2) for (a) summer cyclonic, (b) winter cyclonic, (c) summer anticyclonic and (d) winter anticyclonic conditions.

Composite maps of OMI tropospheric column NO_2 were derived for each of the 11 synoptic and wind direction classes for both winter (October-March) and summer (April-September). Figure 5.2 shows these composites for the cyclonic and anticyclonic conditions

and Figure 5.3. shows the anomaly of each composite from the 7-year seasonal average. This study focuses primarily on the influences of cyclonic and anticyclonic weather patterns, as they have greater occurrence, and are therefore more statistically significant than the wind direction composites.
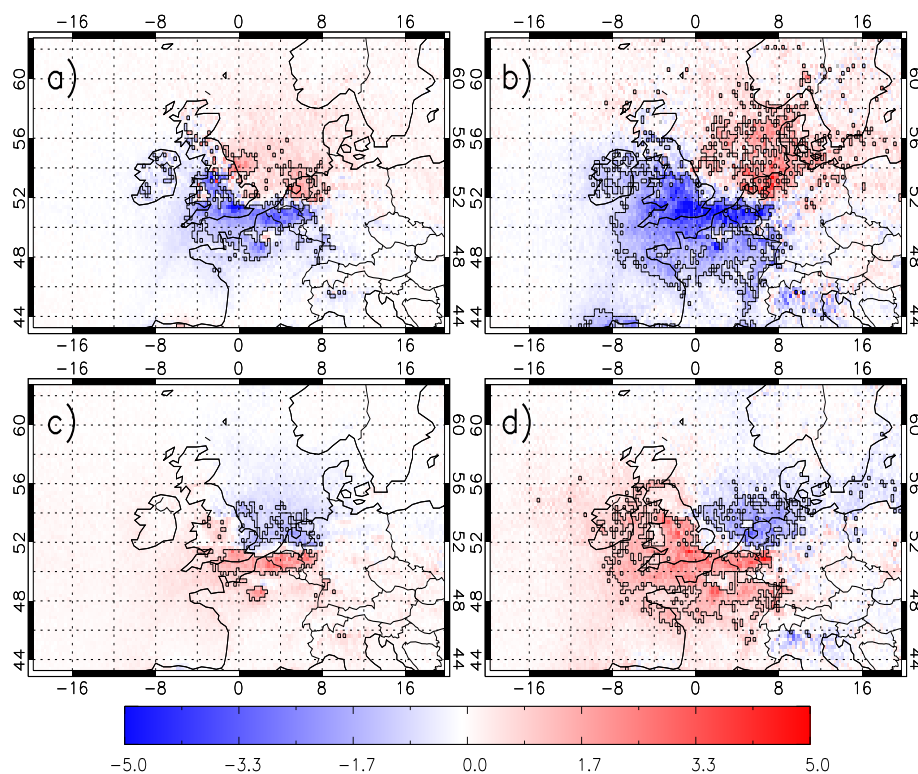
Figure 5.3: Anomalies of OMI column NO_2 composites compared to seasonal 7-year average ($\times 10^{15}$ molecules/cm^2) for (a) summer cyclonic, (b) winter cyclonic, (c) summer anticyclonic and (d) winter anticyclonic conditions. Black boxes indicate where the anomalies are statistically significant at the 95% level.

The summer and winter composites (Figure 5.2) show that NO_2 tropospheric column concentrations peak in the winter, as discussed by Tang et al. (2011), McGregor and Bamzelis (1995), Lesniok et al. (2010) and Demuzere et al. (2009). Winter conditions lead to greater emission of NO_x from power generation. The lower abundance of OH and slower photochemical processes also decrease the loss rate of NO_2. Over the Netherlands source regions, under cyclonic conditions, the peak NO_2 columns are 13 $\times 10^{15}$ molecules/cm^2 in summer and 13-16 $\times 10^{15}$ molecules/cm^2 in winter. Over the UK source regions, the peak UK cyclonic column NO_2 is approximately 13 $\times 10^{15}$ molecules/cm^2 in summer, while only 10 $\times 10^{15}$ molecules/cm^2 in winter. My untested hypothesis is that winter cyclonic transport over the UK is more active than the longer winter NO_2 lifetime in governing the spatial pattern of column NO_2. Therefore, summer source region column NO_2 is greater than that of winter as the slower transport is less efficient at removing

NO_2 despite increased photochemical processes. This is discussed more in Chapter 6. Under anticyclonic conditions, over the UK and Netherlands source regions the summer peak is 16 $\times 10^{15}$ molecules/cm^2, while in winter the NO_2 concentrations reach 20 $\times 10^{15}$ molecules/cm^2.

McGregor and Bamzelis (1995) and Lesniok et al. (2010) noted that air mass stability (instability) under anticyclonic (cyclonic) conditions leads to reduced (increased) transport of NO_2 from sources. This is seen in Figure 5.2 where the NO_2 concentrations over some regions are higher under anticyclonic conditions. In winter the NO_2 concentrations over South East England and Netherlands range from 10-16 $\times 10^{15}$ molecules/cm^2 and 16-20 $\times 10^{15}$ molecules/cm^2 in cyclonic and anticyclonic conditions, respectively. The same occurs in summer, but with lower NO_2 concentrations at 13 $\times 10^{15}$ molecules/cm^2 (cyclonic) and 16 $\times 10^{15}$ molecules/cm^2 (anticyclonic).

To quantify the differences between the synoptic regimes, the 7-year seasonal average (of all weather types) was subtracted from the winter and summer cyclonic and anticyclonic composites (Figure 5.3). We use the Wilcoxon Rank Test (WRT) to examine the significance of the differences, at the 95% significance level ($p < 0.05$), in the composite-total period averages. The WRT is the non-parametric counterpart of the student t-test and so relaxes the constraint on normality of the underlying distributions (Pirovano et al., 2012). In Figure 5.3 areas where the anomalies are significant are outlined with black polygons. In the cyclonic case a significant positive-negative dipole exists, with negative anomalies over the southern UK and positive anomalies over the North Sea. The higher winter NO_2 concentrations lead to an intense dipole, with maximum positive anomalies $> 5 \times 10^{15}$ molecules/cm^2 and the lowest negative anomalies $< -5 \times 10^{15}$ molecules/cm^2. In summer, these anomalies peak at similar values but their spatial extent is much less. Potential reasons why the area of the anomaly is reduced in summer include both the more rapid removal of NO_2 by photochemical processes giving less accumulation under stagnant conditions and lighter winds in the summer causing slower transport from source regions. Typically, cyclonic conditions are indicative of westerly and south-westerly flow. Therefore, the anomalies potentially reveal transport of NO_2 off the UK mainland into the North Sea. In the more stable anticyclonic conditions, the inverse of the cyclonic anomaly dipole exists with positive anomalies, 4-5 $\times 10^{15}$ molecules/cm^2, over the UK and negative anomalies, -3 $\times 10^{15}$ molecules/cm^2, over the North Sea. This occurs for both seasons, but with larger spatial patterns in winter. It is probable that the anomaly pattern occurs as less NO_2 is transported out to the North Sea and more remains over the UK.

This study averaged all OMI pixels within 6°W - 2°E and 50°N - 59°N (see Figure 5.2) to form a UK-average timeseries. Figures 5.4a and 5.4b show the mean annual cycles and their anomalies for the three synoptic classes. The anticyclonic column NO_2 seasonal cycle is well pronounced with maximum (minimum) winter (summer) concentrations of
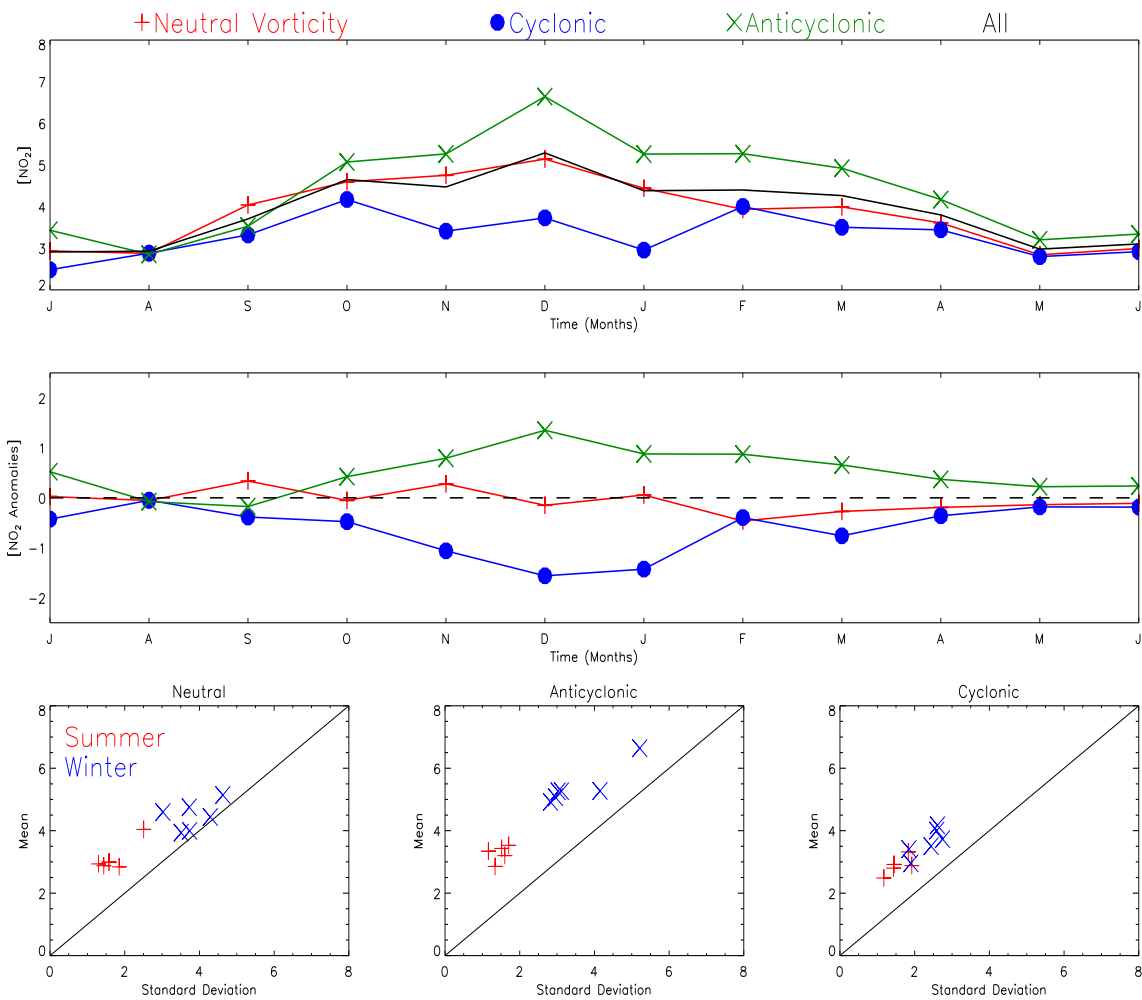
Figure 5.4: OMI NO_2 columns ($\times 10^{15}$ molecules/cm^2) averaged over the UK (see text)
under neutral vorticity, cyclonic and anticyclonic conditions for (a) mean annual cycle of
monthly means, including black line for all conditions, and (b) anomaly of monthly means
with respect to all conditions. Panels (c) - (e) show the correlation of the monthly means
with their standard deviations.

approximately 7 (3) $\times 10^{15}$ molecules/cm^2. The cyclonic column NO_2 cycle is less pro-
nounced with similar concentrations in summer and winter of approximately 3 - 4 $\times 10^{15}$
molecules/cm^2. The neutral conditions show a seasonal pattern between the cyclonic and
anticyclonic conditions, with very similar concentrations to the average of all weather types
in every month. Figures 5.4c -5.4e show the correlation of the UK monthly mean columns
with their standard deviations. The scattered points all sit above the 1:1 line showing
that the monthly mean values are always greater than their temporal variability. Figures
5.4d and 5.4e also emphasise the larger range of mean column NO_2 under anticyclonic
conditions compared to cyclonic conditions. Overall, the largest relative differences are
in winter, likely due to a combination of more intense winter cyclonic and anticyclonic
dynamics and reduced photochemical processes. In winter, increased poleward momen-
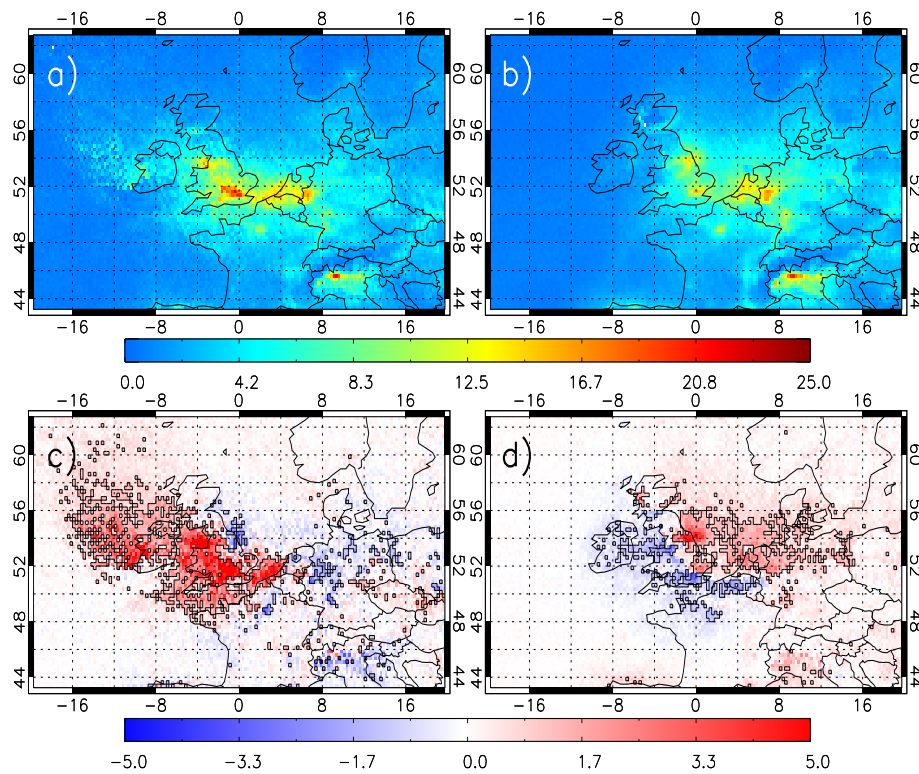
Figure 5.5: Composites of OMI column NO_2 ($\times 10^{15}$ molecules/cm^2) under different wind flow directions and difference of these with respect to 7-year average. (a) South-easterly flow, (b) south-westerly flow, (c) south-easterly anomalies and (d) south-westerly anomalies.

tum flux results in larger atmospheric instabilities. Therefore, the more intense cyclones further reduce column NO_2 above source regions in winter. However, winter anticyclones are associated with cold denser air masses enhancing atmospheric blocking and prolonged stable conditions, therefore, accumulating NO_2 more efficiently. Photochemically, under anticyclonic conditions, in summer stronger photolysis converts more NO_2 to NO, but in winter reduced solar intensity and cloudier conditions limit NO_2 to NO conversion. The neutral vorticity conditions typically have similar concentrations to the cyclonic conditions in summer and anticyclonic conditions in winter over the study period.

This study also finds that the influence of the wind directions on the OMI NO_2 fields can be significant. Note that due to the lower frequency of each of the eight wind directions, these are not seasonal composites but use all seven years of data regardless of season. Two examples of the wind-induced NO_2 transport are shown in Figure 5.5. Figure 5.5a shows the composite of the south-easterly flow off continental Europe, where NO_2 (up to 20×10^{15} molecules/cm^2) is transported away from London and Lancashire towards the Midlands and the Irish Sea, respectively. In Figure 5.5b, the south-westerly flow is transporting NO_2 (up to 13×10^{15} molecules/cm^2) away from London and the M62 corridor out into the
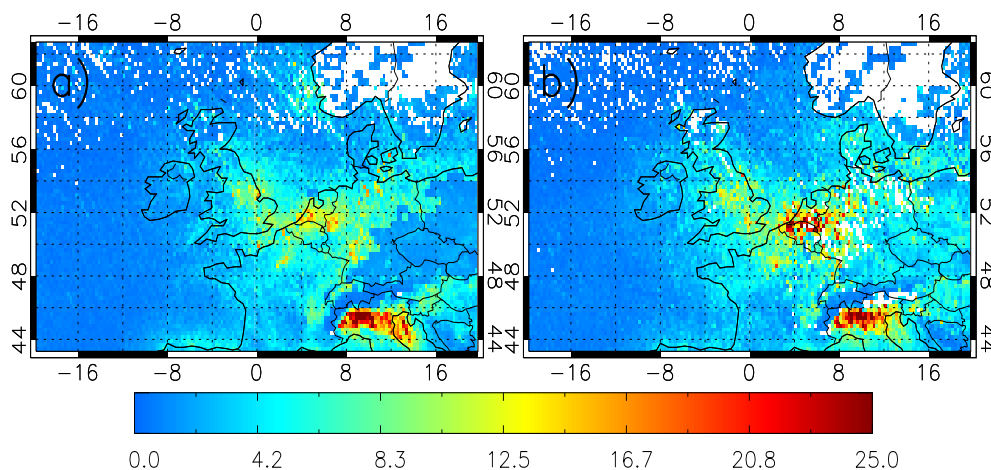
Figure 5.6: OMI column NO_2 ($\times 10^{15}$ molecules/cm^2) composites of DJF 2005-2011 NAO phases (a) positive and (b) negative.

North Sea. The transport impact from the south-easterly flow is much greater, but since these classes can contain different proportions of each vorticity type, this might account for the greater transport when compared with the south-westerly flow. Figures 5.5c and 5.5d show the anomalies in NO_2 for these two flow directions with respect to the 7-year OMI average. The significant positive anomalies suggest south-westerly flow is transporting up to 5×10^{15} molecules/cm^2 away from the source regions. In Figure 5.5d, positive (negative) anomalies, over (under) +(-) 5×10^{15} molecules/cm^2 show where the south-westerly flow has transported NO_2 away from the source regions out into the North Sea.

The link between the winter North Atlantic Oscillation (NAO) and column NO_2 data using the NAO Index from CRU (Jones et al. (1997); available from www.cru.uea.ac.uk/cru /data/nao) was also investigated. However, I could not find any significant spatial differences in the NO_2 columns between the positive and negative NAO phases (Figure 5.6).

5.3.2 Total Column HCHO

Having successfully used the LWTs and OMI column NO_2 to find relationships between air pollutants and synoptic weather, the analysis was repeated with OMI total column HCHO; a significant species in O_3 chemistry. The product is described in more detail in Chapter 3, but cloud fractions and quality flags have been applied to this dataset. The analysis treats the total column as essentially tropospheric as HCHO is produced in the troposphere. As the data is noisy on a grid size of 0.25° latitude x 0.25° longitude, the HCHO data was interpolated onto 0.5° x 0.5° grid. However, the data still experiences striping issues past 2009, so 2005-2009 data is used.

The OMI column HCHO has no noticeable correlation with the LWT wind directions. In winter the product, despite quality filtering of the data, is very noisy with unexpected

features in winter. Figures 5.7a and 5.7b show summer column HCHO under cyclonic and anticyclonic conditions, respectively. Under the cyclonic conditions, there is a clear land-sea gradient with sea and land column HCHO of 15-20 $\times 10^{15}$ molecules/cm^2 and 20-32 $\times 10^{15}$ molecules/cm^2, respectively. Over southern France, column HCHO peaks at approximately 35 $\times 10^{15}$ molecules/cm^2, independent of the LWTs. The anticyclonic conditions still have land-sea gradients of column HCHO, but the concentrations are less, ranging between 15-19 $\times 10^{15}$ molecules/cm^2 over sea and 20-25 $\times 10^{15}$ molecules/cm^2 over land. As the LWTs are focused on the UK, the changes in vorticity over the UK have a limited effect on column HCHO around the edges of the domain, e.g. over southern France (peak domain HCHO concentrations).

Figures 5.7c and 5.7d show the anomalies from the 5-year seasonal average and the black squares indicate the significant differences. Under the cyclonic conditions, there are large positive anomalies of over 5 $\times 10^{15}$ molecules/cm^2 focused on the UK. The anticyclonic conditions, however, show the opposite with negative anomalies between -4 to -2 $\times 10^{15}$ molecules/cm^2. Photolysis has a strong influence on the spatial pattern of column HCHO in summer and I hypothesise that synoptic weather aids or buffers this process.
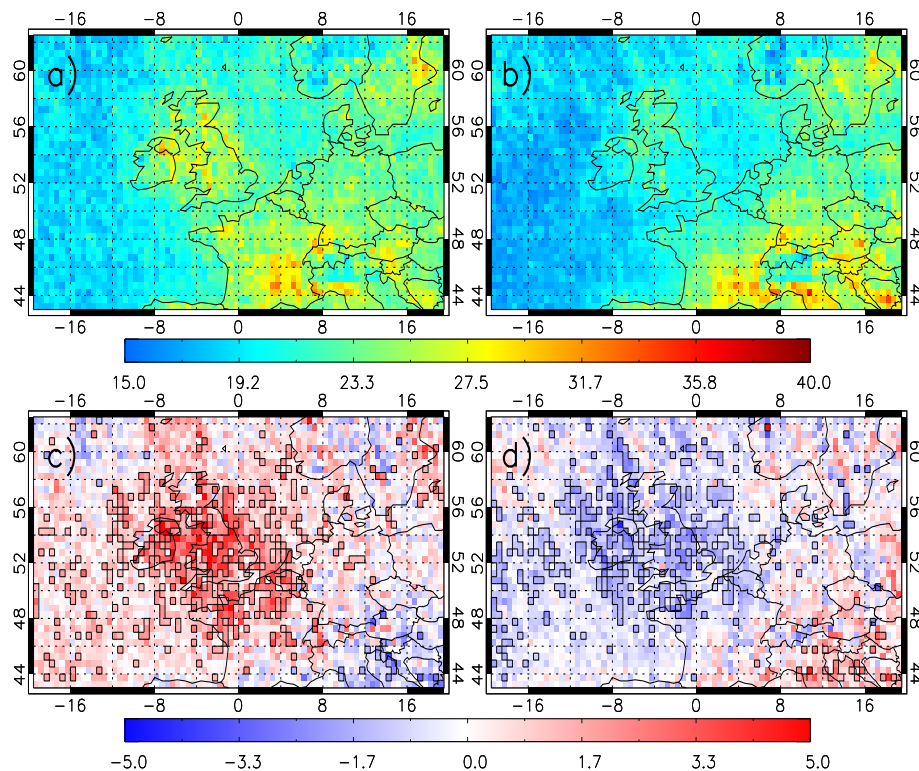
Figure 5.7: Composites of summer OMI column HCHO ($\times 10^{15}$ molecules/cm^2), 2005-2009, for (a) cyclonic conditions, (b) anticyclonic conditions, (c) cyclonic anomalies and (d) anticyclonic anomalies. Black boxes indicate where the anomalies are statistically significant at the 95% level.
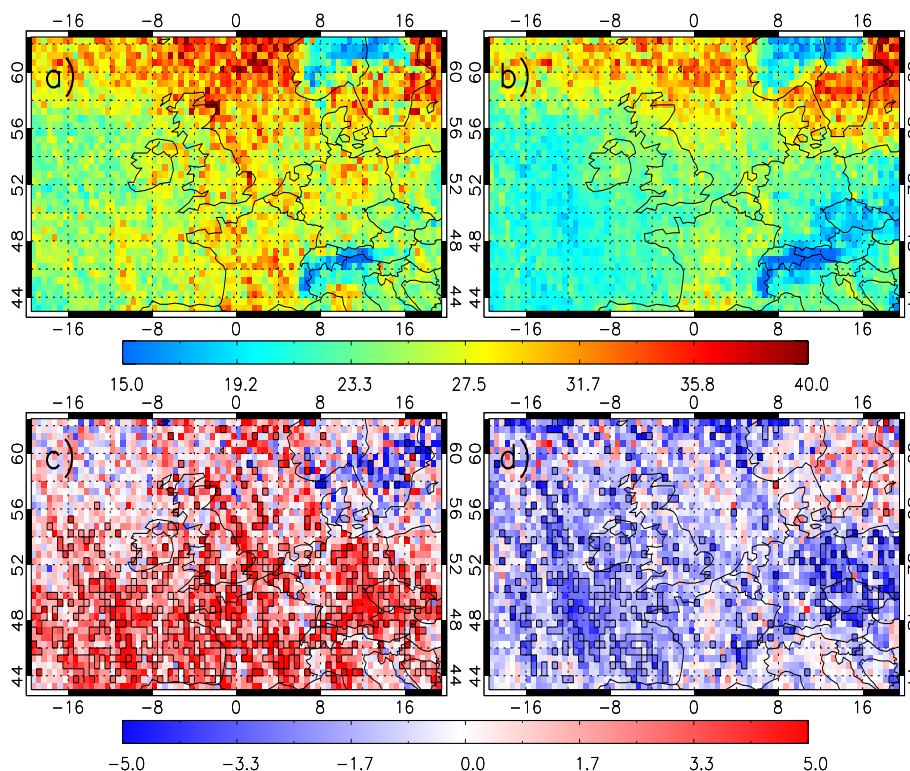
Figure 5.8: Composites of winter OMI column HCHO ($\times 10^{15}$ molecules/cm^2), 2005-2009, for (a) cyclonic conditions, (b) anticyclonic conditions, (c) cyclonic anomalies and (d) anticyclonic anomalies.

Cyclonic conditions are unstable and prone to cloud cover, which reduces the photochemical loss of HCHO, while under anticyclonic conditions, the stable weather is associated with clear skies, which enhances photolysis and HCHO loss.

In the winter case, Figure 5.8, the cyclonic and anticyclonic regimes show similar patterns with higher and lower column HCHO, respectively. This is also seen in the anomaly fields of +/- 5 $\times 10^{15}$ molecules/cm^2 for cyclonic and anticyclonic regimes. However, the spatial patterns of column HCHO are very noisy and there is no coherence spatially in the significant anomalies. There is also a large column HCHO feature in both vorticity regimes at the top of the domain which is suspected to be an OMI artefact. Therefore, no definite conclusions can be drawn from this season for the LWTs and OMI column HCHO.

AQUM summer tropospheric column HCHO was analysed using the same method for OMI summer HCHO. The OMI HCHO product does not contain averaging kernels which could be applied to the AQUM for a more critical comparison. AQUM does produce similar patterns but to a weaker extent where column HCHO over the UK is 5-7 $\times 10^{15}$ and 2-5 $\times 10^{15}$ molecules/cm^2 under cyclonic and anticyclonic conditions, respectively (Figure 5.9a and 5.9b). However, these concentrations are lower by approximately 15-25 $\times 10^{15}$ molecules/cm^2 in places than OMI column HCHO. AQUM vorticity composite anoma-
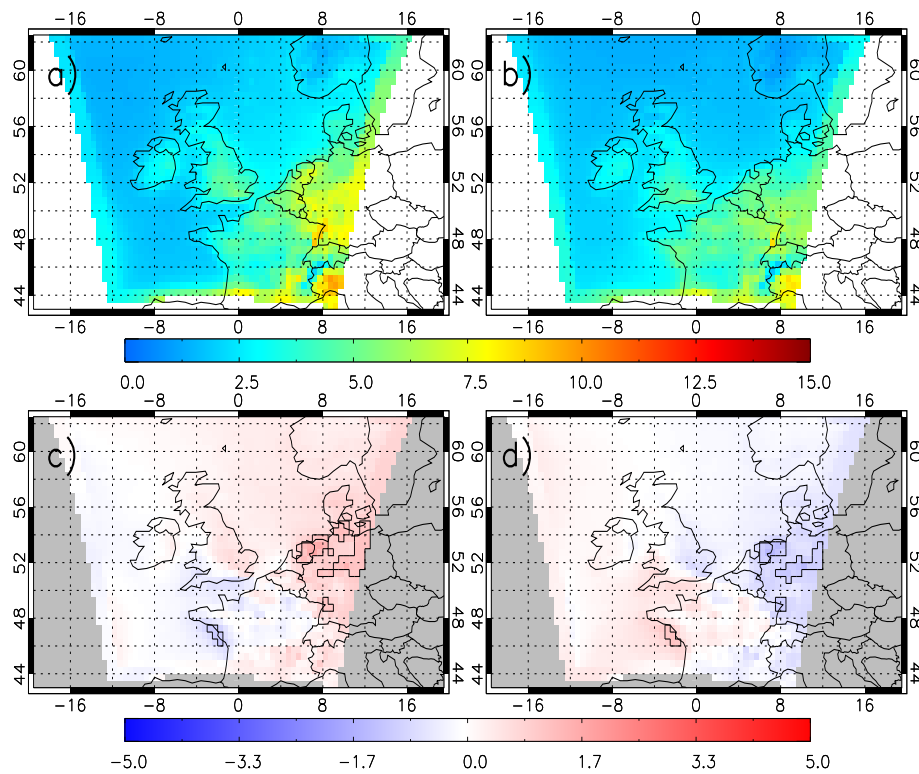
Figure 5.9: Composites of summer AQUM column HCHO ($\times 10^{15}$ molecules/cm^2), 2006-2009, for (a) cyclonic conditions, (b) anticyclonic conditions, (c) cyclonic anomalies and (d) anticyclonic anomalies.

lies are also not statistically significant. Therefore, the results are inconclusive and raise issues either with the model's representation of HCHO, the OMI HCHO product or the comparisons of OMI total column and AQUM tropospheric column HCHO. Comparisons by Barkley et al. (2011) find that over the US, GEOS-Chem is biased against OMI column HCHO by -8% on average. However, when OMI column HCHO is over 5×10^{15} molecules/cm^2, this bias tends to -23%. In Chapter 3, the OMI-AQUM-GEMS column HCHO comparisons for July 2006 show inconsistent patterns making it difficult to determine which data source is most precise.

5.3.3   Surface NO$_2$ and O$_3$

To complement the LWT - OMI NO$_2$ relationships the AURN surface observations for NO$_2$ and O$_3$ have been investigated using the same classifications in Table 5.1. Here the full UK AURN for 2000-2010 has been interpolated onto a 0.25° longitude x 0.25° latitude grid to give larger spatial coverage. The AURN data has been used between 2000-2010 to build up a significantly large spatial network of stations, although not overlapping the satellite record exactly. During this period, the network of stations will change over time as older stations are closed down and new stations introduced. When looking at a case

study of PM_{10} in 2006 there were too few observations to carry out this type of analysis, so longer time periods are required.

Figure 5.10: Composites of summer AURN surface NO_2 (μg/m^3), 2000-2010, for (a) anticyclonic conditions, (b) cyclonic conditions, (c) anticyclonic anomalies and (d) cyclonic anomalies. Black boxes indicate where the anomalies are statistically significant at the 95% level for all surface comparisons in Section 5.3.3.

Figure 5.10 shows surface summer NO_2 under anticyclonic and cyclonic conditions. The black polygons again show where the anomalies from the seasonal average are significant to the 95% level. In Figure 5.10a and 5.10b, there is little difference between the surface NO_2 fields under the two vorticity types, both ranging between 10-70 μg/m^3. In the anomaly fields there are several significant differences but the spatial pattern is noisy. This is inconsistent with spaceborne observations and infers different processes (e.g. boundary layer mixing) could be controlling the surface NO_2 concentrations. In winter, Figure 5.11a and 5.11b, the surface NO_2 tends to be higher (lower) than summer, ranging between 15-80 (15-60) μg/m^3, under the anticyclonic (cyclonic) conditions. In the anomaly fields, Figure 5.11c and 5.11d, there are spatially significant positive (negative) anomalies of 5-15 μg/m^3 (-10 to -2 μg/m^3) over the UK. This is consistent with accumulation (transport) over (away) from source regions, as seen by OMI column NO_2. The fact that in winter emissions are higher and there is reduced photolysis (from more cloud cover and reduced solar intensity) means that concentrations are large enough to be influenced by vorticity regimes.
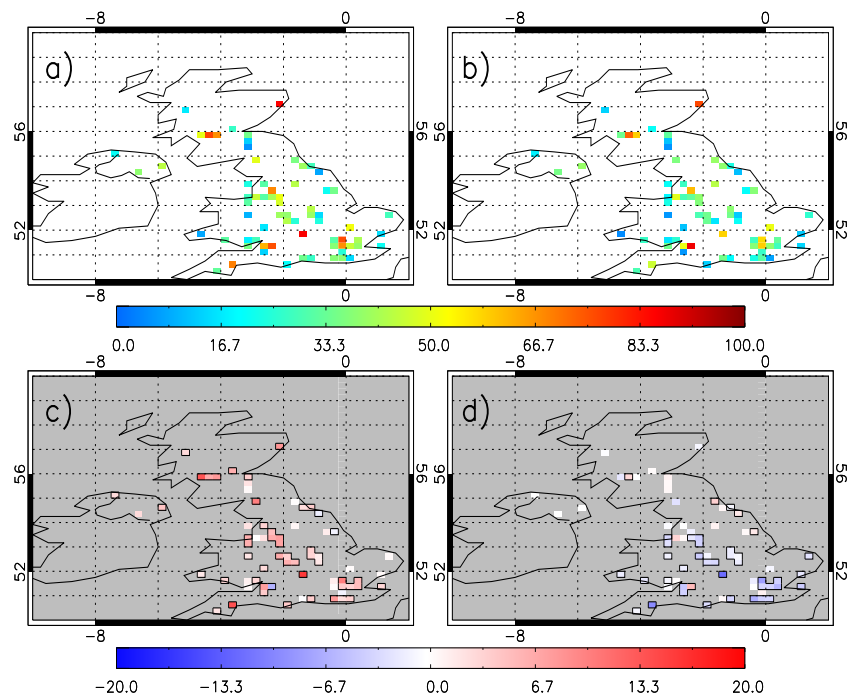
Figure 5.11: Composites of winter AURN surface NO_2 ($\mu g/m^3$), 2000-2010, for (a) anticyclonic conditions, (b) cyclonic conditions, (c) anticyclonic anomalies and (d) cyclonic anomalies.
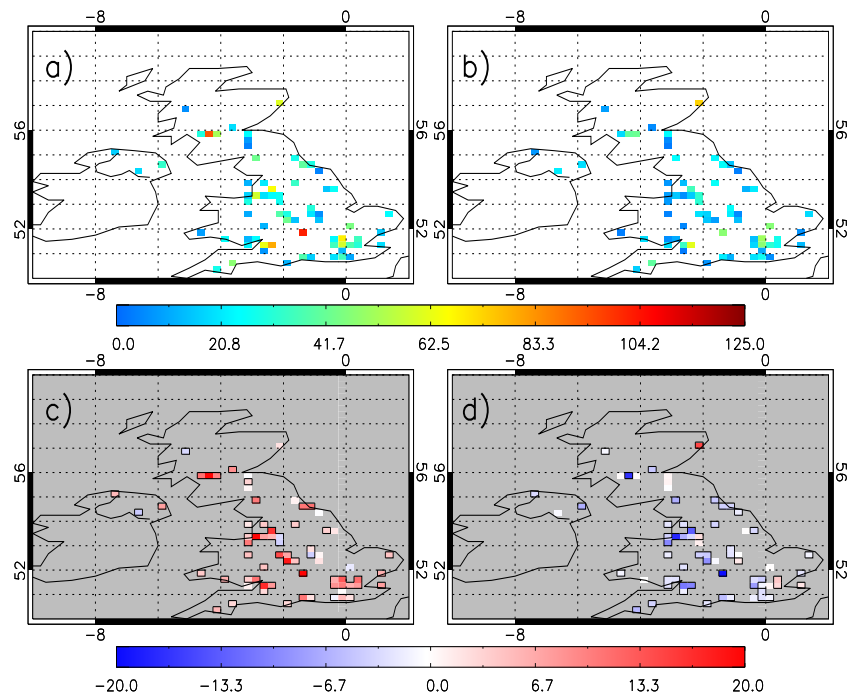
Figure 5.12: Composites of summer AURN surface NO_2 ($\mu g/m^3$), 2000-2010, for (a) south-easterly flow, (b) north-westerly flow, (c) south-easterly anomalies and (d) north-westerly anomalies.

AURN NO_2 was also composited into seasonal south-easterly and north-westerly flow. These two flow regimes appear to have the most significant impact on surface NO_2 concentrations, but others have significant spatial patterns too. In summer, Figure 5.12a and 5.12b, the surface NO_2 ranges between 10-80 $\mu g/m^3$ and 0-50 $\mu g/m^3$ under south-easterly and north-westerly regimes, respectively. In the anomaly fields, Figure 5.12c and 5.12d, there are positive (negative) anomalies of 5-20 $\mu g/m^3$ (-20 to -5 $\mu g/m^3$). The south-easterly flow is off continental Europe where there are high emissions of NO_x (e.g. the Benelux region), which are being transported over the UK. The north-westerly flow is associated with unstable weather and turbulence and clear North Atlantic air. Therefore, there is significant transport of NO_2 away from the UK mainland, replacing it with clearer air. In winter, Figure 5.13, the anomaly fields show similar patterns. However, the significant extent and magnitude of the south-easterly positive anomalies is reduced, while in the north-westerly flow the anomalies have intensified to -20 to -10 $\mu g/m^3$. The intensified north-westerly anomalies potentially highlight enhanced transport of NO_2 away from the UK mainland. This is consistent with more intense unstable weather and turbulence in winter, which is associated with westerly (W, NE, SW) flow regimes. The decrease in positive anomalies under south-easterly flow was unexpected as winter NO_2 concentrations tend to be larger (so more NO_2 transported from Europe). This is the case over the UK as Figure 5.13a (winter south-easterly) tends to have higher NO_2 concentrations
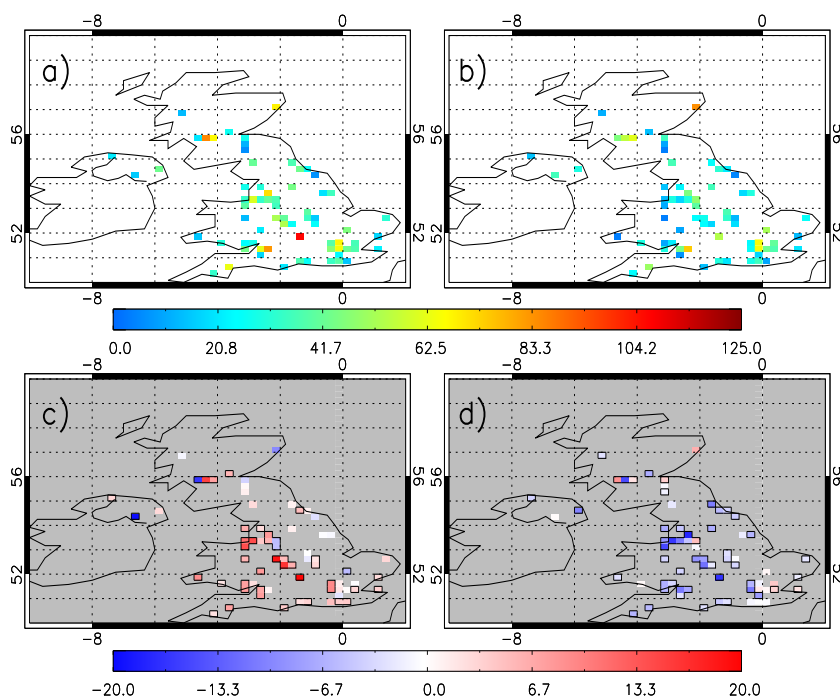
Figure 5.13: Composites of winter AURN surface NO_2 ($\mu g/m^3$), 2000-2010, for (a) south-easterly flow, (b) north-westerly flow, (c) south-easterly anomalies and (d) north-westerly anomalies.
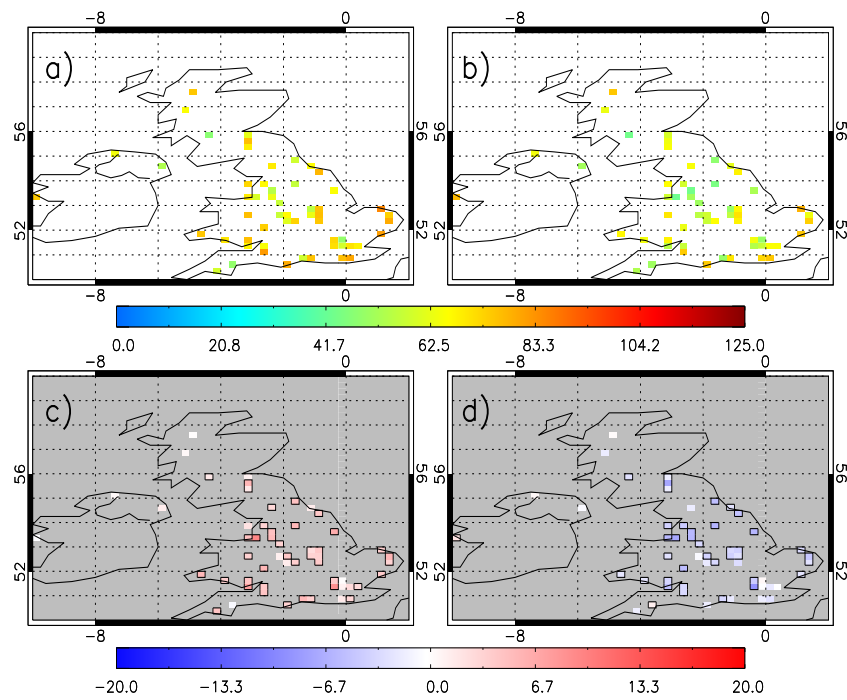
Figure 5.14: Composites of summer AURN surface O$_3$ (μg/m^3), 2000-2010, for (a) anticyclonic conditions, (b) cyclonic conditions, (c) anticyclonic anomalies and (d) cyclonic anomalies.
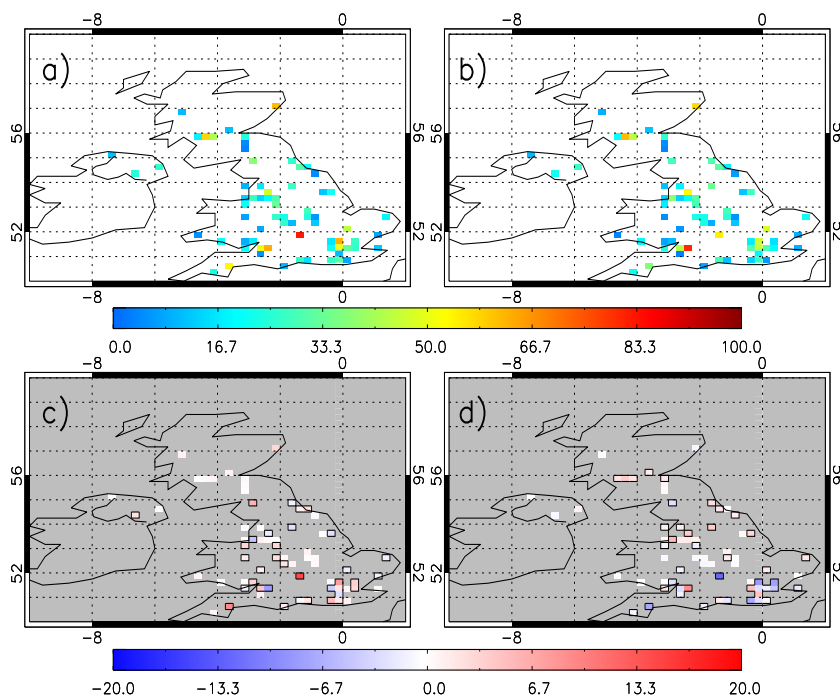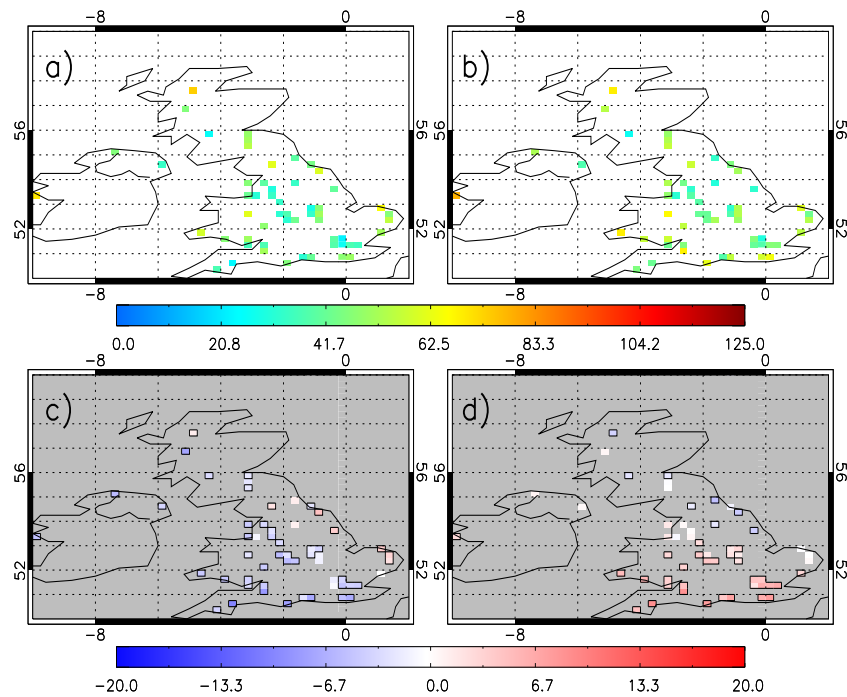

Figure 5.15: Composites of winter AURN surface O$_3$ (μg/m^3), 2000-2010, for (a) anticyclonic conditions, (b) cyclonic conditions, (c) anticyclonic anomalies and (d) cyclonic anomalies.

than Figure 5.12a (summer south-easterly) by 5-10 μg/m^3. It is possible that UK winter
NO$_2$ concentrations are higher than over continental Europe, so transported NO$_2$ only
increases the total slightly and is less significantly different from the seasonal average than
in the summer situation.
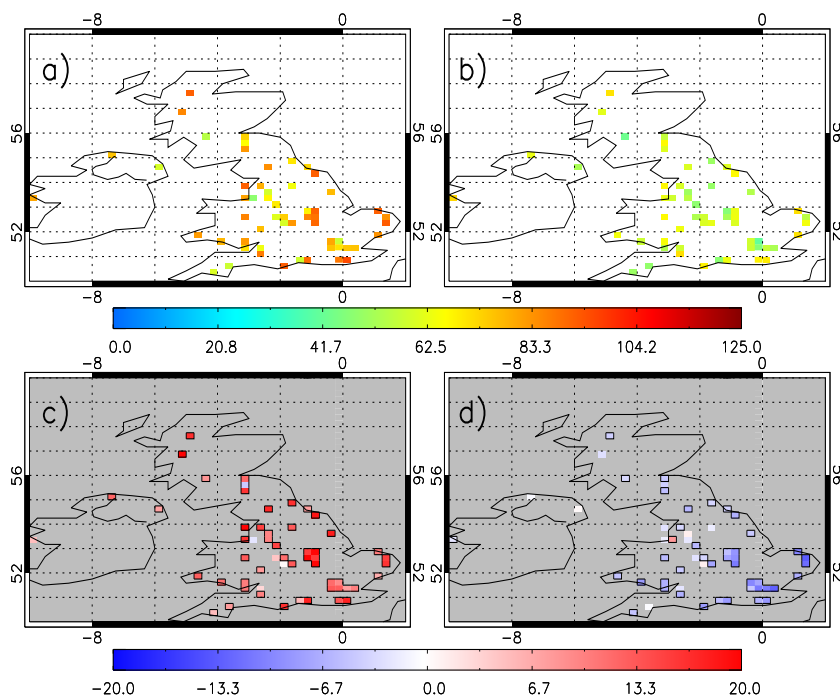
Figure 5.16: Composites of summer AURN surface O$_3$ (μg/m^3), 2000-2010, for (a) south-
easterly flow, (b) north-westerly flow, (c) south-easterly anomalies and (d) north-westerly
anomalies.

Summer AURN O$_3$ concentrations are typically higher under anticyclonic conditions,
but both regimes range between 40-90 μg/m^3. In Figure 5.14c and 5.14d, there are sig-
nificant positive (negative) anomalies over the UK between 0-10 μg/m^3 (-8 to -2 μg/m^3)
under anticyclonic (cyclonic) conditions. This is consistent with elevated photolysis (clear
skies and increased solar intensity) and with NO$_2$ accumulating under anticyclonic condi-
tions leading to higher O$_3$ concentrations. However, under cyclonic conditions the unstable
weather results in greater cloud cover and reduced photochemical ozone formation. Look-
ing at winter, Figure 5.15a and 5.15b, the O$_3$ concentrations are much lower ranging
between 20-65 μg/m^3. However, in the anomaly fields (Figure 5.15c and 5.15d), there
is South West - North East anomaly dipole system. Under anticyclonic conditions the
dipole ranges between -10 to -1 μg/m^3 and 0-5 μg/m^3 in the South West and North East.
However, under cyclonic conditions, the dipole system is reversed between 5-10 μg/m^3 and
-5 to 0 μg/m^3 in the South West and North East, respectively. In each case, the dipole
system is the opposite of the NO$_2$ winter dipole system observed by OMI and AURN.
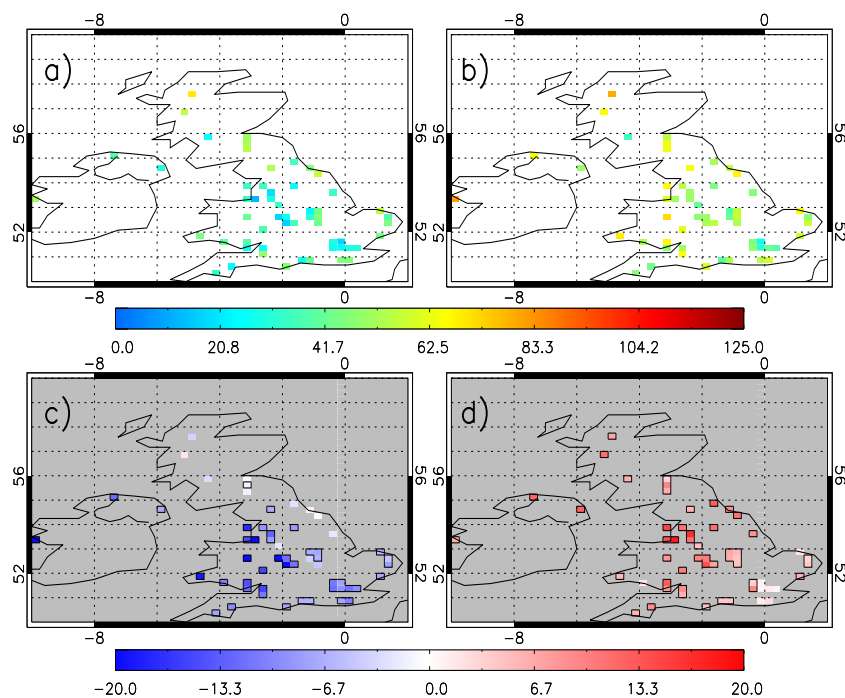
Figure 5.17: Composites of winter AURN surface O_3 (μg/m^3), 2000-2010, for (a) south-easterly flow, (b) north-westerly flow, (c) south-easterly anomalies and (d) north-westerly anomalies.

OMI observes (Figure 5.3), under winter anticyclonic conditions, positive (negative) column NO_2 anomalies of 2-4 (-3 to -1) $\times$ 10^{15} molecules/cm^2 over the UK (North Sea). Under cyclonic conditions this is reversed with negative (positive) anomalies of -5 to -2 (1-3) $\times$ 10^{15} molecules/cm^2 over the UK (North Sea). AURN NO_2, to a lesser extent (Figure 5.11), shows winter positive anomalies, under anticyclonic conditions, across the UK except for the North-East England coast where small negative anomalies exist. Under cyclonic conditions there are negative anomalies over the southern UK but positive anomalies over North East England. Therefore, I hypothesise that surface O_3 anomalies under the two vorticity regimes are negatively corrected with NO_2 anomalies in winter.

In summer, under south-easterly and north-westerly flows (Figure 5.16), the UK surface O_3 ranged between 50-100 μg/m^3 and 40-60 μg/m^3, respectively. The south-easterly anomaly field, Figure 5.16c, has large positive values over 20 μg/m^3, which could be associated with photochemical production of ozone from primary pollutants transported from continental Europe and/or the direct transport of O_3. Easterly flows are generally linked to more stable dry continental weather, which could be aiding the accumulation of O_3 precursors over the UK and O_3 already formed over the continent from clearer skies and more photochemical production. Under north-westerly flow, there are negative anomalies, ranging between -5 to -20 μg/m^3. Again westerly flows are indicative of unstable weather, which is transporting O_3 and O_3 precursors away from the UK mainland. The NO_2 and

O_3 anomalies are the same as each other in summer under these wind regimes. Thus suggesting that the NO_x - O_3 correlations under these summer wind flows are potentially not so active/important. However, in winter the opposite occurs and the O_3 and NO_2 anomalies have different signs. In Figures 5.17a and 5.17b, the O_3 concentrations are lower than summer under south-easterly and north-westerly flow ranging between 15-50 μg/m^3 and 20-70 μg/m^3, respectively. In the anomaly fields, Figure 5.17c and 5.17d, the south-easterly and north-westerly flows introduce large significant magnitude anomalies of under and over 20 μg/m^3. This appears to be strongly correlated (negative correlation) with winter NO_2. Under winter south-easterly and north-westerly flows, the NO_2 anomalies reach over (under) 20 μg/m^3, respectively. This is indicative of synoptic weather influencing the spatial distribution of NO_2 in winter, which impacts on the O_3 spatial pattern through the NO_x - O_3 photochemistry.

5.3.4 Past Weather Code and Tropospheric Column NO_2

Here the Past Weather Code (PWC) is used to analyse OMI tropospheric column NO_2 under different precipitation conditions (similar to the LWTs). The PWC is a descriptive measure of the weather, which, combined with other synoptic observations (e.g. temperature, wind speed), forms the World Meteorological Organisation (WMO)'s SYNOP code. The different PWC weather types are shown in Table 5.2. Weather types 0-3 are classed as "non-significant" (reporting is optional) and 4-9 are "significant" (must be reported), by the WMO. The PWC is recorded over six- and three-hourly periods, starting at 0000, 0600, 1200, 1800 and 0300, 0900, 1500, 2100 respectively (WMO, 1988). As the PWC is hierarchical, only the top two weather types are recorded (W_1, W_2), where W_1 is more significant than W_2. For instance, if PWCs 5, 6 and 9 were observed in a recording period, only 6 and 9 would be recorded (WMO, 1988). Prior to 1st January 1982 only the most significant weather type was recorded (W) (WMO (1988); Dai (2000)).

Other major changes to the PWC around 1st January 1982, applied to both land and marine weather stations, included optional recording of PWC types 0-3 and the introduction of automated stations that had different weather types for PWCs 0-4 (Table 5.2).

Investigation into the PWC as a climate data record has been relatively limited to date. Some previous studies investigating the PWC data include:

- Dai (2000) used both the Past and Present (another descriptive code more common to the USA) Weather Codes to look at global precipitation patterns. He successfully derived global climatologies (DJF and JJA) of precipitation frequency of occurrence between 1975 and 1997.

Table 5.2: World Meteorological Organisation (WMO) Past Weather (W_1W_2) Codes.

	Manual Code: 4561
0	Cloud covering half or less of the sky throughout the period
1	Cloud covering more & less than half the sky in the period
2	Cloud covering more than half the sky throughout the period
3	Sandstorm, duststorm or blowing snow
4	Fog or ice fog or thick haze
5	Drizzle
6	Rain
7	Snow, or rain and snow mixed
8	Shower(s)
9	Thunderstorm(s) with or without precipitation
	Automated Code: 4531
0	No significant weather observed
1	Visibility reduced
2	Blowing phenomenon, visibility reduced
3	Fog
4	Precipitation
5	Drizzle
6	Rain
7	Snow or ice pellets
8	Shower(s) or intermittent precipitation
9	Thunderstorm

- Cacciamani et al. (1995) used Present and Past Weather Code thunderstorm data to create a climatology of the thunderstorm activity in the Po Valley, Italy.

- Olivier (2004) used PWC 4 data to study the frequency of fog events along the West coast of South Africa, which could be a valuable water resource through fog catching.

- Rydock (2007) used the Present Weather Code data to investigate the effect of rainfall on structures (e.g. standing walls) by deriving driving rain maps.

The PWC (W_1) data initially came from the Integrated Surface Database (ISD), which is archived and maintained by the National Oceanic and Atmospheric Administration's (NOAA) National Climatic Data Centre (NCDC) (Lott, 2004). The ISD includes approximately 20,000 weather stations, with the earliest measurements from 1900. All observations used have passed the Lott (2004) quality control process (Flag=1 in ISD dataset). Some other issues encountered by Lott (2004) included:

- Eliminating duplicate stations.

- Combining data from stations with different identification codes in the various datasets.

- Identifying stations whose identification code had changed over time.

However, the Met Office have taken the ISD database and applied their own quality control methodology to it. Even though the PWC data itself in the HadISD dataset is has not been quality controlled, the Met Office Technical Document by Pope et al. (2014b) verified that the data was suitable for scientific study. Therefore, the PWC for the UK was downloaded from http://www.metoffice.gov.uk/hadobs/hadisd/, for between 1st January 2006 - 31st December 2010. The PWC data was downloaded between these dates as it overlapped with the OMI data record and the time range the AQUM can be run.

As stated above, the PWC lower order precipitation type recording practises changed in 1982 and multiple stations have been automated. Therefore, assuming negligible difference between manual and automated reporting practises, only the top 5 PWCs are used as they are consistent in Table 5.2. Therefore, this study focuses on PWCs 5 (Drizzle), 6 (Rainfall), 7 (Snowfall), 8 (Showers) and 9 (Thunderstorms). These PWC types were then used to derive weather type days, similar to the LWTs, which were used to composite the OMI NO_2 record under different precipitation types. Firstly, out of the UK stations, subjectively analysing PWC stations records, 24 had sufficient PWC data to give a good PWC timeseries. Then, on each day of the PWC record, the closest observation (e.g. of any PWC) within 6 hours of the OMI overpass (13.00 LT) was set as the daily precipitation type. Out of these 24 stations, if 50% or more of them were the same PWC type then that code would be classified as the UK weather at the OMI overpass on that day (e.g. 50% of the UK stations show PWC 5 then it is a UK Drizzle Day). The percentage of Drizzle, Rain, Snow, Showers and Thunderstorm days were 9.0%, 41.9%, 0.2%, 39.8% and 0.2%, respectively.

Using this UK PWC precipitation type timeseries, the OMI data was composited up. In the case of PWC 7 (Snowfall) and 9 (Thunderstorms), there were insufficient observations of these PWC types to get a reliable OMI column NO_2 composite. This is unfortunate as lightning can be a significant source of NO_2 and it would have been interesting to see if this source could be detected from space. The PWC 5 (Drizzle) and 6 (Rainfall) OMI column NO_2 composites were similar, but the Drizzle features were more spatially extensive. Therefore, our analysis focuses on non-seasonal Drizzle and Showers precipitation type patterns.

Figure 5.18 shows the OMI column NO_2 composites under Drizzle (a) and Showers (b) and their anomalies respective to the 5-year non-season column average. The black polygons in Figure 5.18c and 5.18d are significant anomalies to the 95% level using the WRT (same test used for the LWTs). Under the Drizzle conditions column NO_2 peaks

over London, the Benelux region and Po Valley between 17-21 $\times 10^{15}$ molecules/cm^2. The Showers column NO_2 composite, however, has much lower concentrations over the source region of 12-13 $\times 10^{15}$ molecules/cm^2. In the anomaly fields, the Drizzle conditions lead to significant positive anomalies of 3-5 $\times 10^{15}$ molecules/cm^2 over the source regions and English Channel. In the case of Showers, there are significant negative anomalies 2-3 $\times 10^{15}$ molecules/cm^2 over the source regions. I hypothesised that Drizzle, defined as "precipitation droplets less than 0.5 mm in diameter" by the Met Office (http://www.metoffice.gov.uk/learning/rain/what-is-precipitation), is a proxy for stable conditions and frontal systems, and Showers, defined as short periods of precipitation, are a proxy for unstable and convection weather. Therefore, the stable conditions governing the Drizzle precipitation, like anticyclonic conditions seen using the LWTs, aid the accumulation of NO_2 over the source regions. The unstable conditions associated with the Showers precipitation result in the transport of NO_2 away from the source regions.

Figure 5.18: Composites of OMI column NO_2 ($\times 10^{15}$ molecules/cm^2) between 2006-2010 for (a) PWC 5 (Drizzle) conditions, (b) PWC 8 (Showers) conditions, (c) PWC 5 (Drizzle) anomalies and (d) PWC 8 (Showers) anomalies. Black boxes indicate where the anomalies are statistically significant at the 95% level.

To test this hypothesis I ran AQUM for the same time period, 2006-2010, and it has been composited up under the PWC time series. Since the AQUM is a regional NWP model, it has accurate representation of weather systems through the LBCs from

the Met Office's global forecast model, I justify using the PWC time series to directly composite up the model NO_2 fields. In all cases, AQUM has been co-located in time and space with OMI and the averaging kernels applied. Again, under the Drizzle conditions (Figure 5.19a), there are higher NO_2 columns over the source regions peaking between 20-25 $\times 10^{15}$ molecules/cm^2. This is higher than OMI column NO_2 under Drizzle conditions; however, as shown in Chapter 4, the lack of heterogeneous chemistry in AQUM leads to an overestimation of column NO_2 in the model. In Figure 5.19b, AQUM has lower column NO_2, similar to OMI now, between 12-13 $\times 10^{15}$ molecules/cm^2 over the source regions. The anomaly fields, Figures 5.19c (Drizzle) and 5.19d (Showers), confirm what OMI sees with positive and negative anomalies of 3-5 $\times 10^{15}$ molecules/cm^2 and 2-3 $\times 10^{15}$ molecules/cm^2, respectively. In the Drizzle anomalies though, the spatial significance is larger. Therefore, the AQUM is reproducing the signals seen by OMI, but does not necessary prove that the precipitation types are a proxy for atmospheric stability and transport.
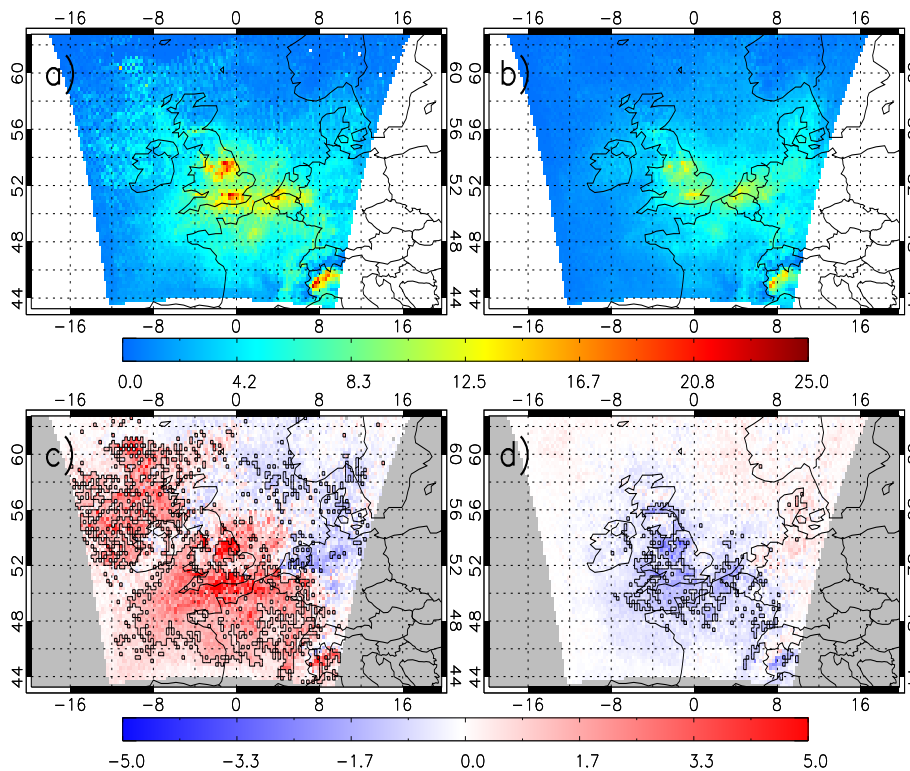
Figure 5.19: Composites of AQUM column NO_2 ($\times 10^{15}$ molecules/cm^2) between 2006-2010 for (a) PWC 5 (Drizzle) conditions, (b) PWC 8 (Showers) conditions, (c) PWC 5 (Drizzle) anomalies and (d) PWC 8 (Showers) anomalies.

An idealised (non reacting) tracer in the NO_x emissions, with a life time of a day - similar to the tracer in Chapter 4, was introduced into AQUM for the 5 year run to investigate how it would be influenced by precipitation types. As the tracer has a fixed

lifetime, its concentration is only affected by transport processes in the model (including large scale winds, convection and boundary layer turbulence) and not by changes in chemistry due to cloud cover changes for example. This provides an insight into whether changes in transport or chemistry linked to PWCs are more important. Comparing Figures 5.20a and b, the tracer columns are significantly higher under Drizzle than Showers conditions with peaks of 25 $\times 10^{15}$ and 15 $\times 10^{15}$ molecules/cm^2, respectively. The tracer columns are significantly higher than that of AQUM and OMI column NO$_2$ which suggests that the chosen lifetime of the tracer is much longer than the lifetime of NO$_2$ in the atmosphere on average. However, in the anomaly plots, Figures 5.20c and 5.20d, there are significant positive (over 5 $\times 10^{15}$ molecules/cm^2) and negative anomalies (-3 to -2 $\times 10^{15}$ molecules/cm^2) over the UK for the Drizzle and Showers, respectively. The spatial pattern of the tracer fields to that of AQUM and OMI column NO$_2$ is more extensive. However, since the core anomaly fields remain, it proves that transport processes of the chemical species are causing these column NO$_2$ composite patterns and that the PWC Drizzle and Showers precipitation types are good proxies of atmospheric transport. In Figure 5.20c, there are some negative anomalies occurring on the eastern side of the domain. In the case of OMI and AQUM column NO$_2$, I suggest that the chemical loss of
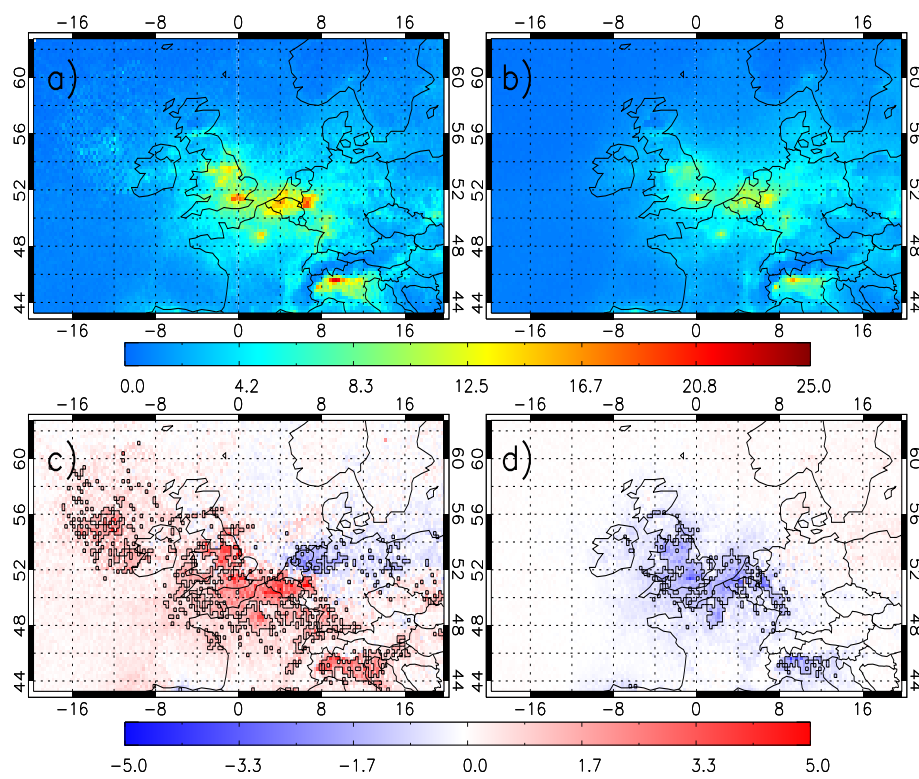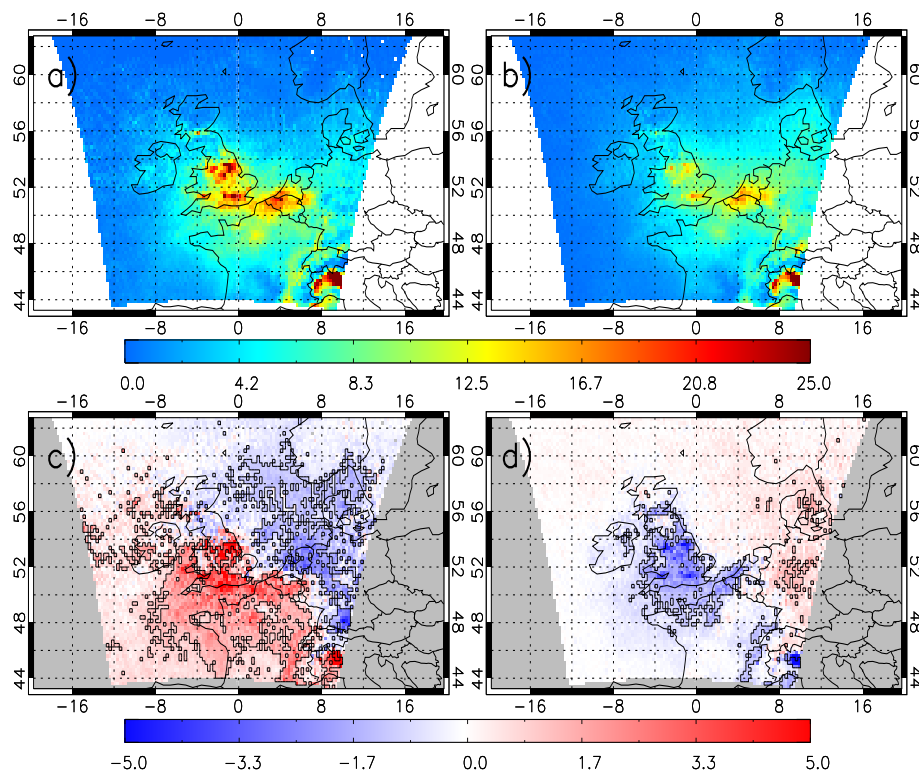

Figure 5.20: Composites of AQUM column tracer ($\times 10^{15}$ molecules/cm^2) between 2006-2010 for (a) PWC 5 (Drizzle) conditions, (b) PWC 8 (Showers) conditions, (c) PWC 5 (Drizzle) anomalies and (d) PWC 8 (Showers) anomalies.

the species means that no significant anomalies are seen here. However, the tracer, which is not chemically lost, is transported here under average conditions, but under the stable Drizzle conditions, there is a reduced transport to this region and the negative anomalies, -3 to -5 $\times 10^{15}$ molecules/cm^2, result.

5.4   Conclusions

This chapter has shown that the OMI NO$_2$ tropospheric column product can be used to detect the influences of synoptic meteorology on NO$_2$ tropospheric columns over the UK. UK column NO$_2$ peaks in winter (October-March) under anticyclonic conditions. It is likely that increased winter NO$_x$ emissions from energy generation coupled with more stable conditions and reduced photolysis allow for the accumulation of NO$_2$ above the source regions. The cyclonic conditions have a less defined seasonal pattern, but column NO$_2$ over the UK source regions is slightly higher in summer (April-September). This is consistent with more intense winter cyclonic conditions, which reduce column NO$_2$ concentrations and has more impact than NO$_2$ loss in summer from enhanced photolysis. The influence of transport of NO$_2$ by wind flow directions can also be seen in the OMI NO$_2$ data, with good examples being the south-easterly and south-westerly flow directions. The spatial patterns in the NO$_2$ fields associated with these transport regimes are significantly different at a 95% confidence level using the Wilcoxon Rank Test.

These statistically significant meteorology-atmospheric chemistry relationships, seen by OMI, can potentially be used as a model validation tool. This dataset will allow progress beyond simply using the satellite data for operational model validation (calculation of means and biases, see Dennis et al. (2010)) and can be used to test the model's ability to reproduce the influence of meteorology on NO$_2$ (dynamic model evaluation). For chemistry-climate models this can also be used to evaluate the model under each of the synoptic regimes, rather than just using averages over seven or so years.

This method using the LWTs was also applied to OMI total column HCHO data. In winter, the HCHO data appears to be very noisy and it is difficult to detect any coherent spatially significant signals. In summer though, the data signal-to-noise ratio is better and clear increases and reductions in UK HCHO can be seen under cyclonic and anticyclonic conditions, respectively. The hypothesis is that reduced photolysis of HCHO under cyclonic conditions leads to increased concentrations. However, anticyclonic conditions are associated with clear skies and greater loss of HCHO from photolysis. The AQUM column HCHO, sampled by the LWTs, did not reveal any statistical relationships. There is a clear bias between AQUM and OMI, where OMI column HCHO ranges between 15-25 $\times 10^{15}$ molecules/cm^2 more in places.

Surface observations from the AURN network of NO_2 and O_3 show clear UK patterns of O_3 and NO_2 accumulations under summer and winter anticyclonic conditions, respectively. Winter NO_x emissions are larger and anticyclonic conditions aid its accumulation over the source regions. Elevated summer O_3 under anticyclonic conditions is consistent with the trapping of O_3 precursors under high pressure and clear skies leading to their photochemical loss and O_3 production.

Under south-easterly and north-westerly flows, NO_2 concentrations are elevated and reduced, respectively, independent of season. Summer O_3 under south-easterly flow is also enhanced. Here, I speculate that south-easterly flow transports air pollution from continental Europe to over the UK. North-westerly flow transports NO_2 off the UK mainland, out into the North Sea and replaces it with clearer North Atlantic air. In the other examples presented in Section 5.3.3, the NO_2 and O_3 concentrations appear to be negatively correlated; governed by NO_x-O_3 cyclical reaction.

Finally, the PWC was used, like the LWTs, to composite the OMI column NO_2. Under PWC 5 (Drizzle) conditions, there is a significant increase in column NO_2. While under PWC 8 (Showers), there is a significant decrease in column NO_2. This study hypothesis that the precipitation types are a proxy for atmospheric stability. AQUM column NO_2, sampled under the PWC, shows similar anomalies where Drizzle and Showers significantly increase and reduce column NO_2, respectively. An idealised tracer was introduced into the NO_x emission sources with a life time of one day. The tracer columns showed similar patterns to OMI and AQUM column NO_2 confirming that precipitation can be a proxy for atmospheric stability (Drizzle = stable, Showers = unstable) and resulted in the accumulation and transport of NO_2 at/away from source regions. It would have been interesting to look at Snowfall and Thunderstorm influences on column NO_2, especially thunderstorms as it can be a significant source of NO_x. However, the data was too sparse temporally.

Overall, synoptic weather has a significant impact on atmospheric chemistry throughout the troposphere. Atmospheric stability can lead to the direct accumulation and transport of primary pollutants. Indirect effects of atmospheric stability, e.g. cloud cover, can control the levels of photolysis which can affect air pollutant concentrations. Modelling was used at the end of this chapter to prove that precipitation type can be used as a proxy for atmospheric stability and respective pollution levels. However, the next chapter, Chapter 6, investigates whether AQUM can reproduce the observed relationships found here in Section 5.3.1. Secondly, it investigates if atmospheric chemistry or dynamics are more active in governing these synoptic weather - air pollution relationships.

Chapter 6

Influence of synoptic weather regimes on UK air quality: Model results

6.1 Introduction

Chapter 5 showed that the influence of synoptic weather on UK air quality can be detected in column NO_2 observed by OMI. This chapter builds on these findings by using AQUM to investigate the patterns between OMI NO_2 and the LWTs. In Chapter 4, "Operational" model evaluation was performed using statistical analysis aimed at determining the agreement between the model and observations (Dennis et al., 2010). In contrast, in this chapter, "Dynamical" model evaluation of AQUM is used to assess the ability of the regional model to simulate changes in air quality stemming from changes in emissions and/or meteorology (Dennis et al., 2010). In this case, I investigate whether AQUM can reproduce the air quality relationships seen by OMI when sampled under the LWTs. AQUM is then used to explore the differences in these air quality-synoptic weather relationships between weather types and season, e.g. is chemistry or weather more active in governing these relationships in different seasons?

Section 6.2 describes the AQUM model setup. Section 6.3 discusses the OMI-LWT relationships over the period 2006-2010 which overlaps with the AQUM simulation. The results comparing AQUM column NO_2 and LWTs are presented in Section 6.4. Section 6.5 discusses model experiments using idealised tracers with different lifetimes to examine these air quality - synoptic weather relationships. The conclusions are summarised in Section 6.6.

6.2   Model Setup

AQUM was run for 5 years from 1st January 2006 - 31st December 2010. The set up is similar to the 2006 AQUM runs in Chapter 4, but uses the MACC LBCs as those from GEMS only exist up till 2008. This is only the second time that the AQUM has been run for such a multiannual period as the model is normally used for short-term NWP studies. Five years provides a sufficient model data record to reproduce the OMI column NO_2 - LWT relationships. Therefore, we focus only on 5 years and not the 7 year period used for the OMI - LWT comparisons in Chapter 5. There are few missing days for the 5-year simulation as the MACC LBCs do not exist over the full period (e.g. 4th-6th June 2007 are missing).

These runs do not use the N_2O_5 heterogeneous chemistry recommended in Chapter 4 (this work was undertaken before the experimentation with heterogeneous chemistry). Again, the 2007 emissions with ENTEC shipping lane emissions are used for the 2006 simulation, instead of the coarser EMEP emissions. Model fields are output at 13.00 LT to match the OMI London overpass time. As AQUM is a limited area NWP model, the representation of weather systems through the LBCs should have high accuracy. Therefore, the large-scale flow from the NCEP reanalyses, used to calculate the LWTs, is likely to be highly consistent with the AQUM large-scale flow through the LBCs. Jones et al. (2014) show good skill in the LWT development based on the NCEP reanalyses against the original objective and subjective methods. As a result, AQUM column NO_2 fields are directly sampled under the classifications derived from the LWTs in 5.1.

6.3   OMI Column NO_2 - LWTs Relationships: 2006-2010

As AQUM was run between 2006-2010, the OMI column NO_2 - LWT analyses from Chapter 5 are repeated for this time period. Figures 6.1 and 6.2 show the influences of cyclonic and anticyclonic conditions in winter and summer on column NO_2. The LWTs are grouped into the cyclonic and anticyclonic conditions based on the approach presented again in Table 5.1. Under cyclonic conditions, column NO_2 is transported away from the source regions, while anticyclonic conditions aid its accumulation. Figure 6.2 highlights significant, 95% confidence level, anomalies of $\pm 5 \times 10^{15}$ molecules/cm^2 over the North Sea/UK under cyclonic conditions. The reverse is found under anticyclonic conditions. The spatial extent of the anomalies is greatest in winter for both vorticity regimes.

Figure 6.3 shows that between 2006-2010 (non-seasonal) there is source region leeward transport of column NO_2 seen by OMI. In the case of south-easterly flow, there is a significant transport of column NO_2 away from London and northern England of over 5 $\times 10^{15}$ molecules/cm^2 towards the Midlands and the Irish Sea, respectively. Under south-westerly flow, column NO_2 is transported away from London and Yorkshire out into the

Figure 6.1: Composites of OMI column NO$_2$ (10^{15} molecules/cm^2) for 2006-2010 for (a) summer cyclonic, (b) summer anticyclonic, (c) winter cyclonic and (d) winter anticyclonic conditions.

North Sea; inferred by the positive (3-5 $\times 10^{15}$ molecules/cm^2) and negative (-3 to -1 $\times 10^{15}$ molecules/cm^2) column NO$_2$ anomalies, respectively. The transport under south-easterly flow potentially has higher anomalies because it also transportes pollution off continental Europe, while south-westerly flow brings in relatively clear air from the Atlantic.

There are no significant differences between the synoptic weather - air quality relationships based on the 5- and 7- year comparisons. Therefore, the LWT-OMI 5-year comparisons accurately represent the relationships seen in Chapter 5 and act as baseline for comparisons between AQUM column NO$_2$ and the LWTs.

6.4   AQUM Column NO$_2$ - LWTs Relationships

AQUM column NO$_2$, composited under the LWTs, displays similar patterns to OMI. For this comparison, AQUM has been co-located spatially and temporally with each OMI retrieval and the averaging kernel applied. In winter, under cyclonic conditions AQUM column NO$_2$ ranges between 10-13 $\times 10^{15}$ molecules/cm^2 over the UK and Benelux source regions (Figure 6.4c). Over the western and eastern domain, column NO$_2$ ranges between 0-4 $\times 10^{15}$ molecules/cm^2 and 5-8 $\times 10^{15}$ molecules/cm^2, respectively. Under winter anticyclonic conditions column NO$_2$ over UK and Benelux source regions is 16-20 $\times 10^{15}$

Figure 6.2: Anomalies of OMI column NO_2 composites compared to the seasonal 5-year average (10^{15} molecules/cm^2) for (a) summer cyclonic, (b) summer anticyclonic, (c) winter cyclonic and (d) winter anticyclonic conditions. Black boxes indicate where the anomalies are statistically significant at the 95% level.

molecules/cm^2 and the background column NO_2 ranges between 5-8 $\times 10^{15}$ molecules/cm^2 (Figure 6.4d). Larger column NO_2 over the North Sea in Figure 6.4c is indicative of cyclonic westerly transport off the UK mainland, while larger source region column NO_2, in Figure 6.4d than 6.4c, highlights anticyclonic accumulation of NO_2.

When compared with OMI (Figure 6.1c) the AQUM sampled under the winter cyclonic conditions shows greater column NO_2 transport over North Sea ranging between 5-8 $\times 10^{15}$ molecules/cm^2 and covering a larger spatial extent. Under anticyclonic conditions, column NO_2 ranges between 16-20 $\times 10^{15}$ molecules/cm^2 and is similar over London to that of OMI. However, AQUM column NO_2 is lower/higher than OMI over the Benelux region/northern England by 2-3 $\times 10^{15}$ molecules/cm^2. The AQUM-OMI winter anticyclonic background column NO_2 ranges between 5-10 $\times 10^{15}$ molecules/cm^2, but AQUM has larger spatial coverage. Both OMI and AQUM show similar patterns in summer for both vorticity types but with lower spatial extent than winter. Interestingly, the OMI cyclonic UK source region column NO_2 is larger in summer (8-10 $\times 10^{15}$ molecules/cm^2) than winter (6-8 $\times 10^{15}$ molecules/cm^2), but AQUM does not simulate this. AQUM summer cyclonic UK source region NO_2 ranges between 6-8 $\times 10^{15}$ molecules/cm^2, while in winter it is 10-12

Figure 6.3: Composites of OMI column NO$_2$ (10^{15} molecules/cm^2) under different wind flow directions and the differences of these with respect to the 5-year average. (a) South-easterly flow, (b) south-westerly flow, (c) south-easterly difference and (d) south-westerly difference.

$\times 10^{15}$ molecules/cm^2.

The AQUM and OMI transport and accumulation differences can be seen in Figure 6.5 which shows anomalies between composite averages and the 5-year seasonal means. Under winter cyclonic conditions, both AQUM and OMI show significant negative/positive anomalies of similar magnitude over the UK/North Sea. However, the AQUM column NO$_2$ dipole is spatially larger and covers the full domain (Figure 6.5c). This implies that there is either too much AQUM column NO$_2$ being transported under cyclonic conditions or AQUM's dynamics are too strong. However, as these runs do not include N$_2$O$_5$ heterogeneous chemistry and use the MACC LBC (positive O$_3$ bias which enhances column NO$_2$ - Chapter 4), this probably accounts for the AQUM-OMI differences under this regime and season. The same arguments apply to Figure 6.5d, where the accumulation of AQUM column NO$_2$, causing significant positive anomalies of 1-3 $\times 10^{15}$ molecules/cm^2, covers the UK and the south-western domain. OMI, on the other hand, only observes anomalies between 1-3 $\times 10^{15}$ molecules/cm^2 over the UK. In summer, N$_2$O$_5$ hydrolysis on aerosol is reduced so the AQUM - OMI anomaly composites are similar.

Under the (non-seasonal) wind flow regimes, AQUM again has larger column NO$_2$ than
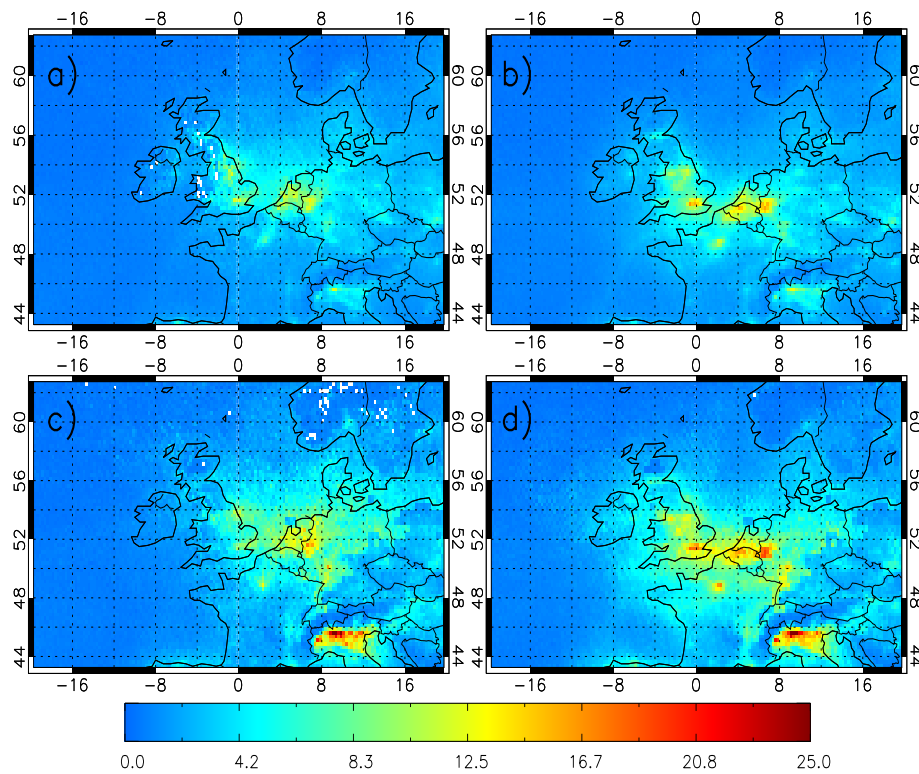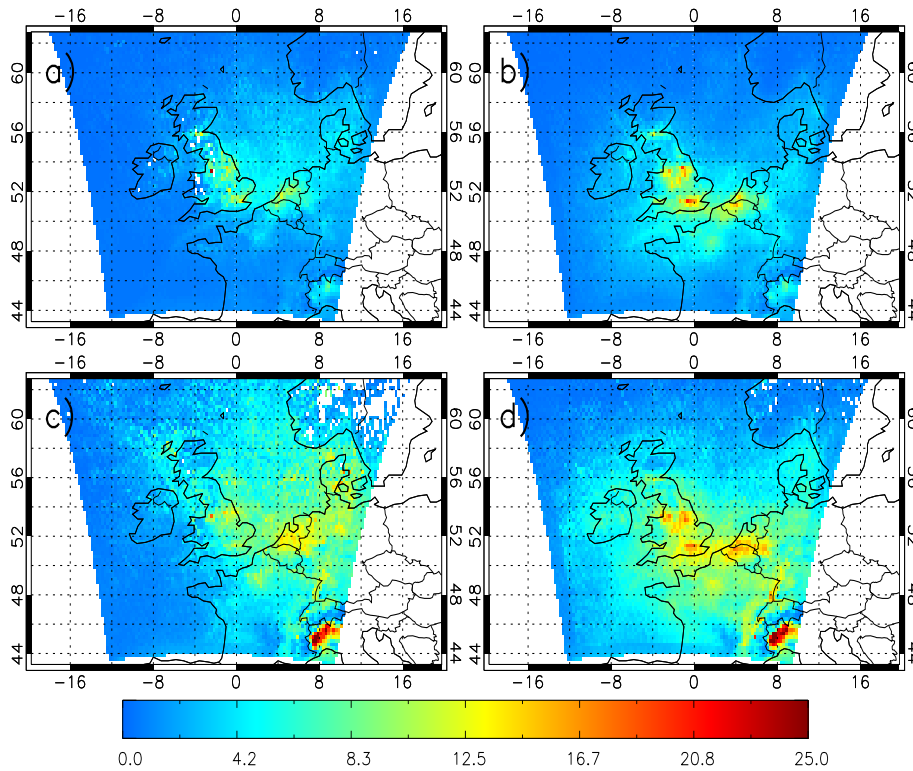
Figure 6.4: Composites of AQUM column NO_2 (10^{15} molecules/cm^2)for 2006-2010 for (a) summer cyclonic, (b) summer anticyclonic, (c) winter cyclonic and (d) winter anticyclonic conditions.

OMI. South-easterly flow highlights the same leeward transport of column NO_2 away from the source regions where AQUM peaks at approximately 20×10^{15} molecules/cm^2 over London and northern England (Figure 6.6a). OMI column NO_2 is the same over London but lower (12-15 $\times 10^{15}$ molecules/cm^2) over northern England (Figure 6.3a). South-westerly source region leeward transport of column NO_2 again results in similar London concentrations, but overestimates in northern England by approximately 3-4 $\times 10^{15}$ molecules/cm^2 (Figure 6.6b). The overestimation of column NO_2 in northern England is discussed in Chapter 4.

The south-easterly anomaly fields (Figure 6.3c and 6.6c) show good agreement between OMI and AQUM, where column NO_2, is being transported way from London and northern England towards the Midlands and Irish Sea, respectively. Over continental Europe negative anomalies of -3 to -1 $\times 10^{15}$ molecules/cm^2 are more prominent in AQUM column NO_2. This shows that more NO_2 has been transported in AQUM than in the real atmosphere observed by OMI. The south-westerly flow shows similar leeward positive anomalies of 1-3 $\times 10^{15}$ molecules/cm^2 over the North Sea from northern England in both datasets. However, AQUM (Figure 6.6d) simulates stronger transport of column NO_2 from the Benelux region than OMI with more extensive significant pixels. Over the UK,
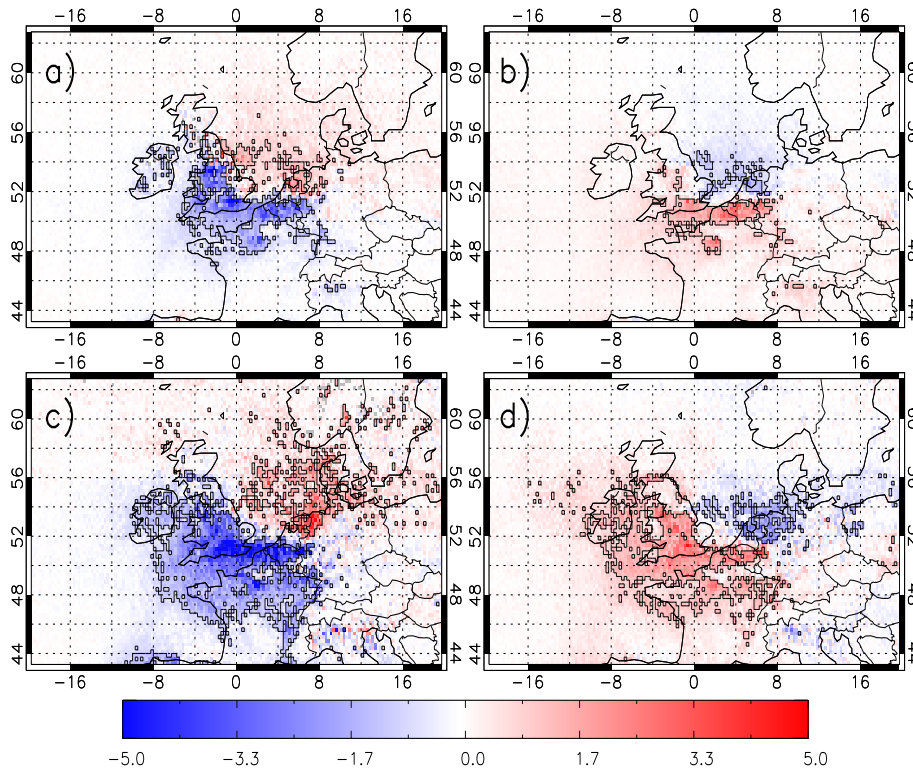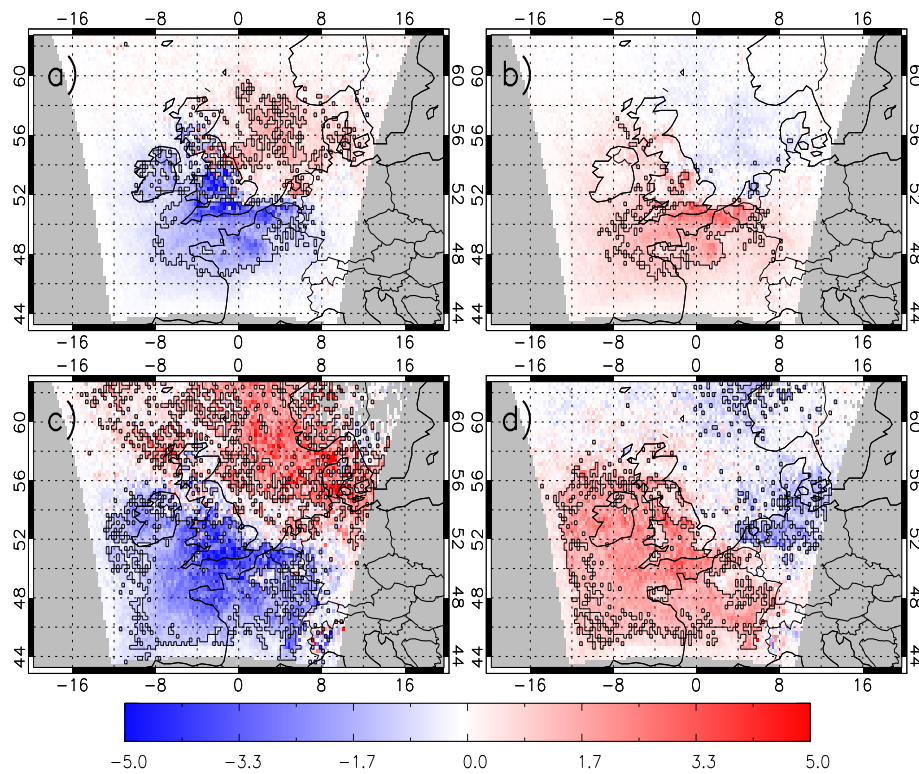
Figure 6.5: Anomalies of AQUM column NO$_2$ composites compared to the seasonal 5-year average (10^{15} molecules/cm^2) for (a) summer cyclonic, (b) summer anticyclonic, (c) winter cyclonic and (d) winter anticyclonic conditions.

negative anomalies of -3 to -1 $\times 10^{15}$ molecules/cm^2 for AQUM and OMI show the removal of column NO$_2$ off the mainland. Again this is spatially more extensive in AQUM.

On the regional scale, AQUM captures the OMI column NO$_2$ - LWT relationships with similar significant anomalies from the period average. However, the missing NO$_x$ sink of N$_2$O$_5$ hydrolysis on aerosol leads to higher composite column NO$_2$, primarily in winter, and can result in over representation of the winter anomaly dipole systems seen by OMI under the synoptic regimes. The use of the MACC LBCs, which enhances NO$_2$ concentrations through positive O$_3$ biases, could also be contributing to elevated AQUM column NO$_2$.

For a more complete dynamical model evaluation the differences between AQUM and OMI column NO$_2$ have been quantified. To compare the spatial extent of the anomaly fields from AQUM and OMI under the different seasonal weather regimes metrics such as correlation, regression and RMSE could be used, but these have limitations. Correlation only accounts for the spatial patterns of the anomalies and not the magnitude. Also, it does not account for the significance of the pixels. Linear regression should indicate the best AQUM-OMI agreement when tending towards a 1:1 fit. However, this metric does not account for anomaly significance either. RMSE gives a good indication of the error
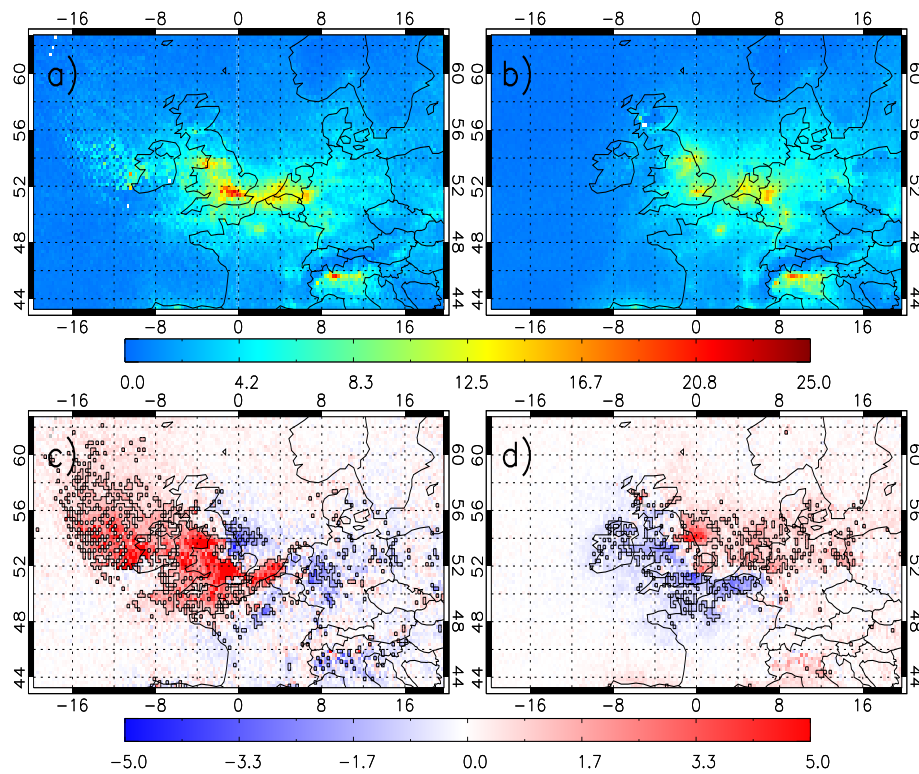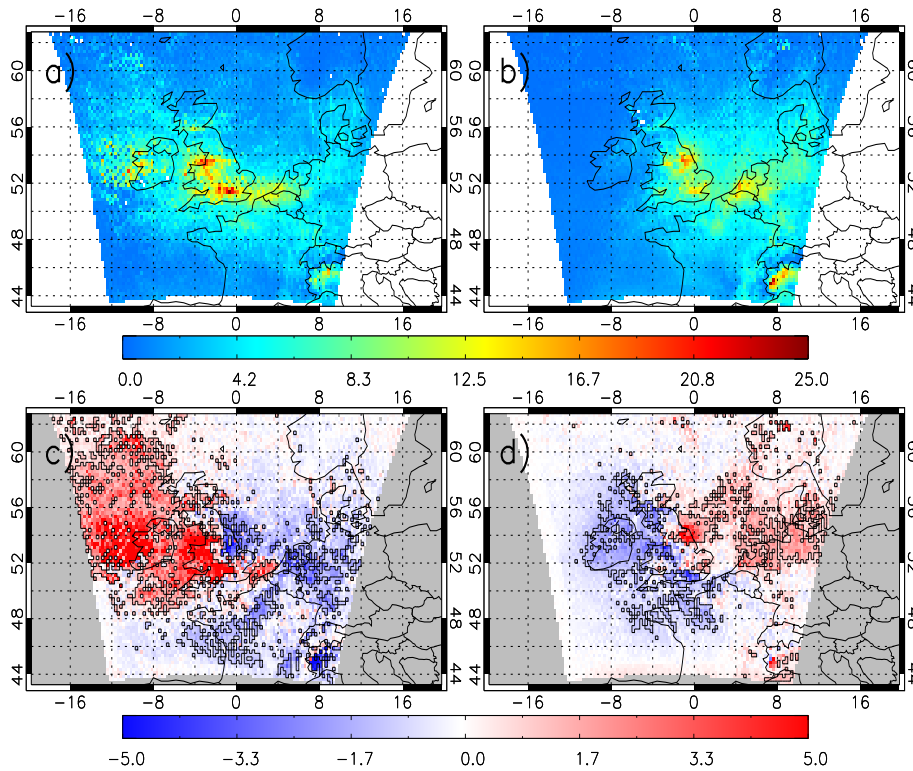
Figure 6.6: Composites of AQUM column NO_2 (10^{15} molecules/cm^2) under different wind flow directions and the differences of these with respect to the 5-year average. (a) South-easterly flow, (b) south-westerly flow, (c) south-easterly difference and (d) south-westerly difference.

in the anomaly field magnitudes and the spatial extent of the significant anomaly clusters indirectly. For instance, if an anomaly cluster for AQUM has a smaller spatial extent than OMI, the error magnitudes will be larger where the two are different, degrading the comparisons. However, comparisons can also be degraded if the anomalies in AQUM and OMI are similar but offset slightly (e.g. the model anomaly cluster is offset to the east by 0.5°).

A more appropriate method to compare AQUM and OMI column NO_2 under the four regimes, therefore, is to analyse both the spatial extent of the significant anomalies and their magnitude. For each of the seasonal synoptic regimes the number of significant positive and negative column NO_2 anomalies were calculated. This represents the spatial extent of significance. The anomalies were grouped into separate counts of the positive and negative anomaly clusters as they show independent features across the UK. To ascertain the magnitude of the anomaly clusters, the average positive and negative anomaly was calculated. Therefore, the spatial extent and size of the anomalies are accounted for.

To compare the similarity of the AQUM and OMI anomaly for each regime, the size of the AQUM positive and negative clusters were presented as a percentage of OMI column
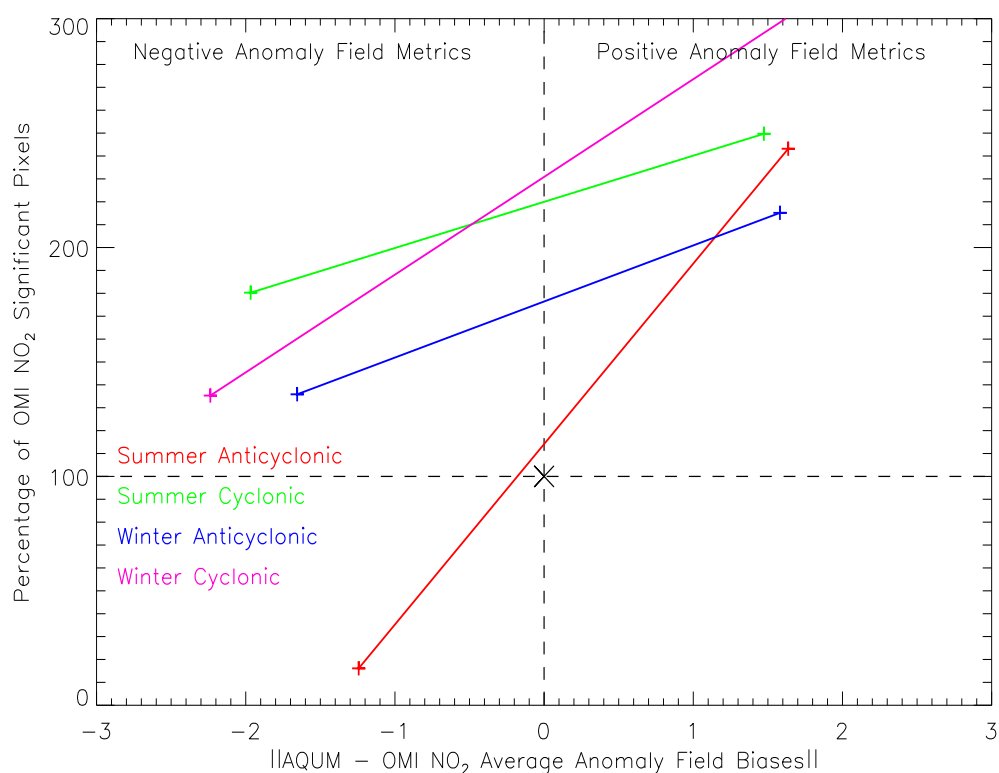
Figure 6.7: AQUM-OMI column NO$_2$ anomaly comparisons for summer and winter anti-cyclonic and cyclonic conditions. Left and right hand sides are the negative and positive anomaly cluster metrics per plot. The percentage of significant AQUM anomalies for positive and negative clusters are presented as a percentage of the respective OMI significant anomalies (y-axis). The x-axis represents the AQUM-OMI absolute mean cluster anomaly bias ($\times 10^{15}$ molecules/cm^2) for the negative (LHS) and positive (RHS) AQUM-OMI anomaly clusters in the synoptic weather-air pollution comparisons.

NO$_2$ positive and negative anomalies. Then, the absolute bias between the AQUM-OMI column NO$_2$ positive and negative anomaly cluster averages were obtained. Here the term "absolute bias" is used to describe the difference between the AQUM and OMI NO$_2$ anomaly cluster averages. This results in four pieces of information; the negative and positive anomaly cluster size (%) and the absolute bias between the positive and negative anomaly cluster averages. This methodology is shown in Figure 6.7 where the metrics plotted are the absolute AQUM-OMI column NO$_2$ cluster bias (negative and positive cluster metrics on the left and right hand sides) against the AQUM-OMI anomaly cluster size percentage. The two points are plotted as a line for each seasonal regime and the best comparison between AQUM and OMI will have cluster size percentages closest to 100% and absolute AQUM-OMI NO$_2$ average cluster biases of 0. The "goal zone" for best AQUM representation of OMI column NO$_2$ under the respective regimes is centred on (x=0, y=100).

In general, Figure 6.7 confirms that AQUM overestimates column NO$_2$, which results

in larger anomalies (spatially and in magnitude), as seen in Figures 3.2 and 3.5. For all the seasonal weather regimes, the AQUM-OMI anomaly cluster biases range between 1-2 $\times 10^{15}$ molecules/cm^2 and the spatial extent is overestimated by 30-150%. Winter anticyclonic conditions appear to have the best comparisons with biases of approximately 2 $\times 10^{15}$ molecules/cm^2 for each anomaly cluster, but with better spatial representation of 130-220%. Therefore, even though there are some large differences between AQUM and OMI column NO$_2$ under the different regimes, the spatial patterns look similar in Figures 3.2 and 3.5.

6.5   AQUM Column Tracer - LWTs Relationships

Section 6.4 has shown that AQUM successfully reproduces the relationships seen by OMI column NO$_2$ when sampled under the LWTs, despite overestimation of column NO$_2$. Therefore, AQUM can be used as a tool to diagnose the influence on meteorology and chemistry on the distribution of NO$_2$ under the seasonal weather regimes. In this section idealised tracers are introduced into the AQUM NO$_x$ emissions with chemical lifetimes of 1, 3, 6, 12, 24 and 48 hours. The idealised tracers will indicate of the importance of transport and atmospheric chemistry governing the relationships between column NO$_2$ and seasonal synoptic weather. If transport is the only factor governing the air quality distribution under the different synoptic regimes, then a fixed lifetime tracer would have the similar anomaly fields as NO$_2$. On the other hand, if changes in chemistry are driving or partially accounting for the different regime anomalies, then a certain fixed lifetime tracer would be unable to capture the observed differences. Therefore, depending on which of the tracers with different lifetimes results in anomaly fields most similar to the AQUM column NO$_2$ anomalies, for winter and summer cyclonic and anticyclonic regimes, the relative importance of the processes can be determined. As the chemistry of NO$_x$ is complex, with non-linear relations via ozone, diurnal cycles and varying emissions, a simple e-folding tracer will never truly match the NO$_2$ distribution. Hence, it will indicate transport and chemical representation to a first-order approximation but can still be used to answer relevant questions. For instance, can the tracer be used to explain why the OMI column NO$_2$ summer anomalies (Figure 6.2) are less spatially significant? Is the chemical lifetime of summer NO$_2$ shorter than that of winter, so synoptic meteorology has smaller NO$_2$ columns to influence? This method of using e-folding tracers has been applied in inverse modelling of NO$_x$ emissions from satellite data. Richter et al. (2004) used SCIAMACHY column NO$_2$ measurements and simple approximations of NO$_x$ loss (i.e. a fixed lifetime of NO$_x$) to develop shipping emissions over the Red Sea.

Figure 6.8 shows AQUM column tracer$_{24}$ (i.e. tracer with a lifetime of 24 hours), sampled under the LWTs, to illustrate how it compares to AQUM column NO$_2$. The other
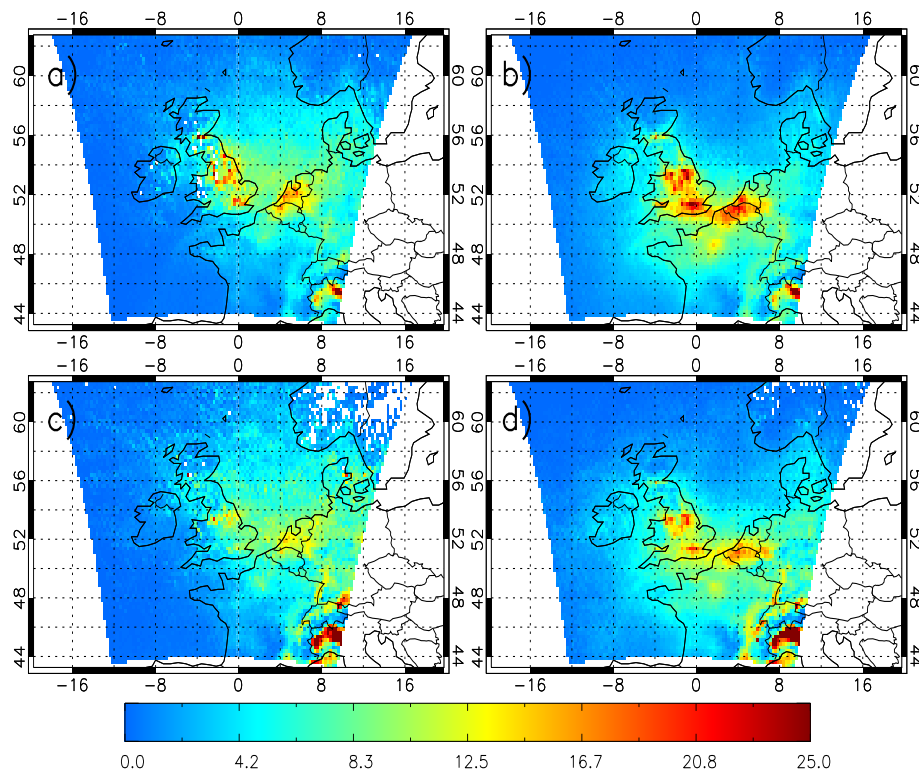
Figure 6.8: Composites of AQUM (AKs applied) column tracer$_{24}$ (i.e. tracer with a lifetime of 24 hours) ($\times 10^{15}$ molecules/cm^2) for 2006-2010 for (a) summer cyclonic, (b) summer anticyclonic, (c) winter cyclonic and (d) winter anticyclonic conditions.

tracer lifetimes are then analysed using the methodology shown in Figure 6.7. In summer cyclonic conditions, peak column tracer$_{24}$ is located over the source regions with values of approximately 20 $\times 10^{15}$ molecules/cm^2, but there is clear transport over the North Sea with values between 10-12 $\times 10^{15}$ molecules/cm^2. Under summer anticyclonic conditions (Figure 6.8b) the column tracer$_{24}$ peaks at similar values of 20-25 $\times 10^{15}$ molecules/cm^2 to Figure 6.8a, but the accumulation of the tracer over the source regions results in significantly larger spatial extents. In winter (Figures 6.8c and 6.8d), the column tracer$_{24}$ has similar, but generally smaller, spatial patterns under the respective weather regimes to that of summer. As NO$_x$ emissions tend to be greater in winter, more column trace$_{24}$ would be expected over the source regions (as seen for OMI column NO$_2$). As discussed in Chapter 4, the seasonal cycle in the AQUM NO$_x$ emissions is larger in winter than summer. Also, Zhou et al. (2012) show that maximum column NO$_2$ over the UK occurs in winter/spring. AQUM and OMI column NO$_2$ are greater in winter, apart from OMI observed UK source region column NO$_2$ under summer cyclonic conditions when compared with winter cyclonic conditions. However, column tracer$_{24}$ has larger summer source and background concentrations than winter. This implies that either the tracer lifetime is too long and not representative of the true NO$_2$ lifetime or transport is stronger in winter.

Analysis of the other tracer lifetimes (Figures 6.9 and 6.10) highlights a similar pattern where summer source region and background column tracer, under either synoptic regime, is always larger than winter. Therefore, this suggests winter meteorology is dispersing the tracer from the source regions more efficiently than in summer. Figure 6.11 highlights the difference between the 2006-2010 winter and summer average wind flows over the UK from ECMWF ERA-Interim. AQUM wind data were not output in the model runs, but as the AQUM meteorology is heavily dependent on the LBCs, the ECMWF ERA-Interim data likely gives a representative picture of winds simulated in AQUM. The winter windspeeds tend to be larger than summer by 2-3 m/s over the northern and western domains, with a range between 5-12 m/s. In summer the range is between 3-9 m/s, indicating that the winter transport is stronger.
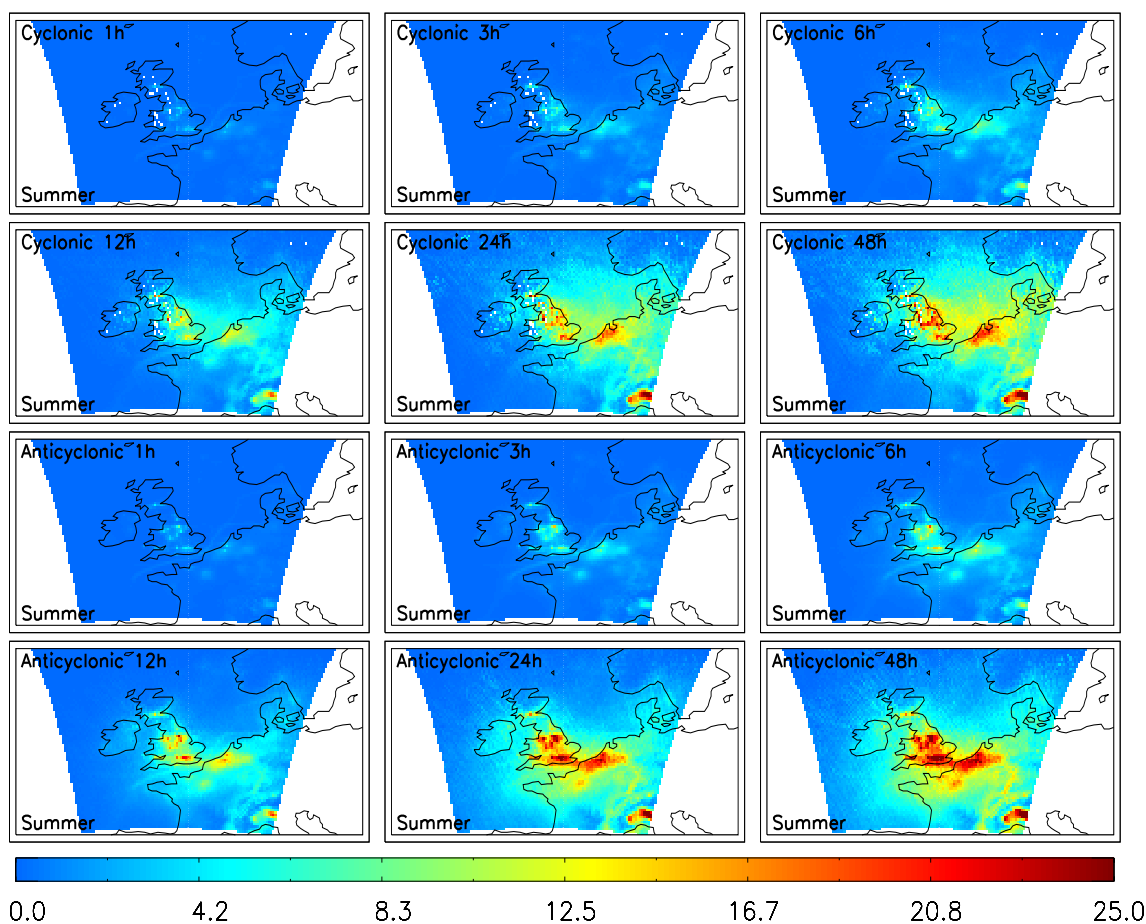
Figure 6.9: Summer AQUM column abundances of tracers with different lifetimes for cyclonic and anticyclonic conditions.

Figure 6.12 shows AQUM $tracer_{24}$ anomalies from the seasonal mean. For both synoptic regimes, the anomalies are similar in winter and summer. Under cyclonic conditions, the summer and winter anomaly dipoles have similar spatial extents. Positive peak anomalies of 2-5 $\times 10^{15}$ molecules/cm^2 occur over the North Sea and are indicative of westerly
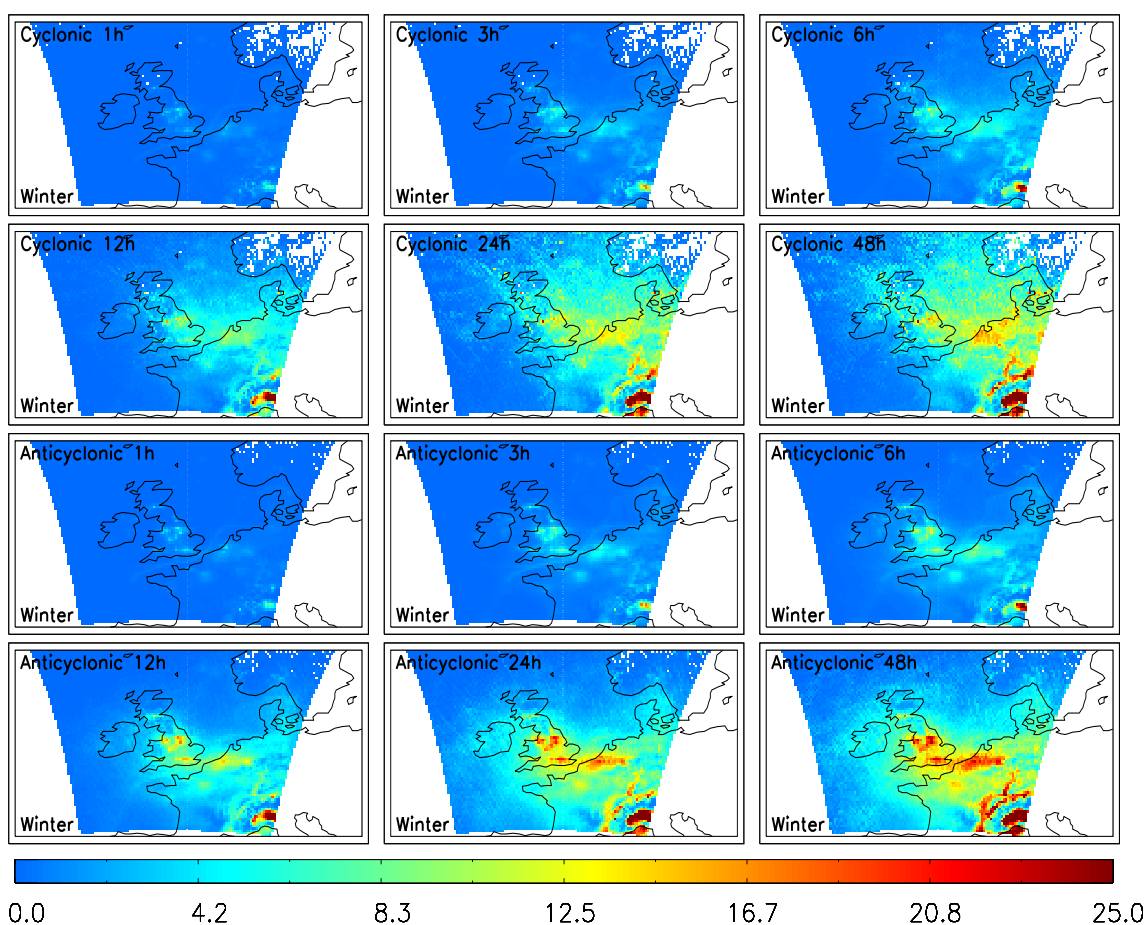
Figure 6.10: Winter AQUM column abundances of tracers with different lifetimes for cyclonic and anticyclonic conditions.
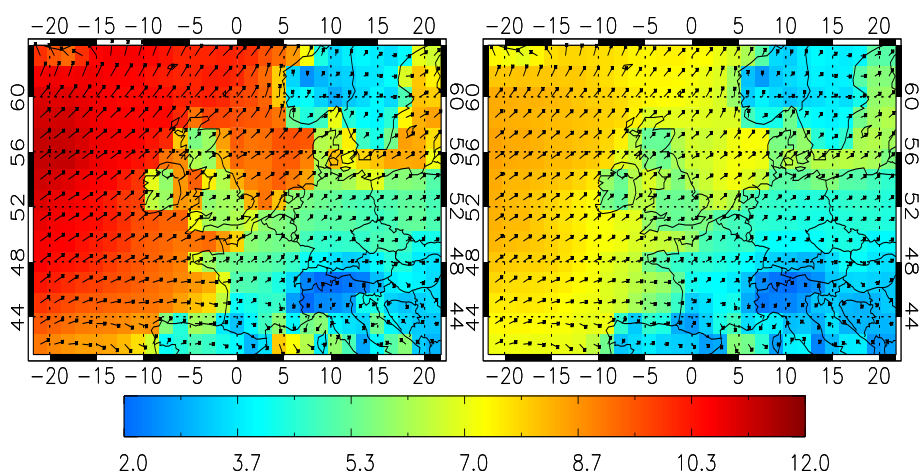
Figure 6.11: ECMWF ERA-Interim 12:00 UT 2006-2010 mean wind speeds (m/s) and directions for (left) winter and (right) summer.

transport off the UK mainland associated with cyclonic systems. Negative anomalies over the UK range between -5 to -3 $\times 10^{15}$ molecules/cm^2. Under anticyclonic regimes, accu-
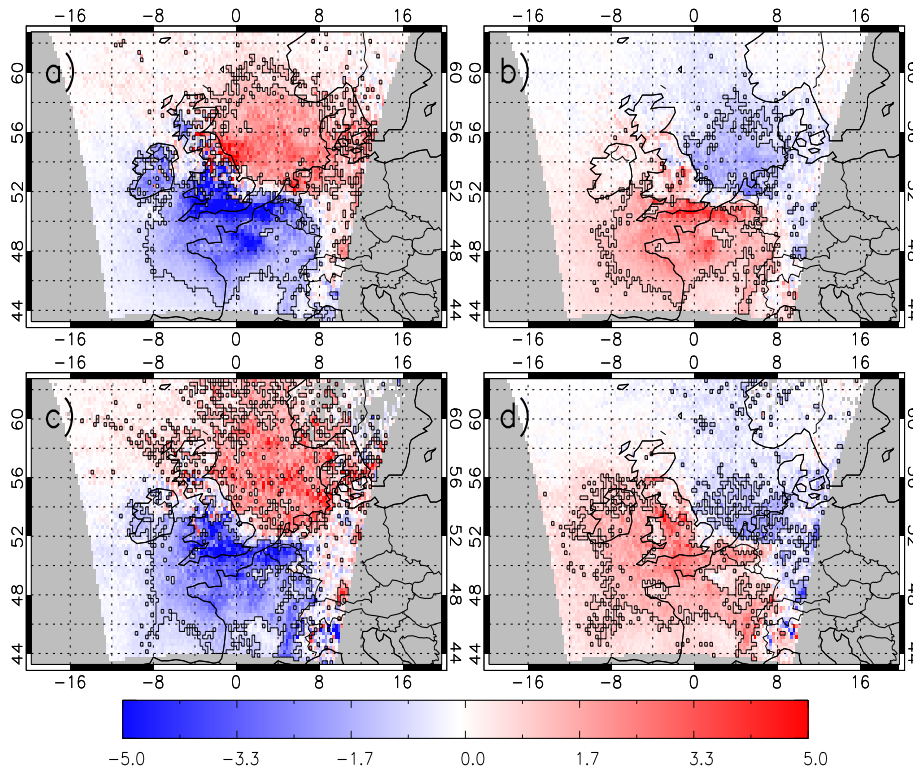
Figure 6.12: Anomalies of AQUM (AKs applied) column tracer$_{24}$ composites compared to seasonal 5-year average ($\times 10^{15}$ molecules/cm^2) for (a) summer cyclonic, (b) summer anticyclonic, (c) winter cyclonic and (d) winter anticyclonic conditions.

mulation of column tracer$_{24}$ results in positive anomalies of 1-5 $\times 10^{15}$ molecules/cm^2 and negative anomalies of 1-3 $\times 10^{15}$ molecules/cm^2 over the UK and North Sea. Comparing the winter column tracer$_{24}$ anomalies (Figures 6.12c and d) with winter AQUM column NO$_2$ anomalies (Figure 6.5c and d), the spatial patterns and anomaly magnitudes are similar for both synoptic regimes, unlike summer, where the spatial extent and magnitudes of the anomalies are much stronger for column tracer$_{24}$. This suggests that in winter, a lifetime of 24 hours is a good approximation for NO$_2$. In summer as the column tracer$_{24}$ anomalies are more spatially extensive than the AQUM NO$_2$ anomalies, the lifetime of 24 hours is too long. Therefore, this indicates to a first-order approximation that transport processes are more active in the column NO$_2$ - LWT relationships than atmospheric chemistry in winter under both synoptic regimes.

Figure 6.13 shows that the impact of wind direction on the column tracer$_{24}$ is similar to that on OMI and AQUM column NO$_2$, although, the concentrations are larger. The wind flows show significant leeward transport of column tracer$_{24}$ away from the source regions. Under south-westerly flow, column tracer$_{24}$ ranges between 20-25 $\times 10^{15}$ molecules/cm^2 leeward of the source regions. Positive anomalies of 2-5 $\times 10^{15}$ molecules/cm^2 can also be seen leeward of the source regions. Negative anomalies of -5 to -2 $\times 10^{15}$ molecules/cm^2 occur
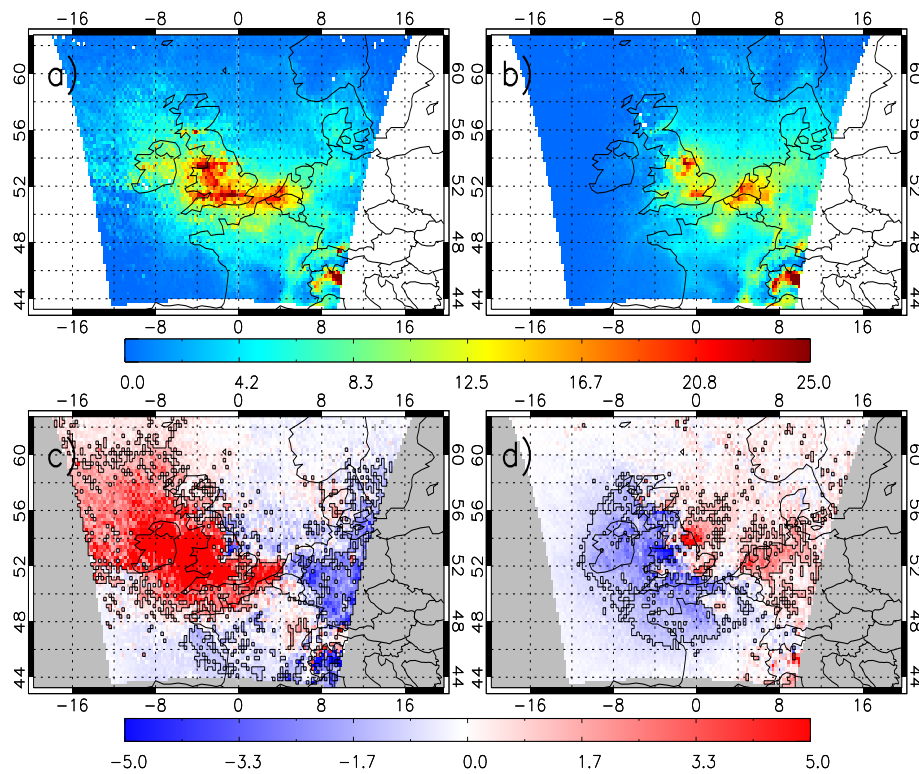
Figure 6.13: Composites of AQUM (AKs applied) column tracer$_{24}$ ($\times 10^{15}$ molecules/cm^2) under different wind flow directions and difference of these with respect to the 5-year average. (a) South-easterly flow, (b) south-westerly flow, (c) south-easterly difference and (d) south-westerly difference.

over the western UK where polluted air is transported westward and replaced with cleaner North Atlantic air. Under the south-easterly wind regime, column tracer$_{24}$ is transported away from the source regions with positive anomalies of over 5×10^{15} molecules/cm^2. However, the lifetime of the tracer appears to be too long as UK-wide column tracer$_{24}$ ranges between 20-25 $\times 10^{15}$ molecules/cm^2. Therefore, there is a much larger spatial extent and magnitude of positive anomalies leeward of London and northern England source regions when compared with OMI and AQUM column NO$_2$.

Overall, tracer$_{24}$ gives reasonable representation of how column NO$_2$ is influenced under different synoptic weather regimes, although other tracer lifetimes may give more accurate representation under different seasons and/or weather types.

To quantify which tracer life times are most representative of NO$_2$ under the different seasonal weather regimes, the methodology presented in Figure 6.7 is used. Under summer anticyclonic conditions, the 48, 24 and 12-hour lifetime tracers resulted in relatively small biases between 0-0.5 $\times 10^{15}$ molecules/cm^2 for the two anomaly clusters (Figure 6.14). However, these tracer lifetimes result in much larger significant positive and negative spatial significance extents with values between 200-6000%. All percentages over 500% have

been plotted at 500% for figure clarity. Tracer lifetimes of 1 and 3 hours did not result in any significant negative anomalies, so have not been plotted. Tracer$_6$ gives the best representation of the regime column NO_2 with absolute anomaly biases 0-0.25 $\times 10^{15}$ molecules/cm^2 and percentages between 20-150% (Figure 6.14). Therefore, 6 hours appears to be the best representation of the column NO_2 lifetime under summer anticyclonic conditions.
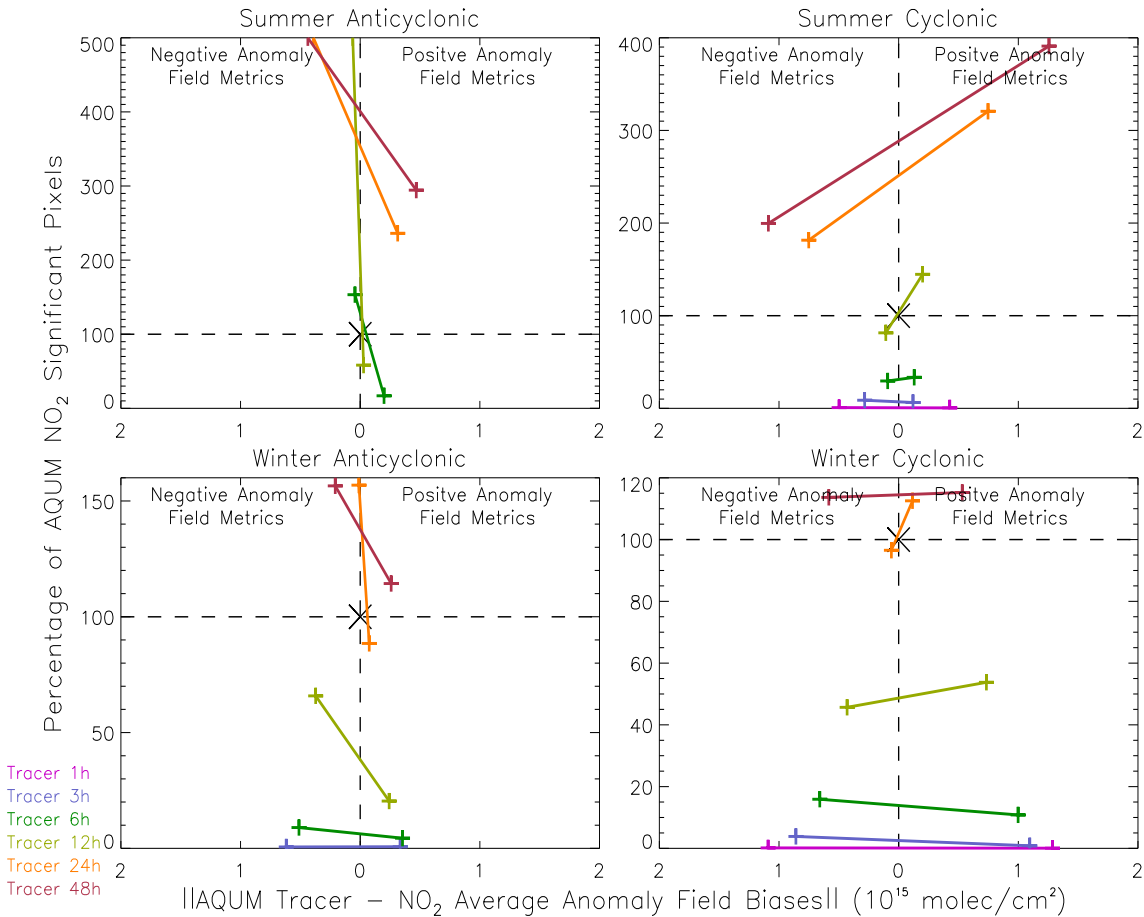
Figure 6.14: AQUM column tracer - NO_2 anomaly comparisons for summer and winter anticyclonic and cyclonic conditions. Left and right hand sides are the negative and positive anomaly cluster metrics per plot. The different colour bars represent different tracer lifetimes. The percentage of significant tracer anomalies for positive and negative clusters are presented as a percentage of the respective column NO_2 significant anomalies (y-axis). The x-axis represents the tracer-NO_2 absolute mean cluster anomaly bias ($\times 10^{15}$ molecules/cm^2) for the negative (LHS) and positive (RHS) AQUM tracer and NO_2 anomaly clusters in the synoptic weather-air pollution comparisons.

The summer cyclonic situations show similar patterns for tracers$_{24\&48}$ as they result in the largest biases of approximately 1 $\times 10^{15}$ molecules/cm^2 and spatial significance extents of 200-400%. Tracers$_{1,3\&6}$ show smaller absolute biases of between 0-0.5, but they under-

represent the spatial extent with low percentages of 0-20% (Figure 6.14). $Tracer_{12}$ is the most representative of the NO_2 lifetime under summer cyclonic conditions with biases between 0-0.25 $\times 10^{15}$ molecules/cm^2 and spatial extents of 80-150%. Under cyclonic conditions, there is more cloud coverage, so it can be inferred that NO_2 photolysis is reduced. However, anticyclonic conditions are more indicative of clear skies and greater losses of NO_2 from photolysis. This is consistent with a longer NO_2 lifetime, i.e. 12 hours, under cyclonic conditions.

Winter anticyclonic conditions suggest that either $tracer_{24}$ or $tracer_{48}$ best represent the regime NO_2 lifetime. $Tracer_1$ had insufficient data as its rapid loss resulted is no significant anomalies. $Tracer_{3,6\&12}$ have larger absolute biases between 0-0.5 $\times 10^{15}$ molecules/cm^2 and lower spatial significance percentages ranging from 0-70% (Figure 6.14). $Tracer_{48}$ has slightly larger absolute biases than $tracer_{24}$ by approximately 0.25 $\times 10^{15}$ molecules/cm^2. $Tracer_{24}$ captures the anomaly magnitude of the column NO_2 anomalies well with near zero biases. The spatial significance is similar for the negative clusters for $tracer_{24\&48}$ at approximately 150%. The positive clusters were approximately 90 and 115%. Therefore, $tracer_{24}$ gives a better representation of the column NO_2 with similar spatial significance percentage spreads from the "goal zone" (i.e. 0,100) as $tracer_{48}$, but with lower absolute biases.

Under winter cyclonic conditions, $tracers_{1,3,6\&12}$ all have too low spatial significance percentages and larger absolute biases. $Tracer_{24}$ again gives the best agreement to the column NO_2 anomalies under this regime with the lowest absolute biases and closest spatial significance percentages. $Tracer_{48}$ gives the next best agreement, but is not as close as $tracer_{24}$ in winter anticyclonic conditions. Therefore, 24 hours is the best representation of the NO_2 lifetime in winter.

6.6   Summary

Investigation of AQUM's ability to capture the synoptic weather - column NO_2 relationships, discussed in Chapter 5, meant the original analysis between the LWTs and OMI column NO_2 for 7 years was repeated over 5 years to match AQUM's simulation period of 2006-2010. There were no significant differences in the relationships between the 5 and 7 year comparisons, so the 5 year relationships were used as the baseline to compare with AQUM.

AQUM column NO_2 was composited up in the same way using the LWTs directly and successfully captured the OMI column NO_2 - LWT relationships in Chapter 5. Under anticyclonic conditions, AQUM column NO_2 accumulates over the source regions, while is transported away under cyclonic conditions. This is important as it highlights AQUM's ability to simulate potentially hazardous air pollution events under anticyclonic conditions.

This study argues that the representation of weather systems through the model LBCs (a NWP model so included high accuracy meteorology) is sufficiently consistent with the NCEP reanalyses used to produce the LWTs. Despite the agreement, AQUM column NO_2 anomaly fields tend to be more spatially significant than OMI. Chapter 4 shows that heterogeneous chemistry of N_2O_5 is required in the model, so the elevated column NO_2 state in AQUM mean more NO_2 is present to be influenced by the synoptic weather regimes. Hence, the spatial extent of the AQUM anomalies are more significant than OMI.

To determine which processes are important in driving these relationships, idealised (non-reacting) tracers were introduced into model using the NO_x emission sources and selected lifetimes of 1, 3, 6, 12, 24 and 48 hours. Analysis of the 24-hour lifetime tracer (tracer$_{24}$) showed similar patterns in winter to AQUM column NO_2 under both regions. Similar patterns were found in summer, but the lifetime was too long so more column tracer$_{24}$ remained in the domain and the column tracer anomalies where much larger than AQUM column NO_2 anomalies. However, as the tracer cannot be lost other than via its specified lifetime, these runs demonstrate that synoptic weather (accumulation and transport - strong and weak) is driving the air pollution over the UK and North-west Europe in winter and summer. Therefore, this is potentially important for policy makers when trying to mitigate or advise the public of poor air quality episodes.

To find the most accurate tracer lifetime of the column NO_2 under the seasonal weather regimes, a more complex method was required than regression or correlation between the AQUM column NO_2 and different tracer life time anomaly fields. For instance, neither correlation nor regression would account for the significance of the anomalies between the fields. Therefore, this study devised a method of comparing the average absolute bias and the spatial size of the significant anomalies between AQUM column NO_2 and tracer anomaly fields to find the most representative tracer lifetime under the seasonal weather regimes. In winter, tracer$_{24}$ has the most representative lifetime of column NO_2 in the troposphere under both vorticity regimes. However, in summer, tracer$_6$ and tracer$_{12}$ are more representative under anticyclonic and cyclonic conditions, respectively. This therefore shows that to a first-order approximation that atmospheric chemistry, as expected, is more influential in summer as the NO_2 lifetime decreases (enhanced photolysis of NO_2) and explains the less spatially significant summer synoptic weather-air pollution relationships detected in OMI column NO_2 in Chapter 5.

Chapter 7

Conclusions and Outlook

7.1   Completion of Aims

This project aimed to test the ability of satellite atmospheric trace gas observations to monitor UK air quality, evaluate AQUM's representation of UK air quality and investigate the links between air quality and synoptic weather in combination with AQUM. These aims have been achieved through the results discussed in Chapters 3, 4, 5 and 6.

Chapter 3 investigated the ability of satellite measurements of atmospheric chemistry (NO_2, O_3, HCHO and aerosol optical depth) to monitor UK air quality. Tropospheric column NO_2 data from the Ozone Monitoring Instrument (OMI) appears to be the best product to monitor air quality because of its multiple viewing angles, good signal-to-noise ratio and high resolution ($0.25° \times 0.25°$). SCIAMACHY column NO_2 can successfully detect the UK air pollution source regions, however, the number of observations are fewer and the resolution is coarser of $0.5° \times 0.5°$. OMI total column HCHO, on a coarser grid of ($0.5° \times 0.5°$), captures the spatial pattern of the land-sea mask, where peak concentrations exist over land and minimum values over the sea. However, the signal-to-noise ratio is much worse than that of OMI column NO_2. MODIS and OMI AOD on a $0.25° \times 0.25°$ grid are not really suitable for quantifying air quality on a regional scale. When detecting Saharan dust events, these global signals will stand out from the noise in the data, but over the UK aerosol events are not so prominent and are not well observed.

Ozone proved to be a challenge because products suitable for measuring tropospheric O_3 at high spatial and temporal resolutions were limited. Because the bulk of atmospheric O_3 is in the stratosphere, the sensitivity of satellites to tropospheric concentrations is limited. As a result the OMI subcolumn product had limited sensitivity to the troposphere. Other instruments, like TES, measure O_3 in the troposphere but have small footprints and limited sampling orbits. Therefore, it is difficult to get spatial information on a regional scale as interpolating TES swath data onto high resolution grids leaves a lot a data gaps. OMI-MLS tropospheric column O_3, despite its coarse resolution of $1.0° \times 1.0°$, gives the best spatial representation of European air quality. However, as the data product is

provided as monthly means, comparisons between the satellite and model at this temporal resolution will have significant sampling errors. The best O_3 product for model evaluation at least appears to be tropospheric retrievals from GOME-2. It has a coarse resolution that needs to be gridded to a $1.0° \times 1.0°$ or $1.5° \times 1.5°$ grid. But it does highlight European O_3 spatial features and the swath data can be co-located with model profiles and satellite averaging kernels applied to the model.

Chapter 4 investigated the validation of AQUM against OMI column NO_2 data, the satellite errors (random, systematic and smoothing) for DOAS retrieved species and an algorithm was derived. This reduces the retrieval random error component when averaging retrievals, which allows more critical AQUM-satellite comparisons as the time average random error component can be reduced by 30-70% in all seasons. Based on the summer and winter comparisons of 2006, the standard (operational) AQUM significantly overestimates OMI column NO_2 over northern England/Scotland and the North Sea above the UK, respectively. From multiple sensitivity experiments on the UK NO_x point source emissions I conclude that it was AQUM's representation of these emissions which caused the northern England/Scotland summer biases. By emitting an idealised tracer in the NO_x points sources I found a significant correlation of the peak tracer columns to the AQUM - OMI MBs. Introducing N_2O_5 heterogeneous chemistry into AQUM improves the AQUM - OMI comparisons in both seasons. In winter, the spatial extent of positive biases decreases; in summer, the northern England biases also decrease spatially. Therefore, this suggests that in summer the AQUM's representation of NO_x point sources is inaccurate but can be partially masked by the introduction of N_2O_5 heterogeneous chemistry, which is a well-known process and needs to be included in AQUM.

This study also aimed to quantify the relationships between synoptic weather and air pollution over the UK. In Chapter 5, OMI tropospheric column NO_2, composited up under different synoptic regimes, successfully detected the influences of synoptic meteorology on UK column NO_2. These relationships were to a statistically significant confidence level of 95%. The stable weather associated with anticyclonic conditions leads to the accumulation of column NO_2 over the UK source regions. This process is most efficient in winter at trapping higher levels of pollution from increased NO_x emissions and reduced photochemical loss of NO_2 over populated regions. This can potentially lead to dangerous levels of poor air quality, resulting in adverse health effects in the population. Under cyclonic conditions, atmospheric instability transports column NO_2 away from source regions, typically out into the North Sea due to the westerly flow associated with low pressure systems. The influence of transport of NO_2 by wind flow directions can also be seen in the OMI NO_2 data, with good examples being the south-easterly and south-westerly flow directions.

Based on the results in Chapter 5, AQUM column NO_2, in Chapter 6, was also composited up under different synoptic weather regimes to test if the model could reproduce

these important synoptic weather - air pollution events seen by OMI. AQUM does successfully capture these relationships, however, they tend to be more spatially significant than OMI because of the higher NO_2 concentrations resulting from missing N_2O_5 heterogeneous chemical sinks of NO_x. To determine which processes are important in driving these relationships, a set of idealised (non-reacting) tracers were introduced into the NO_x emission sources with lifetimes of 1, 3, 6, 12, 24 and 48 hours. In winter, the spatial patterns of AQUM column NO_2 were most accurately reproduced by the 24 and 48 hour tracer lifetimes. As the tracer is non reacting and only lost via a simple e-folding term, the transport of the tracer proves that meteorology is primarily driving these spatial patterns of air pollution in winter when compared to summer. In summer, the tracer lifetimes of 24 and 48 hours were too long leading to large overestimations in the summer synoptic spatial extents of AQUM column NO_2. However, tracer lifetimes of 6 and 12 hours gave a much better agreement. This therefore shows to a first-order approximation that atmospheric chemistry is more influential in summer as the NO_2 lifetime decreases (enhanced photolysis of NO_2) and explains the less spatially significant summer synoptic weather-air pollution relationships detected in OMI and AQUM column NO_2.

From this thesis, I conclude that OMI tropospheric column NO_2 is currently the best Earth Observation product of atmospheric trace gases with which to monitor air quality over the UK. Comparisons between AQUM and OMI highlight that AQUM's representation of point source (power station) emissions and missing N_2O_5 heterogeneous chemistry (a standard reaction) needs addressing. The compositing of OMI column NO_2 data under the LWTs shows that under cyclonic conditions there is a transport of column NO_2 away from source regions, while there is an accumulation over source regions under anticyclonic conditions. This process is more evident in winter. Dynamical model evaluation of AQUM shows it successfully reproduces these relationships found in the OMI column NO_2, giving confidence in its ability to forecast air pollution under synoptic conditions favourable in enhancing poor air quality events.

7.2   Future Work

From the evaluation of AQUM, the model performed well in capturing the column NO_2 seen from space. There is good agreement in the background concentrations and over many of the UK source regions. However, AQUM's treatment of point source NO_x emissions, especially in summer, is inaccurate and needs improving. Heterogeneous chemistry partially improves this but investigation of new methods to treat these point source emissions is needed. For instance, the introduction of a stack plume model for AQUM point source emissions at known power station locations. The hydrolysis of N_2O_5 with the reaction of water on aerosol is a standard reaction and an important sink of NO_x. Therefore,

this chemistry should be included in the operational AQUM, with an uptake value of 0.02 (Macintyre and Evans, 2010). The NO_x emissions over continental Europe are also a concern as comparisons with multiple satellite instruments showing that AQUM column NO_2 here is significantly underestimated. So in the future, as new improved emission datasets become available (e.g. satellite top-down emissions), the coarse EMEP emissions should be replaced or modified.

The statistically significant meteorology-atmospheric chemistry relationships, seen by OMI, can potentially be used as a model validation tool. This dataset will allow progress beyond simply using the satellite data for operational model validation (calculation of means and biases, see Dennis et al. (2010)) and can be used to test the model's ability to reproduce the influence of meteorology on NO_2 (dynamic model evaluation). This has been started here with the multiple tracer life times, but investigation of some of the atmospheric chemistry should be undertaken. For instance, sensitivity experiments on the model photolysis scheme could confirm whether or not AQUM column NO_2 photochemical loss is significantly effected between seasons. It might also be worth exploring the links between other meteorological variables and air pollution (e.g. relative humidity, wind speed and temperature etc).

The monitoring of air quality in the UK (and elsewhere - e.g. China, a developing country, with serious air quality problems) will be greatly improved as newer higher resolution and sampling (geostationary) instruments are deployed in future satellite missions. For instance, the ESA/GMES Sentinel 5 Precursor mission (polar orbiter), due to be launched in 2016, will carry TROPOspheric Monitoring Instrument (TROPOMI), which will monitor species such as NO_2 and O_3 at a resolution of 7×7 km^2 (TROPOMI, 2014). Future geostationary satellite missions will provide continuous observation of atmospheric trace gases over a designated region. TEMPO (Tropospheric Emissions: Monitoring of Pollution) will be launched in 2018-2019 and monitor air quality over North America (ESA, 2014). The higher resolution of these instruments means areas of poor air quality and emission sources can be more accurately quantified. The continuous temporal observations from geostationary instruments should allow the more accurate understanding of the evolution and diurnal cycles of air quality episodes.

Appendix A

AQUM Chemistry Mechanism

Below is the AQUM chemical mechanism from Savage et al. (2013), which is stored as supplementary information at http://www.geosci-model-dev.net/6/353/2013/gmd-6-353-2013-supplement.pdf.

Supplementary Online Material

Air quality modelling using the Met Office Unified Model:
model description and initial evaluation

N. H. Savage, P. Agnew, L. S. Davis, C. Ordóñez, R. Thorpe,

C. E. Johnson, F. M. O'Connor and M. Dalvi

Met Office, Fitzroy Road, Exeter, EX1 3PB, United Kingdom

Table S1. Chemical species present in the RAQ gas phase chemistry scheme of the model.

Item	Tracer name	Species name	Advected	Dry dep.	Wetdep.	Emitted
1	O(3P)	$O(^3P)$	-	-	-	-
2	O(1D)	$O(^1D)$	-	-	-	-
3	OH	OH	-	-	-	-
4	O3	O_3	Yes	Yes	-	-
5	NO	NO	Yes	-	-	Yes
6	NO3	NO_3	Yes	-	Yes	-
7	NO2	NO_2	Yes	Yes	-	-
8	N2O5	N_2O_5	Yes	-	Yes	-
9	HO2NO2	HO_2NO_2	Yes	-	Yes	-
10	HONO2	HNO_3	Yes	Yes	Yes	-
11	H2O2	H_2O_2	Yes	Yes	Yes	-
12	CH4	CH_4	Yes	Yes	-	Yes
13	CO	CO	Yes	Yes	-	Yes
14	HCHO	HCHO (formaldehyde)	Yes	-	Yes	Yes
15	HO2	HO_2	-	-	Yes	-
16	MeOO	CH_3OO	-	-	Yes	-
17	MeOOH	CH_3OOH	Yes	Yes	Yes	-
18	EtOO	C_2H_5OO	-	-	-	-
19	C2H6	C_2H_6 (ethane)	Yes	-	-	Yes
20	MeCO3	CH_3COO_2	-	-	-	-
21	EtOOH	C_2H_5OOH	Yes	Yes	Yes	-
22	MeCHO	CH_3CHO (acetaldehyde)	Yes	-	-	Yes
23	PAN	$CH_3COO_2NO_2$ (peroxyacetyl nitrate)	Yes	Yes	-	-
24	s-BuOO	$s-C_4H_9OO$	-	-	-	-
25	C3H8	C_3H_8 (propane)	Yes	-	-	Yes

26	i-PrOOH	i-C$_3$H$_7$OOH	Yes	Yes	Yes	-
27	Me2CO	CH$_3$COCH$_3$ (acetone)	Yes	-	-	Yes
28	O3S	O$_3$ (stratospheric tracer)	Yes	Yes	-	-
29	C5H8	C$_5$H$_8$ (isoprene)	Yes	-	-	Yes
30	i-PrOO	i-C$_3$H$_7$OO	-	-	-	-
31	ISOOH	HOC$_5$H$_8$OOH	Yes	Yes	Yes	-
32	ISON	(NO$_3$)C$_4$H$_6$CHO	Yes	-	Yes	-
33	MGLY	CH$_3$COCHO (methyl glyoxal)	Yes	-	Yes	-
34	MVK	CH$_2$CHCOCH$_3$ (methyl vinyl ketone and other species lumped)	Yes	-	-	-
35	MVKOOH	CH$_3$COCH(OH)CH$_2$OH	Yes	Yes	Yes	-
36	MeCOCH2OO	CH$_3$COCH$_2$O$_2$	-	-	-	-
37	MEKO2	CH$_3$COCH(O$_2$)CH$_3$	-	-	-	-
38	HOC2H4O2	HOC$_2$H$_4$O$_2$	-	-	-	-
39	ORGNIT	Lumped organic nitrates	Yes	Yes	Yes	-
40	HOC3H6O2	CH$_3$CHO$_2$CH$_2$OH	-	-	-	-
41	CH3OH	CH$_3$OH (methanol)	Yes	-	Yes	Yes
42	OXYL1	HOC$_6$H$_4$(CH$_3$)$_2$O$_2$	-	-	-	-
43	H2	H$_2$	Yes	Yes	-	Yes
44	MEMALD1	CHOCH(OH)CO$_2$CH$_3$CHO	-	-	-	-
45	RNC2H4	CH$_2$(NO$_3$)CHO	Yes	-	-	-
46	HOIPO2	HOC$_5$H$_8$O$_2$	-	-	-	-
47	RNC3H6	CH$_3$CH(NO$_3$)CHO	Yes	-	-	-
48	HOMVKO2	CH$_3$COCH(OH)CH$_2$O$_2$	-	-	-	-
49	C2H4	C$_2$H$_4$ (ethene)	Yes	-	-	Yes
50	C3H6	C$_3$H$_6$ (propene)	Yes	-	-	Yes
51	C4H10	C$_4$H$_{10}$ (butane)	Yes	-	-	Yes

52	s-BuOOH	s-C$_4$H$_9$OOH	Yes	Yes	Yes	-
53	MEK	CH$_3$COC$_2$H$_5$	Yes	-	-	-
54	TOLUENE	toluene	Yes	-	-	Yes
55	TOLP1	HOC$_6$H$_5$CH$_3$O$_2$	-	-	-	-
56	MEMALD	CH$_3$COCHCHCHO (methyl maleic dialdehyde)	Yes	-	-	-
57	GLY	CHOCHO (glyoxal)	Yes	-	Yes	-
58	oXYLENE	o-xylene	Yes	-	-	Yes

Table S2. Bimolecular reactions in the RAQ mechanism.

Reaction	K (cm^3 molecule^{-1} s^{-1})	Notes
O(^{1}D) + H$_2$O → 2 OH	2.2 · 10^{-10}	Atk1
NO + O$_3$ → NO$_2$ + O$_2$	1.4 · 10^{-12} · exp(-1310/T)	Atk1
NO$_2$ + O$_3$ → NO$_3$ + O$_2$	1.4 · 10^{-13} · exp(-2470/T)	Atk1
OH + O$_3$ → HO$_2$ + O$_2$	1.7 · 10^{-12} · exp(-940/T)	Atk1
HO$_2$ + O$_3$ → OH + 2O$_2$	2.03 · 10^{-16} · (T/300)$^{4.57}$ · exp(693/T)	Atk1
NO + NO$_3$ → 2 NO$_2$	1.8 · 10^{-11} · exp(110/T)	Atk1
NO$_2$ + O(^{3}P) → NO + O$_2$	5.5 · 10^{-12} · exp(188/T)	Atk1
NO + HO$_2$ → OH + NO$_2$	3.6 · 10^{-12} · exp(270/T)	Atk1
NO$_2$ + NO$_3$ → NO + NO$_2$ + O$_2$	4.5 · 10^{-14} · exp(-1260/T)	C97
HO$_2$NO$_2$ + OH → NO$_2$ + H$_2$O + O$_2$	3.2 · 10^{-13} · exp(690/T)	IUP1
NO$_3$ + NO$_3$ → 2 NO$_2$ + O$_2$	8.5 · 10^{-13} · exp(-2450/T)	NIST
HO$_2$ + OH → H$_2$O + O$_2$	4.8 · 10^{-11} · exp(250/T)	Atk1
OH + H$_2$O$_2$ → HO$_2$ + H$_2$O	2.9 · 10^{-12} · exp(-160/T)	C97
OH + H$_2$ + O$_2$ → HO$_2$ + H$_2$O	5.5 · 10^{-12} · exp(-2000/T)	C97
NO$_3$ + HO$_2$ → HNO$_3$ + O$_2$	4.2 · 10^{-12}	NIST
NO$_3$ + HO$_2$ → OH + NO$_2$ + O$_2$	3.5 · 10^{-12}	NIST
OH + CH$_3$OOH → CH$_3$O$_2$ + H$_2$O	2.66 · 10^{-12} · exp(200/T)	NIST [(*)]
OH + CH$_3$OOH → HCHO + OH	1.14 · 10^{-12} · exp(200/T)	NIST
OH + C$_2$H$_5$OOH → C$_2$H$_5$O$_2$ + H$_2$O	2.66 · 10^{-12} · exp(200/T)	assumed as *
OH + i-C$_3$H$_7$OOH → i-C$_3$H$_7$O$_2$ + H$_2$O	2.66 · 10^{-12} · exp(200/T)	assumed as *
OH + s-C$_4$H$_9$OOH → s-C$_4$H$_9$O$_2$ + H$_2$O	2.66 · 10^{-12} · exp(200/T)	assumed as *
OH + CH$_4$ + O$_2$ → CH$_3$O$_2$ + H$_2$O	1.85 · 10^{-12} · exp(-1690/T)	Atk2
NO + CH$_3$O$_2$ + O$_2$ → HCHO + NO$_2$ + HO$_2$	2.3 · 10^{-12} · exp(360/T)	Atk2
CH$_3$OH + OH + O$_2$ → HCHO + HO$_2$ + H$_2$O	7.3 · 10^{-12} · exp(-620/T)	NIST
CH$_3$O$_2$ + HO$_2$ → CH$_3$OOH + O$_2$	4.1 · 10^{-13} · exp(750/T)	C97
OH + HCHO + O$_2$ → HO$_2$ + CO + H$_2$O	5.4 · 10^{-12} · exp(135/T)	Atk2
NO$_3$ + HCHO → HO$_2$ + CO + HNO$_3$	5.8 · 10^{-16}	C97
OH + C$_2$H$_6$ → C$_2$H$_5$O$_2$	6.9 · 10^{-12} · exp(-1000/T)	Atk2
C$_2$H$_5$O$_2$ + NO → CH$_3$CHO + NO$_2$ + HO$_2$	2.6 · 10^{-12}	NIST
C$_2$H$_5$O$_2$ + CH$_3$O$_2$ + O$_2$ → CH$_3$CHO + HCHO + 2 HO$_2$	2.0 · 10^{-13}	NIST
OH + CH$_3$CHO + O$_2$ → CH$_3$COO$_2$ + H$_2$O	4.4 · 10^{-12} · exp(365/T)	Atk2
CH$_3$COO$_2$ + NO + O$_2$ → CH$_3$O$_2$ + NO$_2$ + CO$_2$	2.0 · 10^{-11}	C97
OH + n-C$_4$H$_{10}$ + O$_2$ → s-C$_4$H$_9$O$_2$ + H$_2$O	7.9 · 10^{-13} · (T/300)^2 · exp(300/T)	based on C97
s-C$_4$H$_9$O$_2$ + NO → CH$_3$COC$_2$H$_5$ + NO$_2$ + HO$_2$	2.54 · 10^{-12} · exp(360/T)	based on C97

s-$C_4H_9O_2$ + CH_3O_2 + O_2 → $CH_3COC_2H_5$ + 2 HO_2 + HCHO	$2.5 \cdot 10^{-13}$	based on C97 & NIST
OH + $CH_3COC_2H_5$ + O_2 → $CH_3COCH(O_2)CH_3$ + H_2O	$1.3 \cdot 10^{-12} \cdot exp(-25/T)$	IUP2
$C_2H_5O_2$ + $C_2H_5O_2$ → 2 CH_3CHO + 2 HO_2	$6.4 \cdot 10^{-14}$	IUP2
CH_3COO_2 + CH_3COO_2 + O_2 → 2CH_3O_2 + 2 CO_2	$2.9 \cdot 10^{-12} \cdot exp(500/T)$	IUP2
OH + C_3H_8 → i-$C_3H_7O_2$ + H_2O	$7.6 \cdot 10^{-12} \cdot exp(-585/T)$	IUP2
i-$C_3H_7O_2$ + NO → NO_2 + HO_2 + CH_3COCH_3	$2.7 \cdot 10^{-12} \cdot exp(360/T)$	IUP2
$CH_3COCH_2O_2$ + NO → NO_2 + HCHO + CH_3COO_2	$2.45 \cdot 10^{-12} \cdot exp(360/T)$	based on C99 & NIST
$CH_3COCH_2O_2$ + CH_3O_2 → HO_2 + 2 HCHO + CH_3COO_2	$3.8 \cdot 10^{-12}$	NIST
i-$C_3H_7O_2$ + CH_3O_2 → 2HO_2 + HCHO + CH_3COCH_3	$4.0 \cdot 10^{-14}$	C99
OH + PAN → NO_3 + HCHO	$9.5 \cdot 10^{-13} \cdot exp(-650/T)$	NIST
HO_2 + $C_2H_5O_2$ → C_2H_5OOH + O_2	$3.8 \cdot 10^{-13} \cdot exp(900/T)$	IUP2
OH + C_2H_5OOH → CH_3CHO + OH + H_2O	$8.0 \cdot 10^{-12}$	based on C99
HO_2 + i-$C_3H_7O_2$ → i-C_3H_7OOH + O_2	$1.51 \cdot 10^{-13} \cdot exp(1300/T)$	based on C99
OH + i-C_3H_7OOH → CH_3COCH_3 + OH + H_2O	$1.66 \cdot 10^{-11}$	based on C99
HO_2 + s-$C_4H_9O_2$ → s-C_4H_9OOH + O_2	$1.82 \cdot 10^{-13} \cdot exp(1300/T)$	based on C99
OH + s-C_4H_9OOH → $CH_3COC_2H_5$ + OH + H_2O	$2.15 \cdot 10^{-11}$	based on C99 & NIST
NO + $CH_3COCH(O_2)CH_3$ → CH_3COO_2 + NO_2 + CH_3CHO	$2.54 \cdot 10^{-12} \cdot exp(360/T)$	based on C97 & NIST
CH_3O_2 + $CH_3COCH(O_2)CH_3$ + O_2 → HCHO + HO_2 + CH_3CHO + CH_3COO_2	$8.8 \cdot 10^{-13}$	based on C99
$CH_2O_2CH_2OH$ + NO → 2HCHO + HO_2 + NO_2	$9.0 \cdot 10^{-12}$	C97
CH_3O_2 + $CH_2O_2CH_2OH$ + O_2 → 3HCHO + 2 HO_2	$2.0 \cdot 10^{-12}$	based on C97
O_3 + C_2H_4 → HCHO + 0.31 CO + 0.13 H_2 + 0.2 HO_2 + 0.47 HCHO	$1.2 \cdot 10^{-14} \cdot exp(-2630/T)$	C97
O_3 + C_3H_6 → HCHO + 0.3 CH_4 + 0.4 CO + 0.28 OH + 0.3HO_2 + 0.58CH_3O_2 + 0.12CH_3OH + 0.6CO_2	$2.75 \cdot 10^{-15} \cdot exp(-1878/T)$	MCM
O_3 + C_3H_6 → CH_3CHO + 0.24 H_2 + 0.58 CO + 0.18 HO_2	$2.75 \cdot 10^{-15} \cdot exp(-1878)$	MCM
$CH_3CHO_2CH_2OH$ + NO → HCHO + HO_2 + CH_3CHO + NO_2	$2.54 \cdot 10^{-12} \cdot exp(360/T)$	based on C97
CH_3O_2 + $CH_3CHO_2CH_2OH$ + O_2 → 2 HCHO + 2 HO_2 + CH_3CHO	$6.0 \cdot 10^{-13}$	based on C97
O_3 + C_5H_8 → $CH_2CHCOCH_3$ + 0.78 CO + 0.22 HCHO + 0.27 HO_2 + 0.27 OH	$7.86 \cdot 10^{-15} \cdot exp(-1913/T)$	C99, MCM
O_3 + $CH_2CHCOCH_3$ → CH_3COCHO + 0.76 CO + 0.24 HCHO + 0.36 HO_2 + 0.36 OH	$7.56 \cdot 10^{-16} \cdot exp(-1521/T)$	C99
CH_3COO_2 + HO_2 → 0.3 O3 + 0.8 CH_3O_2 + 0.2 CH_3COO_2	$5.2 \cdot 10^{-13} \cdot exp(980/T)$	IUP2

Reaction	Rate	Reference
$HOC_5H_8O_2 + CH_3O_2 \rightarrow CH_2CHCOCH_3 + HCHO + 2\,HO_2$	$5.0 \cdot 10^{-13}$	based on C97 & MIM
$CH_3COCH(OH)CH_2O_2 + CH_3O_2 \rightarrow CH_3COCHO + HCHO + 2\,HO_2$	$2.0 \cdot 10^{-12}$	MIM
$HOC_5H_8O_2 + HO_2 \rightarrow HOC_5H_8OOH + O_2$	$2.45 \cdot 10^{-13} \cdot exp(1250/T)$	C99
$HOC_5H_8OOH + OH \rightarrow CH_2CHCOCH_3 + HCHO + OH$	$4.2 \cdot 10^{-11}$	C99
$CH_3COCH(OH)CH_2O_2 + HO_2 \rightarrow CH_3COCH(OH)CH_2OH$	$2.23 \cdot 10^{-13} \cdot exp(1250/T)$	C99
$CH_3COCH(OH)CH_2OH + OH \rightarrow CH_3COCHO + HCHO + OH$	$5.77 \cdot 10^{-11}$	C99
$CH_3COCHO + OH \rightarrow CH_3COO_2 + CO$	$1.72 \cdot 10^{-11}$	C99
$CHOCHO + OH \rightarrow HO_2 + 2\,CO$	$1.14 \cdot 10^{-11}$	C99
$OH + C_5H_8 + O_2 \rightarrow HOC_5H_8O_2$	$2.54 \cdot 10^{-11} \cdot exp(410/T)$	C97, MCM
$HOC_5H_8O_2 + NO \rightarrow CH_2CHCOCH_3 + NO_2 + HCHO + HO_2$	$2.08 \cdot 10^{-12} \cdot exp(180/T)$	based on MIM
$OH + CH_2CHCOCH_3 + O_2 \rightarrow CH_3COCH(OH)CH_2O_2$	$4.13 \cdot 10^{-12} \cdot exp(452/T)$	based on MIM
$CH_3COCH(OH)CH_2O_2 + NO \rightarrow NO_2 + HO_2 + HCHO + CH_3COCHO$	$2.5 \cdot 10^{-12} \cdot exp(360/T)$	MIM
$NO_3 + C_2H_6 \rightarrow C_2H_5O_2 + HNO_3$	$5.7 \cdot 10^{-12} \cdot exp(-4426/T)$	NIST
$NO_3 + n\text{-}C_4H_{10} \rightarrow s\text{-}C_4H_9O_2 + HNO_3$	$2.8 \cdot 10^{-12} \cdot exp(-3280/T)$	NIST
$NO_3 + C_2H_4 \rightarrow CH_2(NO_3)CHO + HO_2$	$3.3 \cdot 10^{-12} \cdot (T/300)^2 \cdot exp(-2880/T)$	based on C97, IUP2, Atk2
$CH_2(NO_3)CHO + OH \rightarrow HCHO + NO_2 + CO_2$	$4.95 \cdot 10^{-12}$	estimated
$NO_3 + C_3H_6 \rightarrow CH_3CH(NO_3)CHO + HO_2$	$4.59 \cdot 10^{-13} \cdot exp(-1156/T)$	Atk2, NIST
$CH_3CH(NO_3)CHO + OH \rightarrow CH_3CHO + NO_2$	$5.25 \cdot 10^{-12}$	estimated
$NO_3 + CH_3CHO \rightarrow CH_3COO_2 + HNO_3$	$1.4 \cdot 10^{-12} \cdot exp(-1860/T)$	Atk2
$NO_3 + C_5H_8 \rightarrow (NO_3)C_4H_6CHO + HO_2$	$3.03 \cdot 10^{-12} \cdot exp(-446/T)$	MIM, MCM
$(NO_3)C_4H_6CHO + OH \rightarrow CH_2CHCOCH_3 + NO_2$	$4.16 \cdot 10^{-11}$	based on MIM
$OH + o\text{-xylene} \rightarrow HO_2 + 0.8\,CH_3COCHCHCHO + 0.8\,CH_3COCHO$	$1.36 \cdot 10^{-11}$	MCM
$NO_2 + HOC_6H_4(CH_3)_2O_2 \rightarrow ORGNIT$	$1.0 \cdot 10^{-11}$	estimated
$OH + CH_3COCHCHCHO \rightarrow CHOCH(OH)CO_2CH_3CHO$	$5.6 \cdot 10^{-11}$	C97
$CHOCH(OH)CO_2CH_3CHO + NO \rightarrow HO_2 + NO_2 + CHOCHO + CH_3COCHO$	$2.54 \cdot 10^{-12} \cdot exp(360/T)$	based on C97 & MIM
$OH + toluene \rightarrow HO_2 + CH_3COCHCHCHO + CHOCHO$	$1.18 \cdot 10^{-12} \cdot exp(338/T)$	based on MCM
$OH + toluene \rightarrow HOC_6H_5CH_3O_2$	$3.6 \cdot 10^{-13}$	based on MCM
$OH + o\text{-xylene} \rightarrow HOC_6H_4(CH_3)_2O_2$	$1.36 \cdot 10^{-11}$	MCM
$OH + ORGNIT \rightarrow CH_3COCHCHCHO + CHOCHO + NO_2$	$2.7 \cdot 10^{-12}$	estimated

$NO_3 + ORGNIT \rightarrow CH_3COCHCHCHO + CHOCHO + 2\ NO_2$	$7.0 \cdot 10^{-14}$	estimated
$HOC_6H_4(CH_3)_2O_2 + HO_2 \rightarrow CH_3COCHCHCHO + CH_3COCHO$	$2.5 \cdot 10^{-13} \cdot \exp(1300/T)$	MCM
$CHOCH(OH)CO_2CH_3CHO + CH_3O_2 \rightarrow 2HO_2 + HCHO + CHOCHO + CH_3COCHO$	$1.0 \cdot 10^{-13}$	C97
$HO_2 + HOC_6H_5CH_3O_2 \rightarrow CH_3COCHCHCHO + CHOCHO + OH$	$1.0 \cdot 10^{-11}$	estimated
$NO_2 + HOC_6H_5CH_3O_2 \rightarrow ORGNIT$	$1.0 \cdot 10^{-11}$	estimated

Values of the reaction rates are based on the following references:

C97: Collins et al., 1997.

C99: Collins et al., 1999.

Atk1: Atkinson et al., ACP, 2004.

Atk2: Atkinson et al., ACP, 2006a.

IUP1: Atkinson et al., IUPAC web – O_x, HO_x, NO_x and SO_x reactions, 2006b.

IUP2: Atkinson et al., IUPAC web – Organic reactions, 2006c.

NIST: http://kinetics.nist.gov/kinetics, 2007.

MCM: http://mcm.leeds.ac.uk/MCMv3.1, 2008.

MIM (Mainz Isoprene Mechanism): von Kuhlmann and Lawrence, 2006.

For organic reactions where different product routes are possible, we used branching ratios from the Master Chemical Mechanism (MCMv3.1).

Table S3. Termolecular reactions in RAQ mechanism.

	Termolecular reactions	$k = (k_0\ [M] / (1 + k_0\ [M] / k_\infty))\ \text{x}\ F_c^n$ $n = \{1 + (\log_{10}(k_0\ [M] / k_\infty))^2\}^{-1}$	Notes
T1.	$O(^3P) + NO\ (+ M) \rightarrow NO_2\ (+ M)$	$k_0 = 1.0 \cdot 10^{-31} \cdot (T/300)^{-1.6}$ $k_\infty = 3.0 \cdot 10^{-11} \cdot (T/300)^{0.3}$ $F_c = 0.85$	Atk1
T2.	$NO_2 + NO_3\ (+ M) \rightarrow N_2O_5\ (+ M)$	$k_0 = 3.6 \cdot 10^{-30} \cdot (T/300)^{-4.1}$ $k_\infty = 1.9 \cdot 10^{-12} \cdot (T/300)^{0.2}$ $F_c = 0.35$	Atk1
T3.	$NO_2 + OH\ (+ M) \rightarrow HNO_3\ (+ M)$	$k_0 = 3.3 \cdot 10^{-30} \cdot (T/300)^{-3.0}$ $k_\infty = 4.1 \cdot 10^{-11}$ $F_c = 0.4$	Atk1
T4.	$NO_2 + HO_2\ (+ M) \rightarrow HO_2NO_2\ (+ M)$	$k_0 = 1.8 \cdot 10^{-31} \cdot (T/300)^{-3.2}$ $k_\infty = 4.7 \cdot 10^{-12}$ $F_c = 0.6$	Atk1
T5.	$HO_2NO_2\ (+ M) \rightarrow HO_2 + NO_2\ (+ M)$	$k_0 = 4.1 \cdot 10^{-5} \cdot \exp(-10650/T)$ $k_\infty = 4.8 \cdot 10^{15} \cdot \exp(-11170/T)$ $F_c = 0.6$	Atk1
T6.	$N_2O_5\ (+ M) \rightarrow NO_2 + NO_3\ (+ M)$	$k_0 = 1.3 \cdot 10^{-3} \cdot (T/300)^{-3.5} \cdot \exp(-11000/T)$ $k_\infty = 9.7 \cdot 10^{14} \cdot (T/300)^{0.1} \cdot \exp(-11080/T)$ $F_c = 0.35$	Atk1
T7.	$CH_3COO_2 + NO_2\ (+ M) \rightarrow PAN\ (+ M)$	$k_0 = 2.7 \cdot 10^{-28} \cdot (T/300)^{-7.1}$ $k_\infty = 1.2 \cdot 10^{-11} \cdot (T/300)^{-0.9}$ $F_c = 0.3$	Atk2
T8.	$PAN\ (+ M) \rightarrow CH_3COO_2 + NO_2\ (+ M)$	$k_0 = 4.9 \cdot 10^{-3} \cdot \exp(-12100/T)$ $k_\infty = 5.4 \cdot 10^{16} \cdot \exp(-13830/T)$ $F_c = 0.3$	Atk2
T9.	$OH + C_2H_4\ (+ M) \rightarrow CH_2O_2CH_2OH\ (+ M)$	$k_0 = 8.6 \cdot 10^{-29} \cdot (T/300)^{-3.1}$ $k_\infty = 9.0 \cdot 10^{-12} \cdot (T/300)^{-0.85}$ $F_c = 0.48$	IUP2
T10.	$OH + C_3H_6\ (+ M) \rightarrow CH_3CHO_2CH_2OH\ (+ M)$	$k_0 = 8.0 \cdot 10^{-27} \cdot (T/300)^{-3.5}$ $k_\infty = 3.0 \cdot 10^{-11} \cdot (T/300)^{-1.0}$ $F_c = 0.5$	IUP2

Table S4. Complex reactions in RAQ mechanism. The overall rate k is used in the model for each group of complex reactions unless otherwise indicated.

	Reaction	K (cm^3 molecule^{-1} s^{-1})	Notes
R1.	$O(^3P) + O_2 + M \rightarrow O_3 + M$	$k_1 = 6.0 \cdot 10^{-34} \cdot (T/300)^{-2.6}$	Atk1
		$k = k_1 \cdot [M] \cdot [O_2]$	
R6.	$O(^1D) + M \rightarrow O(^3P) + M$	$k_6 = 3.2 \cdot 10^{-11} \cdot \exp(70/T)$	C97
R7.	$O(^1D) + M \rightarrow O(^3P) + M$	$k_7 = 1.8 \cdot 10^{-11} \cdot \exp(110/T)$	
		$k = k_6 \cdot [O_2] + k_7 \cdot [N_2]$	
R50.	$OH + HNO_3 \rightarrow NO_3 + H_2O$	$k_{50} = 2.7 \cdot 10^{-17} \cdot \exp(2199/T)$	C97
R51.	$OH + HNO_3 \rightarrow NO_3 + H_2O$	$k_{51} = 6.5 \cdot 10^{-34} \cdot \exp(1335/T)$	
R35.	$OH + HNO_3 \rightarrow NO_3 + H_2O$	$k_{35} = 2.4 \cdot 10^{-14} \cdot \exp(460/T)$	
		$k = k_{35} + k_{51} \cdot [M] / (1 + k_{51} \cdot [M] / k_{50})$	
R37.	$HO_2 + HO_2 (+M) \rightarrow H_2O_2 + O_2 (+M)$	$k_{37} = 1.9 \cdot 10^{-33} \cdot \exp(980/T)$	C97
R38.	$HO_2 + HO_2 (+H_2O) \rightarrow H_2O_2 + O_2 (+H_2O)$	$k_{38} = 1.4 \cdot 10^{-21} \cdot \exp(2200/T)$	
R36.	$HO_2 + HO_2 (+M) \rightarrow H_2O_2 + O_2 (+M)$	$k_{36} = 2.2 \cdot 10^{-13} \cdot \exp(600/T)$	
		$k = (k_{36} + k_{37} \cdot [M]) \cdot (1 + k_{38} \cdot [H_2O])$	
R61.	$CH_3O_2 + CH_3O_2 \rightarrow 2HCHO + 2\,HO_2$	$k_{61} = 7.4 \cdot 10^{-13} \cdot \exp(-520/T)$	C97
R62.	$CH_3O_2 + CH_3O_2 \rightarrow HCHO + CH_3OH$	$k_{62,0} = 1.03 \cdot 10^{-13} \cdot \exp(365/T)$	
		$k_{62} = k_{62,0} - k_{61}$	
		(both branches considered, with rates k_{61} & k_{62})	
R69.	$OH + CO \rightarrow HO_2 + CO_2$	$k_{69} = 3.54 \cdot 10^{-33}$ (pressure dependent term)	C97
R70.	$OH + CO \rightarrow HO_2 + CO_2$	$k_{70} = 1.5 \cdot 10^{-13}$	
		$k = k_{70} + k_{69} \cdot [M]$	
R74.	$CH_3O_2 + CH_3COO_2 \rightarrow 2\,HCHO$	$k_{74,0} = 4.4 \cdot 10^{5} \cdot \exp(-3910/T)$	C97
R80.	$CH_3O_2 + CH_3COO_2 \rightarrow HCHO + HO_2 + CH_3O_2 + CO_2$	$k_{80,0} = 1.1 \cdot 10^{-11}$	
		$k_{74} = k_{80,0} \cdot \{1 - k_{74,0} / (1 + k_{74,0})\}$	
		$k_{80} = k_{80,0} \cdot \{k_{74,0} / (1 + k_{74,0})\}$	
		(both branches considered, with rates k_{74} & k_{80})	
R89.	$CH_3COCH_3 + OH \rightarrow CH_3COCH_2O_2 + H_2O$	$k_{89} = 8.8 \cdot 10^{-12} \cdot \exp(-1320/T)$	IUP2
R94.	$CH_3COCH_3 + OH \rightarrow CH_3COCH_2O_2 + H_2O$	$k_{94} = 1.7 \cdot 10^{-14} \cdot \exp(423/T)$	
		$k = k_{89} + k_{94}$	

[M], [O$_2$], [N$_2$]: molecular density (in cm^{-3}) of air, O$_2$ and N$_2$, respectively.

Table S5. Photochemical reactions in RAQ mechanism.

J1.	$O_3 + h\nu$	$\rightarrow$	$O(^3P)$
J2.	$O_3 + h\nu$	$\rightarrow$	$O(^1D)$
J3.	$NO_2 + h\nu$	$\rightarrow$	$NO + O(^3P)$
J4.	$H_2O_2 + h\nu$	$\rightarrow$	$OH + OH$
J5.	$HNO_3 + h\nu$	$\rightarrow$	$NO_2 + OH$
J6.	$HCHO + h\nu$	$\rightarrow$	$CO + HO_2 + HO_2$
J7.	$HCHO + h\nu$	$\rightarrow$	$CO + H_2$
J8.	$CH_3CHO + h\nu$	$\rightarrow$	$CH_3O_2 + HO2 + CO$
J9.	$CH_3COC_2H_5 + h\nu$	$\rightarrow$	$C_2H_5O_2 + CH_3COO_2$
J10.	$CH_3COCH_3 + h\nu$	$\rightarrow$	$CH_3COO_2 + CH_3O_2$
J11.	$HO_2NO_2 + h\nu$	$\rightarrow$	$HO_2 + NO_2$
J12.	$CH_3COCHO + h\nu$	$\rightarrow$	$CH_3COO2 + HO2 + CO$
J13.	$CHOCHO + h\nu$	$\rightarrow$	$HO_2 + HO_2 + CO + CO$
J14.	$NO_3 + h\nu$	$\rightarrow$	$NO + O_2$
J15.	$NO_3 + h\nu$	$\rightarrow$	$NO_2 + O(^3P)$
J16.	$N_2O_5 + h\nu$	$\rightarrow$	$NO_2 + NO_3$
J17.	$CH_3OOH + h\nu$	$\rightarrow$	$HCHO + HO_2 + OH$
J18.	$PAN + h\nu$	$\rightarrow$	$CH_3COO_2 + NO_2$
J19.	$C_2H_5OOH + h\nu$	$\rightarrow$	$OH + HO_2 + CH_3CHO$
J20.	$i\text{-}C_3H_7OOH + h\nu$	$\rightarrow$	$OH + HO_2 + CH_3COCH_3$
J21.	$s\text{-}C_4H_9OOH + h\nu$	$\rightarrow$	$OH + HO_2 + CH_3COC_2H_5$
J22.	$HOC_5H_8OOH + h\nu$	$\rightarrow$	$OH + CH_2CHCOCH_3 + HCHO + HO_2$
J23.	$CH_3COCH(OH)CH_2OH + h\nu$	$\rightarrow$	$OH + CH_3COCHO + HCHO + HO_2$

Table S6. Henry's Law constants for the species which undergo wet deposition in the RAQ mechanism.

Species	k_1 (M atm^{-1})	c_1 (K)	k_2 (M atm^{-1})	c_2 (K)	Reference for k_1 and c_1
NO3	2.0	2000	--	--	Sander (1999)
N2O5	2.1×10^5	8700	0.2000×10^2	--	Assumed as HNO3
HO2NO2	1.3×10^4	6900	0.1000×10^{-4}	--	Sander (1999)
HONO2	2.1×10^5	8700	0.2000×10^2	--	Sander (1999)
H2O2	8.3×10^4	7400	0.2400×10^{-11}	-3730	Sander (1999)
HCHO	3.3×10^3	6500	--	--	Sander (1999)
MeOO	2.0×10^3	6600	--	--	Sander (1999)
HO2	4.0×10^3	5900	0.2000×10^{-4}	--	Sander (1999)
MeOOH	3.1×10^2	5000	--	--	Sander (1999)
EtOOH	3.4×10^2	5700	--	--	Sander (1999)
i-PrOOH	3.4×10^2	5700	--	--	Assumed as EtOOH
ISOOH	1.7×10^6	9700	--	--	Staudinger & Roberts (1996)
ISON	3.0×10^3	7400	--	--	Staudinger & Roberts (1996)
MGLY	3.5×10^3	7200	--	--	Sander (1999)
MVKOOH	1.7×10^6	9700	--	--	Assumed as ISOOH
ORGNIT	1.3×10^2	--	--	--	Average of values in Schwarzenbach et al. (1988)
CH3OH	2.2×10^2	5200	--	--	Sander (1999)
s-BuOOH	3.4×10^2	5700	--	--	Assumed as EtOOH
GLY	3.6×10^5	--	--	--	Sander (1999)

Temperature dependent Henry's law coefficients are calculated as:

$$k_h = k_1 \times \exp\left[c_1\left(\frac{1}{T} - \frac{1}{T_0}\right)\right]$$

where

$T_0 = 298.15$ K
T = ambient temperature (K)

This equation only accounts for physical solubility. If the species dissociates in the aqueous phase then k_h is multiplied by a second term to calculate the effective Henry's law coefficient, which also considers the effects of complex formation:

$$k_{eff} = k_h \times k_2 \times \exp\left[c_2\left(\frac{1}{T} - \frac{1}{T_0}\right)\right]$$

References

Atkinson, R., Baulch, D. L., Cox, R. A., Crowley, J. N., Hampson, R. F., Hynes, R. G., Jenkin, M. E., Rossi, M. J., and Troe, J.: Evaluated kinetic and photochemical data for atmospheric chemistry: Volume I – gas phase reactions of Ox, HOx, NOx and SOx species, Atmos. Chem. Phys., 4, 1461–1738, 2004.

Atkinson, R., Baulch, D. L., Cox, R. A., Crowley, J. N., Hampson, R. F., Hynes, R. G., Jenkin, M. E., Rossi, M. J., and Troe, J.: Evaluated kinetic and photochemical data for atmospheric chemistry: Volume II – gas phase reactions of organic species, Atmos. Chem. Phys., 6, 3625–4055, 2006a.

Atkinson, R., Cox, R. A. Crowley, J. N., Hampson, Jr, R. F., Hynes, R. G., Jenkin, M. E., Kerr, J. A., Rossi, M. J., and Troe, J.: Summary of Evaluated Kinetic and Photochemical Data for Atmospheric Chemistry, Section I – Ox, HOx, NOx and SOx Reactions. IUPAC Subcommittee on Gas Kinetic Data Evaluation for Atmospheric Chemistry, Web Version October 2006, http://www.iupac-kinetic.ch.cam.ac.uk, 2006b.

Atkinson, R., Cox, R. A. Crowley, J. N., Hampson, Jr, R. F., Hynes, R. G., Jenkin, M. E., Kerr, J. A., Rossi, M. J., and Troe, J.: Summary of Evaluated Kinetic and Photochemical Data for Atmospheric Chemistry, Section II - Organic Reactions. IUPAC Subcommittee on Gas Kinetic Data Evaluation for Atmospheric Chemistry, Web Version February 2006, http://www.iupac-kinetic.ch.cam.ac.uk, 2006c.

Collins, W. J., Stevenson, D. S, Johnson, C. E., and Derwent, R. G.: Tropospheric Ozone in a Global-Scale Three-Dimensional Lagrangian Model and Its Response to NO_x Emission Controls, J. Atmos. Chem., 26, 223–274, 1997.

Collins, W. J., Stevenson, D. S., Johnson, C. E., and. Derwent, R. G.: Role of convection in determining the budget of odd hydrogen in the upper troposphere, J. Geophys. Res., 104, D21, 26,927-26,941, 1999.

Master Chemical Mechanism (MCM), http://mcm.leeds.ac.uk/MCMv3.1, last accessed in May 2008,

National Institute of Standards and Technology (NIST), Chemical Kinetics Database on the Web, Standard Reference Database 17, Version 7.0 (Web Version), Release 1.5 http://kinetics.nist.gov/kinetics, 2007.

Sander, R: Compilation of Henry's Law Constants for Inorganic and Organic Species of Potential Importance in Environmental Chemistry (Version 3), http://www.henrys-law.org, 1999.

Schwarzenbach, R. P., Stierli, R., Folsom, B. R., and Zeyer, J.: Compound properties relevant for assessing the environmental partitioning of nitrophenols, Environ. Sci. Technol., 22 , 83–92, 1988.

Staudinger, J. and Roberts, P. V.: A critical review of Henry's law constants for environmental applications, Crit. Rev. Environ. Sci. Technol., 26 , 205–297, 1996.

von Kuhlmann, R. and Lawrence, M. G.: The impact of ice uptake of nitric acid on atmospheric chemistry, Atmos. Chem. Phys., 6, 225-235, doi:10.5194/acp-6-225-2006, 2006.

References

Ahrens, C.: Meteorology Today - Ninth Edition, Brooks/Cole CENGAGE Learning, Belmont, USA, 2009. ix, 7

Barkley, M. P., Palmer, P. I., Ganzeveld, L., Arneth, A., Hagberg, D., Karl, T., Guenther, A., Paulot, F., Wennberg, P. O., Mao, J., Kurosu, T. P., Chance, K., Mller, J.-F., De Smedt, I., Van Roozendael, M., Chen, D., Wang, Y., and Yantosca, R. M.: Can a state of the art chemistry transport model simulate Amazonian tropospheric chemistry?, Journal of Geophysical Research: Atmospheres, 116, n/a–n/a, doi:10.1029/2011JD015893, http://dx.doi.org/10.1029/2011JD015893, 2011. 91

Barnaba, F. and Gobbi, G. P.: Lidar estimation of tropospheric aerosol extinction, surface area and volume: Maritime and desert-dust cases, Journal of Geophysical Research: Atmospheres, 106, 3005–3018, doi:10.1029/2000JD900492, http://dx.doi.org/10.1029/2000JD900492, 2001. 57

BBC: EU Commission launches legal action over UK air quality, http://www.bbc.co.uk/news/science-environment-26257703 (last accessed June 2014), 2014. 2

Beirle, S., Boersma, K. F., Platt, U., Lawrence, M. G., and Wagner, T.: Megacity Emissions and Lifetimes of Nitrogen Oxides Probed from Space, Science, 333, 1737–1739, doi:10.1126/science.1207824, http://www.sciencemag.org/content/333/6050/1737.abstract, 2011. 81

Bellouin, N., Rae, J., Jones, A., Johnson, C., Haywood, J., and Boucher, O.: Aerosol forcing in the Climate Model Intercomparison Project (CMIP5) simulations by HadGEM2-ES and the role of ammonium nitrate, Journal of Geophysical Research: Atmospheres (1984–2012), 116, 2011. 22

Blond, N., Boersma, K. F., Eskes, H. J., van der A, R. J., Van Roozendael, M., De Smedt, I., Bergametti, G., and Vautard, R.: Intercomparison of SCIAMACHY nitrogen dioxide observations, in situ measurements and air quality modelling results over Western Europe, Journal of Geophysical Research: Atmospheres, 112, n/a–n/a, doi:10.1029/2006JD007277, http://dx.doi.org/10.1029/2006JD007277, 2007. 47

Boersma, K., Eskes, H., and Brinksma, E.: Error analysis for tropospheric NO_2 retrieval from space, Journal of Geophysical Research: Atmospheres (1984–2012), 109, 2004. 50, 51, 52

Boersma, K., Eskes, H., Veefkind, J. P., Brinksma, E., Van Der A, R., Sneep, M., Van Den Oord, G., Levelt, P., Stammes, P., Gleason, J., et al.: Near-real time retrieval of tropospheric NO_2 from OMI, Atmospheric Chemistry and Physics, 7, 2103–2118, 2007. 51, 52

Boersma, K., Jacob, D., Bucsela, E., Perring, A., Dirksen, R., van der A, R., Yantosca, R., Park, R., Wenig, M., Bertram, T., and Cohen, R.: Validation of {OMI} tropospheric {NO2} observations during INTEX-B and application to constrain emissions over the eastern United States and Mexico, Atmospheric Environment, 42, 4480 – 4497, doi: http://dx.doi.org/10.1016/j.atmosenv.2008.02.004, http://www.sciencedirect.com/science/article/pii/S1352231008001258, 2008a. 47, 48

Boersma, K., Eskes, H., Dirksen, R., Veefkind, J., Stammes, P., Huijnen, V., Kleipool, Q., Sneep, M., Claas, J., Leitão, J., et al.: An improved tropospheric NO_2 column retrieval algorithm for the Ozone Monitoring Instrument, Atmospheric Measurement Techniques Discussions, 4, 2329–2388, 2011a. 48

Boersma, K., Braak, R., and van der A, R.: Dutch OMI NO_2 (DOMINO) data product v2.0, Tropospheric Emissions Monitoring Internet Service on-line documentation, p. http://www.temis.nl/docs/OMI_NO2_HE5_2.0_2011.pdf, 2011b. 27, 48, 49

Boersma, K. F., Jacob, D. J., Eskes, H. J., Pinder, R. W., Wang, J., and van der A, R. J.: Intercomparison of SCIAMACHY and OMI tropospheric NO2 columns: Observing the diurnal evolution of chemistry and emissions from space, Journal of Geophysical Research: Atmospheres, 113, n/a–n/a, doi:10.1029/2007JD008816, http://dx.doi.org/10.1029/2007JD008816, 2008b. 48, 58, 59

Braak, R.: Row Anomaly Flagging Rules Lookup Table, KNMI Technical Document TN-OMIE-KNMI-950, 2010. 48

Bush, M., Bell, S., Christidis, N., Renshaw, R., MacPherson, B., and Wilson, B.: Development of the North Atlantic European model (NAE) into an operational model, Forecasting Research Technical Report No. 47, Met Office, UK, 2006. 21

Cacciamani, C., Battaglia, F., Patruno, P., Pomi, L., Selvini, A., and Tibaldi, S.: A climatological study of thunderstorm activity in the Po Valley, Theoretical and Applied Climatology, 50, 185–203, doi:10.1007/BF00866116, 1995. 99

CMEAP: Quantification of the Medical Effects of Air Pollution in the United Kingdom (1998), Committee on Medical Effects of Air Pollution, Department of Health, 1998. 1

Dai, A.: Global Precipitation and Thunder Storm Frequencies. Part 1: Seasonal and Interannual Variations, Journal of Climate, 14, 1092–1111, 2000. 98

Davies, T., Cullen, M. J. P., Malcolm, A. J., Mawson, M. H., Staniforth, A., White, A. A., and Wood, N.: A new dynamical core for the Met Office's global and regional modelling of the atmosphere, Quarterly Journal of the Royal Meteorological Society, 131, 1759–1782, doi:10.1256/qj.04.101, http://dx.doi.org/10.1256/qj.04.101, 2005. 21

Davies, T. D., Dorling, S. R., Pierce, C. E., Barthelmie, R. J., and Farmer, G.: The meteorological control on the anthropogenic ion content of precipitation at three sites in the UK: The utility of lamb weather types, International Journal of Climatology, 11, 795–807, doi:10.1002/joc.3370110706, http://dx.doi.org/10.1002/joc.3370110706, 1991. 80

Davis, J. M., Bhave, P. V., and Foley, K. M.: Parameterization of N_2O_5 reaction probabilities on the surface of particles containing ammonium, sulfate, and nitrate, Atmospheric Chemistry and Physics, 8, 5295–5311, doi:10.5194/acp-8-5295-2008, http://www.atmos-chem-phys.net/8/5295/2008/, 2008. 55

de Haan, J. and Veefkind, J.: OMO3PR README, NASA, http://disc.sci.gsfc.nasa.gov/Aura/data-holdings/OMI/documents/v003/OMO3PRO_README.html, 2012. 36

DEFRA: The Air Quality Strategy for England, Scotland, Wales and Northern Ireland, https://www.gov.uk/government/uploads/system/uploads/attachment_data/file/69336/pb12654-air-quality-strategy-vol1-070712.pdf (last accessed June 2014), 1, 2011a. 1

DEFRA: UK and EU Air Quality Policy Context, http://uk-air.defra.gov.uk/air-pollution/uk-eu-policy-context (last accessed June 2014), 2011b. 1, 2

DEFRA: Automatic Urban and Rural Network (AURN), http://uk-air.defra.gov.uk/networks/network-info?view=aurn (last accessed June 2014), 2012. 2, 53

DEFRA: Daily Air Quality Index, http://uk-air.defra.gov.uk/air-pollution/daqi (last accessed June 2014), 2013. ix, 2, 17

Demuzere, M., Trigo, R. M., Vila-Guerau de Arellano, J., and van Lipzig, N. P. M.: The impact of weather and atmospheric circulation on O_3 and PM_{10} levels at a rural mid-latitude site, Atmospheric Chemistry and Physics, 9, 2695–2714, doi:10.5194/acp-9-2695-2009, http://www.atmos-chem-phys.net/9/2695/2009/, 2009. 80, 84

Dennis, R., Fox, T., Fuentes, M., Gilliland, A., Hanna, S., Hogrefe, C., Irwin, J., Rao, S., Scheffe, R., Schere, K., Steyn, D., and Venkatram, A.: A framework for evaluating regional-scale numerical photochemical modelling systems, Environmental Fluid Mechanics, 10, 471–489, doi:10.1007/s10652-009-9163-2, http://dx.doi.org/10.1007/s10652-009-9163-2, 2010. 104, 107, 128

Dirksen, R. J., Boersma, K. F., Eskes, H. J., Ionov, D. V., Bucsela, E. J., Levelt, P. F., and Kelder, H. M.: Evaluation of stratospheric NO2 retrieved from the Ozone Monitoring Instrument: Intercomparison, diurnal cycle, and trending, Journal of Geophysical Research: Atmospheres, 116, n/a–n/a, doi:10.1029/2010JD014943, http://dx.doi.org/10.1029/2010JD014943, 2011. 51

Edwards, J. M. and Slingo, A.: Studies with a flexible new radiation code. I: Choosing a configuration for a large-scale model, Quarterly Journal of the Royal Meteorological Society, 122, 689–719, doi:10.1002/qj.49712253107, http://dx.doi.org/10.1002/qj.49712253107, 1996. 22

ESA: TEMPO, https://directory.eoportal.org/web/eoportal/satellite-missions/t/tempo, 2014. 128

Eskes, H.: DOAS retrieval errors, Personal Communication, KNMI, Netherlands, 2012. 52

Eskes, H. and Boersma, K.: Averaging kernels for DOAS total-column satellite retrievals, Atmospheric Chemistry and Physics, 3, 1285–1291, 2003. 25, 48

Essery, R., Best, M., Betts, R., Cox, P., and Taylor, C.: Explicit Representation of Subgrid Heterogeneity in a GCM Land Surface Scheme, Journal of Hydrometeorology, 4, 530–543, 2003. 22

Fitzgerald, J. W.: Approximation formulas for the equilibrium size of an aerosol particle as a function of its dry size and composition and the ambient relative humidity, Journal of Applied Meteorology, 14, 1044–1049, 1975. 56

Foley, K., Roselle, S., Appel, K., Bhave, P., Pleim, J., Otte, T., Mathur, R., Sarwar, G., Young, J., Gilliam, R., et al.: Incremental testing of the Community Multiscale Air Quality (CMAQ) modelling system version 4.7, Geoscientific Model Development, 3, 205–226, 2010. 15, 55

Gottwald, M. and Bovernsmann, H.: SCIAMACHY: Exploring the Changing Earth's Atmosphere, Springer, 2006. 14

Gregory, D. and Rowntree, P.: A mass flux convection scheme with representation of cloud ensemble characteristics and stability-dependent closure, Monthly Weather Review, 118, 1483–1506, 1990. 21

Guardian: Air pollution: European commission launches legal action against the UK, http://www.theguardian.com/environment/2014/feb/20/air-pollution-european-commission-legal-action-uk-nitrogen-dioxide (last accessed June 2014), 2014. 2

Han, K., Lee, C., Lee, J., Kim, J., and Song, C.: A comparison study between model-predicted and OMI-retrieved tropospheric NO_2 columns over the Korean peninsula, Atmospheric Environment, 45, 2962–2971, 2011. 15, 24, 26

Hayn, M., Beirle, S., Hamprecht, F. A., Platt, U., Menze, B. H., and Wagner, T.: Analysing spatio-temporal patterns of the global NO_2-distribution retrieved from GOME satellite observations using a generalised additive model, Atmospheric Chemistry and Physics, 9, 6459–6477, doi:10.5194/acp-9-6459-2009, http://www.atmos-chem-phys.net/9/6459/2009/, 2009. 81

HoC: House of Commons Environmental Audit Report (HCEA): Air Quality: Vol 1 (2009-2010), http://www.publications.parliament.uk/pa/cm200910/cmselect/cmenvaud/229/229i.pdf (last accessed February 2014), 2010. 1

Hollaway, M.: Modelling Interactions Between Vegetation and Tropospheric Ozone, University of Leeds, Leeds, UK, 2012. xvii, 8

Hollaway, M., Arnold, S., Challinor, A., and Emberson, L.: Intercontinental transboundary contributions to ozone-induced crop yield losses in the Northern Hemisphere, Biogeosciences, 9, 271–292, 2012. 1

Hollingsworth, A., Engelen, R., Benedetti, A., Dethof, A., Flemming, J., Kaiser, J., Morcrette, J., Simmons, A., Textor, C., Boucher, O., et al.: Towards a monitoring and forecasting system for atmospheric composition: The GEMS project, Bulletin of the American Meteorological Society, 89, 1147–1164, 2008. 23

Huijnen, V., Eskes, H., Poupkou, A., Elbern, H., Boersma, K., Foret, G., Sofiev, M., Valdebenito, A., Flemming, J., Stein, O., et al.: Comparison of OMI NO_2 tropospheric columns with an ensemble of global and European regional air quality models, Atmospheric Chemistry and Physics, 10, 3273–3296, 2010. 15, 19, 49, 50, 79

Inness, A., Engelen, R., and Flemming, J.: The MACC reanalysis: An 8-year data set of atmospheric composition, in: EGU General Assembly Conference Abstracts, vol. 14, p. 7347, 2012. 53

Irie, H., Kanaya, Y., Akimoto, H., Tanimoto, H., Wang, Z., Gleason, J. F., and Bucsela, E. J.: Validation of OMI tropospheric NO_2 column data using MAX-DOAS measurements deep inside the North China Plain in June 2006: Mount Tai Experiment 2006, Atmospheric Chemistry and Physics, 8, 6577–6586, doi:10.5194/acp-8-6577-2008, http://www.atmos-chem-phys.net/8/6577/2008/, 2008. 47

Jacob, D.: Introduction to Atmospheric Chemistry, Princeton University Press, Princeton, New Jersey, USA, 1999. ix, 6, 8, 12

Jenkinson, A. and Collison, F.: An initial climatology of gales over the North Sea, Synoptic Branch Memorandum No. 62, Met Office, Exeter, 1977. 81

Jones, P. D., Jonsson, T., and Wheeler, D.: Extension to the North Atlantic oscillation using early instrumental pressure observations from Gibraltar and south-west Iceland, International Journal of Climatology, 17, 1433–1450, doi:10.1002/(SICI)1097-0088(19971115)17:13⟨1433::AID-JOC203⟩3.0.CO;2-P, http://dx.doi.org/10.1002/(SICI)1097-0088(19971115)17:13⟨1433:: AID-JOC203⟩3.0.CO;2-P, 1997. 88

Jones, P. D., Harpham, C., and Briffa, K. R.: Lamb weather types derived from reanalysis products, International Journal of Climatology, 33, 1129–1139, doi:10.1002/joc.3498, http://dx.doi.org/10.1002/joc.3498, 2013. 79, 82

Jones, P. D., Osborn, T. J., Harpham, C., and Briffa, K. R.: The development of Lamb weather types: from subjective analysis of weather charts to objective approaches using reanalyses, Weather, 69, 128–132, doi:10.1002/wea.2255, http://dx.doi.org/10. 1002/wea.2255, 2014. 108

Kalnay, E., Kanamitsuand, M., Kistler, R., Collins, W., Deaven, D., Gandin, L., Iredell, M., Saha, S., White, G., Wollen, J., Zhu, Y., Chelliah, M., Ebisuzaki, W., Higgins, W., Janowiak, J., Mo, K., Ropelewski, C., Wang, J., Leetmaa, A., Reynolds, R., Jenne, R., and Joseph, D.: The NCEP/NCAR 40 year reanalysis project, Bulletin of the American Meteorological Society, 77, 437–471, 1996. 82

Lamb, H.: British Isles Weather types and a register of daily sequence of circulation patterns, 1861-1971, Geophysical Memoir, HMSO, London, 116, 85, 1972. xii, 81, 82

Lawrence, M. G., Jöckel, P., and von Kuhlmann, R.: What does the global mean OH concentration tell us?, Atmospheric Chemistry and Physics, 1, 37–49, doi:10.5194/ acp-1-37-2001, http://www.atmos-chem-phys.net/1/37/2001/, 2001. 8

Lesniok, M., Malarzewski, L., and Niedzwiedz, T.: Classification of circulation types for Southern Poland with an application to air pollution concentration in Upper Silesia, Physics and Chemistry of the Earth, 35, 516 – 522, doi:http://dx.doi.org/10.1016/j.pce.2009.11.006, 2010. 79, 80, 84, 85

Lock, A., Brown, A., Bush, M., Martin, G., and Smith, R.: A New Boundary Layer Mixing Scheme. Part I: Scheme Description and Single-Column Model Tests, Monthly Weather Review, 128, 3187–3199, 2000. 21

Lott, N.: The quality control of the integrated surface hourly database, 84th American Meteorological Society Annual Meeting, 2004, Seattle, WA, American Meteorological Society, Boston, MA, 2004. 99

MACC: GEMS Reanalysis, ECMWF, http://www.gmes-atmosphere.eu/d/services/gac/reanalysis/gems/, 2014. 30, 39

MacCarthy, J., Pang, Y., Murrells, T., Passant, N., Martinez, C., Thomas, J., Thistlethawaite, G., and Misselbrook, T.: Air quality pollutant inventories for England, Scotland, Wales and Northern Ireland, AEA report number AEAT/ENV/R/3225, pp. 1990–2009, 2011. 23

Macintyre, H. and Evans, M.: Sensitivity of a global model to the uptake of N_2O_5 by tropospheric aerosol, Atmospheric Chemistry and Physics, 10, 7409–7414, 2010. 55, 128

Magi, B. I. and Hobbs, P. V.: Effects of humidity on aerosols in southern Africa during the biomass burning season, Journal of Geophysical Research: Atmospheres (1984–2012), 108, 2003. 56

McGregor, G. and Bamzelis, D.: Synoptic typing and its application to the investigation of weather air pollution relationships, Birmingham, United Kingdom, Theoretical and Applied Climatology, 51, 223–236, doi:10.1007/BF00867281, http://dx.doi.org/10.1007/BF00867281, 1995. 84, 85

Menut, L., Bessagnet, B., Khvorostyanov, D., Beekmann, M., Blond, N., Colette, A., Coll, I., Curci, G., Foret, G., Hodzic, A., Mailler, S., Meleux, F., Monge, J.-L., Pison, I., Siour, G., Turquety, S., Valari, M., Vautard, R., and Vivanco, M. G.: CHIMERE 2013: a model for regional atmospheric composition modelling, Geoscientific Model Development, 6, 981–1028, doi:10.5194/gmd-6-981-2013, http://www.geosci-model-dev.net/6/981/2013/, 2013. 55

Monks, S., Arnold, S., and Chipperfield, M.: Evidence for El Niño–Southern Oscillation (ENSO) influence on Arctic CO interannual variability through biomass burning emissions, Geophysical Research Letters, 39, 2012. 14

NASA: NASA A-Train, NASA, http://glory.gsfc.nasa.gov/images/a-train.jpg, 39, 2012. ix, 24

Nassar, R., Logan, J. A., Worden, H. M., Megretskaia, I. A., Bowman, K. W., Osterman, G. B., Thompson, A. M., Tarasick, D. W., Austin, S., Claude, H., Dubey, M. K., Hocking, W. K., Johnson, B. J., Joseph, E., Merrill, J., Morris, G. A., Newchurch, M., Oltmans, S. J., Posny, F., Schmidlin, F. J., Vmel, H., Whiteman, D. N., and Witte, J. C.: Validation of Tropospheric Emission Spectrometer (TES) nadir ozone profiles using ozonesonde measurements, Journal of Geophysical Research: Atmospheres, 113, n/a–n/a, doi:10.1029/2007JD008819, http://dx.doi.org/10.1029/2007JD008819, 2008. 35

O'Connor, F. M., Johnson, C. E., Morgenstern, O., Abraham, N. L., Braesicke, P., Dalvi, M., Folberth, G. A., Sanderson, M. G., Telford, P. J., Voulgarakis, A., Young, P. J., Zeng, G., Collins, W. J., and Pyle, J. A.: Evaluation of the new UKCA climate-composition model-Part 2: The Troposphere, Geoscientific Model Development, 7, 41–91, doi:10.5194/gmd-7-41-2014, http://www.geosci-model-dev.net/7/41/2014/, 2014. 23

O'Hare, G. and Wilby, R.: A Review of Ozone Pollution in the United Kingdom and Ireland with an Analysis Using Lamb Weather Types, The Geographical Journal, 161, pp. 1–20, http://www.jstor.org/stable/3059923, 1995. 79, 80, 83

Olivier, J.: Fog harvesting: An alternative source of water supply on the West Coast of South Africa, GeoJournal, 61, 203–214, doi:10.1007/s10708-004-2889-y, 2004. 99

Osterman, G. B., Kulawik, S. S., Worden, H. M., Richards, N. A. D., Fisher, B. M., Eldering, A., Shephard, M. W., Froidevaux, L., Labow, G., Luo, M., Herman, R. L., Bowman, K. W., and Thompson, A. M.: Validation of Tropospheric Emission Spectrometer (TES) measurements of the total, stratospheric, and tropospheric column abundance of ozone, Journal of Geophysical Research: Atmospheres, 113, n/a–n/a, doi:10.1029/2007JD008801, http://dx.doi.org/10.1029/2007JD008801, 2008. 35

Paton-Walsh, C., Emmons, L. K., and Wilson, S. R.: Estimated total emissions of trace gases from the Canberra Wildfires of 2003: a new method using satellite measurements of aerosol optical depth & the MOZART chemical transport model, Atmospheric Chemistry and Physics, 10, 5739–5748, doi:10.5194/acp-10-5739-2010, http://www.atmos-chem-phys.net/10/5739/2010/, 2010. 16, 24

Peters, W., Krol, M., Dentener, F., Thompson, A. M., and Lelieveld, J.: Chemistry-transport modelling of the satellite observed distribution of tropical tropospheric ozone,

Atmospheric Chemistry and Physics, 2, 103–120, doi:10.5194/acp-2-103-2002, `http://www.atmos-chem-phys.net/2/103/2002/`, 2002. 15

PHE: Public Health England, Available at: http://www.hpa.org.uk/ProductsServices /ChemicalsPoisons/Environment/Air/ (last accessed June 2014), 2014. 1

Pirovano, G., Balzarini, A., Bessagnet, B., Emery, C., Kallos, G., Meleux, F., Mitsakou, C., Nopmongcol, U., Riva, G., and Yarwood, G.: Investigating impacts of chemistry and transport model formulation on model performance at European scale, Atmospheric Environment, 53, 93–109, doi:http://dx.doi.org/10.1016/j.atmosenv.2011.12.052, 2012. 85

Pope, R., Willett, K., Osborn, T., and Thorne, P.: Investigation and quality assessment of the Past Weather Code from the Integrated Surface Database, Hadley Centre Technical Note 97, Met Office, Exeter, UK, 2014b. 100

Pope, R. J., Savage, N. H., Chipperfield, M. P., Arnold, S. R., and Osborn, T. J.: The influence of synoptic weather regimes on UK air quality: analysis of satellite column NO2, Atmospheric Science Letters, 15, 211–217, doi:10.1002/asl2.492, `http://dx.doi.org/10.1002/asl2.492`, 2014a. 58, 81

Rebetez, M., Dupont, O., and Giroud, M.: An analysis of the July 2006 heatwave extent in Europe compared to the record year of 2003, Theoretical and Applied Climatology, 95, 1–7, doi:10.1007/s00704-007-0370-9, `http://dx.doi.org/10.1007/s00704-007-0370-9`, 2009. ix, 19, 20

Richards, N. A. D., Osterman, G. B., Browell, E. V., Hair, J. W., Avery, M., and Li, Q.: Validation of Tropospheric Emission Spectrometer ozone profiles with aircraft observations during the Intercontinental Chemical Transport Experiment-B, Journal of Geophysical Research: Atmospheres, 113, n/a–n/a, doi:10.1029/2007JD008815, `http://dx.doi.org/10.1029/2007JD008815`, 2008. 24, 27, 34, 35

Richards, N. A. D., Arnold, S. R., Chipperfield, M. P., Miles, G., Rap, A., Siddans, R., Monks, S. A., and Hollaway, M. J.: The Mediterranean summertime ozone maximum: global emission sensitivities and radiative impacts, Atmospheric Chemistry and Physics, 13, 2331–2345, doi:10.5194/acp-13-2331-2013, `http://www.atmos-chem-phys.net/13/2331/2013/`, 2013. 41

Richter, A., Eyring, V., Burrows, J. P., Bovensmann, H., Lauer, A., Sierk, B., and Crutzen, P. J.: Satellite measurements of NO2 from international shipping emissions, Geophysical Research Letters, 31, n/a–n/a, doi:10.1029/2004GL020822, `http://dx.doi.org/10.1029/2004GL020822`, 2004. 116

Rydock, J.: Validation of a present weather observation method for driving rain mapping, Building and Environment, 42, 566 – 571, doi:http://dx.doi.org/10.1016/j.buildenv.2005.09.017, 2007. 99

Sarwar, G., Godowitch, J., Henderson, B. H., Fahey, K., Pouliot, G., Hutzell, W. T., Mathur, R., Kang, D., Goliff, W. S., and Stockwell, W. R.: A comparison of atmospheric composition using the Carbon Bond and Regional Atmospheric Chemistry Mechanisms, Atmospheric Chemistry and Physics, 13, 9695–9712, doi:10.5194/acp-13-9695-2013, http://www.atmos-chem-phys.net/13/9695/2013/, 2013. 55

Savage, N., Agnew, P., Davis, L., Ordóñez, C., Thorpe, R., Johnson, C., O'Connor, F., and Dalvi, M.: Air quality modelling using the Met Office Unified Model (AQUM OS24-26): model description and initial evaluation, Geoscientific Model Development, 6, 353–372, 2013. ix, 16, 21, 22, 23, 26, 53, 64, 65, 66, 67, 77, 129

Savage, N. H., Law, K. S., Pyle, J. A., Richter, A., Nüß, H., and Burrows, J. P.: Using GOME NO_2 satellite data to examine regional differences in TOMCAT model performance, Atmospheric Chemistry and Physics, 4, 1895–1912, doi:10.5194/acp-4-1895-2004, http://www.atmos-chem-phys.net/4/1895/2004/, 2004. 14, 15

Savage, N. H., Pyle, J. A., Braesicke, P., Wittrock, F., Richter, A., Nüß, H., Burrows, J. P., Schultz, M. G., Pulles, T., and van Het Bolscher, M.: The sensitivity of Western European NO_2 columns to interannual variability of meteorology and emissions: a model-GOME study, Atmospheric Science Letters, 9, 182–188, 2008. 15, 81

Schmidt, A., Ostro, B., Carslaw, K. S., Wilson, M., Thordarson, T., Mann, G. W., and Simmons, A. J.: Excess mortality in Europe following a future Laki-style Icelandic eruption, Proceedings of the National Academy of Sciences, 108, 15 710–15 715, doi: 10.1073/pnas.1108569108, http://www.pnas.org/content/108/38/15710.abstract, 2011. ix, 2

Seigneur, C., Pun, B., Pai, P., Louis, J.-F., Solomon, P., Emery, C., Morris, R., Zahniser, M., Worsnop, D., Koutrakis, P., et al.: Guidance for the performance evaluation of three-dimensional air quality modelling systems for particulate matter and visibility, Journal of the Air & Waste Management Association, 50, 588–599, 2000. 16

Seinfeld, J. and Pandis, S.: Atmospheric Chemistry and Physics: From Air Pollution to Climate Change - Second Edition, John Wiley and Sons Inc, New Jersey, USA, 2006. 7

Singh, H.: Reactive nitrogen in the troposphere, Environmental Science & Technology, 21, 320–327, 1967. 8

Smith, R. N. B.: A scheme for predicting layer clouds and their water content in a general circulation model, Quarterly Journal of the Royal Meteorological Society, 116, 435–460, doi:10.1002/qj.49711649210, http://dx.doi.org/10.1002/qj.49711649210, 1990. 22

Steinbacher, M., Zellweger, C., Schwarzenbach, B., Bugmann, S., Buchmann, B., Ordez, C., Prevot, A. S. H., and Hueglin, C.: Nitrogen oxide measurements at rural sites in Switzerland: Bias of conventional measurement techniques, Journal of Geophysical Research: Atmospheres, 112, n/a–n/a, doi:10.1029/2006JD007971, http://dx.doi.org/10.1029/2006JD007971, 2007. 65

Stevenson, D. S., Dentener, F. J., Schultz, M. G., Ellingsen, K., van Noije, T. P. C., Wild, O., Zeng, G., Amann, M., Atherton, C. S., Bell, N., Bergmann, D. J., Bey, I., Butler, T., Cofala, J., Collins, W. J., Derwent, R. G., Doherty, R. M., Drevet, J., Eskes, H. J., Fiore, A. M., Gauss, M., Hauglustaine, D. A., Horowitz, L. W., Isaksen, I. S. A., Krol, M. C., Lamarque, J.-F., Lawrence, M. G., Montanaro, V., Mller, J.-F., Pitari, G., Prather, M. J., Pyle, J. A., Rast, S., Rodriguez, J. M., Sanderson, M. G., Savage, N. H., Shindell, D. T., Strahan, S. E., Sudo, K., and Szopa, S.: Multimodel ensemble simulations of present-day and near-future tropospheric ozone, Journal of Geophysical Research: Atmospheres, 111, n/a–n/a, doi:10.1029/2005JD006338, http://dx.doi.org/10.1029/2005JD006338, 2006. 8

Tang, L., Rayner, D., and Haeger-Eugensson, M.: Have Meteorological Conditions Reduced NO2 Concentrations from Local Emission Sources in Gothenburg?, Water, Air, & Soil Pollution, 221, 275–286, doi:10.1007/s11270-011-0789-6, http://dx.doi.org/10.1007/s11270-011-0789-6, 2011. 80, 83, 84

Tie, X., Emmons, L., Horowitz, L., Brasseur, G., Ridley, B., Atlas, E., Stround, C., Hess, P., Klonecki, A., Madronich, S., et al.: Effect of sulfate aerosol on tropospheric NO_x and ozone budgets: Model simulations and TOPSE evidence, Journal of Geophysical Research: Atmospheres (1984–2012), 108, 2003. 55

TROPOMI: TROPOMI, http://www.tropomi.eu/TROPOMI/Instrument.html, 2014. 128

van der A, R. J., Eskes, H. J., Boersma, K. F., van Noije, T. P. C., Van Roozendael, M., De Smedt, I., Peters, D. H. M. U., and Meijer, E. W.: Trends, seasonal variability and dominant NOx source derived from a ten year record of NO2 measured from space, Journal of Geophysical Research: Atmospheres, 113, n/a–n/a, doi:10.1029/2007JD009021, http://dx.doi.org/10.1029/2007JD009021, 2008. 81

Varutbangkul, V., Brechtel, F., Bahreini, R., Ng, N., Keywood, M., Kroll, J., Flagan, R., Seinfeld, J., Lee, A., and Goldstein, A.: Hygroscopicity of secondary organic aerosols

formed by oxidation of cycloalkenes, monoterpenes, sesquiterpenes, and related compounds, Atmospheric Chemistry and Physics, 6, 2367–2388, 2006. 56

Visschedijk, A., Zanveld, P., and van der Gon, H.: A high resolution gridded European emission database for the EU integrated project GEMS, TNO report 2007-A-R0233/B, 2007. 23

Wallace, J. and Hobbs, P.: Atmospheric Science: An Introductory Survey - Second Edition, Elsevier Academic Press, New York, USA, 2006. 7

Wayne, R.: Chemistry of Atmospheres - Third Edition, Oxford University Press, Oxford, UK, 2000. 5, 7, 8

Whall, C., Scarborough, T., Stavrakaki, A., Green, C., Squire, J., and Noden, R.: UK Ship Emissions Inventory, Entec UK Ltd, London, UK, available at: http://uk-air.defra.gov.uk/reports/cat15/101213145921897FinalReport291110.pdf, 2010. 23

WHO: World Health Organisation (WHO): Air Quality and Health, http://www.who.int/mediacentre/factsheets/fs313/en/ (last accessed February 2014), 2014. 1

Wilson, D. R. and Ballard, S. P.: A microphysically based precipitation scheme for the UK meteorological office unified model, Quarterly Journal of the Royal Meteorological Society, 125, 1607–1636, doi:10.1002/qj.49712555707, http://dx.doi.org/10.1002/qj.49712555707, 1999. 22

WMO: Manual on Codes: Volume I-International Codes, World Meteorological Organisation (WMO) No. 306, pp. 203, Geneva, Switzerland, 1988. 98

Zhang, Y., Sartelet, K., Wu, S.-Y., and Seigneur, C.: Application of WRF/Chem-MADRID and WRF/Polyphemus in Europe? Part 1: Model description, evaluation of meteorological predictions, and aerosol-meteorology interactions, Atmospheric Chemistry and Physics, 13, 6807–6843, doi:10.5194/acp-13-6807-2013, http://www.atmos-chem-phys.net/13/6807/2013/, 2013. 55

Zhou, Y., Brunner, D., Hueglin, C., Henne, S., and Staehelin, J.: Changes in {OMI} tropospheric {NO2} columns over Europe from 2004 to 2009 and the influence of meteorological variability, Atmospheric Environment, 46, 482–495, doi:http://dx.doi.org/10.1016/j.atmosenv.2011.09.024, 2012. 81, 117

Ziemke, J. R., Chandra, S., Labow, G. J., Bhartia, P. K., Froidevaux, L., and Witte, J. C.: A global climatology of tropospheric and stratospheric ozone derived from Aura

OMI and MLS measurements, Atmospheric Chemistry and Physics, 11, 9237–9251, doi: 10.5194/acp-11-9237-2011, http://www.atmos-chem-phys.net/11/9237/2011/, 2011. 38